



2012

# SHEAR STRENGTH OF WEB-TAPERED I-SHAPED MEMBERS

Ryan Paul Studer

*University of Kentucky*, [ryanstuder15@gmail.com](mailto:ryanstuder15@gmail.com)

**[Click here to let us know how access to this document benefits you.](#)**

---

## Recommended Citation

Studer, Ryan Paul, "SHEAR STRENGTH OF WEB-TAPERED I-SHAPED MEMBERS" (2012). *Theses and Dissertations--Civil Engineering*. 1.

[https://uknowledge.uky.edu/ce\\_etds/1](https://uknowledge.uky.edu/ce_etds/1)

This Master's Thesis is brought to you for free and open access by the Civil Engineering at UKnowledge. It has been accepted for inclusion in Theses and Dissertations--Civil Engineering by an authorized administrator of UKnowledge. For more information, please contact [UKnowledge@lsv.uky.edu](mailto:UKnowledge@lsv.uky.edu).

**STUDENT AGREEMENT:**

I represent that my thesis or dissertation and abstract are my original work. Proper attribution has been given to all outside sources. I understand that I am solely responsible for obtaining any needed copyright permissions. I have obtained and attached hereto needed written permission statements(s) from the owner(s) of each third-party copyrighted matter to be included in my work, allowing electronic distribution (if such use is not permitted by the fair use doctrine).

I hereby grant to The University of Kentucky and its agents the non-exclusive license to archive and make accessible my work in whole or in part in all forms of media, now or hereafter known. I agree that the document mentioned above may be made available immediately for worldwide access unless a preapproved embargo applies.

I retain all other ownership rights to the copyright of my work. I also retain the right to use in future works (such as articles or books) all or part of my work. I understand that I am free to register the copyright to my work.

**REVIEW, APPROVAL AND ACCEPTANCE**

The document mentioned above has been reviewed and accepted by the student's advisor, on behalf of the advisory committee, and by the Director of Graduate Studies (DGS), on behalf of the program; we verify that this is the final, approved version of the student's dissertation including all changes required by the advisory committee. The undersigned agree to abide by the statements above.

Ryan Paul Studer, Student

Dr. Douglas Bradley Davis, Major Professor

Dr. Kamyar C. Mahboub, Director of Graduate Studies

---

# SHEAR STRENGTH OF WEB-TAPERED I-SHAPED MEMBERS

---

THESIS

---

A thesis submitted in partial fulfillment of the requirements for the degree of Master of Science in Civil Engineering in the College of Engineering

By

Ryan Paul Studer

Lexington, Kentucky

Director: Dr. Douglas Bradley Davis, Professor of Civil Engineering

Lexington, Kentucky

2012

Copyright © Ryan Paul Studer 2012

## ABSTRACT OF THESIS

### SHEAR STRENGTH OF WEB-TAPERED I-SHAPED MEMBERS

Plate girders are fabricated in situations where standard structural shapes do not possess the required strength necessary to carry applied loads. In many instances, plate girders are tapered so that the resistance to bending is proportional to the bending moment, creating cost effective, aesthetically pleasing structures. The AISC 2010 *Specifications* accurately predict the flexural capacity of tapered plate girders but recent research has suggested that the required shear strength is overly conservative. The researchers postulate that the required shear strength is overly conservative due to an effect known as modified shear that has been neglected from the AISC 2010 *Specifications* but has been suggested by several authors.

This research investigates both analytically and experimentally, tapered member ultimate shear strength considering a “modified” and “unmodified” applied shear approach. A new design formula introduced by Lee et al. (2008) will be used in conjunction with the AISC 2010 *Specification* in making ultimate shear strength comparisons. A total of 12 specimens are tested to failure, ten tapered and two prismatic built-up plate girders.

**KEYWORDS:** modified shear, ultimate shear strength, web buckling, shear contribution, strain gage

Ryan Paul Studer

April 30, 2012

SHEAR STRENGTH OF WEB-TAPERED I-SHAPED MEMEBERS

By

Ryan Paul Studer

Dr. Douglas Bradley Davis  
Director of Thesis

Dr. Kamyar C. Mahboub  
Director of Graduate Studies

April 30, 2012

## ACKNOWLEDGEMENTS

I would like to thank Dr. Brad Davis for his support throughout the duration of this project. His insight and unwavering support were influential in the writing of this thesis. I would also like to thank Dr. George Blandford and Dr. Issam Harik for their thoughtful review of my work as being part of my committee. The financial support for this project was made possible by the Metal Building Manufacturers Association and was invaluable towards the completion of this research.

The faculty and staff at the Civil Engineering Department provided the administrative and technical support that made this research possible and I would like to recognize: Shelia Williams, Abheetha Peiris, and Gene Yates. I would also like to acknowledge Herb Mefford and Bottoms Engineering who machined much of the research equipment used during the duration of the experimental stage.

My colleagues and friends Dave Murray, Di Liu, Drew Thompson, Matthew Hansman, and Aaron Thomas helped with portions of the analytical and experimental setup of my research and I appreciate all their hard work. Last but not least, I want to thank my family members - none of this would be possible without your loving support.

## TABLE OF CONTENTS

Chapter 1	Introduction and Literature Review.....	1
1.1	Introduction.....	1
1.2	Literature Review .....	2
1.2.1	Web Shear Force Determination.....	2
1.2.2	Plate Girder Shear Strength.....	6
Chapter 2	Experimental Program.....	16
2.1	Test Setup .....	16
2.2	Specimens .....	17
2.3	Load Frame and Boundary Conditions.....	19
2.4	Instrumentation .....	22
2.5	Web Initial Out-of-Plane Measurements .....	26
2.6	Testing Procedure .....	31
2.7	Material Properties.....	32
2.8	Right vs. Normal Cross Sectional Properties.....	34
2.9	Measured Web and Flange Forces.....	35
Chapter 3	Analytical Predictions .....	39
3.1	Predicted Web and Flange Forces .....	39
3.2	Ultimate Shear Strength.....	40
3.2.1	AISC Specification / MBMA/AISC Design Guide 25 Web Shear Strength Prediction Method.....	41
3.2.2	Lee et al. (2008) Method.....	42
Chapter 4	Comparisons of Measurements and Predictions.....	43
4.1	Tapered 1a.....	44
4.1.1	Web and Flange Shear Contributions.....	44
4.1.2	Failure Loads.....	45
4.2	Tapered 1b .....	48
4.2.1	Web and Flange Shear Contributions.....	49
4.2.2	Failure Loads.....	50
4.3	Tapered 1c.....	52
4.3.1	Web and Flange Shear Contributions.....	53
4.3.2	Failure Loads.....	53
4.4	Tapered 2a.....	55
4.4.1	Web and Flange Shear Contributions.....	56

4.4.2	Failure Loads.....	57
4.5	Tapered 2b .....	59
4.5.1	Web and Flange Shear Contributions.....	60
4.5.2	Failure Loads.....	61
4.6	Tapered 2c.....	63
4.6.1	Web and Flange Shear Contributions.....	65
4.6.2	Failure Loads.....	66
4.7	Tapered 3 .....	68
4.7.1	Web and Flange Shear Contributions.....	70
4.7.2	Failure Loads.....	71
4.8	Tapered 4 .....	73
4.8.1	Web and Flange Shear Contributions.....	74
4.8.2	Failure Loads.....	75
4.9	Tapered 5 .....	77
4.9.1	Web and Flange Shear Contributions.....	78
4.9.2	Failure Load .....	79
4.10	Tapered 6 .....	81
4.10.1	Web and Flange Shear Contributions.....	82
4.10.2	Failure Load .....	83
4.11	Prismatic 1 .....	85
4.11.1	Failure Load .....	86
4.12	Prismatic 2 .....	87
4.12.1	Failure Load .....	88
4.13	Summary of Comparisons .....	89
Chapter 5	Conclusions .....	94
5.1	Web and Flange Shear Contributions .....	94
5.2	Ultimate Shear Strength of Tapered Members .....	95
5.3	Ultimate Shear Strength of Prismatic Members .....	97
5.4	Flexural Strength.....	97
Chapter 6	Recommendations for Future Research.....	100
Appendices.....		101
Appendix A	Tapered 1a Results.....	102
Appendix B	Tapered 1b Results.....	109
Appendix C	Tapered 1c Results.....	116



Appendix D	Tapered 2a Results.....	123
Appendix E	Tapered 2b Results.....	129
Appendix F	Tapered 2c Results .....	136
Appendix G	Tapered 3 Results .....	144
Appendix H	Tapered 4 Results .....	151
Appendix I	Tapered 5 Results .....	158
Appendix J	Tapered 6 Results.....	166
Appendix K	Prismatic 1 Results .....	173
Appendix L	Prismatic 2 Results.....	179
References	.....	186
Vita	.....	188

## LIST OF FIGURES

Figure 1-1 Williams and Harris Modified Shear .....	4
Figure 1-2 Blodgett's Modified Shear (Decrease Web Shear).....	5
Figure 1-3 Blodgett's Modified Shear (Increase Web Shear) .....	6
Figure 2-1 Metal Building Moment Frame Shear and Moment Diagrams.....	16
Figure 2-2 Specimen Elevation.....	17
Figure 2-3 Overall Setup With Load Shown .....	20
Figure 2-4 Pinned and Roller Supports.....	21
Figure 2-5 Hydraulic Ram and Load Cell .....	21
Figure 2-6 Flange Lateral Brace (Watt's Linkage).....	22
Figure 2-7 Cable-Extension Displacement Sensor .....	23
Figure 2-8 LVDTs for Web Out-of-Plane Measurements .....	24
Figure 2-9 Strain Gage Locations at a Measurement Station .....	24
Figure 2-10 "Tapered 2" Strain Gage Locations at a Measurement Station .....	25
Figure 2-11 "Tapered 5" Strain Gage Locations at a Measurement Station .....	26
Figure 2-12 Carriage .....	27
Figure 2-13 Initial Out-Of-Plane Grid Spacing .....	28
Figure 2-14 Transverse Out of Plane Tolerance.....	29
Figure 2-15 Longitudinal Out of Plane Tolerance.....	29
Figure 2-16 Specimen Cross Sectional Properties.....	34
Figure 2-17 Measured Modified Shear Diagram .....	36
Figure 4-1 "Tapered 1a" $V_{meas.} / V_{pred.}$ (%).....	45
Figure 4-2 "Tapered 1a" $V_{meas.} / V_{pred.}$ .....	45
Figure 4-3 AISC Predicted Failure Loads "Tapered 1a" .....	46
Figure 4-4 Lee et al. (2008) Predicted Failure Loads "Tapered 1a".....	47
Figure 4-5 "Tapered 1b" $V_{meas.} / V_{pred.}$ (%) .....	49
Figure 4-6 "Tapered 1b" $V_{meas.} / V_{pred.}$ .....	49
Figure 4-7 "Tapered 1b" AISC Predicted Failure Loads.....	51
Figure 4-8 "Tapered 1b" Lee et al. (2008) Predicted Failure Loads .....	52
Figure 4-9 "Tapered 1c" $V_{meas.} / V_{pred.}$ (%).....	53
Figure 4-10 "Tapered 1c" $V_{meas.} / V_{pred.}$ .....	53
Figure 4-11 "Tapered 1c" AISC Predicted Failure Loads .....	54
Figure 4-12 "Tapered 1c" Lee et al. (2008) Predicted Failure Loads.....	55
Figure 4-13 "Tapered 2a" $V_{meas.} / V_{pred.}$ (%).....	56
Figure 4-14 "Tapered 2a" $V_{meas.} / V_{pred.}$ .....	57
Figure 4-15 "Tapered 2a" AISC Predicted Failure Loads .....	58
Figure 4-16 "Tapered 2a" Lee et al. (2008) Predicted Failure Loads.....	59
Figure 4-17 "Tapered 2b" $V_{meas.} / V_{pred.}$ (%) .....	60
Figure 4-18 "Tapered 2b" $V_{meas.} / V_{pred.}$ .....	61
Figure 4-19 "Tapered 2b" AISC Predicted Failure Loads.....	62
Figure 4-20 "Tapered 2b" Lee et al. (2008) Predicted Failure Loads .....	63
Figure 4-21 "Tapered 2c" $V_{meas.} / V_{pred.}$ (%).....	65
Figure 4-22 "Tapered 2c" $V_{meas.} / V_{pred.}$ .....	66
Figure 4-23 "Tapered 2c" AISC Predicted Failure Loads .....	67
Figure 4-24 "Tapered 2c" Lee et al. (2008) Predicted Failure Loads.....	68
Figure 4-25 "Tapered 3" $V_{meas.} / V_{pred.}$ (%) .....	70

Figure 4-26 “Tapered 3” $V_{meas.} / V_{pred.}$ .....	70
Figure 4-27 “Tapered 3” AISC Predicted Failure Loads.....	72
Figure 4-28 “Tapered 3” Lee et al. (2008) Predicted Failure Loads .....	73
Figure 4-29 “Tapered 4” $V_{meas.} / V_{pred.}$ (%) .....	74
Figure 4-30 “Tapered 4” $V_{meas.} / V_{pred.}$ .....	75
Figure 4-31 “Tapered 4” AISC Predicted Failure Loads.....	76
Figure 4-32 “Tapered 4” Lee et al. (2008) Predicted Failure Loads .....	77
Figure 4-33 “Tapered 5” $V_{meas.} / V_{pred.}$ (%) .....	78
Figure 4-34 “Tapered 5” $V_{meas.} / V_{pred.}$ .....	79
Figure 4-35 “Tapered 5” AISC Predicted Failure Loads.....	80
Figure 4-36 “Tapered 5” Lee et al. (2008) Predicted Failure Loads .....	81
Figure 4-37 “Tapered 6” $V_{meas.} / V_{pred.}$ (%) .....	82
Figure 4-38 “Tapered 6” $V_{meas.} / V_{pred.}$ .....	83
Figure 4-39 “Tapered 6” AISC Predicted Failure Loads.....	84
Figure 4-40 “Tapered 6” Lee et al. (2008) Predicted Failure Loads .....	85
Figure 4-41 “Prismatic 1” $V_{meas.} / V_{pred.}$ .....	85
Figure 4-42 “Prismatic 1” Predicted Failure Loads.....	87
Figure 4-43 “Prismatic 2” $V_{meas.} / V_{pred.}$ .....	87
Figure 4-44 “Prismatic 2” Predicted Failure Loads.....	89

LIST OF TABLES

Table 2-1 Specimen Summary..... 19  
Table 2-2 Web Initial Out-of-Plane MBMA Tolerance Check ..... 30  
Table 2-3 Web Initial Out-of-Plane Measurements for Failed Specimens..... 30  
Table 2-4 Coupon Results..... 33  
Table 2-5 “Tapered 2” Specimen Geometric Property Comparisons..... 35  
Table 4-1 Tapered Specimens Shear Force Contribution..... 90  
Table 4-2 Tapered Specimens AISC Measured / Predicted Failure Loads ..... 91  
Table 4-3 Tapered Specimens Lee et al. (2008) Measured / Predicted Failure Loads ..... 92  
Table 4-4 Prismatic Specimens Measured / Predicted Failure Loads ..... 93  
Table 5-1 Summary of Web Shear Prediction Accuracy..... 95  
Table 5-2 Summary of Shear Strength Measurements and Predictions ..... 96  
Table 5-3 Shear Strength Prediction Methods..... 96

## LIST OF EQUATIONS

(1-1) .....	4
(1-2) .....	4
(1-3) .....	5
(1-4) .....	5
(1-5) .....	7
(1-6) .....	8
(1-7) .....	8
(1-8) .....	8
(1-9) .....	9
(1-10) .....	9
(1-11) .....	10
(1-12) .....	10
(1-13) .....	11
(1-14) .....	11
(1-15) .....	11
(1-16) .....	11
(1-17) .....	14
(1-18) .....	14
(1-19) .....	15
(1-20) .....	15
(1-21) .....	15
(1-22) .....	15
(1-23) .....	15
(2-1) .....	36
(2-2) .....	37
(2-3) .....	37
(2-4) .....	38
(2-5) .....	38
(3-1) .....	39
(3-2) .....	39
(3-3) .....	41
(3-4) .....	41
(3-5) .....	41
(3-6) .....	41
(3-7) .....	41
(3-8) .....	42

## Chapter 1 Introduction and Literature Review

### 1.1 Introduction

Historically, it has been common practice among metal building manufacturers to evaluate shear in tapered I-shaped members using a “modified shear” approach which accounts for the shear components of the inclined flange forces. Concisely, the modified shear approach is summarized as follows: (1) the required web shear is not the entire shear at a section, but is the total shear at a section minus the transverse component of each flange force, and (2) the required web shear is compared to the web shear yielding or buckling strength computed using the *AISC Specification for Structural Steel Buildings* (AISC 2010) or some other source. The modified shear approach is usually economically advantageous, is rational from an engineering mechanics standpoint, has been recommended by Blodgett (1966), among others, and has not resulted in failures of frames in-service, to the investigators’ knowledge.

The most modern guidance for the design of tapered I-shaped members is the *MBMA/AISC Design Guide 25, Frame Design Using Web-Tapered Members* (Kaehler et al. 2011). In the last paragraph of Section 5.6, the authors state that the modified shear approach “has not been included here due to the lack of research to validate the procedure.” Previous research studies by Sumner (1995) and Redmond (2007) included the knee regions of moment frames and thus did not provide conclusive evidence for or against the modified shear approach used in member strength checks. However, their results seem to indicate that simply comparing the total shear at a section to the *AISC Specification* shear strength is conservative, and perhaps very conservative.

Therefore, the objectives of this research project were: (1) to investigate the internal force distribution in tapered members to determine whether the web resists the portion of the shear predicted using the modified shear approach, and (2) to determine an accurate method for predicting the shear strength of tapered members.

## **1.2 Literature Review**

Over the last five decades, steel plate girder shear strength has been the subject of numerous research projects, most of which focused on quantifying the ultimate strength including post-buckling strength (tension field action (TFA)) of web panels bounded by transverse stiffeners. Few projects have been completed on unstiffened plate girders such as those of interest in the current project. Similarly, few projects have been completed on the subject of tapered member shear, and even fewer on the subject of shear strength of unstiffened tapered members. However, several papers contain research findings that are helpful toward accomplishing the objectives of the current project, and those are the focus of this literature review.

For a complete literature review of all but the most recent research on plate girders, see the SSRC *Guide to Stability Design Criteria for Metal Structures* (Ziemian, 2010) Chapter 6. There is also a series of newer papers not mentioned in the SSRC *Guide*, mostly by Dr. S.C. Lee and Dr. C.H. Yoo, that contain important new behavioral theories—see Yoo and Lee (2006) and Lee et al. (2009) for citations.

### *1.2.1 Web Shear Force Determination*

The simplest assumption, which is consistent with the AISC *Specification* Chapter G, is that the web shear strength must resist the entire shear force at a section. The

authors are aware of three other methods (Williams and Harris 1957, Blodgett (1966), and Bresler (1968)) for manually computing the internal shear forces present in a tapered member. The primary assumption used in each method is that each flange force vertical component resists a portion of the applied shear and the web must only resist the remainder. (Note that, depending on the taper angle, the flange force vertical components can be in the opposite direction as the applied shear and thus cause the web shear to exceed the applied shear, but this is less common.) These three methods are referred to as modified shear methods. Williams and Harris (1957) and Blodgett (1966) are described below. Bresler et al. (1968) was not used in this research study, so is not described herein.

Williams and Harris (1957) proposed the modified shear method depicted in Figure 1-1. In this method, the principal stresses in the flanges due to flexure are parallel to the angle of taper.



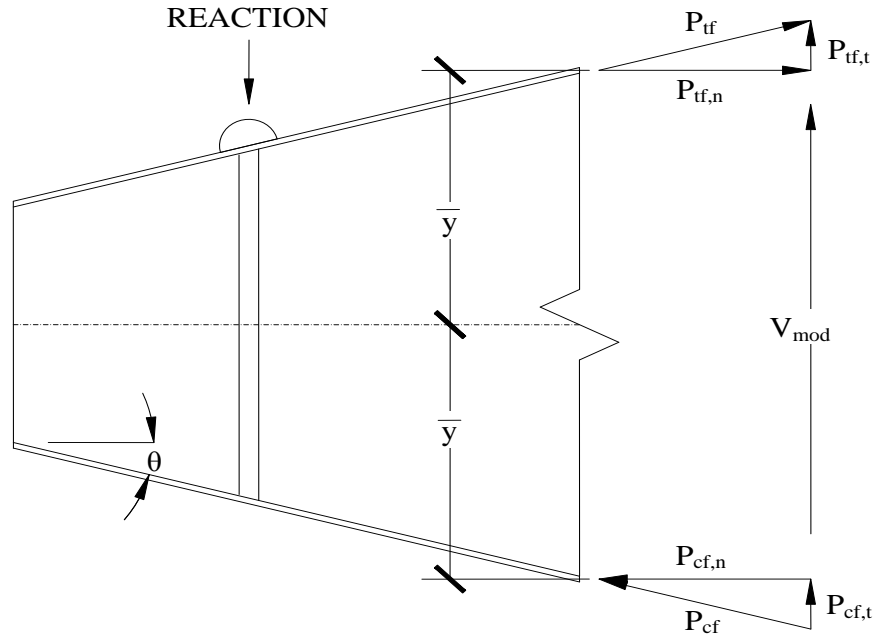


Figure 1-1 Williams and Harris Modified Shear

Using an elastic stress distribution, the principal force in the compression flange is calculated as follows:

$$P_{cf} = A_f \frac{M\bar{y}}{I} \frac{1}{\cos \theta} \quad (1-1)$$

where

- $P_{cf}$  = principal compression flange force
- $A_f$  = area of flange plate (product of  $b_f$  and  $t_f$ )
- $\bar{y}$  = distance from elastic neutral axis to flange centroid
- $I$  = strong-axis moment of inertia (computed using  $A_f$  (not  $A_f/\cos(\theta)$ ))

The transverse component of the compression flange force is:

$$P_{cf,t} = P_{cf} \sin \theta \quad (1-2)$$

The transverse component of the tension flange force,  $P_{tf,t}$ , is found similarly and the modified shear force resisted by the web is:

$$V_{Web} = V_{mod} = V - P_{cf,t} - P_{tf,t} \quad (1-3)$$

In 1966, Blodgett published *Design of Welded Structures* and describes a modified shear force used in bridge girders of variable depth. Blodgett's method is essentially identical to the one proposed by Williams and Harris (1957) except that Blodgett slightly simplifies the calculations by assuming that the moment is resisted only by the flanges as shown in Figure 1-2. The transverse (vertical) component of the compression flange is:

$$P_{cf,t} = P_{cf,n} \tan \theta = \frac{M}{h_o} \tan \theta \quad (1-4)$$

The tension flange vertical component is computed similarly. Blodgett points out the fact that if the applied shear force opposes the vertical components of the flange force, the web shear will actually increase to satisfy vertical force equilibrium. This situation is depicted in Figure 1-3.

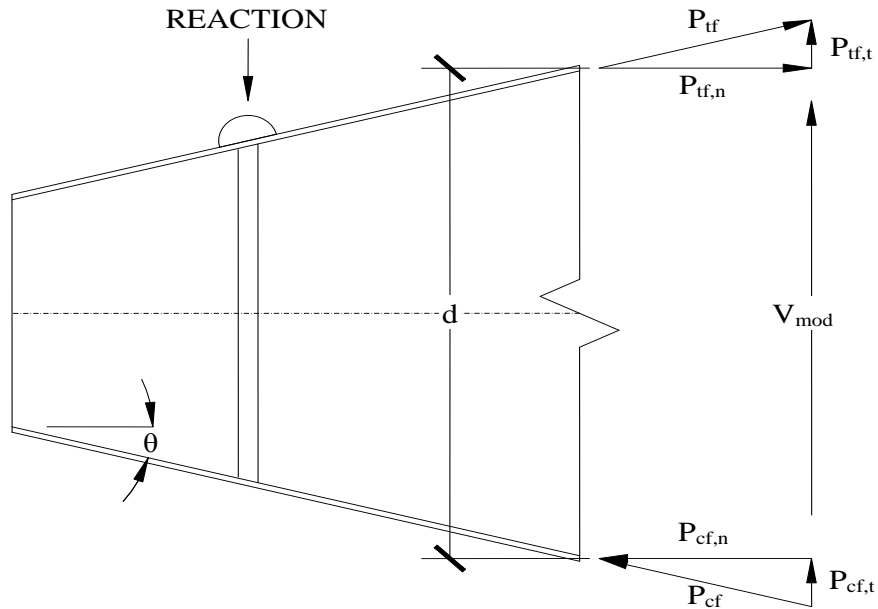


Figure 1-2 Blodgett's Modified Shear (Decrease Web Shear)

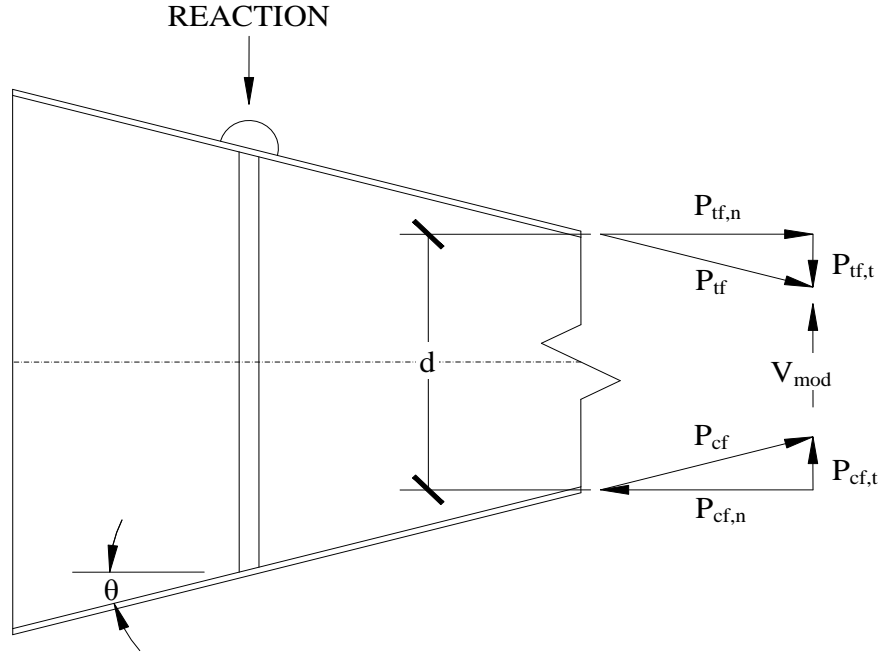


Figure 1-3 Blodgett's Modified Shear (Increase Web Shear)

### 1.2.2 Plate Girder Shear Strength

As previously mentioned, numerous authors have researched the shear strength of plate girders with slender webs, but the vast majority of those studies focused on the ultimate strength of short prismatic shear panels bounded by transverse stiffeners. This section only includes publications useful toward the objectives of the current research project.

The most widely cited research, published by Basler in 1961, forms the basis of the current AISC *Specification* (2010) Sections G2 and G3. Basler (1961) stated that the ultimate shear strength is the sum of the shear buckling and post-buckling strength provided by tension field action (TFA). The fundamental assumption is that, at loads below the shear buckling load, the web is subjected to a stress state with pure shear

(equal compressive and tensile principal stresses), but the compressive stress does not increase after shear buckling. Therefore, to allow the tensile stress field to further increase, some other element must provide the equilibrating compressive force (or otherwise, vertical equilibrium is not satisfied for a free body diagram of a portion of the web). Basler (1961) reasoned that transverse (shear) stiffeners provide the necessary compressive force and the plate girder performed much like a Pratt truss with the diagonals in tension and vertical stiffeners in compression. Therefore, by Basler's reasoning, unstiffened plate girders such as those used by MBMA member companies have no tension field action, so the total shear strength is the shear buckling strength.

To compute the shear buckling strength, Basler started with the classical plate buckling equation which is presented in numerous textbooks including Bleich (1952), Timoshenko and Gere (1961), and Salmon, Johnson, and Malhas (2008):

$$\tau_e = \frac{k_v \pi^2 E}{12(1 - \nu^2)(h/t_w)^2} \quad (1-5)$$

where

- $k_v$  = plate shear buckling coefficient for shear stress
- $h$  = web plate height
- $t_w$  = web thickness

The plate shear buckling coefficient,  $k_v$ , is a function of the web panel aspect ratio ( $a/h$ , where  $a$  is the clear distance between transverse stiffeners) and the type of boundary condition at the flange—simply supported (hinged), fixed, or something in between. Basler (1961) chose the most conservative boundary condition option: simply supported connection between the web and flanges. Bleich (1952) provided the following equations for the simply supported web shear buckling coefficient, denoted here as  $k_{ss}$  (the first

subscript to denote shear; the second subscript indicates simply supported connection at the flanges). These equations are also shown in Lee et al. (1996). For long panels such as the ones of interest in the present study, the shear buckling coefficient,  $k_v = 5.34$  which is approximately the value adopted by the AISC *Specification* (AISC 2010) Section G2,  $k_v = 5$ .

$$k_{ss} = 5.34 + \frac{4}{(a/h)^2} \text{ for } a/h \geq 1 \quad (1-6)$$

$$k_{ss} = 4 + \frac{5.34}{(a/h)^2} \text{ for } a/h < 1 \quad (1-7)$$

Basler's equations were first adopted into the AISC *Specification* in 1963, and have been carried forward to the 2010 *Specification*, as shown below.

$$V_n = 0.6F_y A_w C_v \quad (1-8)$$

$C_v$  is the ratio of the shear buckling strength to the plastic (full yield) shear strength, determined as follows:

When  $h/t_w \leq 1.10\sqrt{k_v E/F_y}$ , the web is stocky enough to achieve the plastic shear strength without shear buckling, so  $C_v = 1.0$ . For unstiffened webs, the plate buckling coefficient is  $k_v = 5.0$  which is slightly different from that shown above.

When  $1.10\sqrt{k_v E/F_y} < h/t_w \leq 1.37\sqrt{k_v E/F_y}$ , the web is stocky enough to develop limited yielding, but not the full plastic shear strength, so the anticipated failure behavior is inelastic buckling. Basler (1961) chose a nonlinear transition equation of the form  $\tau_{cr} = (\tau_{pr})^n (\tau_e)^{1-n}$  where  $\tau_{pr}$  is the proportional limit for shear stress. Test data led him

to choose  $\tau_{pr} = 0.8 \tau_y = 0.8(0.577F_y)$  and  $n = 0.5$ , resulting in  $\tau_{cr} = \sqrt{\tau_{pr}\tau_e}$  and  $C_v = 1.1\sqrt{k_v/E}/(h/t_w)$ .

When  $h/t_w > 1.37\sqrt{k_v E/F_y}$ , the web is so slender that it is expected to undergo shear buckling at such a low stress (below the proportional limit,  $\tau_{pr}$ ) that no part of the web has yielded. The anticipated failure behavior is elastic buckling, so the classical plate buckling equation given above applies directly. It is simplified and manipulated to result in  $C_v = (1.51k_v E)/(h/t_w)^2 F_y$ .

Over the years, alternative behavioral theories have been developed by several researchers. The main idea remains the same, though: the shear strength is the sum of the buckling strength and the post-buckling strength.

Several researchers have proposed shear buckling coefficients other than the one shown above, the most conservative value, applying to simply-supported web panels. On the other end of the spectrum, according to Lee et al. (1996), the shear buckling coefficient for a rectangular web plate is rotationally fixed at the flanges (moment connected to the flanges, so the flange torsional stiffness provides rotational stiffness at the web interface),  $k_{sf}$ , is given by the following equations. For panels with large  $a/h$ ,  $k_v = 8.98$ , a result also given by Timoshenko and Gere (1961).

$$k_{sf} = 8.98 + \frac{5.61}{(a/h)^2} - \frac{1.99}{(a/h)^3} \text{ for } a/h \geq 1 \quad (1-9)$$

$$k_{sf} = \frac{5.34}{(a/h)^2} + \frac{2.31}{a/h} - 3.44 + 8.39 \frac{a}{h} \text{ for } a/h < 1 \quad (1-10)$$

Authors have used different plate shear buckling coefficients over the years. Porter et al. (1975) also used  $k_{ss}$ , the most conservative value. Chern and Ostapenko (1969) used  $k_{sf}$  in their research. Lee et al. (1996) examined finite element analysis (FEA) results for over 300 hypothetical specimens and concluded that the shear buckling coefficient is a function of the flange-to-web thickness ratio ( $t_f/t_w$ ), and is between  $k_{ss}$  and  $k_{sf}$ . They proposed the following shear buckling coefficient equations for rectangular panels of I-shaped beams:

$$k_v = k_{ss} + 0.8(k_{sf} - k_{ss}) \left[ 1 - \frac{2}{3} \left( 2 - \frac{t_f}{t_w} \right) \right] \text{ for } 0.5 < \frac{t_f}{t_w} < 2 \quad (1-11)$$

$$k_v = k_{ss} + 0.8(k_{sf} - k_{ss}) \text{ for } \frac{t_f}{t_w} > 2 \quad (1-12)$$

Dr. S.C. Lee and Dr. C.H. Yoo published a series of papers (Lee and Yoo (1998), Lee and Yoo (1999), Yoo and Lee (2006)) in which they explain an alternative theory for post-buckling strength of stiffened rectangular plate girders. (Because the current study is concerned with unstiffened panels, some of their results are not directly applicable. However, some of their results are applicable, and some serve as the foundation of Lee et al. (2008) which is directly applicable.) In Lee et al. (2008), they performed geometric and material nonlinear FEA on hypothetical plate girders to quantify buckling, post-buckling, and overall strength. From those synthesized specimens, the researchers observed that the post-buckling strength is approximately 40% of the difference between the elastic shear buckling strength and the plastic shear strength. They proposed the following equations, with slight nomenclature changes to be more consistent with AISC variable names, which predict strengths that almost exactly match the FEA predictions.

$$V_n = V_{cr} + V_{PB} = V_{cr} + 0.4(V_p - V_{cr}) = 0.6V_{cr} + 0.4V_p \quad (1-13)$$

The plastic shear strength,  $V_p = 0.58F_y t_w h$ , is almost identical to the AISC *Specification* shear yield strength. The 0.58 factor is the theoretical value per the von Mises yield criterion, and the calculations are done in terms of the web depth,  $h$ . However the difference between  $V_p$  and the AISC *Specification* yield strength is quite small.

Introducing the variable  $C_v$ , as in the AISC *Specification*, the proposed nominal strength is  $V_n = V_p(0.6C_v + 0.4)$ .  $C_v$  is a three-part function almost identical (slight round-off differences) to the one given in the AISC *Specification* (2010).

$$C_v = 1 \quad h/t_w \leq 1.12 \sqrt{k_v E / F_y} \quad (1-14)$$

$$C_v = \frac{1.10 \sqrt{k_v E / F_y}}{(h/t_w)} \quad 1.12 \sqrt{k_v E / F_y} < h/t_w \leq 1.4 \sqrt{k_v E / F_y} \quad (1-15)$$

$$C_v = \frac{(1.57 k_v E)}{(h/t_w)^2 F_y} \quad h/t_w > 1.4 \sqrt{k_v E / F_y} \quad (1-16)$$

Lee et al. (2008) provided several important findings. First, because the equations shown above produced shear buckling and ultimate strengths that nearly exactly matched the FEA results, the shear buckling coefficients proposed in Lee et al. (1996) are shown to be accurate.

During a series of analyses intended to assess the influence of flange stiffness on post-buckling strength, Lee et al. (1998) made the very interesting discovery that web panels with no flange possess nearly the same post-buckling strength as panels with very



heavy flanges. This led them to put forth a profound new theory to explain the post-buckling strength of stiffened panels.

Lee and Yoo (1999) reported experimental findings that were generated to verify the equations and theories proposed in Lee et al. (1998). During the experimental program, they tested ten plate girders to failure ( $a/h$  ranging from 1.0 to 3.0, so these were stiffened panels), with eight of them failing in shear.

One objective was to investigate the restraint at the web-to-flange connection and verify the shear buckling coefficient proposed in Lee et al. (1996). Because of large initial imperfections, obvious bifurcation buckling was not observed, so it was not possible to identify the elastic shear buckling strength and thus not possible to infer the boundary conditions from the buckling load. However, the researchers inspected the final buckled shape for two specimens, finding that they resembled the buckling mode shape of a fixed-fixed column, thus implying that “the boundary condition at the flange-web juncture is very close to the fixity (*sic*).”

Lee and Yoo (1999) also showed that the shear strength equation presented in Lee et al. (1998) was indeed very accurate, with an average measured-to-predicted ultimate shear strength ratio 1.01 (COV=4%) for the specimens that failed by shear buckling.

They also concluded that through-thickness (out-of-plane) bending of the web has a significant effect near failure. Finally, probably the most important result toward the current project’s objectives is the conclusion that “an anchoring system, such as the flanges, is not needed for the development of postbuckling strength.” This conclusion sheds light on the source of postbuckling strength for unstiffened panels.

Yoo and Lee (2006) studied and explained the source of postbuckling strength for stiffened panels. They stated that the fundamental assumption in the classical failure theories is that the “compressive stresses that develop in the direction perpendicular to the tension diagonal do not increase any further once elastic buckling has taken place.”

Lee and Yoo (2006) did not state the following, but this fundamental theory runs completely contrary to what is common knowledge among those familiar with plate buckling: upon buckling, the portions of the plate far from supports become more flexible so do not accept further load, but the portions of the plate near the support continue to accept additional stress. This is the basis for the effective width concepts used to develop the effective widths used in the AISC *Specification* Section E7 and explained in Salmon, Johnson, and Malhas (2008).

Lee and Yoo (2006) performed material and geometric nonlinear FEA of hypothetical specimens and investigated changes in the tension and compression stress fields. They discovered that the compression stress field does, in fact, increase near the supports, which for their stiffened panels, are the flanges and stiffeners.

Lee et al. (2008) extended their previous work to long web panels such as those of interest for the current study in their paper “Ultimate Shear Strength of Long Web Panels.” They performed nonlinear FEA on hypothetical plate girders with  $a/h$  ratios ranging from three to six. It can be concluded from their Table 2 that the shear buckling strength equation (using the shear buckling coefficient from Lee et al. (1996)) accurately and slightly conservatively predicted the shear buckling prediction from the FEA.

The researchers also compared predictions from the ultimate shear strength equations from Lee and Yoo (1998) to the FEA predictions, indicating that the equations

are accurate for low  $h/t_w$  ratios, but are unconservative by 12-40% for  $h/t_w$  ratios between 210 and 300 for  $a/h = 6$ . Their FEA results indicated that significant postbuckling strength existed in the hypothetical specimens, although the researchers did not explain the source. It seems reasonable to assume that the postbuckling strength is due to a similar compression field stress redistribution as that described in Lee and Yoo (2006), although less efficient as indicated by the fact that the Lee and Yoo (1998) equations slightly over-predict the ultimate strength compared to the strength predicted by FEA.

Because the Lee and Yoo (1998) equation over-predicted the ultimate strength for long panels, Lee et al. (2008) developed an adjustment factor,  $\lambda$ , to bring the equations into agreement with the FEA. When the equations from Lee and Yoo (1998) are multiplied by  $\lambda$ , the equations provide slightly conservative results compared to the FEA predictions, with the ratio of FEA-to-equation result ranging from 1.00 to 1.04 for  $a/h = 6$ . They also observed that real plate girders have larger initial imperfections ( $h/120$ ) than those used in the models, so they re-analyzed the hypothetical specimens with larger initial imperfections, indicating that a further adjustment factor is necessary. They were able to locate one directly applicable experimental test specimen, and their equation almost exactly predicted the failure load, giving an indication of its accuracy.

The following is their strength prediction equation, which account for realistic initial imperfections.

$$V_n = R\lambda V_p(0.6C_v + 0.4) \quad (1-17)$$

The high slenderness factor,  $\lambda$  is given by the following:

$$\lambda = 1.0 \quad C_v \geq 0.3 \quad (1-18)$$

$$\lambda = 1.35C_v + 0.6 \qquad 0.1 < C_v < 0.3 \qquad (1-19)$$

$$\lambda = 5.62C_v + 0.145 \qquad C_v = 0.1 \qquad (1-20)$$

The geometric imperfection factor,  $R$  is given by the following:

$$R = 1.0 - 0.2 \frac{h/t_w \sqrt{F_y/k_v E}}{1.10} \qquad h/t_w < 1.10 \sqrt{\frac{Ek_v}{F_y}} \qquad (1-21)$$

$$R = 0.8 + 0.2 \frac{h/t_w \sqrt{F_y/k_v E} - 1.10}{1.10} \qquad 1.10 \sqrt{\frac{Ek_v}{F_y}} \leq h/t_w \leq 2.20 \sqrt{\frac{Ek_v}{F_y}} \qquad (1-22)$$

$$R = 1.0 \qquad h/t_w > 2.20 \sqrt{\frac{Ek_v}{F_y}} \qquad (1-23)$$

## Chapter 2 Experimental Program

### 2.1 Test Setup

Using the modified shear approach, the required web shear is a function of the shear and bending moment. Therefore, it was important for the test setup to result in shear and bending moment diagrams of the same or similar shape as those in metal building moment frames such as the one shown in Figure 2-1.

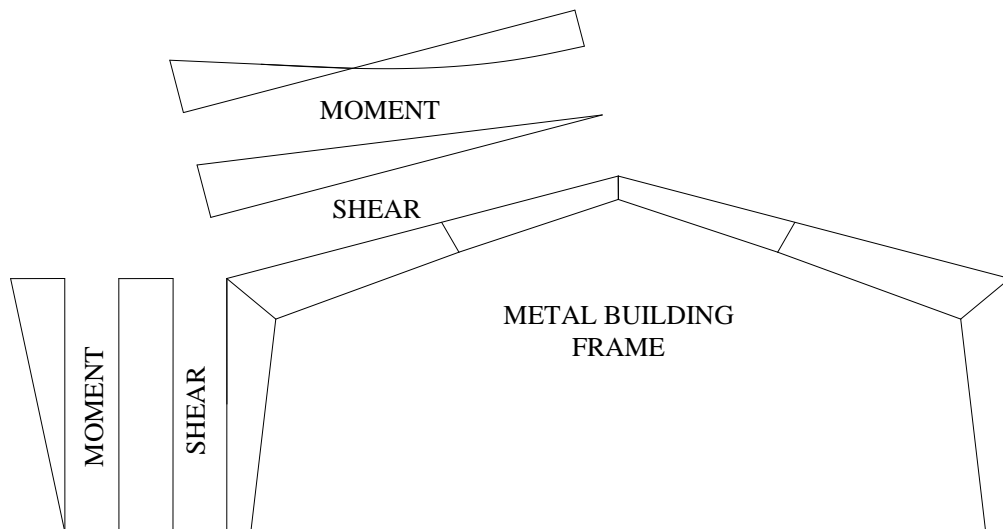


Figure 2-1 Metal Building Moment Frame Shear and Moment Diagrams

A simply supported beam specimen with a midspan point load exactly simulates the shear and moment diagrams of the column shown in Figure 2-1 and approximates the shear and moment diagrams in the portion of the rafter between the knee and the rafter splice. Therefore, the overall configuration shown in

Figure 2-2 was chosen for all specimens. This specimen configuration also excludes complications associated with connection at the knee region. A moment end

plate splice was included at midspan to allow the specimens to be more easily handled and transported into the laboratory, to prevent web local crippling, and to provide a bearing surface for the hydraulic ram. The moment end plate was flush at the bottom, extended at the top, and had two interior rows of bolts at the top to more uniformly distribute flexural stresses into the flange and web.

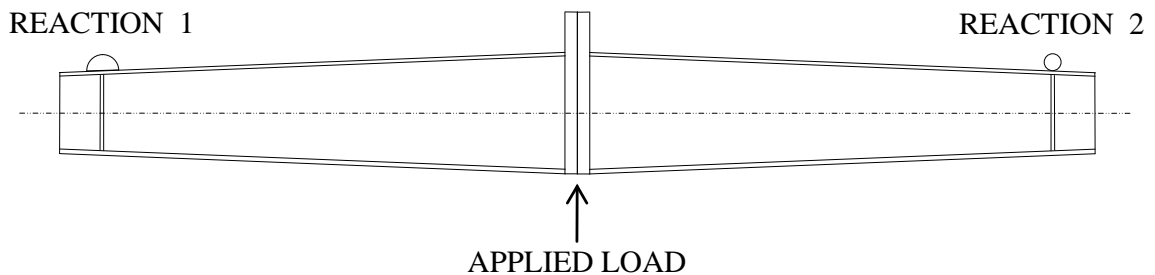


Figure 2-2 Specimen Elevation

## 2.2 Specimens

A summary of specimen dimensions is shown in Table 2-1. Flange and web sizes were similar to those commonly used by MBMA companies. Each web was flexurally slender at midspan and had  $h/t_w$  large enough that elastic shear buckling was the anticipated behavior. Three specimens (“Tapered 4,” “Tapered 5,” and “Tapered 6”) had different flange sizes, two of which had a larger compression flange. Taper angles varied between 5 deg. to 10 deg. which is in the normal range of taper angles used by MBMA companies. Combinations of taper angle, depths, web thickness, and flange sizes were selected to fail in shear without having unrealistically large flanges or  $a/h$  less than three, which is the AISC demarcation between stiffened and unstiffened panels.

Specimen “Tapered 6” was included with a reverse taper angle, meaning that it was shallower at midspan than at the supports, because the modified shear approach

predicts that the transverse component of each flange force actually adds to the web shear for that configuration. Two prismatic specimens were also included to allow investigation of the shear strength without the effect of the transverse component of each flange force.

Each web-to-flange fillet weld was on one side only except for short segments of weld near the ends of the members. Bearing stiffeners were included at the ends of the members to prevent web local yielding and web local crippling. The left half of each specimen had the web thickness listed in Table 2-1; the right half had a web thickness that was a size or two larger to ensure that it did not fail, thus saving fabrication, transportation, and instrumentation expense.

Table 2-1 Specimen Summary

Designation	Length (ft)	$d_{\text{End}}$ (in.)	$d_{\text{Midspan}}$ (in.)	Taper Angle (deg.)	$t_w$ (in.)	Bottom Flange		Top Flange		$h/t_w$		$a/h$
						$b_f$ (in.)	$t_f$ (in.)	$b_f$ (in.)	$t_f$ (in.)	End	Midspan	Average
Prismatic 1	15	20	20	0	0.125	6	0.313	6	0.313	155	155	4.51
Prismatic 2	12	20	20	0	0.125	6	0.625	6	0.625	150	150	3.65
Tapered 1a	15	12	20	5.1	0.125	6	0.313	6	0.313	91	155	5.66
Tapered 1b	15	12	20	5.1	0.125	6	0.313	6	0.313	91	155	5.66
Tapered 1c	15	12	20	5.1	0.125	6	0.313	6	0.313	91	155	5.66
Tapered 2a	15	10	25	9.5	0.156	8	0.500	8	0.500	58	154	5.22
Tapered 2b	15	10	25	9.5	0.156	8	0.500	8	0.500	58	154	5.22
Tapered 2c	15	10	25	9.5	0.156	8	0.500	8	0.500	58	154	5.22
Tapered 3	12	13	20	5.6	0.125	6	0.625	6	0.625	94	150	4.46
Tapered 4	12	12	22	7.9	0.125	8	0.625	8	0.375	88	168	4.29
Tapered 5	13.5	16	23	5	0.156	8	0.500	8	0.75	95	139	4.23
Tapered 6	12	22	14	6.5	0.135	8	0.500	8	0.375	157	98	4.03



### 2.3 Load Frame and Boundary Conditions

The vertical reaction at each end of the specimen was provided by a heavy HSS load frame which was connected to the 24 in. thick reinforced concrete reaction floor using 2 in. high strength all-thread rods as shown at the far end in Figure 2-3. The left and right end, respectively, were pinned and roller supports shown in Figure 2-4. Load was applied to the underside of the moment end plates at midspan using the hydraulic ram shown in Figure 2-5.



Figure 2-3 Overall Setup With Load Shown



Figure 2-4 Pinned and Roller Supports



Figure 2-5 Hydraulic Ram and Load Cell

Flange lateral braces were provided at a 3 ft spacing to prevent lateral-torsional buckling (LTB) and global twist of the specimen. See Figure 2-3 and Figure 2-6. A

system based on “Watt’s linkage” was developed to restrain lateral movement while allowing vertical displacement, longitudinal displacement, and rotation. The braces were connected to vertical HSS6x6 columns which cantilevered from base plates connected to the reaction floor. The system was designed to provide the required stiffness and strength for a beam nodal lateral brace per the AISC *Specification* Appendix 6.

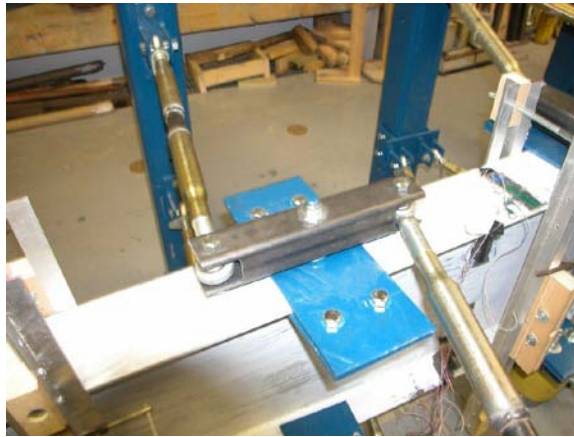


Figure 2-6 Flange Lateral Brace (Watt’s Linkage)

## 2.4 Instrumentation

Several types of sensors were used during the tests to measure the load, displacements, and strains at various locations on the specimens. In general, the measurement stations were placed at the anticipated failure locations. The appendices provide detailed information on the instrumentation locations for each specimen. Measurements were recorded using a Vishay Micro-Measurements System 7000 running “StrainSmart” software.

**Load Cell.** A 200 kip load cell was placed between the hydraulic ram and the moment end plate to measure the load applied to the specimen. See Figure 2-5.

**Cable-Extension Displacement Sensor (CDS).** CDS were used to measure the vertical displacement at each end of the member, and at midspan. The specimen's shear and bending displacement at midspan is the midspan displacement minus the average of the two end displacements. See Figure 2-5 and Figure 2-7 .

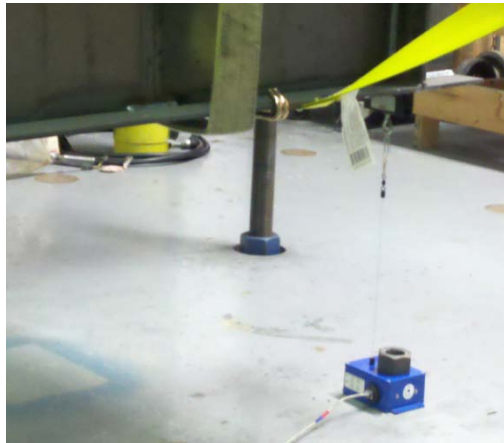


Figure 2-7 Cable-Extension Displacement Sensor

**LVDT.** Three LVDTs were used to measure the web out-of-plane displacement during the tests. These were connected to small aluminum and wood frames attached to the flanges to allow the web displacement relative to the flanges to be measured. See Figure 2-8. The location of the LVDTs for each individual test can be found in the appendices.

**Strain Gages.** Figure 2-9 shows typical strain gage locations at a strain gage station for most MBMA test specimens. Four strain gages were placed on each flange at each station, two on the outside of the flange and two on the inside as shown in the left hand figure. Two strain gage rosettes were placed on each face of the web at each station as shown in the right hand figure. They were aligned vertically at one-third and two-third the web height as shown in the left-hand figure. The mid-thickness strain is

approximated by averaging opposing strain gage readings. Strains  $\epsilon_1$ ,  $\epsilon_2$ , and  $\epsilon_3$  are transformed to  $\epsilon_x$ ,  $\epsilon_y$ , and  $\gamma_{xy}$  using basic mechanics of materials equations.



Figure 2-8 LVDTs for Web Out-of-Plane Measurements

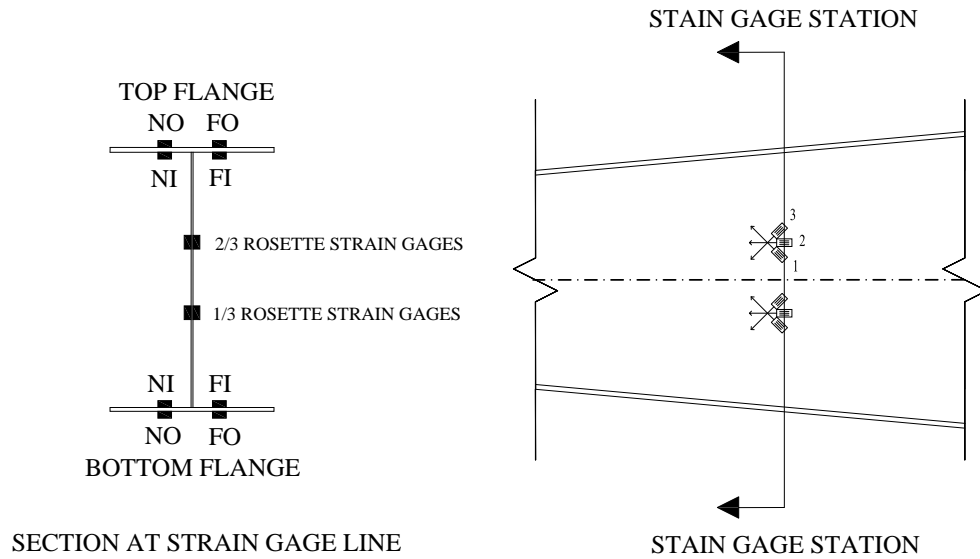


Figure 2-9 Strain Gage Locations at a Measurement Station

where

- N = near side
- F = far side
- O = outside flange face
- I = inside flange face

Another strain gage layout was used for “Tapered 2a, 2b, and 2c.” It was thought to be easier to transform the strains  $\epsilon_1$ ,  $\epsilon_2$ , and  $\epsilon_3$  into  $\epsilon_x$ ,  $\epsilon_y$ , and  $\gamma_{xy}$ , as shown in Figure 2-10. It became apparent after performing the “Tapered 2a, 2b, and 2c” tests, that the original format in Figure 2-9 was a simpler method of aligning the strain gage grid lines at the one-third and two-thirds web heights and this layout was used for the duration of the testing program.

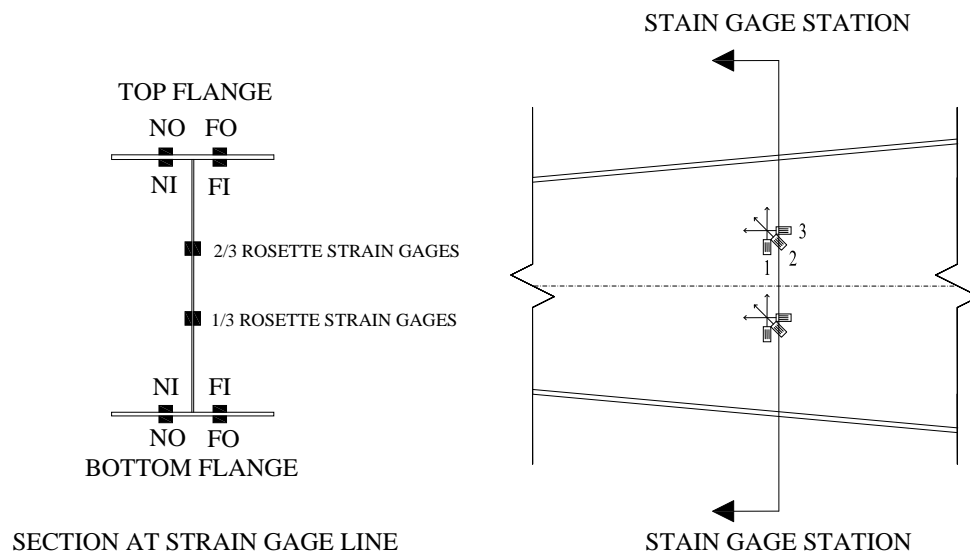


Figure 2-10 “Tapered 2” Strain Gage Locations at a Measurement Station

where

- N = near side
- F = far side
- O = outside flange face
- I = inside flange face

To ensure that flange and web strains were indeed representative of the entire web and flange surfaces, a third formation was used on “Tapered 5.” In this formation, eight uniaxial strain gages were placed on each flange at each station, four on the outside of the flange and four on the inside, as shown in Figure 2-11. Three strain gage rosettes were

placed on each face of the web at a station, as shown in the right hand figure. They were aligned vertically at one-quarter, half, and three-quarter the web height as shown in the left-hand figure.

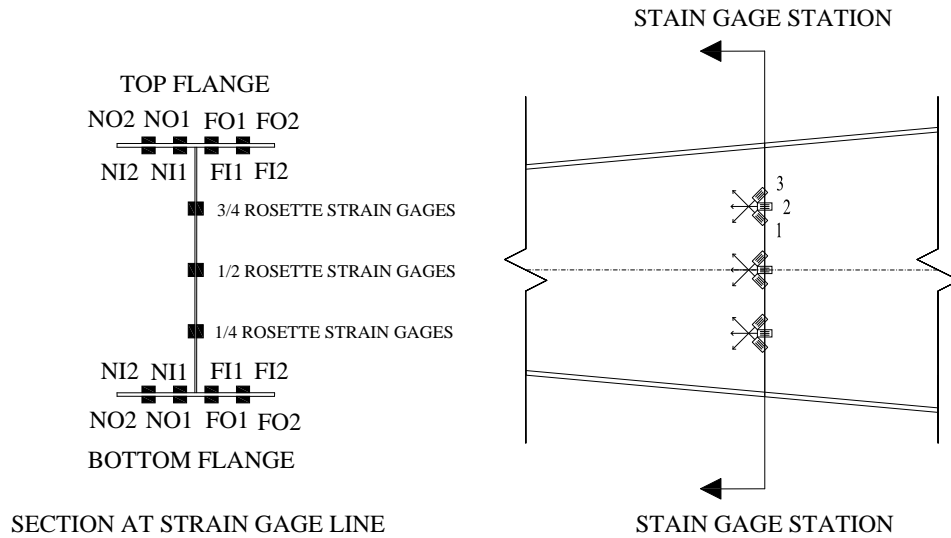


Figure 2-11 “Tapered 5” Strain Gage Locations at a Measurement Station where

- N = near side
- F = far side
- O = outside flange face
- I = inside flange face
- 1 = inner
- 2 = outer

## 2.5 Web Initial Out-of-Plane Measurements

Three out of the twelve specimens had visible initial out-of-plane imperfections in the web. In the interest of quantifying the variations in the initial shape, measurements were made of each specimen prior to testing and compared to tolerance limits established by MBMA. The measurements were made using a displacement transducer (LVDT) mounted to a carriage as shown in Figure 2-12. It was assumed that the flanges and the

bottom portion of the carriage, which slid along the flanges, were perpendicular to each other. The accuracy of the LVDT used was  $\pm 0.0001$  in.



Figure 2-12 Carriage

Each specimen was marked with gridlines on a coordinate system with the origin located at the intersection of the stiffener centerline and the geometric centerline of the specimen – the positive  $x$  axis and the positive  $y$  axis were oriented towards the moment plate and the top flange respectively. Positive  $z$  values were oriented away from the specimen because the “Strain Smart” software recorded positive displacements as the plunger of the LVDT retracted. The gridlines were tapered according to the geometry of a particular test specimen as shown in Figure 2-13. This grid layout was representative for all specimens; the only difference among specimens was the interval used for the  $x$  coordinate. The points can be categorized into two groups: boundary points and quarter points.



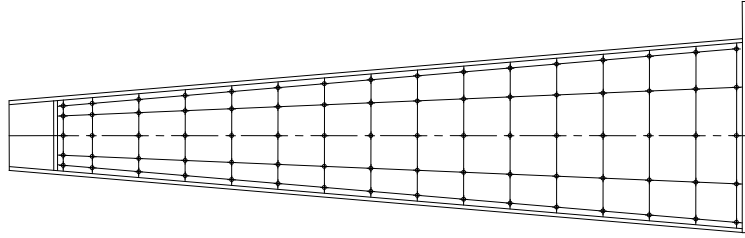


Figure 2-13 Initial Out-Of-Plane Grid Spacing

1. **Boundary Points:** Points taken three quarters of an inch off the outside face of a boundary condition (top flange, bottom flange, moment end plate, and stiffener) at  $x$  coordinate intervals.
2. **Quarter Points:** Points taken at quarter points of the web depth at  $x$  coordinate intervals.

The Metal Building Manufacturers Association gives two tolerance limits for deviation from a plane allowed in the webs of built up plate girders (MBMA 2006). One limit refers to deviations from a plane on a transverse cross-section and the associated variables are shown in Figure 2-14. In this research study, the plane of a transverse cross section was defined as the slope of the line formed from the two boundary points;  $C$  was therefore the deviation from this plane at the quarter points.

The second limit refers to the deviation in the web along a longitudinal cross-section which is shown in Figure 2-15. In this case, similar to the plane of a transverse section, the plane of a longitudinal cross section was defined as the slope of the line formed from the two boundary points;  $f$  was therefore the deviation from this plane at each  $x$  interval for the quarter points.

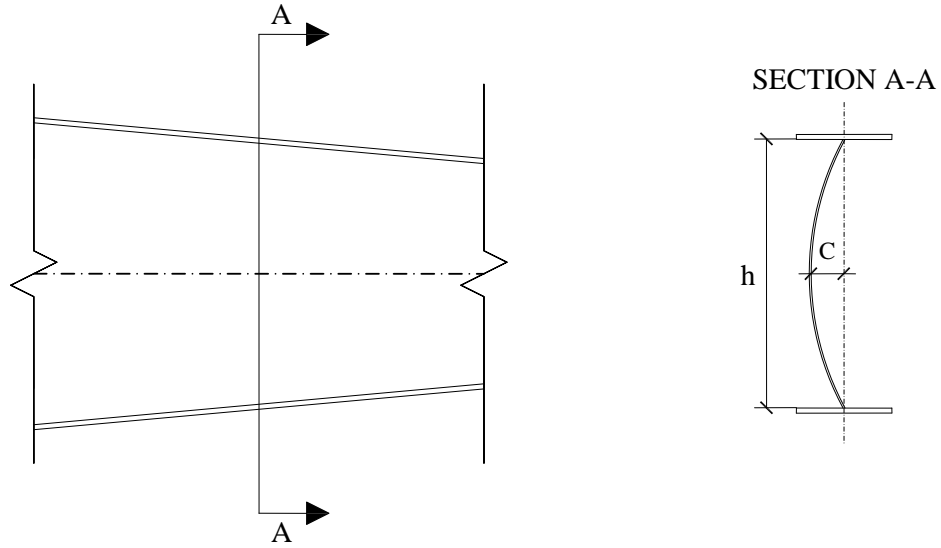


Figure 2-14 Transverse Out of Plane Tolerance

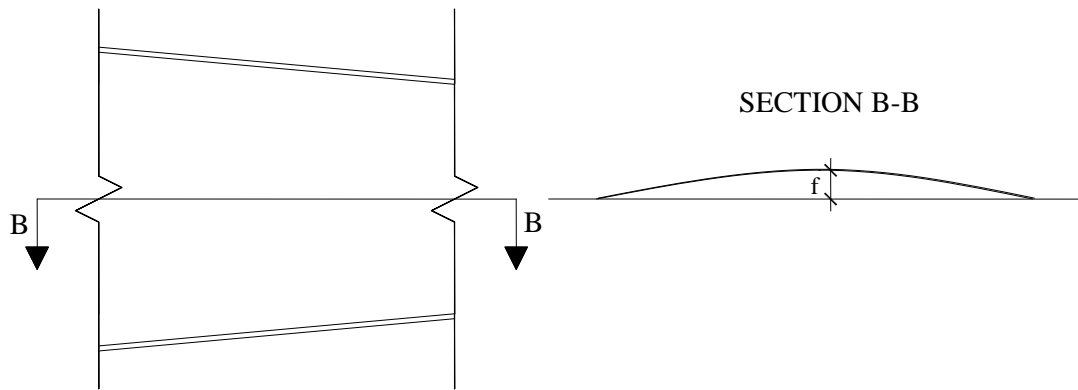


Figure 2-15 Longitudinal Out of Plane Tolerance

The tolerance allowed for both of these cases according to MBMA is  $h/72$ , where  $h$  is the web height as shown in Figure 2-14 –  $h$  was assumed to be the average web height of the specimen in the longitudinal tolerance case. Due to the limiting nature of the carriage, points could not be taken across the full depth of the member. Instead, the distance between the boundary points was used to define  $h$ . Table 2-2 lists a general summary of each specimen based on whether it passed the MBMA tolerance

specifications and Table 2-3 shows the values of the initial imperfections for those failed specimens.

Table 2-2 Web Initial Out-of-Plane MBMA Tolerance Check

Designation	Pass / Fail	Location of failure (x , y) (in.)	Ratio of <i>C</i> or <i>f</i> to <i>h</i> /72	
Prismatic 1	Pass	NA	NA	
Prismatic 2	Pass	NA	NA	
Tapered 1a	Fail	(18.25, -3.39)	c	1.024
		(18.25, -3.39)	f	1.090
Tapered 1b	Pass	NA	NA	
Tapered 1c	Pass	NA	NA	
Tapered 2a	Pass	NA	NA	
Tapered 2b	Pass	NA	NA	
Tapered 2c	Pass	NA	NA	
Tapered 3	Fail	(21.25, -3.80)	f	1.143
		(27.25, -3.95)	f	1.035
Tapered 4	Fail	(21.25, -3.82)	f	1.168
		(21.25, 0)	f	1.132
		(27.25, -4.03)	f	1.217
		(27.25, 0)	f	1.103
		(33.25, -4.24)	f	1.171
		(39.25, -4.46)	f	1.084
Tapered 5	Pass	NA	NA	
Tapered 6	Pass	NA	NA	

NA = Not Applicable

Table 2-3 Web Initial Out-of-Plane Measurements for Failed Specimens

Designation	<i>C</i>	<i>f</i>
Tapered 1a	<i>h</i> /70	<i>h</i> /66
Tapered 3	NA	<i>h</i> /63
	NA	<i>h</i> /70
Tapered 4	NA	<i>h</i> /62
	NA	<i>h</i> /64
	NA	<i>h</i> /59
	NA	<i>h</i> /65
	NA	<i>h</i> /61
	NA	<i>h</i> /66

NA = Not Applicable

## 2.6 Testing Procedure

Before testing, each test specimen's web was checked for initial out of plane measurements according to the Metal Buildings System Manual (MBMA 2006) tolerance specifications, the full details of which are described in the Web Initial Out-of-Plane Measurements section. Uniaxial strain gages and rosette strain gages were installed prior to placing the test specimen into the loading frame.

Once in the load frame, the moment end plates were bolted together and snug-tightened with pipe wrenches. The test specimen was then adjusted to make sure it was plumb within the reaction frame and subsequently engaged at the reactions points with the overhead crane. At this point, the lateral bracing system was installed. After the CDS sensors and the LVDTs were in place, the lead wires were unraveled from the gages and attached to the Micro Measurements System 7000 Data Acquisition System. To zero out the specimen, the procedure was as follows:

1. Calculate weight of test specimen
2. Zero out Micro Measurements System 7000 Data Acquisition System
3. Engage 200 kip load cell with test specimen using the Enerpac RC-1006 Cylinder
4. Load until double the specimen weight is reached (specimen is now engaged within reaction frame).
5. Release the straps from the overhead crane (straps are carrying zero load at this point)
6. Re-zero Micro Measurements System 7000 Data Acquisition System

The application of loading from underneath the specimen required the weight to be doubled to account for the initial weight of the specimen. Specimens were initially loaded to 25% of the predicted failure load according to AISC *Specification G2* and the load-displacement plot was graphed to check whether the measured and predicted stiffness correlated.

Once confirmed, the load was returned to zero to start the official test. Loading proceeded in intervals, different for each test specimen, and stiffness was checked at each interval manually in Microsoft Excel - data was continuously obtained between load intervals by the data acquisition system software. When the load reached the AISC *Specification G2* failure load without modified shear, smaller intervals were used to capture the deviation of the experimental stiffness plot from the theoretical. Upon significant loss of stiffness, displacement control was initiated until ultimate failure, which was defined as the test specimen being unable to withstand further load. Additional displacement was applied to accentuate the buckled shape after failure.

## **2.7 Material Properties**

Rectangular steel pieces were torched from the existing specimens at low stress areas and were milled into coupons according to ASTM E8/E8M-09. The coupons were tested with a 300 kip Satec Universal Testing Machine. The results of the coupon test are shown below in Table 2-2.

Table 2-4 Coupon Results

Designation	Plate	Yield Load (kip)	Yield Stress (ksi)	Ultimate Load (kip)	Ultimate Stress (ksi)
Tapered 1a	Top Flange	27.1	58.9	35.4	76.8
	Bottom Flange	27.6	60.1	35.5	77.2
	Web	12.8	67.5	14.3	75.9
Tapered 1b	Top Flange	27.6	59.5	35.8	77.1
	Bottom Flange	27.8	60.2	36.1	78.0
	Web	13.3	70.6	14.4	76.2
Tapered 1c	Top Flange	28.2	59.4	36.3	76.5
	Bottom Flange	27.3	58.4	35.9	76.9
	Web	12.8	67.0	14.5	75.8
Tapered 2a	Top Flange	43.3	60.8	60.6	79.6
	Bottom Flange	45.4	59.9	60.8	80.1
	Web	13.8	60.0	15.9	69.3
Tapered 2b	Top Flange	47.0	62.0	60.8	80.0
	Bottom Flange	46.6	61.1	61.3	80.4
	Web	14.2	61.2	16.4	70.8
Tapered 2c	Top Flange	45.9	60.3	61.5	80.7
	Bottom Flange	47.5	62.6	61.1	80.4
	Web	14.3	62.7	16.1	70.6
Tapered 3	Top Flange	51.3	55.5	69.3	74.9
	Bottom Flange	51.1	55.0	68.8	74.2
	Web	11.5	62.1	14.5	78.1
Tapered 4	Top Flange	33.1	58.1	45.6	74.7
	Bottom Flange	53.1	55.2	72.2	75.1
	Web	11.2	56.9	14.0	70.7
Tapered 5	Top Flange	67.4	59.4	85.2	75.1
	Bottom Flange	45.8	71.4	56.5	88.2
	Web	13.8	58.6	18.1	77.2
Tapered 6	Top Flange	33.5	57.9	42.1	72.7
	Bottom Flange	46.2	61.1	55.4	73.4
	Web	13.4	63.7	15.2	72.6
Prismatic 1	Top Flange	27.0	56.8	35.9	75.6
	Bottom Flange	26.8	57.5	35.7	76.6
	Web	13.0	66.2	14.4	73.1
Prismatic 2	Top Flange	49.5	52.6	69.3	73.7
	Bottom Flange	52.1	55.9	68.8	73.9
	Web	11.6	61.3	14.6	77.1

## 2.8 Right vs. Normal Cross Sectional Properties

All geometric calculations are based on right cross sectional properties as opposed to properties along the section cut. Figure 2-16 shows a close up of the bottom flange at a measurement station section cut where  $t$  is the thickness of the bottom flange normal to the face of the flange (right cross sectional property) and  $e$  is the thickness along the section cut (normal cross sectional property). To simplify calculations,  $t$  was used to calculate specimen geometric properties such as elastic section modulus, plastic section modulus, etc...

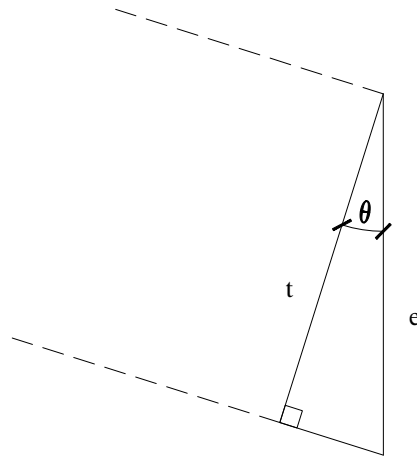


Figure 2-16 Specimen Cross Sectional Properties

Table 3-1 shows the elastic and plastic section modulus of “Tapered 2” (largest tested taper angle, 10 deg.) at several different locations from the stiffener centerline and it is reasonable to conclude that simplifying equations based on specimen geometry does not affect measurement precision. “Tapered 2” was selected because its tapered angle was the largest and would have the most profound effect on geometric properties.

Table 2-5 “Tapered 2” Specimen Geometric Property Comparisons

$x$ (ft)	$S_x^*$ (in. <sup>3</sup> )	$S_x^{**}$ (in. <sup>3</sup> )	% Difference	$Z_x^*$ (in. <sup>3</sup> )	$Z_x^{**}$ (in. <sup>3</sup> )	% Difference
0	38.1	38.0	0.289	41.3	41.2	0.337
1.5	51.7	51.6	0.291	55.8	55.6	0.323
3	65.8	65.6	0.291	70.0	70.8	0.313
4.5	80.3	80.1	0.289	86.9	86.6	0.303
6	95.3	95.0	0.288	103.5	103.2	0.295
7.5	110.7	110.4	0.285	120.8	120.5	0.288

\* Right Cross Sectional Properties

\*\* Normal Sectional Properties

## 2.9 Measured Web and Flange Forces

The first objective of this research study, as stated in Section 1.1, is to investigate the internal force distribution in tapered members to determine whether the web resists the portion of the shear predicted using the modified shear approach. Toward satisfying this objective, the internal force distribution depicted in Figure 2-17 was determined at each strain gage station. Making use of elastic material properties and specimen geometry, internal forces were calculated.

It is rational from an engineering mechanics standpoint to reason that the forces parallel with the tension and compression flange, at mid-thickness flange height, are composed of vertical and horizontal components. The vertical (transverse) components were of interest and are labeled  $P_{f,t}$  and  $P_{cf,t}$ .



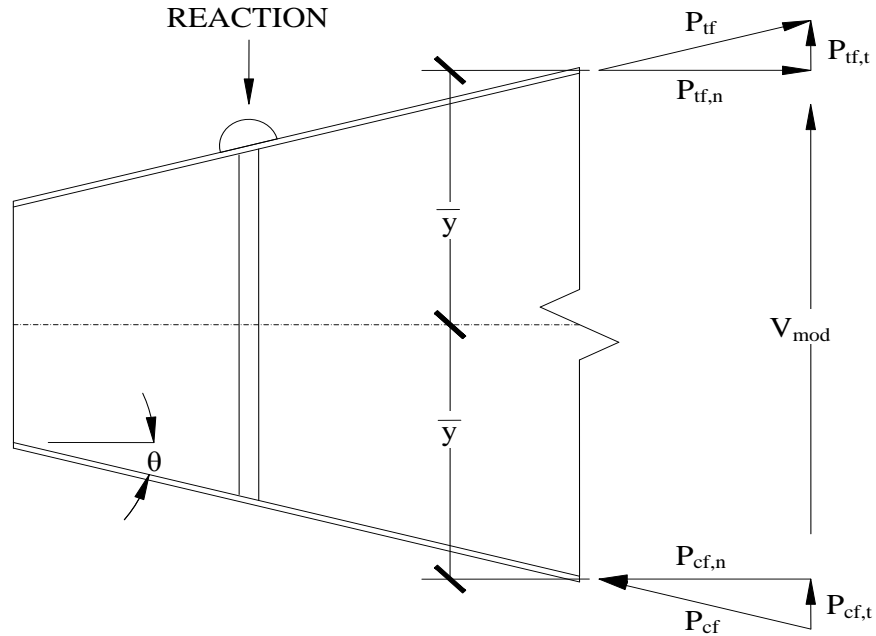


Figure 2-17 Measured Modified Shear Diagram

The web shear force at the station, labeled  $V_{Web}$ , was then calculated by subtracting the flange force transverse components from the applied shear force, which was half the load cell reading. The vertical components were computed as follows. Readings from the four uniaxial strain gages at a station (see Figure 2-9 for locations) were averaged to obtain the average mid-thickness strain. Hooke's Law, Equation (2-1), was then used to convert flange strain (not exceeding the yield strain) to stress (Beer et al. 2006).

$$\sigma = E\varepsilon \quad (2-1)$$

where  $\sigma$  = stress;  $\varepsilon$  = micro strain;  $E$  = modulus of elasticity.

$P_{cf}$  and  $P_{tf}$  were calculated by multiply the cross-sectional area of the flanges by the flange stress. The transverse component of these forces are  $P_{cf,t}$  and  $P_{tf,t}$  and are found by taking  $P_{cf,t} = P_{cf} \sin\theta$  and  $P_{tf,t} = P_{tf} \sin\theta$ .

Web shear forces were also calculated using readings from the rosette strain gages,  $V_{Web*}$ , which were placed on the web. In an effort to remove bending stresses associated with out of plane web displacements, strain gage readings were averaged across the thickness of the web. To calculate the shear at a strain gage station  $\varepsilon_1$ ,  $\varepsilon_2$ , and  $\varepsilon_3$  were transformed to  $\varepsilon_x$ ,  $\varepsilon_y$ , and  $\gamma_{xy}$  by Equation (2-2) (Beer et al. 2006). Refer to Figure 2-9 for the location and orientation of the rosette strain gages on the web.

$$\begin{Bmatrix} \varepsilon_x \\ \varepsilon_y \\ \gamma_{xy} \end{Bmatrix} = \begin{pmatrix} \cos^2 \alpha_1 & \sin^2 \alpha_1 & \sin \alpha_1 \cos \alpha_1 \\ \cos^2 \alpha_2 & \sin^2 \alpha_2 & \sin \alpha_2 \cos \alpha_2 \\ \cos^2 \alpha_3 & \sin^2 \alpha_3 & \sin \alpha_3 \cos \alpha_3 \end{pmatrix} \begin{Bmatrix} \varepsilon_1 \\ \varepsilon_2 \\ \varepsilon_3 \end{Bmatrix} \quad (2-2)$$

where

- $\varepsilon_x$  = normal strain in  $x$  direction
- $\varepsilon_y$  = normal strain in  $y$  direction
- $\gamma_{xy}$  = shear strain
- $\varepsilon_1$  = normal strain at  $\alpha_1 = -45^\circ$
- $\varepsilon_2$  = normal strain at  $\alpha_2 = 0^\circ$
- $\varepsilon_3$  = normal strain at  $\alpha_3 = 45^\circ$

“Tapered 5” follows the same transformation matrix as Equation (2-2) and the location and orientation of the strain gages is shown in Figure 2-11. For “Tapered 2,” Equation (2-2) simplified to Equation (2-3) which was used to transform  $\varepsilon_1$ ,  $\varepsilon_2$ , and  $\varepsilon_3$  into  $\varepsilon_x$ ,  $\varepsilon_y$ , and  $\gamma_{xy}$  (Beer et al. 2006). Refer to Figure 2-10 for the location and orientation of the rosette strain gages for “Tapered 2.”

$$\gamma_{xy} = \varepsilon_1 - 2\varepsilon_2 + \varepsilon_3 \quad (2-3)$$

where

- $\gamma_{xy}$  = shear strain
- $\varepsilon_1$  = normal strain at  $\alpha_1 = -90^\circ$
- $\varepsilon_2$  = normal strain at  $\alpha_2 = -45^\circ$
- $\varepsilon_3$  = normal strain at  $\alpha_3 = 0^\circ$

Hooke's Law for shearing stress and strain below the proportional limit, Equation (2-4), was used to determine the shear stress at a particular rosette strain gage (Beer et al. 2006).

$$\tau_{xy} = G\gamma_{xy} \quad (2-4)$$

where  $\tau_{xy}$  = shear stress;  $\gamma_{xy}$  = shear strain;  $G$  = modulus of rigidity.

The shear force at a particular rosette strain gage was computed using Equation (2-5) (Beer et al. 2006).

$$V_{Web*} = \frac{\tau_{xy}It}{Q} \quad (2-5)$$

where

- $V_{Web*}$  = shear force
- $\tau_{xy}$  = shear stress
- $I$  = moment of inertia
- $Q$  = first moment of area

The shear force at a strain gage station was taken to be the average of the shear force determined at the one-third and two-third rosette strain gages.

## Chapter 3 Analytical Predictions

### 3.1 Predicted Web and Flange Forces

The web shear,  $V_{mod} = V_{Web}$ , and transverse component of flange forces,  $P_{tf,t}$  and  $P_{tf,c}$ , as shown in Figure 2-18, were computed using basic mechanics of materials equations as described in the following.

The flange mid-thickness normal stress horizontal component on a cross section is calculated using Equation 3-1.

$$\sigma = \frac{M\bar{y}}{I} \quad (3-1)$$

where

$M$  = moment

$\bar{y}$  = distance from the neutral axis to flange mid-thickness

$I$  = moment of inertia

The normal flexural stress was converted into a normal force by multiplying stress by the flange cross sectional area. This force was represented by  $P_{tf,n}$  and  $P_{cf,n}$  in Figure 2-17.

The transverse force components,  $P_{cf,t}$  and  $P_{tf,t}$ , are  $P_{cf,t} = P_{cf,n}\tan\theta$  and  $P_{tf,t} = P_{tf,n}\tan\theta$ .

The modified shear concept is that these two transverse components will act at a strain gage station and thus are subtracted from the applied shear force as shown in Equation (3-2). (Note that the transverse force components are additive with the applied shear if the situation is as shown in Figure 1-3, but this is uncommon.)

$$V_{mod} = V_{Web} = V - P_{cf,t} - P_{tf,t} \quad (3-2)$$

where

- $V$  = applied shear force
- $V_{Web}$  = shear force in the web
- $V_{mod.}$  = modified shear force
- $P_{tf,t}$  = transverse component tension flange
- $P_{cf,t}$  = transverse component compression flange

In the case of a singly symmetric specimen with one flange thicker than the other, the flange force transverse components are unequal, with the larger flange force being the larger of the two.

### 3.2 Ultimate Shear Strength

The ultimate shear strength was predicted using the methods described in this section. Because there are two web shear strength prediction methods (*AISC Specification / MBMA/AISC Design Guide 25* and Lee et al. (2008)) and three options for defining the applied shear (web resists entire shear, modified shear per Williams and Harris (1957), and modified shear per Blodgett (1966)), there are actually six candidate methods:

- *AISC Specification* web shear strength; web resists entire shear.
- *AISC Specification* web shear strength; Williams and Harris modified shear.
- *AISC Specification* web shear strength; Blodgett modified shear.
- Lee et al. web shear strength; web resists entire shear.
- Lee et al. web shear strength; Williams and Harris modified shear.
- Lee et al. web shear strength; Blodgett modified shear.

Twelve equally spaced stations were analyzed along each specimen between points that were a member depth from the bearing stiffeners or moment end plate.

### 3.2.1 AISC Specification / MBMA/AISC Design Guide 25 Web Shear Strength

#### Prediction Method

The MBMA/AISC *Design Guide 25, Frame Design Using Web-Tapered Members* (Kaehler et al. 2011) recommends computing the web shear strength using the AISC *Specification* provisions for prismatic members (AISC 2010). The authors recommend that the shear strength be calculated on a cross-section by cross-section basis, with the plate buckling coefficient taken as 5.0 for unstiffened webs such as those of interest in the current study. The web slenderness,  $h/t_w$ , is defined by the geometry at the section being checked.

The AISC *Specification* shear provisions for the nominal shear strength of unstiffened prismatic members are:

$$V_n = 0.6F_y A_w C_v \quad (3-3)$$

$$h/t_w \leq 1.10 \sqrt{k_v E / F_y} \quad C_v = 0.1 \quad (3-4)$$

$$1.10 \sqrt{k_v E / F_y} < h/t_w \leq 1.37 \sqrt{k_v E / F_y} \quad C_v = \frac{1.10 \sqrt{\frac{k_v E}{F_y}}}{\left(\frac{h}{t_w}\right)} \quad (3-5)$$

$$h/t_w > 1.37 \sqrt{k_v E / F_y} \quad C_v = \frac{1.51 k_v E}{\left(\frac{h}{t_w}\right)^2 F_y} \quad (3-6)$$

$$k_v = 5 \quad (3-7)$$

where

- $k_v$  = plate buckling coefficient
- $C_v$  = web shear coefficient
- $E$  = Young's modulus, 200 GPa (29,000 ksi)

- $F_y$  = nominal yield stress
- $h$  = web height at cross section of interest
- $t_w$  = web thickness
- $A_w$  = shear area of web ( $d t_w$ )

The formulation of the preceding equations is described in Section 1.2.2.

### 3.2.2 Lee et al. (2008) Method

As mentioned earlier in Section 1.2.2, a new strength prediction method by Lee et al. (2008) incorporates recently discovered web behavior reported in several Lee and Yoo published journal articles. These key discoveries included a more representative buckling coefficient between  $k_{ss}$  and  $k_{sf}$ , accounting for through thickness bending of the web after initial buckling, and post buckling action without the presence of an anchor system. The Lee et al. (2008) equation revisits the early equation of Lee and Yoo (1998) but is redefined for web panels with high aspect ratios and realistic initial web out-of-planeness. The new equation is as follows:

$$V_n = R\lambda V_p(0.6C_v + 0.4) \quad (3-8)$$

where:

- $R$  = strength reduction caused by large initial imperfections
- $\lambda$  = strength reduction factor due to high slenderness
- $C_v$  = ratio of the shear buckling strength  $V_{cr}$  to shear yielding  $V_p$

The nominal shear strength using Equation (3-8) was checked at critical cross sections as suggested by MBMA/AISC *Design Guide 25, Frame Design Using Web-Tapered Members* (Kaehler et al. 2011).

## Chapter 4 Comparisons of Measurements and Predictions

Measured and predicted flange and web shears were compared toward satisfying the first objective indicated in Section 1.1, which is to investigate the internal force distribution to determine if the web resists the portion of the shear predicted using a modified shear approach. These comparisons were calculated 500 lbs. after initial loading until a significant deviation was noticed between the experimental and theoretical stiffness on the linear-elastic load-displacement plot. For each specimen shown below, there are two plots. The first plot shows the measured and predicted percent of shear force resisted by the web and flange primarily to give the reader a sense of the reduction in web force provided by a modified shear approach, and secondarily to show the accuracy of the predictions. The second plot shows the ratio of measured-to-predicted shear for the web and flanges to indicate the accuracy of the predictions.

There are two measured web shears shown on each plot:  $V_{Web}$  and  $V_{Web^*}$ . The former was computed using the primary method of subtracting the flange transverse components,  $V_{Top\ Flg}$  and  $V_{Bot. Flg}$ , from half the load cell reading as described in Section 2.8. The latter, provided as a verification of the former, uses the strain gage rosettes as described in Section 2.8.

The midspan load vs vertical midspan displacement plot is also shown for each specimen. The plot includes a linearly-elastic predicted load-displacement plot for comparison with the specimen stiffness in the linear range. Also included are horizontal lines indicating the failure loads predicted using the methods listed in Section 3.2. The flexural failure load is also listed for reference.



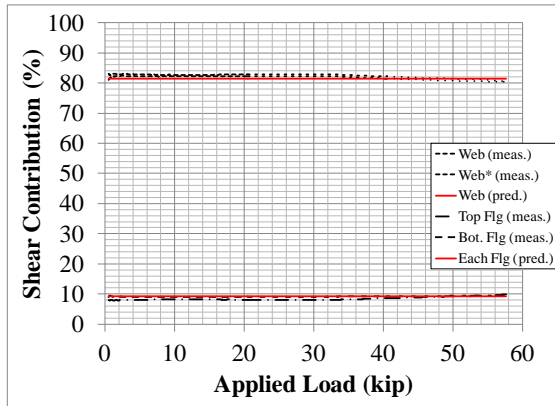
## 4.1 Tapered 1a

A complete list of graphs for test “Tapered 1a” can be found in Appendix A.

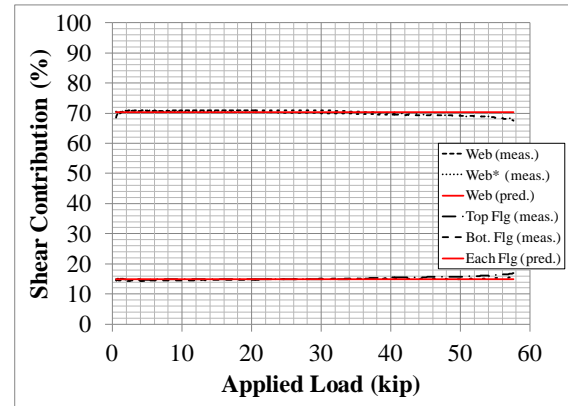
### 4.1.1 Web and Flange Shear Contributions

**Station 1.** Figure 4-1 indicates that the measured and predicted web shear force contributions are 82.2% and 81.4% respectively, for a measured-to-predicted ratio of 1.01 for  $V_{Web}$ . For  $V_{Web^*}$  the measured and predicted web shear contributions are 82.8% and 81.4% respectively, for a measured-to-predicted ratio of 1.02 for  $V_{Web^*}$ . Figure 4-1 also indicates that the measured-to-predicted  $V_{Top\ Flg}$  contributions are 8.1% and 9.3%, respectively, for a measured-to-predicted ratio of 0.874. Finally, it indicates that the measured and predicted  $V_{Bot.\ Flg}$  shear contributions are 9.1% and 9.3%, respectively, for a measured-to-predicted ratio of 0.978.

**Station 2.** Figure 4-1 indicates that the measured and predicted web shear contributions are 70.8% and 70.3% respectively, for a measured-to-predicted ratio of 1.01 for  $V_{Web}$ . For  $V_{Web^*}$  the measured and predicted web shear contributions are 70.3% and 70.3% respectively, for a measured-to-predicted ratio of 1.00 for  $V_{Web^*}$ . Figure 4-1 also indicates that the measured-to-predicted  $V_{Top\ Flg}$  contributions are 14.9% and 14.9%, respectively, for a measured-to-predicted ratio of 1.01. Finally, it indicates that the measured and predicted  $V_{Bot.\ Flg}$  shear contributions are 14.8% and 14.9%, respectively, for a measured-to-predicted ratio of 1.00.



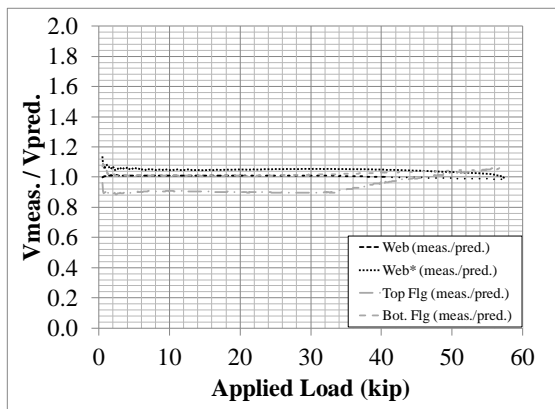
(a) Station 1



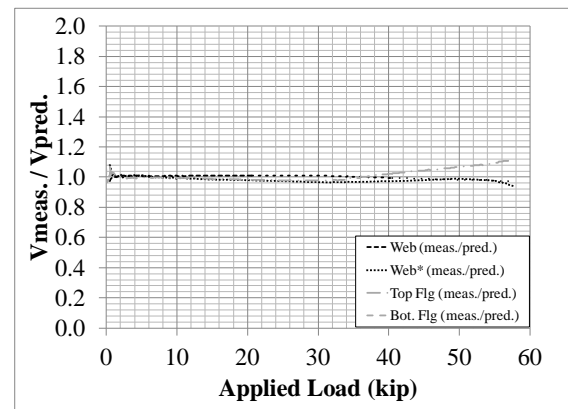
(b) Station 2

Figure 4-1 “Tapered 1a”  $V_{meas.} / V_{pred.}$  (%)

In Figure 4-2,  $V_{meas.} / V_{pred.}$  for each component contributing to the resistance of the applied shear force at Station 1 and Station 2 was computed. At Station 1, the ratios were:  $V_{Web} = 1.01$ ,  $V_{Web^*} = 1.05$ ,  $V_{Top Flg} = 0.903$ , and  $V_{Bot. Flg} = 1.01$ . At Station 2, the ratios were:  $V_{Web} = 1.01$ ,  $V_{Web^*} = 0.980$ ,  $V_{Top Flg} = 0.986$ , and  $V_{Bot. Flg} = 0.976$ .



(a) Station 1



(b) Station 2

Figure 4-2 “Tapered 1a”  $V_{meas.} / V_{pred.}$

#### 4.1.2 Failure Loads

Figure 4-3 shows the measured load-displacement curve (flexural flange local buckling failure near midspan; ultimate load = 57.6 kip) and predicted failure loads using

the AISC *Specification* (2010) Section G2. The lines labeled “AISC,” “AISC + Williams and Harris,” and “AISC + Blodgett” are the predicted failure loads without using modified shear, using the Williams and Harris (1957) modified shear, and using the Blodgett (1966) modified shear method, respectively. If a modified shear method is not used, the predicted failure load is 30.3 kip for a measured-to-predicted ratio of 1.90, indicating that this method is very conservative. Using the William and Harris modified shear, the predicted failure load is 42.7 kip for a measured-to-predicted ratio of 1.35, indicating that the method is conservative. Similarly, using the Blodgett modified shear method, the predicted failure load is 46.3 kip for a measured-to-predicted ratio of 1.25, indicating that the method is conservative.

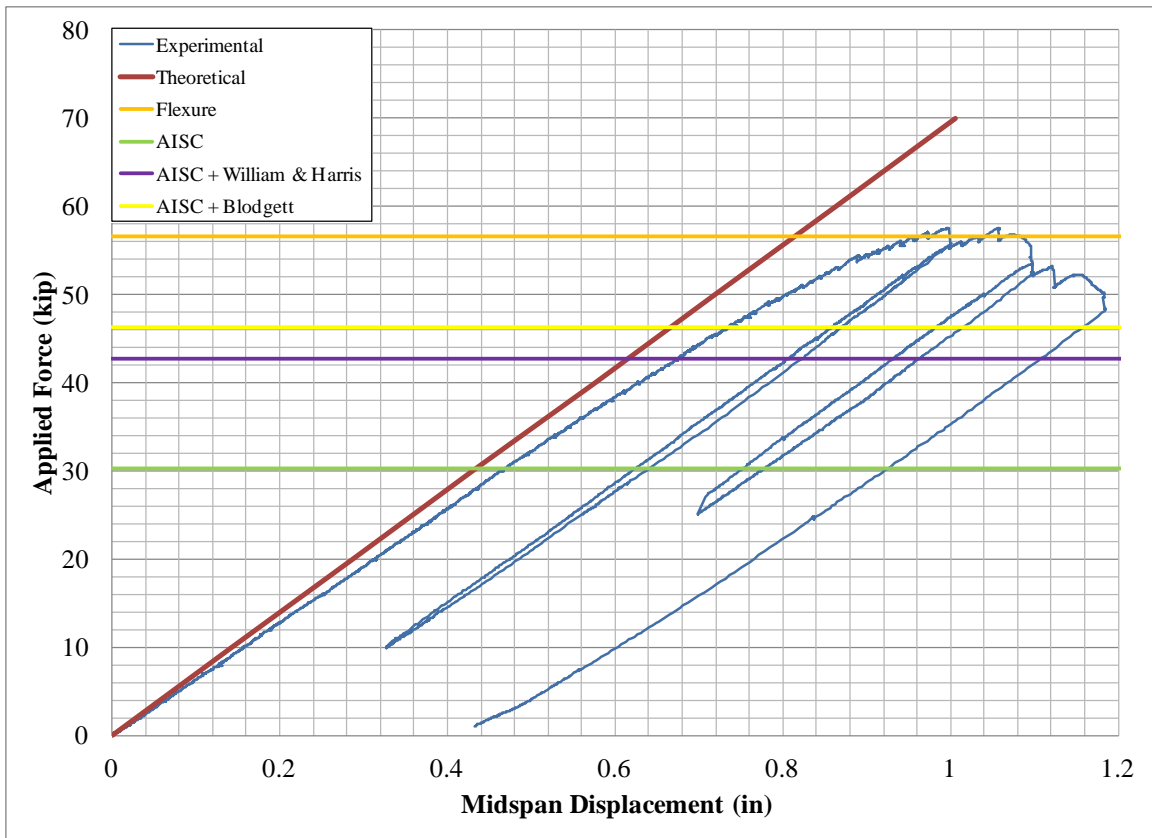


Figure 4-3 AISC Predicted Failure Loads “Tapered 1a”

Figure 4-4 shows the measured load-displacement curve (flexural flange local buckling failure near midspan; ultimate load = 57.6 kip) and predicted failure loads using the equations given by Lee et al. (2008). The lines labeled “Lee et al. 2008,” “Lee et al. (2008) + William and Harris,” and “Lee et al. (2008) + Blodgett” are at the predicted failure loads without using modified shear, using the William and Harris (1957) modified shear, and using the Blodgett (1966) modified shear method, respectively. Because the specimen failed in flexure at a load below the predicted shear failure loads, it is not possible to compare the measured and predicted failure loads. It can only be stated that the three methods did not produce an unconservative predicted failure load for this test.

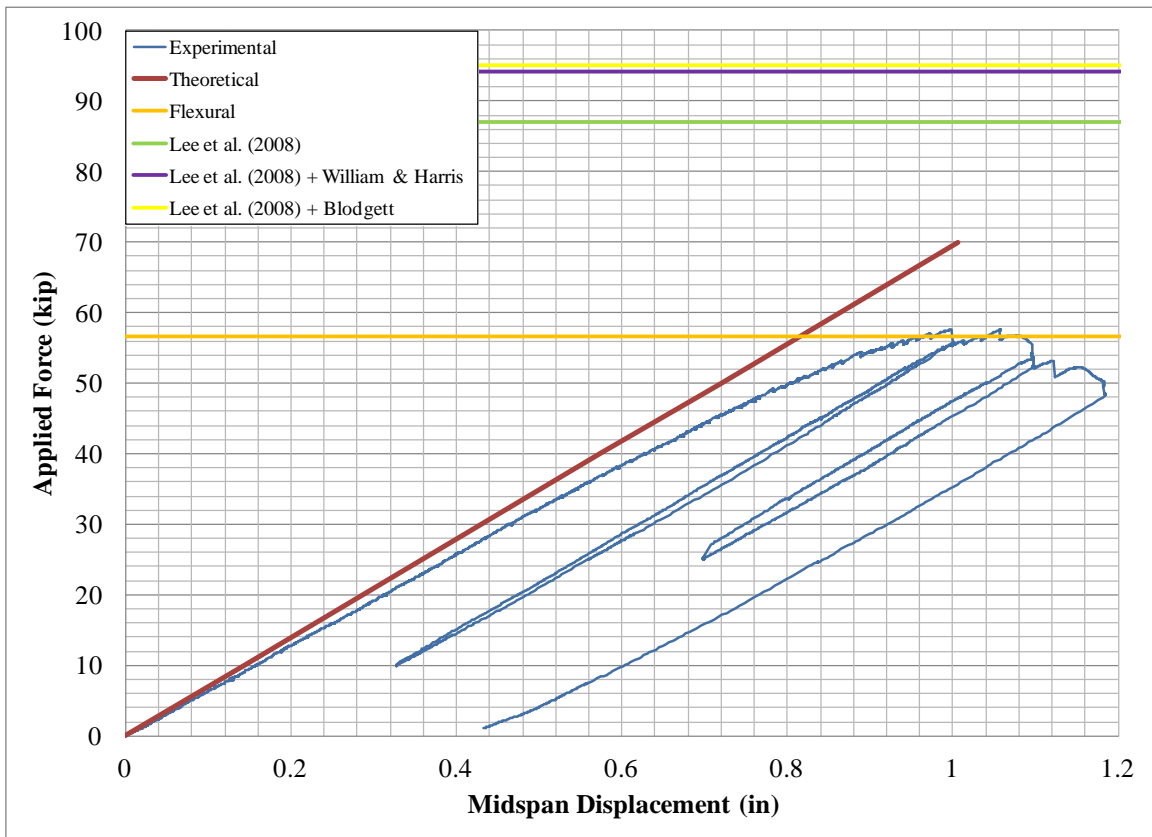


Figure 4-4 Lee et al. (2008) Predicted Failure Loads “Tapered 1a”

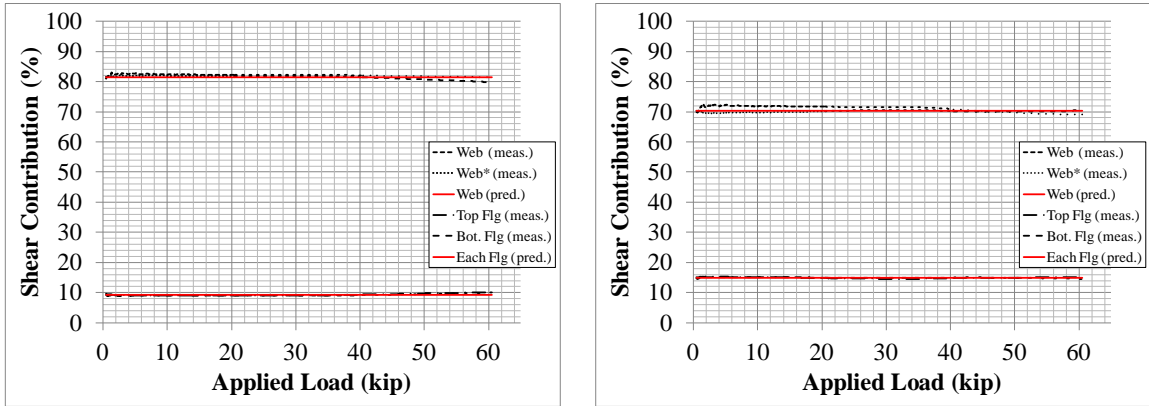
## 4.2 Tapered 1b

A complete list of graphs for test “Tapered 1b” can be found in Appendix B.

**Station 1.** Figure 4-5 indicates that the measured and predicted web shear contributions are 82.3% and 81.4% respectively, for a measured-to-predicted ratio of 1.01 for  $V_{Web}$ . For  $V_{Web^*}$  the measured and predicted web shear contributions are 81.9% and 81.4% respectively, for a measured-to-predicted ratio of 1.01 for  $V_{Web^*}$ . Figure 4-5 also indicates that the measured-to-predicted  $V_{Top\ Flg}$  contributions are 9.1% and 9.3%, respectively, for a measured-to-predicted ratio of 0.979. Finally, it indicates that the measured and predicted  $V_{Bot.\ Flg}$  shear contributions are 9.0% and 9.3%, respectively, for a measured-to-predicted ratio of 0.969.

**Station 2.** Figure 4-5 indicates that the measured and predicted web shear contributions are 71.7% and 70.3% respectively, for a measured-to-predicted ratio of 1.02 for  $V_{Web}$ . For  $V_{Web^*}$  the measured and predicted web shear contributions are 70.2% and 70.3% respectively, for a measured-to-predicted ratio of 0.999 for  $V_{Web^*}$ . Figure 4-5 also indicates that the measured-to-predicted  $V_{Top\ Flg}$  contributions are 14.8% and 14.9%, respectively, for a measured-to-predicted ratio of 1.00. Finally, it indicates that the measured and predicted  $V_{Bot.\ Flg}$  shear contributions are 15.0% and 14.9%, respectively, for a measured-to-predicted ratio of 1.01.

#### 4.2.1 Web and Flange Shear Contributions

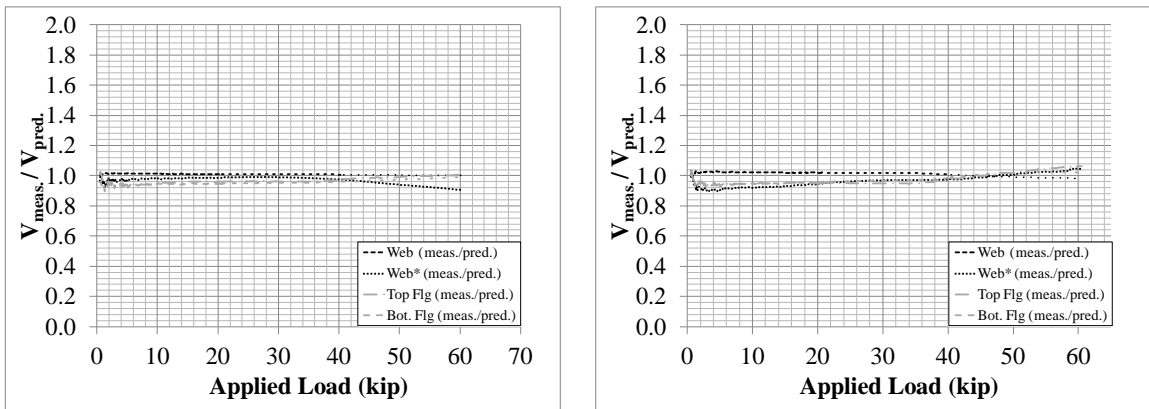


(a) Station 1

(b) Station 2

Figure 4-5 “Tapered 1b”  $V_{meas.} / V_{pred.}$  (%)

In Figure 4-6,  $V_{meas.} / V_{pred.}$  for each component contributing to the resistance of the applied shear force at Station 1 and Station 2 was computed. At Station 1 the ratios were:  $V_{Web} = 1.01$ ,  $V_{Web^*} = 0.983$ ,  $V_{Top\ Flg} = 0.957$ , and  $V_{Bot.\ Flg} = 0.948$ . At Station 2, the ratios were:  $V_{Web} = 1.02$ ,  $V_{Web^*} = 0.949$ ,  $V_{Top\ Flg} = 0.949$ , and  $V_{Bot.\ Flg} = 0.957$ .



(a) Station 1

(b) Station 2

Figure 4-6 “Tapered 1b”  $V_{meas.} / V_{pred.}$

#### 4.2.2 Failure Loads

Figure 4-7 shows the measured load-displacement curve (flexural flange local buckling failure near midspan; ultimate load = 60.5 kip) and predicted failure loads using the AISC *Specification* (2010) Section G2. The lines labeled “AISC,” “AISC + Williams and Harris,” and “AISC + Blodgett” are the predicted failure loads without using modified shear, using the Williams and Harris (1957) modified shear, and using the Blodgett (1966) modified shear method, respectively. If a modified shear method is not used, the predicted failure load is 30.3 kip for a measured-to-predicted ratio of 1.99, indicating that this method is very conservative. Using the William and Harris modified shear, the predicted failure load is 42.7 kip for a measured-to-predicted ratio of 1.42, indicating that the method is conservative. Similarly, using the Blodgett modified shear method, the predicted failure load is 46.3 for a measured-to-predicted ratio of 1.31, indicating that the method is conservative.

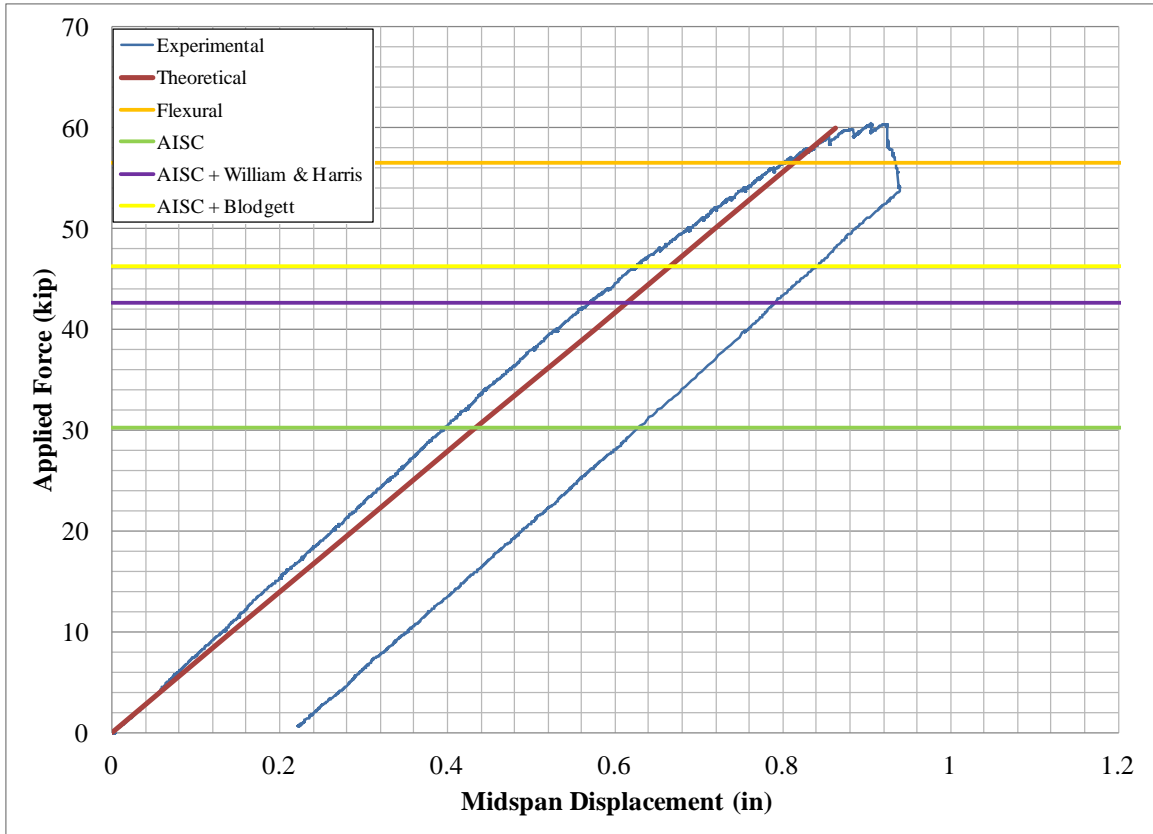


Figure 4-7 “Tapered 1b” AISC Predicted Failure Loads

Figure 4-8 shows the measured load-displacement curve (flexural flange local buckling failure near midspan; ultimate load = 60.5 kip) and predicted failure loads using the equations given by Lee et al. (2008). The lines labeled “Lee et al. (2008),” “Lee et al. (2008) + William and Harris,” and “Lee et al. (2008) + Blodgett” are at the predicted failure loads without using modified shear, using the William and Harris (1957) modified shear, and using the Blodgett (1966) modified shear method, respectively. Because the specimen failed in flexure at a load below the predicted shear failure loads, it is not possible to compare the measured and predicted failure loads. It can only be stated that the three methods did not produce an unconservative predicted failure load for this test.



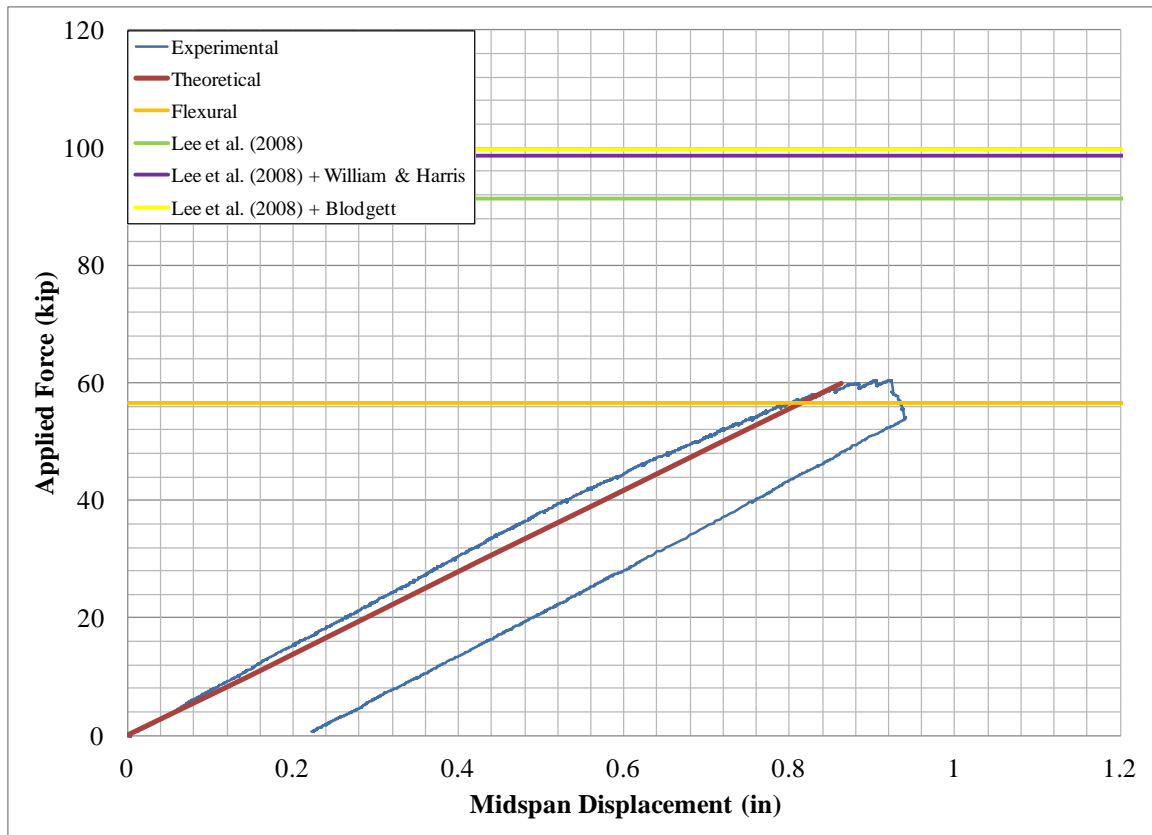


Figure 4-8 “Tapered 1b” Lee et al. (2008) Predicted Failure Loads

### 4.3 Tapered 1c

A complete list of graphs for test “Tapered 1c” can be found in Appendix C.

**Station 1.** Figure 4-9 indicates that the measured and predicted web shear contributions are 70.7% and 70.5% respectively, for a measured-to-predicted ratio of 1.00 for  $V_{Web}$ . For  $V_{Web}^*$  the measured and predicted web shear contributions are 73.7% and 70.5% respectively, for a measured-to-predicted ratio of 1.05 for  $V_{Web}^*$ . Figure 4-9 also indicates that the measured-to-predicted  $V_{Top\ Flg}$  contributions are 13.2% and 14.8%, respectively, for a measured-to-predicted ratio of 0.895. Finally, it indicates that the measured and predicted  $V_{Bot.\ Flg}$  shear contributions are 13.1% and 14.8%, respectively, for a measured-to-predicted ratio of 0.890.

### 4.3.1 Web and Flange Shear Contributions

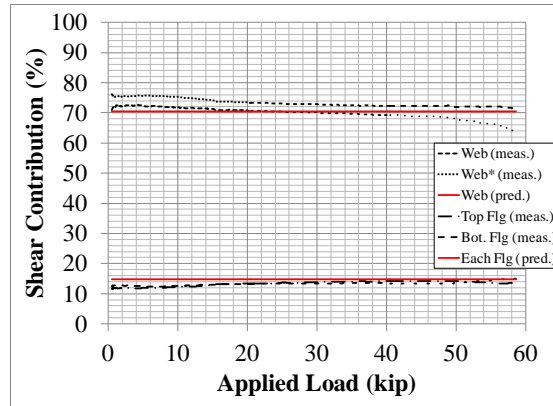


Figure 4-9 “Tapered 1c”  $V_{meas.} / V_{pred.}$  (%)

In Figure 4-10,  $V_{meas.} / V_{pred.}$  for each component contributing to the resistance of the applied shear force at Station 1 and Station 2 was computed. At Station 1 ratios were:  $V_{Web} = 1.00$ ,  $V_{Web^*} = 1.16$ ,  $V_{Top Flg} = 0.994$ , and  $V_{Bot. Flg} = 0.989$ .

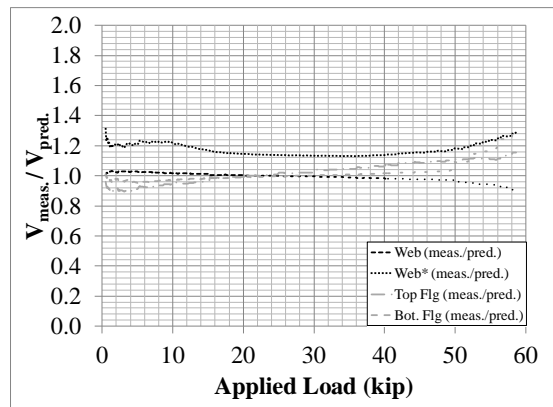


Figure 4-10 “Tapered 1c”  $V_{meas.} / V_{pred.}$

### 4.3.2 Failure Loads

Figure 4-11 shows the measured load-displacement curve (flexural flange local buckling failure near midspan; ultimate load = 58.6 kip) and predicted failure loads using the AISC *Specification* (2010) Section G2. The lines labeled “AISC,” “AISC + Williams and Harris,” and “AISC + Blodgett” are the predicted failure loads without using

modified shear, using the Williams and Harris (1957) modified shear, and using the Blodgett (1966) modified shear method, respectively. If a modified shear method is not used, the predicted failure load is 30.3 kip for a measured-to-predicted ratio of 1.93, indicating that this method is very conservative. Using the William and Harris modified shear, the predicted failure load is 42.7 kip for a measured-to-predicted ratio of 1.37, indicating that the method is conservative. Similarly, using the Blodgett modified shear method, the predicted failure load is 46.3 for a measured-to-predicted ratio of 1.27, indicating that the method is slightly conservative.

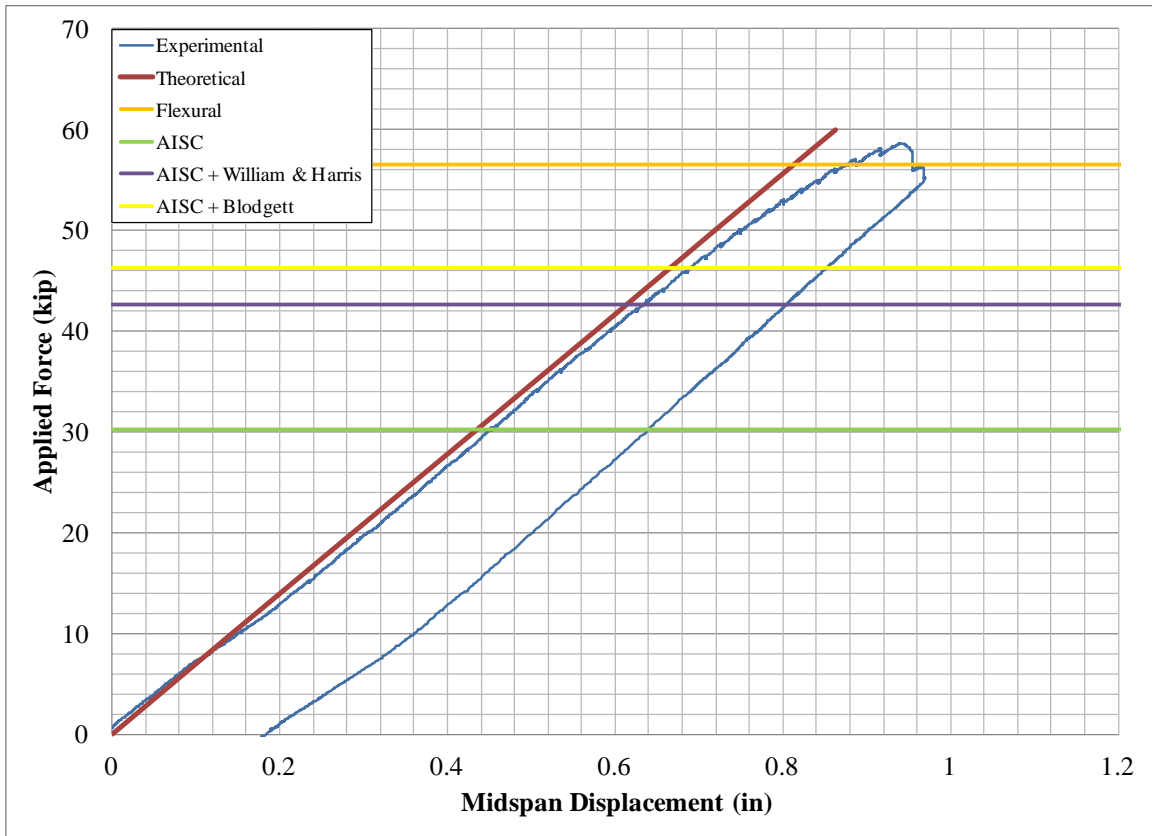


Figure 4-11 “Tapered 1c” AISC Predicted Failure Loads

Figure 4-12 shows the measured load-displacement curve (flexural flange local buckling failure near midspan; ultimate load = 60.5 kip) and predicted failure loads using

the equations given by Lee et al. (2008). The lines labeled “Lee et al. 2008,” “Lee et al. (2008) + William and Harris,” and “Lee et al. (2008) + Blodgett” are at the predicted failure loads without using modified shear, using the William and Harris (1957) modified shear, and using the Blodgett (1966) modified shear method, respectively. Because the specimen failed in flexure at a load below the predicted shear failure loads, it is not possible to compare the measured and predicted failure loads. It can only be stated that the three methods did not produce an unconservative predicted failure load for this test.

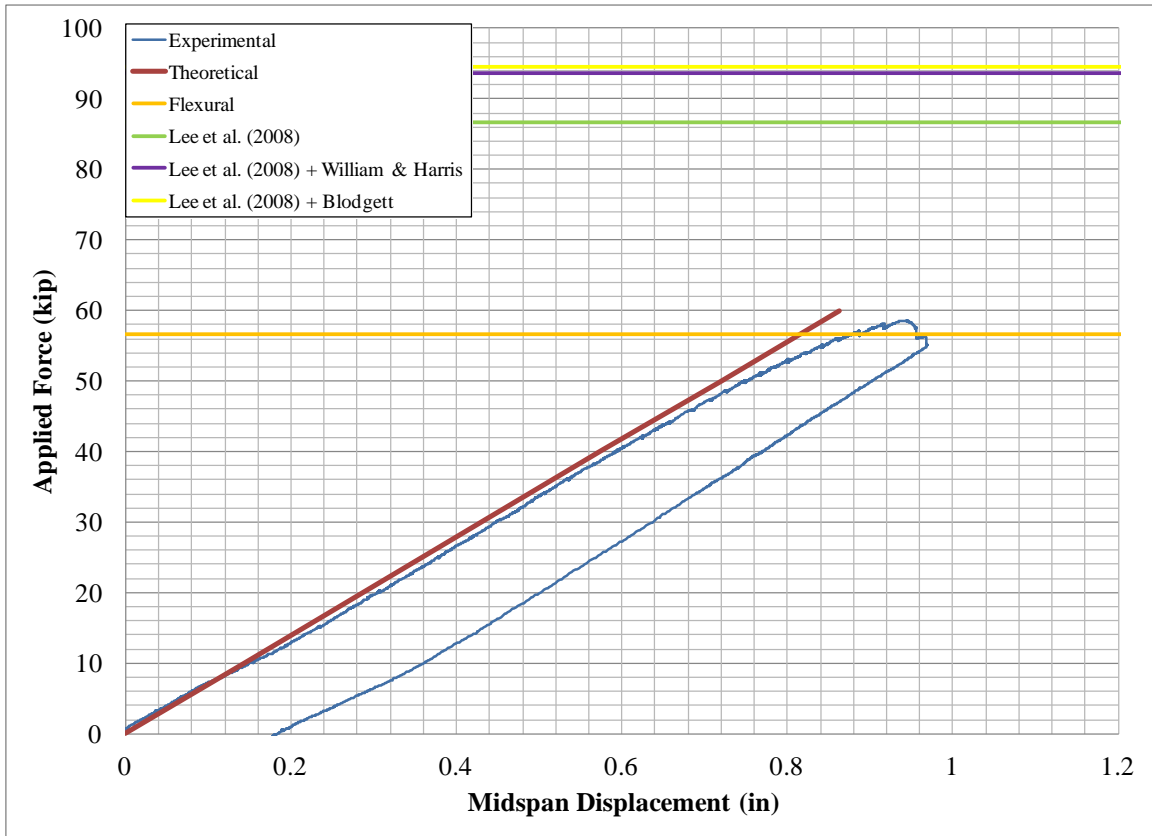


Figure 4-12 “Tapered 1c” Lee et al. (2008) Predicted Failure Loads

#### 4.4 Tapered 2a

A complete list of graphs for test “Tapered 2a” can be found in Appendix D.

**Station 1.** Figure 4-13 indicates that the measured and predicted web shear contributions are 50.9% and 49.4% respectively, for a measured-to-predicted ratio of 1.03 for  $V_{Web}$ . For  $V_{Web^*}$  the measured and predicted web shear contributions are 51.4% and 49.4% respectively, for a measured-to-predicted ratio of 1.04 for  $V_{Web^*}$ . Figure 4-13 also indicates that the measured-to-predicted  $V_{Top Flg}$  contributions are 27.9% and 25.3%, respectively, for a measured-to-predicted ratio of 1.10. Finally, it indicates that the measured and predicted  $V_{Bot. Flg}$  shear contributions are 20.7% and 25.3%, respectively, for a measured-to-predicted ratio of 0.819.

#### 4.4.1 Web and Flange Shear Contributions

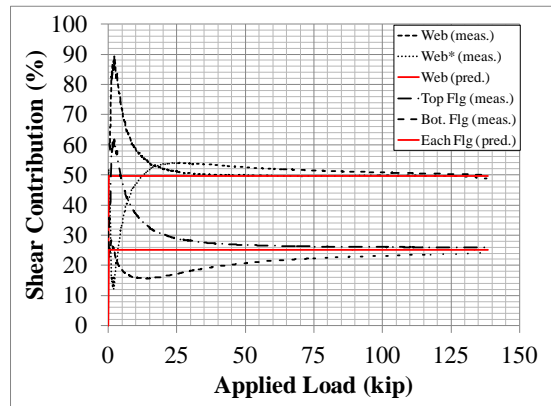


Figure 4-13 “Tapered 2a”  $V_{meas.} / V_{pred.}$  (%)

In Figure 4-14,  $V_{meas.} / V_{pred.}$  for each component contributing to the resistance of the applied shear force at Station 1 and Station 2 was computed. At Station 1 the ratios were:  $V_{Web} = 1.04$ ,  $V_{Web^*} = 1.05$ ,  $V_{Top Flg} = 1.10$ , and  $V_{Bot. Flg} = 0.827$ .

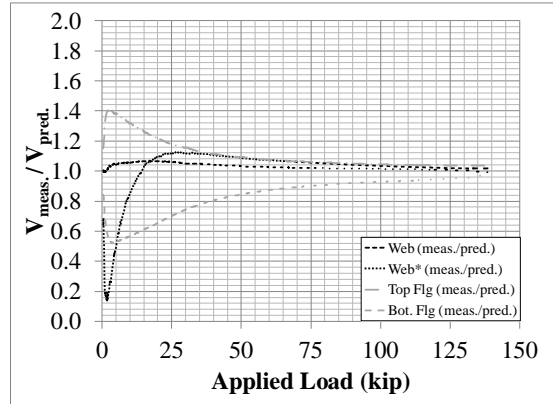


Figure 4-14 “Tapered 2a”  $V_{meas.} / V_{pred.}$

#### 4.4.2 Failure Loads

Figure 4-15 shows the measured load-displacement curve (shear buckling failure ½ ft near the support; ultimate load = 138 kip) and predicted failure loads using the AISC *Specification* (2010) Section G2. The lines labeled “AISC,” “AISC + Williams and Harris,” and “AISC + Blodgett” are the predicted failure loads without using modified shear, using the Williams and Harris (1957) modified shear, and using the Blodgett (1966) modified shear method, respectively. If a modified shear method is not used, the predicted failure load is 53.4 kip for a measured-to-predicted ratio of 2.59, indicating that this method is very conservative. Using the William and Harris modified shear, the predicted failure load is 101 kip for a measured-to-predicted ratio of 1.37, indicating that the method is conservative. Similarly, using the Blodgett modified shear method, the predicted failure load is 113 kip for a measured-to-predicted ratio of 1.22, indicating that the method is conservative.

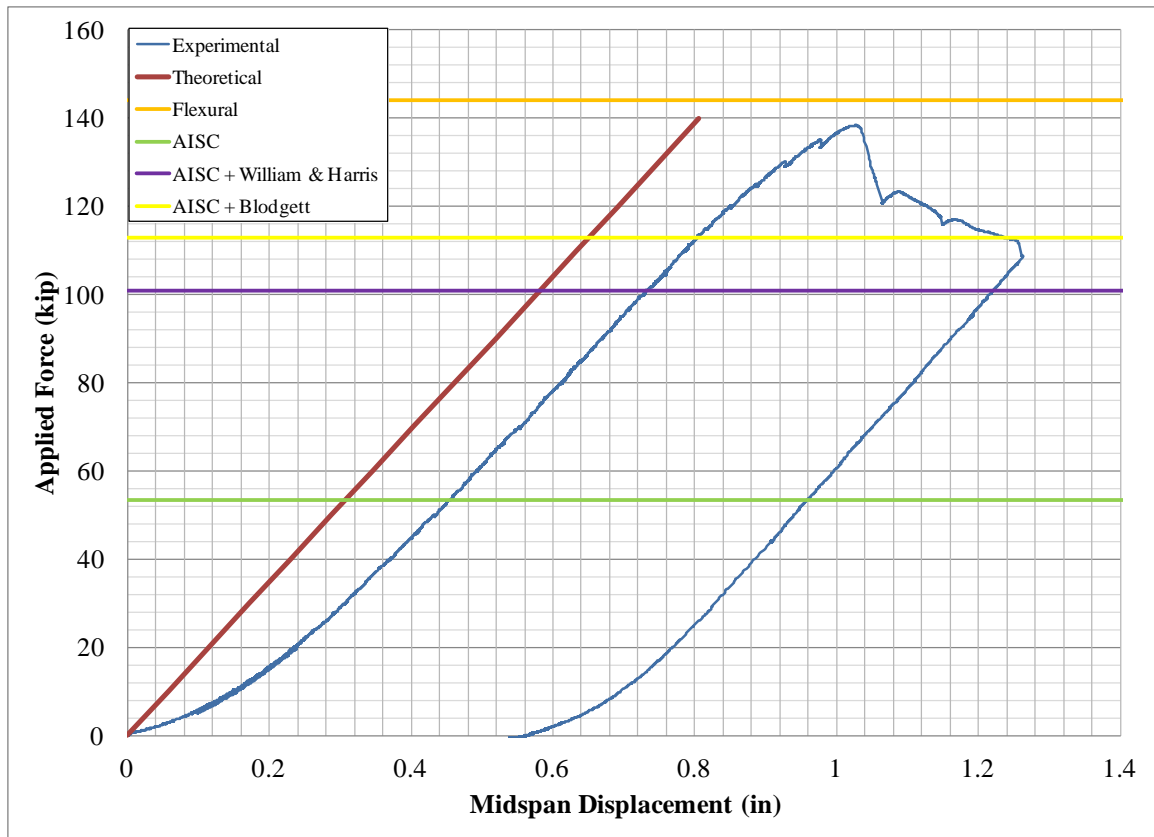


Figure 4-15 “Tapered 2a” AISC Predicted Failure Loads

Figure 4-16 shows the measured load-displacement curve (shear buckling failure  $\frac{1}{2}$  ft near the support; ultimate load = 138 kip) and predicted failure loads using the method proposed by Lee et al. (2008). The lines labeled “Lee et al. (2008),” “Lee et al. (2008) + William and Harris,” and “Lee et al. (2008) + Blodgett” are at the predicted failure loads without using modified shear, using the William and Harris (1957) modified shear, and using the Blodgett (1966) modified shear method, respectively. If a modified shear method is not used, the predicted failure load is 93.4 kip for a measured-to-predicted ratio of 1.48, indicating that this method is conservative. Using the William and Harris modified shear method, the predicted failure load is 109 kip for a measured-to-predicted ratio of 1.27, indicating that the method is slightly conservative. Similarly,

using the Blodgett modified shear method, the predicted failure load is 110 kip for a measured-to-predicted ratio of 1.26, indicating that the method is slightly conservative.

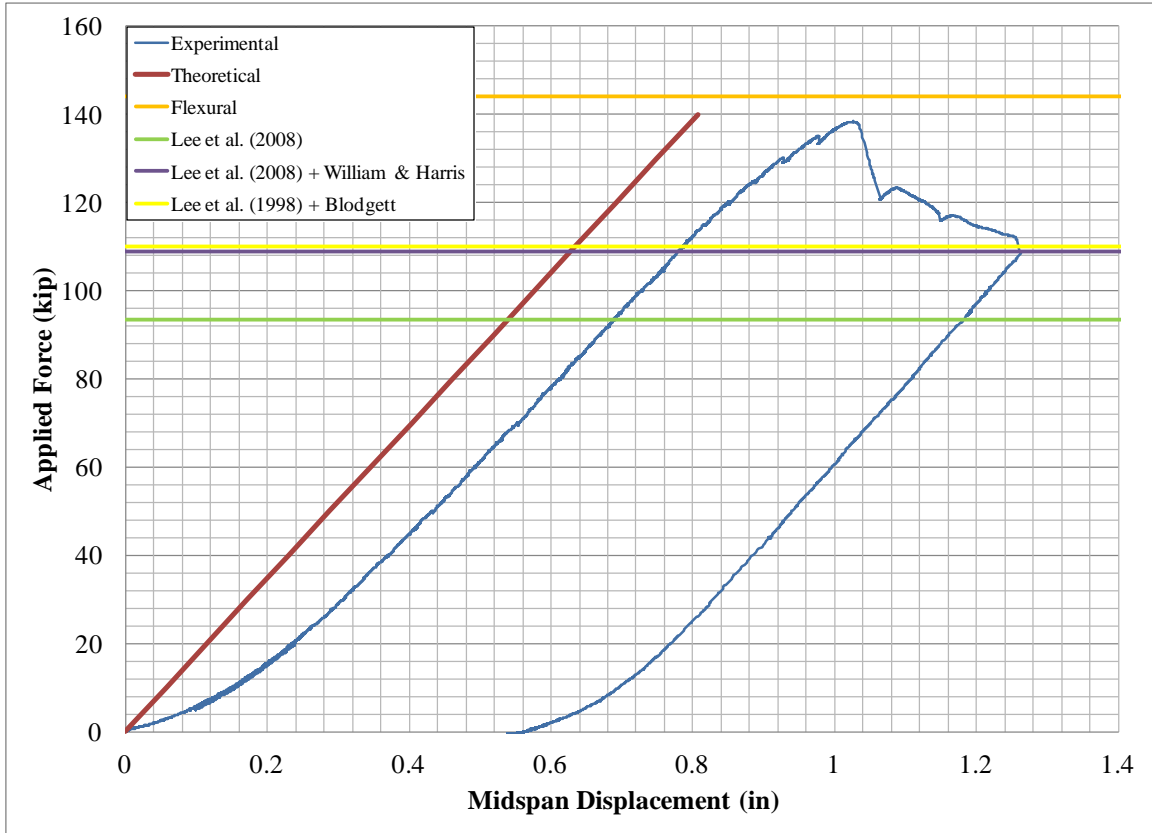


Figure 4-16 “Tapered 2a” Lee et al. (2008) Predicted Failure Loads

#### 4.5 Tapered 2b

A complete list of graphs for test “Tapered 2b” can be found in Appendix E.

**Station 1.** Figure 4-17 indicates that the measured and predicted web shear contributions are 88.7% and 88.4% respectively, for a measured-to-predicted ratio of 1.00 for  $V_{Web}$ . For  $V_{Web}^*$  the measured and predicted web shear contributions are 88.4% and 88.4% respectively, for a measured-to-predicted ratio of 1.00 for  $V_{Web}^*$ . Figure 4-17 also indicates that the measured-to-predicted  $V_{Top Flg}$  contributions are 5.8% and 5.8%, respectively, for a measured-to-predicted ratio of 1.00. Finally, it indicates that the



measured and predicted  $V_{Bot. Flg}$  shear contributions are 5.8% and 5.8%, respectively, for a measured-to-predicted ratio of 0.993.

**Station 2.** Figure 4-17 indicates that the measured and predicted web shear contributions are 82.3% and 81.7% respectively, for a measured-to-predicted ratio of 1.01 for  $V_{Web}$ . For  $V_{Web^*}$  the measured and predicted web shear contributions are 82.2% and 81.7% respectively, for a measured-to-predicted ratio of 1.01 for  $V_{Web^*}$ . Figure 4-17 also indicates that the measured-to-predicted  $V_{Top Flg}$  contributions are 9.1% and 9.2%, respectively, for a measured-to-predicted ratio of 0.987. Finally, it indicates that the measured and predicted  $V_{Bot. Flg}$  shear contributions are 8.7% and 9.2%, respectively, for a measured-to-predicted ratio of 0.954.

#### 4.5.1 Web and Flange Shear Contributions

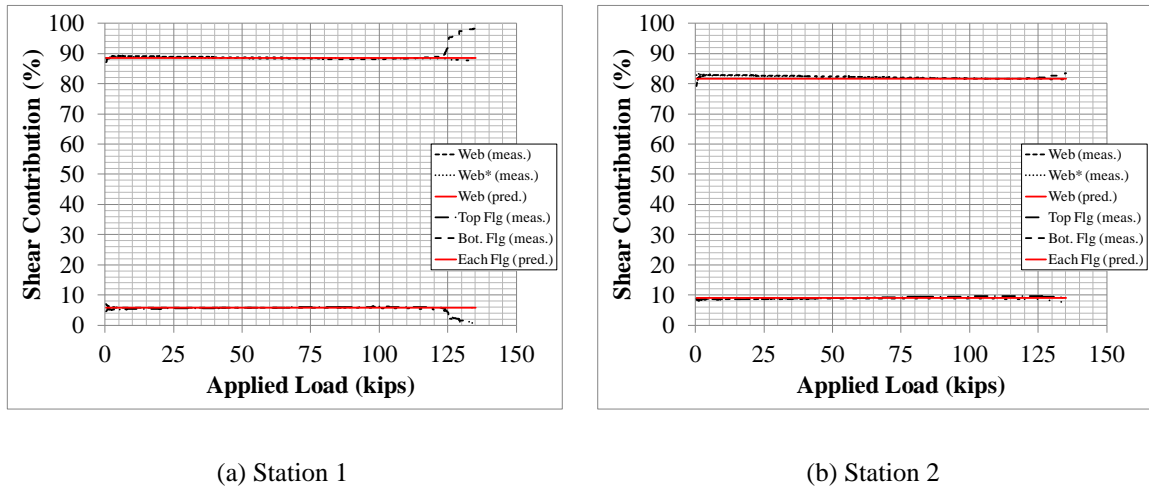


Figure 4-17 “Tapered 2b”  $V_{meas.} / V_{pred.}$  (%)

In Figure 4-18,  $V_{meas.} / V_{pred.}$  for each component contributing to the resistance of the applied shear force at Station 1 and Station 2 was computed. At Station 1 the ratios were:  $V_{Web} = 1.00$ ,  $V_{Web^*} = 0.977$ ,  $V_{Top Flg} = 0.975$ , and  $V_{Bot. Flg} = 0.970$ . At Station 2, the

following unity checks were as follows:  $V_{Web} = 1.01$ ,  $V_{Web^*} = 0.999$ ,  $V_{Top Flg} = 0.980$ , and  $V_{Bot. Flg} = 0.947$ .

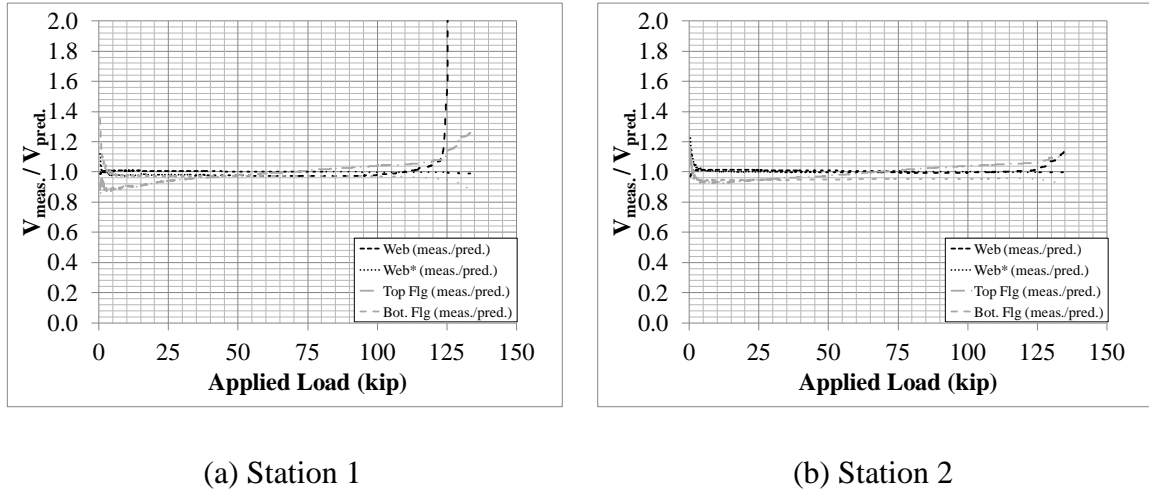


Figure 4-18 “Tapered 2b”  $V_{meas.} / V_{pred.}$

#### 4.5.2 Failure Loads

Figure 4-19 shows the measured load-displacement curve (shear buckling failure ½ ft near the support; ultimate load = 135 kip) and predicted failure loads using the AISC *Specification* (2010) Section G2. The lines labeled “AISC,” “AISC + Williams and Harris,” and “AISC + Blodgett” are the predicted failure loads without using modified shear, using the Williams and Harris (1957) modified shear, and using the Blodgett (1966) modified shear method, respectively. If a modified shear method is not used, the predicted failure load is 53.4 kip for a measured-to-predicted ratio of 2.59, indicating that this method is very conservative. Using the William and Harris modified shear, the predicted failure load is 101 kip for a measured-to-predicted ratio of 1.34, indicating that the method is conservative. Similarly, using the Blodgett modified shear method, the predicted failure load is 113 for a measured-to-predicted ratio of 1.19, indicating that the method is slightly conservative.

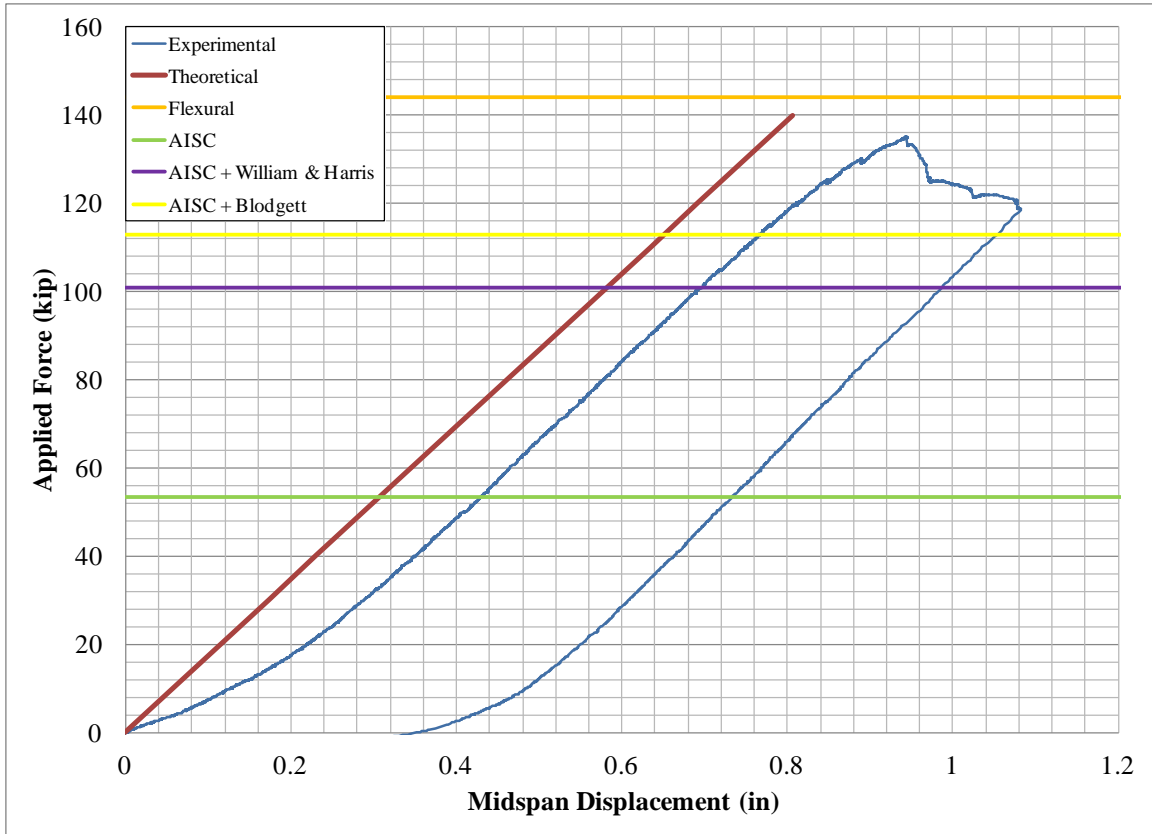


Figure 4-19 “Tapered 2b” AISC Predicted Failure Loads

Figure 4-20 shows the measured load-displacement curve (shear buckling failure ½ ft near the support; ultimate load = 135 kip) and predicted failure loads using the method proposed by Lee et al. (2008). The lines labeled “Lee et al. (2008),” “Lee et al. (2008) + William and Harris,” and “Lee et al. (2008) + Blodgett” are at the predicted failure loads without using modified shear, using the William and Harris (1957) modified shear, and using the Blodgett (1966) modified shear method, respectively. If a modified shear method is not used, the predicted failure load is 95.1 kip for a measured-to-predicted ratio of 1.42, indicating that this method is conservative. Using the William and Harris modified shear method, the predicted failure load is 111 kip for a measured-to-predicted ratio of 1.22, indicating that the method is slightly conservative. Similarly,

using the Blodgett modified shear method, the predicted failure load is 112 kip for a measured-to-predicted ratio of 1.21, indicating that the method is slightly conservative.

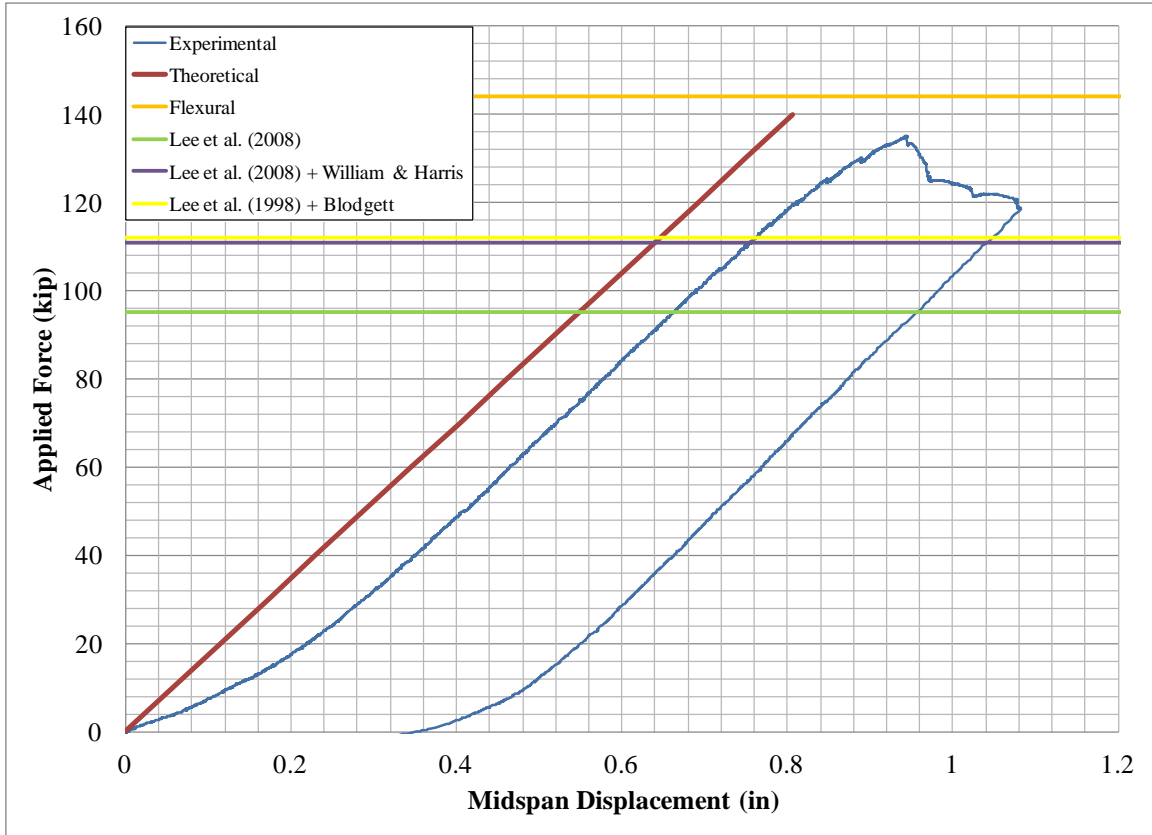


Figure 4-20 “Tapered 2b” Lee et al. (2008) Predicted Failure Loads

#### 4.6 Tapered 2c

A complete list of graphs for test “Tapered 2c” can be found in Appendix F.

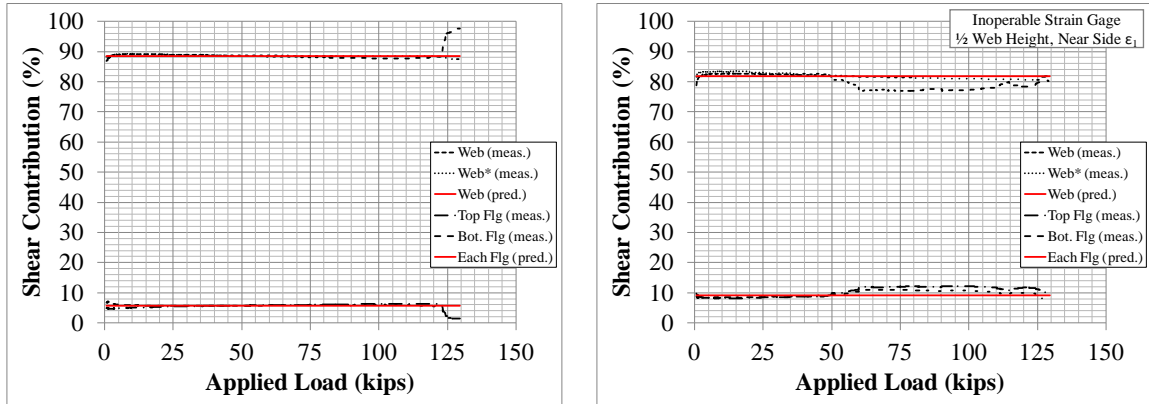
**Station 1.** Figure 4-21 indicates that the measured and predicted web shear contributions are 88.7% and 88.4% respectively, for a measured-to-predicted ratio of 1.00 for  $V_{Web}$ . For  $V_{Web^*}$  the measured and predicted web shear contributions are 88.4% and 88.4% respectively, for a measured-to-predicted ratio of 1.00 for  $V_{Web^*}$ . Figure 4-21 also indicates that the measured-to-predicted  $V_{Top Flg}$  contributions are 5.8% and 5.8%, respectively, for a measured-to-predicted ratio of 1.00. Finally, it indicates that the

measured and predicted  $V_{Bot. Flg}$  shear contributions are 5.8% and 5.8%, respectively, for a measured-to-predicted ratio of 1.01.

**Station 2.** Figure 4-21 indicates that the measured and predicted web shear contributions are 81.8% and 81.7% respectively, for a measured-to-predicted ratio of 1.00 for  $V_{Web}$ . For  $V_{Web^*}$  the measured and predicted web shear contributions are 79.9% and 81.7% respectively, for a measured-to-predicted ratio of 0.978 for  $V_{Web^*}$ . Figure 4-21 also indicates that the measured-to-predicted  $V_{Top Flg}$  contributions are 10.4% and 9.2%, respectively, for a measured-to-predicted ratio of 1.13. Finally, it indicates that the measured and predicted  $V_{Bot. Flg}$  shear contributions are 9.7% and 9.2%, respectively, for a measured-to-predicted ratio of 1.06.

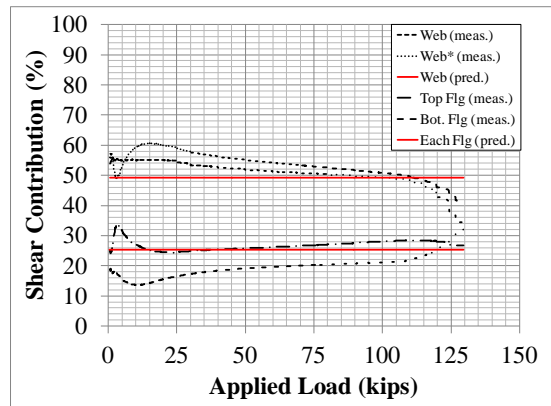
**Station 3.** Figure 4-21 indicates that the measured and predicted web shear contributions are 51.7% and 49.1% respectively, for a measured-to-predicted ratio of 1.05 for  $V_{Web}$ . For  $V_{Web^*}$  the measured and predicted web shear contributions are 54.6% and 49.1% respectively, for a measured-to-predicted ratio of 1.11 for  $V_{Web^*}$ . Figure 4-21 also indicates that the measured-to-predicted  $V_{Top Flg}$  contributions are 26.5% and 25.4%, respectively, for a measured-to-predicted ratio of 1.04. Finally, it indicates that the measured and predicted  $V_{Bot. Flg}$  shear contributions are 18.9% and 25.4%, respectively, for a measured-to-predicted ratio of 0.743.

#### 4.6.1 Web and Flange Shear Contributions



(a) Station 1

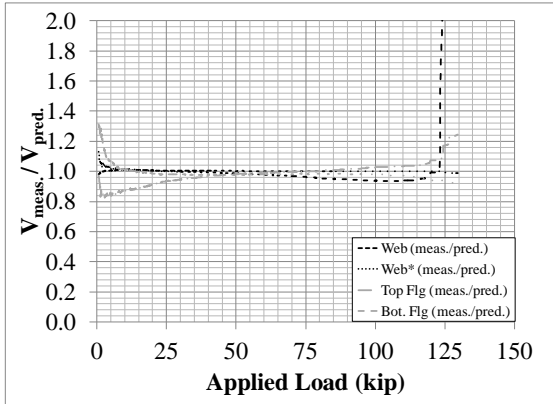
(b) Station 2



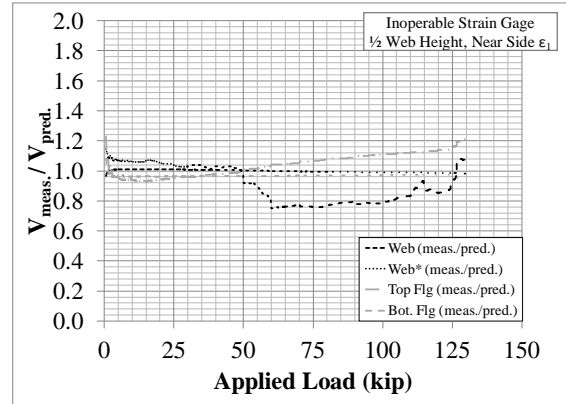
Station 3

Figure 4-21 “Tapered 2c”  $V_{meas.} / V_{pred.}$  (%)

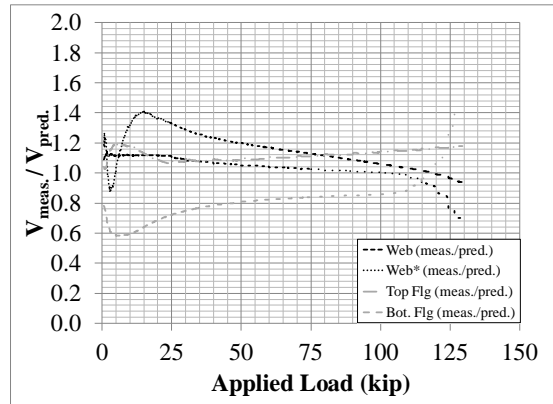
In Figure 4-22,  $V_{meas.} / V_{pred.}$  for each component contributing to the resistance of the applied shear force at Station 1 and Station 2 was computed. At Station 1 the ratios were:  $V_{Web} = 1.00$ ,  $V_{Web^*} = 0.975$ ,  $V_{Top\ Flg} = 0.973$ , and  $V_{Bot.\ Flg} = 0.980$ . At Station 2, the ratios were:  $V_{Web} = 1.00$ ,  $V_{Web^*} = 0.903$ ,  $V_{Top\ Flg} = 1.02$ , and “Bot. Flg” = 0.964. At Station 3, the ratios were:  $V_{Web} = 1.05$ ,  $V_{Web^*} = 1.19$ ,  $V_{Top\ Flg} = 1.11$ , and  $V_{Bot.\ Flg} = 0.789$ .



Station 1



Station 2



Station 3

Figure 4-22 “Tapered 2c”  $V_{meas.} / V_{pred.}$

#### 4.6.2 Failure Loads

Figure 4-23 shows the measured load-displacement curve (shear buckling failure  $\frac{1}{2}$  ft near the support; ultimate load = 130 kip) and predicted failure loads using the AISC *Specification* (2010) Section G2. The lines labeled “AISC,” “AISC + Williams and Harris,” and “AISC + Blodgett” are the predicted failure loads without using modified shear, using the Williams and Harris (1957) modified shear, and using the Blodgett (1966) modified shear method, respectively. If a modified shear method is not used, the predicted failure load is 53.4 kip for a measured-to-predicted ratio of 2.43, indicating that

this method is very conservative. Using the William and Harris modified shear, the predicted failure load is 101 kip for a measured-to-predicted ratio of 1.29, indicating that the method is slightly conservative. Similarly, using the Blodgett modified shear method, the predicted failure load is 113 for a measured-to-predicted ratio of 1.15, indicating that the method is slightly conservative.

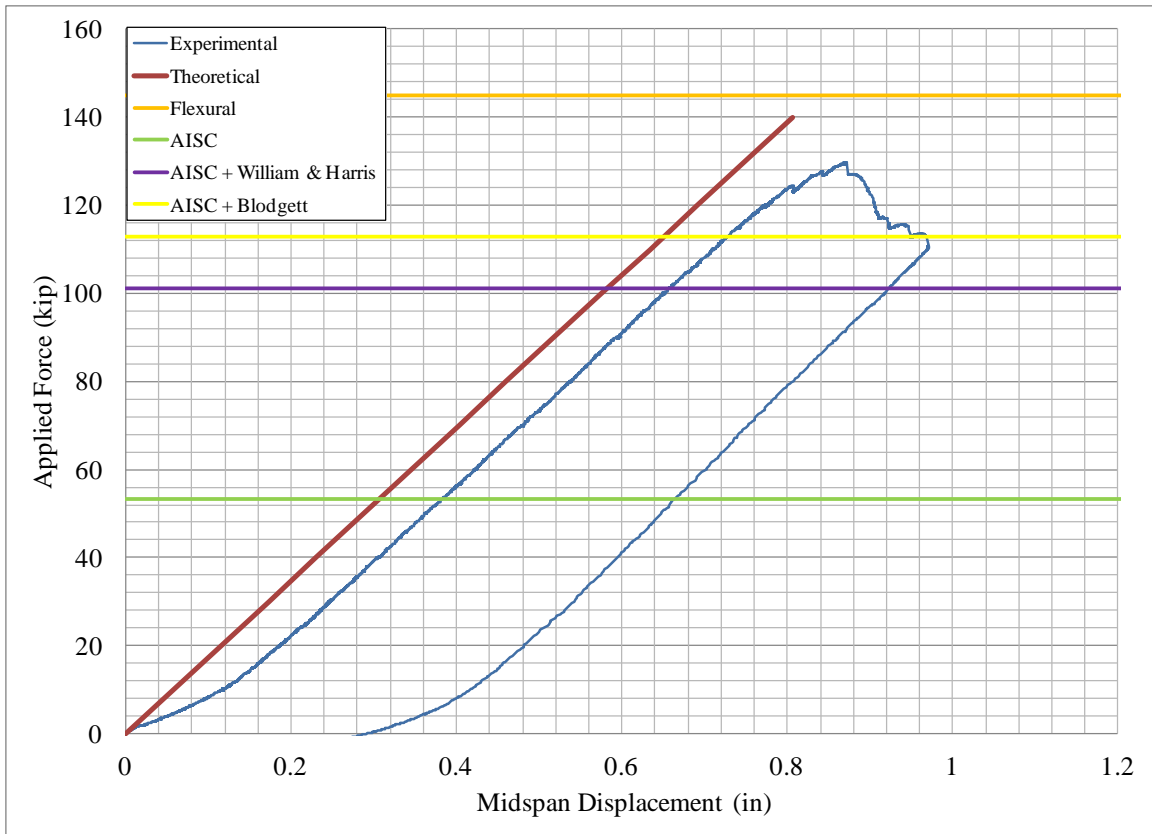


Figure 4-23 “Tapered 2c” AISC Predicted Failure Loads

Figure 4-24 shows the measured load-displacement curve (shear buckling failure ½ ft near the support; ultimate load = 130 kip) and predicted failure loads using the method proposed by Lee et al. (2008). The lines labeled “Lee et al. (2008),” “Lee et al. (2008) + William and Harris,” and “Lee et al. (2008) + Blodgett” are at the predicted failure loads without using modified shear, using the William and Harris (1957) modified



shear, and using the Blodgett (1966) modified shear method, respectively. If a modified shear method is not used, the predicted failure load is 97.3 kip for a measured-to-predicted ratio of 1.33, indicating that this method is conservative. Using the William and Harris modified shear method, the predicted failure load is 114 kip for a measured-to-predicted ratio of 1.14, indicating that the method is slightly conservative. Similarly, using the Blodgett modified shear method, the predicted failure load is 115 kip for a measured-to-predicted ratio of 1.13, indicating that the method is slightly conservative.

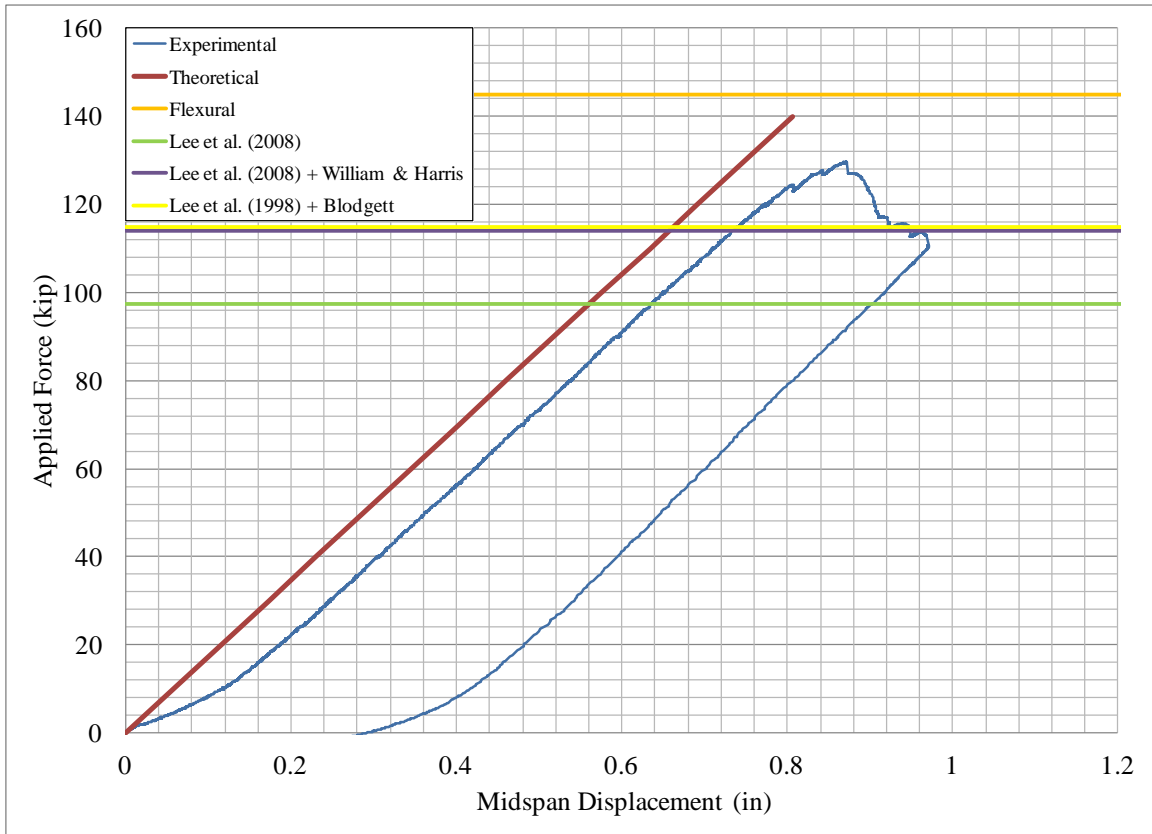


Figure 4-24 “Tapered 2c” Lee et al. (2008) Predicted Failure Loads

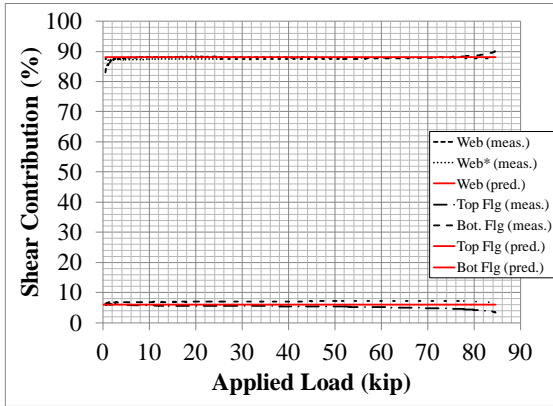
#### 4.7 Tapered 3

A complete list of graphs for test “Tapered 3” can be found in Appendix G.

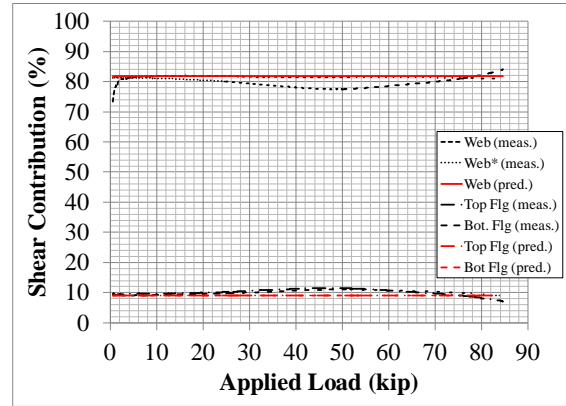
**Station 1.** Figure 4-25 indicates that the measured and predicted web shear contributions are 88.1% and 88% respectively, for a measured-to-predicted ratio of 1.00 for  $V_{Web}$ . For  $V_{Web^*}$  the measured and predicted web shear contributions were 87.4% and 88.0% respectively, for a measured-to-predicted ratio of 0.994 for  $V_{Web^*}$ . Figure 4-25 also indicates that the measured-to-predicted  $V_{Top Flg}$  contributions are 5.6% and 6.0%, respectively, for a measured-to-predicted ratio of 0.924. Finally, it indicates that the measured and predicted  $V_{Bot. Flg}$  shear contributions are 7.0% and 6.0%, respectively, for a measured-to-predicted ratio of 1.17.

**Station 2.** Figure 4-25 indicates that the measured and predicted web shear contributions are 81.6% and 81.8% respectively, for a measured-to-predicted ratio of 0.998 for  $V_{Web}$ . For  $V_{Web^*}$  the measured and predicted web shear contributions are 79.3% and 81.8% respectively, for a measured-to-predicted ratio of 0.970 for  $V_{Web^*}$ . Figure 4-25 also indicates that the measured-to-predicted  $V_{Top Flg}$  contributions are 10.6% and 9.1%, respectively, for a measured-to-predicted ratio of 1.16. Finally, it indicates that the measured and predicted  $V_{Bot. Flg}$  shear contributions are 10.1% and 9.1%, respectively, for a measured-to-predicted ratio of 1.11.

#### 4.7.1 Web and Flange Shear Contributions



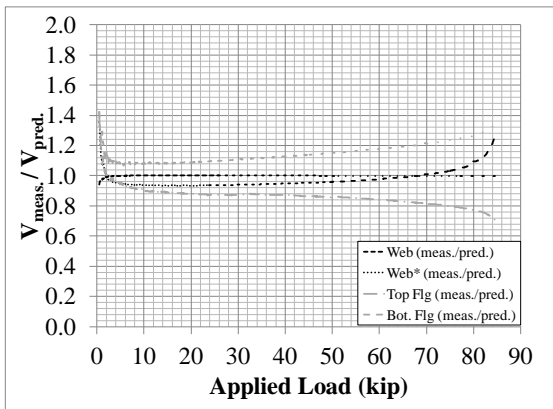
(a) Station 1



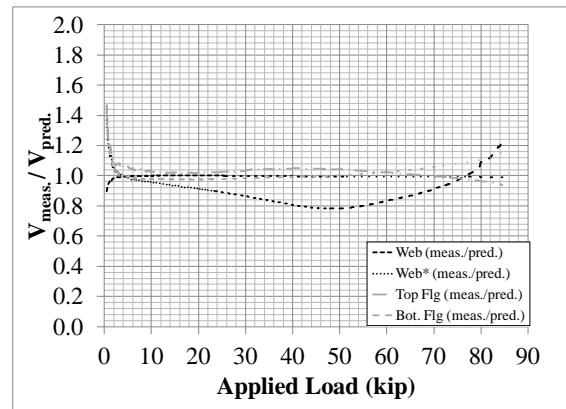
(b) Station 2

Figure 4-25 “Tapered 3”  $V_{meas.} / V_{pred.}$  (%)

In Figure 4-26,  $V_{meas.} / V_{pred.}$  for each component contributing to the resistance of the applied shear force at Station 1 and Station 2 was computed. At Station 1 the ratios were:  $V_{Web} = 1.00$ ,  $V_{Web^*} = 0.944$ ,  $V_{Top Flg} = 0.878$ , and  $V_{Bot. Flg} = 1.11$ . At Station 2, the ratios were:  $V_{Web} = 0.998$ ,  $V_{Web^*} = 0.867$ ,  $V_{Top Flg} = 1.03$ , and  $V_{Bot. Flg} = 0.985$ .



(a) Station 1



(b) Station 2

Figure 4-26 “Tapered 3”  $V_{meas.} / V_{pred.}$

#### 4.7.2 Failure Loads

Figure 4-27 shows the measured load-displacement curve (shear buckling failure; ultimate load = 84.6 kip) and predicted failure loads using the AISC *Specification* (2010) Section G2. The lines labeled “AISC,” “AISC + Williams and Harris,” and “AISC + Blodgett” are the predicted failure loads without using modified shear, using the Williams and Harris (1957) modified shear, and using the Blodgett (1966) modified shear method, respectively. If a modified shear method is not used, the predicted failure load is 32.5 kip for a measured-to-predicted ratio of 2.61, indicating that this method is very conservative. Using the William and Harris modified shear, the predicted failure load is 43.5 kip for a measured-to-predicted ratio of 1.95, indicating that the method is very conservative. Similarly, using the Blodgett modified shear method, the predicted failure load is 44.8 kip for a measured-to-predicted ratio of 1.89, indicating that the method is very conservative.

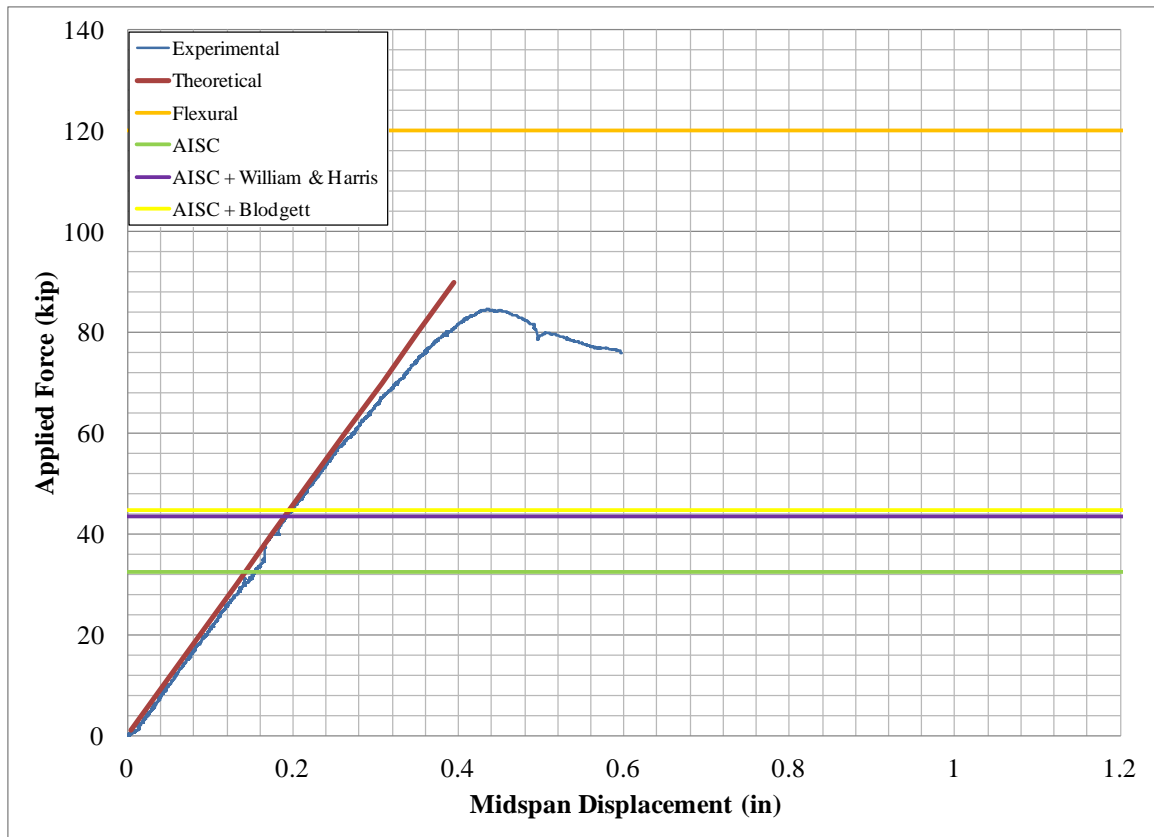


Figure 4-27 “Tapered 3” AISC Predicted Failure Loads

Figure 4-28 shows the measured load-displacement curve (shear buckling failure ½ ft near the support; ultimate load = 84.6 kip) and predicted failure loads using the method proposed by Lee et al. (2008). The lines labeled “Lee et al. (2008),” “Lee et al. (2008) + William and Harris,” and “Lee et al. (2008) + Blodgett” are at the predicted failure loads without using modified shear, using the William and Harris (1957) modified shear, and using the Blodgett (1966) modified shear method, respectively. If a modified shear method is not used, the predicted failure load is 72.3 kip for a measured-to-predicted ratio of 1.17, indicating that this method is slightly conservative. Using the William and Harris modified shear method, the predicted failure load is 79.5 kip for a measured-to-predicted ratio of 1.06, indicating that the method is slightly conservative.

Similarly, using the Blodgett modified shear method, the predicted failure load is 80.0 kip for a measured-to-predicted ratio of 1.06, indicating that the method is slightly conservative.

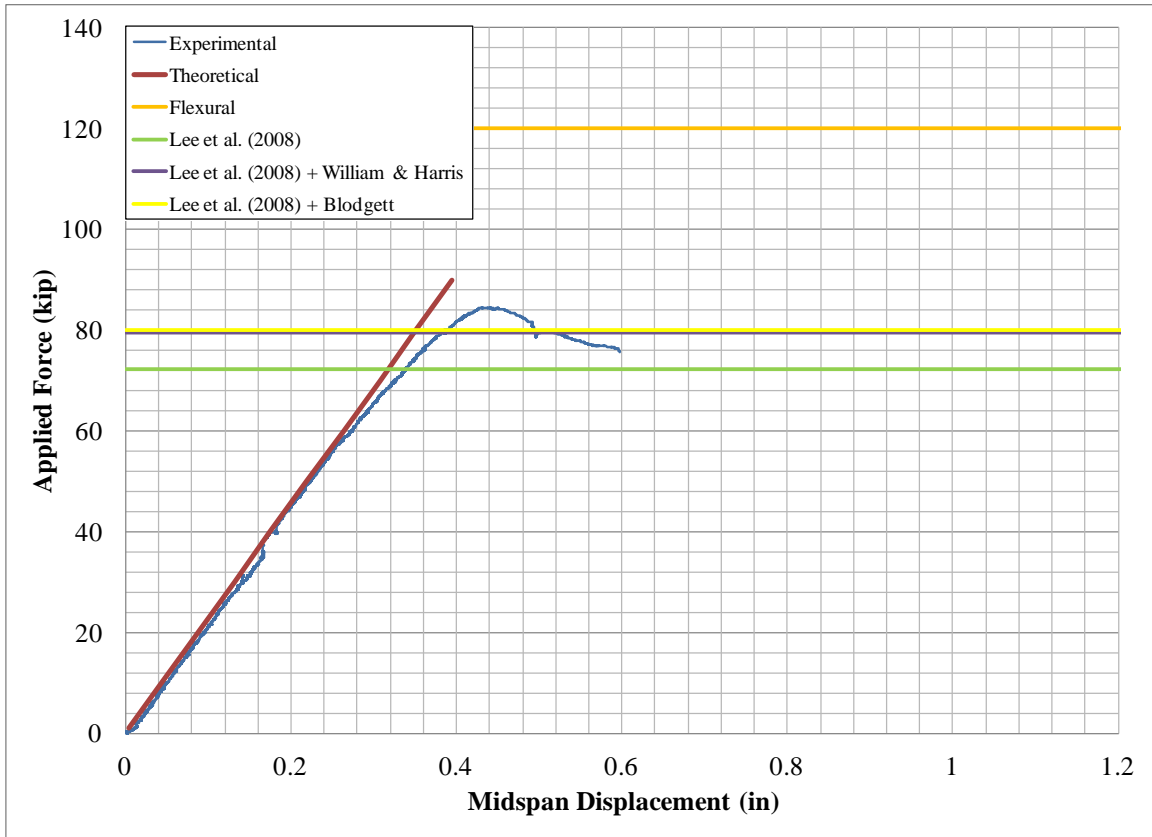


Figure 4-28 “Tapered 3” Lee et al. (2008) Predicted Failure Loads

#### 4.8 Tapered 4

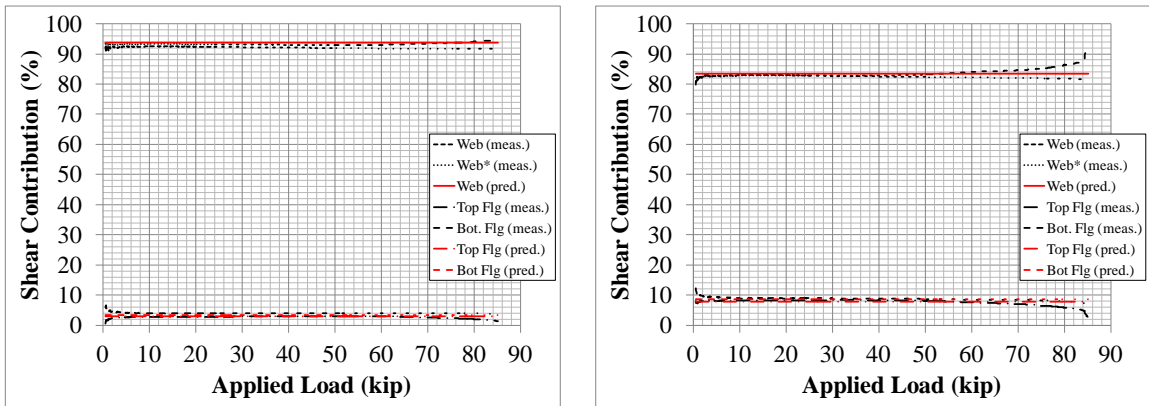
A complete list of graphs for test “Tapered 4” can be found in Appendix H.

**Station 1.** Figure 4-29 indicates that the measured and predicted web shear contributions are 92.2% and 93.7% respectively, for a measured-to-predicted ratio of 0.984 for  $V_{Web}$ . For  $V_{Web}^*$  the measured and predicted web shear contributions are 93.1% and 93.7% respectively, for a measured-to-predicted ratio of 0.994 for  $V_{Web}^*$ . Figure 4-29 also indicates that the measured-to-predicted  $V_{Top Flg}$  contributions are 2.9% and 3.0%,

respectively, for a measured-to-predicted ratio of 0.963. Finally, it indicates that the measured and predicted  $V_{Bot. Flg}$  shear contributions are 4.0% and 3.3%, respectively, for a measured-to-predicted ratio of 1.21.

**Station 2.** Figure 4-29 indicates that the measured and predicted web shear contributions are 82.7% and 83.5% respectively, for a measured-to-predicted ratio of 0.991 for  $V_{Web}$ . For  $V_{Web^*}$  the measured and predicted web shear contributions are 83.0% and 83.5% respectively, for a measured-to-predicted ratio of 0.994 for  $V_{Web^*}$ . Figure 4-29 also indicates that the measured-to-predicted  $V_{Top Flg}$  contributions are 8.2% and 7.9%, respectively, for a measured-to-predicted ratio of 1.04. Finally, it indicates that the measured and predicted  $V_{Bot. Flg}$  shear contributions are 8.9% and 8.7%, respectively, for a measured-to-predicted ratio of 1.02.

#### 4.8.1 Web and Flange Shear Contributions



(a) Station 1

(b) Station 2

Figure 4-29 “Tapered 4”  $V_{meas.} / V_{pred.}$  (%)

In Figure 4-30,  $V_{meas.} / V_{pred.}$  for each component contributing to the resistance of the applied shear force at Station 1 and Station 2 was computed. At Station 1 the ratios

were:  $V_{Web} = 0.984$ ,  $V_{Web^*} = 1.13$ ,  $V_{Top Flg} = 1.09$ , and  $V_{Bot. Flg} = 1.37$ . At Station 2, the ratios were:  $V_{Web} = 0.991$ ,  $V_{Web^*} = 1.01$ ,  $V_{Top Flg} = 1.06$ , and  $V_{Bot. Flg} = 1.04$ .

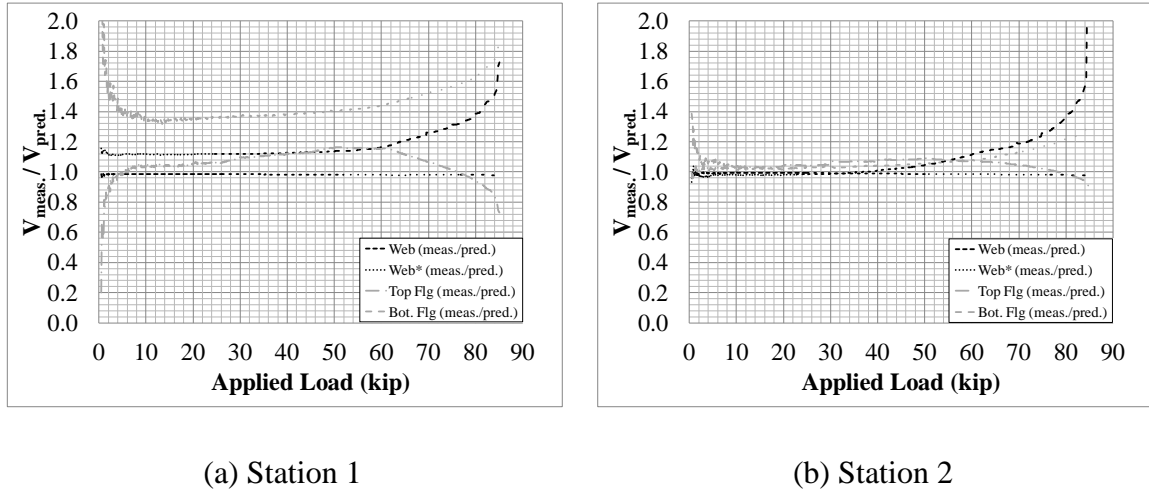


Figure 4-30 “Tapered 4”  $V_{meas.} / V_{pred.}$

#### 4.8.2 Failure Loads

Figure 4-31 shows the measured load-displacement curve (shear buckling failure; ultimate load = 85.1 kip) and predicted failure loads using the AISC *Specification* (2010) Section G2. The lines labeled “AISC,” “AISC + Williams and Harris,” and “AISC + Blodgett” are the predicted failure loads without using modified shear, using the Williams and Harris (1957) modified shear, and using the Blodgett (1966) modified shear method, respectively. If a modified shear method is not used, the predicted failure load is 29.9 kip for a measured-to-predicted ratio of 2.84, indicating that this method is very conservative. Using the William and Harris modified shear, the predicted failure load is 44.1 kip for a measured-to-predicted ratio of 1.93, indicating that the method is very conservative. Similarly, using the Blodgett modified shear method, the predicted failure load is 46.2 for a measured-to-predicted ratio of 1.84, indicating that the method is very conservative.



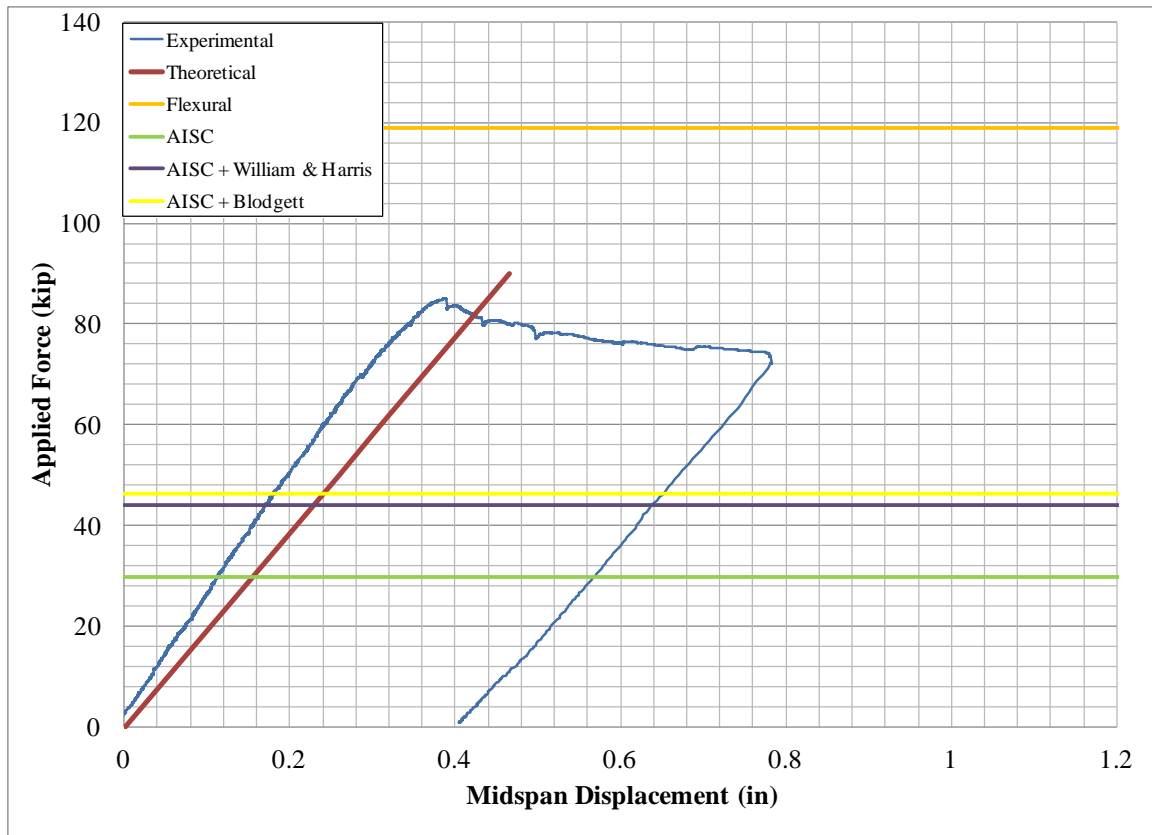


Figure 4-31 “Tapered 4” AISC Predicted Failure Loads

Figure 4-32 shows the measured load-displacement curve (shear buckling failure ½ ft near the support; ultimate load = 85.1 kip) and predicted failure loads using the method proposed by Lee et al. (2008). The lines labeled “Lee et al. (2008),” “Lee et al. (2008) + William and Harris,” and “Lee et al. (2008) + Blodgett” are at the predicted failure loads without using modified shear, using the William and Harris (1957) modified shear, and using the Blodgett (1966) modified shear method, respectively. If a modified shear method is not used, the predicted failure load is 64.6 kip for a measured-to-predicted ratio of 1.32, indicating that this method is conservative. Using the William and Harris modified shear method, the predicted failure load is 73.6 kip for a measured-to-predicted ratio of 1.16, indicating that the method is slightly conservative. Similarly,

using the Blodgett modified shear method, the predicted failure load is 74.2 kip for a measured-to-predicted ratio of 1.15, indicating that the method is conservative.

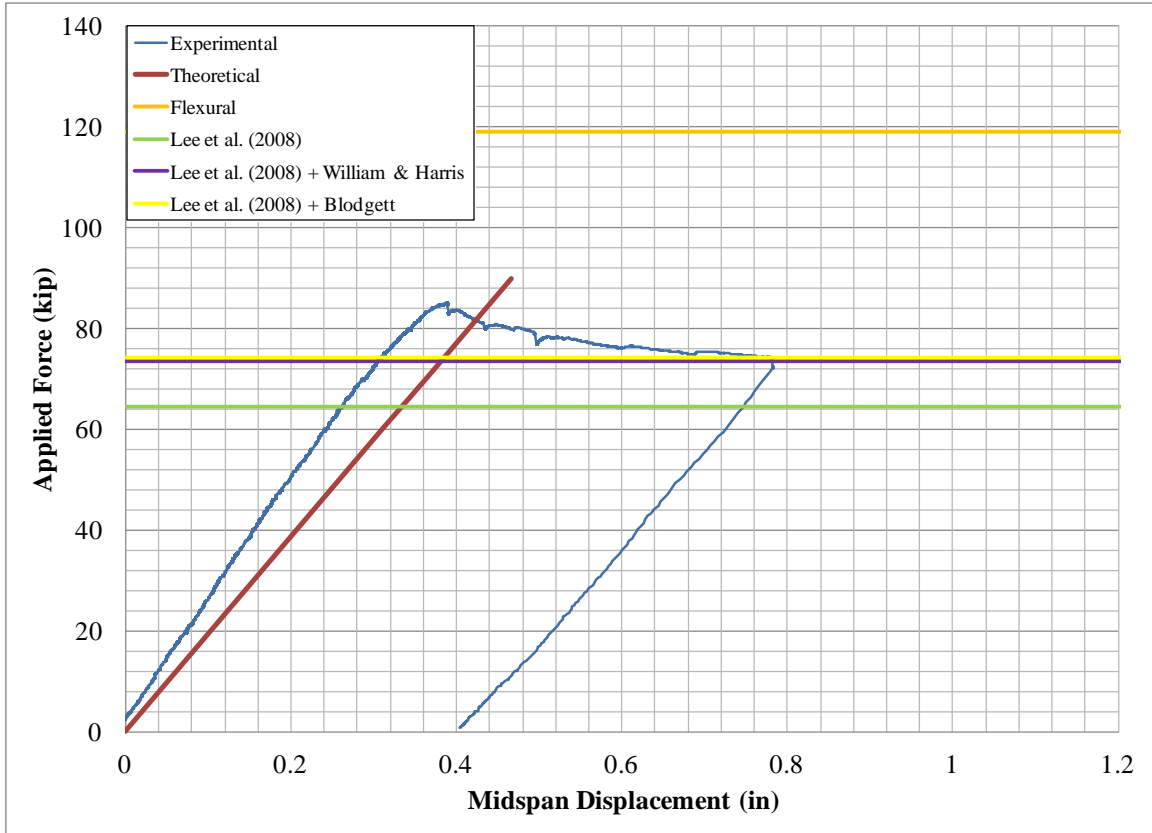


Figure 4-32 “Tapered 4” Lee et al. (2008) Predicted Failure Loads

#### 4.9 Tapered 5

A complete list of graphs for test “Tapered 5” can be found in Appendix I. The “Tapered 5” had only one strain gage station that had a denser grouping of strain gages on the flanges and web. The orientation of these strain gages can be seen in Section 2.4. Web and flange strains exhibited a consistent distribution across the web height and flange width therefore confirming the sparser placement of strain gages throughout the testing program.

**Station 1.** Figure 4-33 indicates that the measured and predicted web shear contributions are 91.6% and 91.4% respectively, for a measured-to-predicted ratio of 1.00 for  $V_{Web}$ . For  $V_{Web^*}$  the measured and predicted web shear contributions are 90.9% and 91.4% respectively, for a measured-to-predicted ratio of 0.995 for  $V_{Web^*}$ . Figure 4-33 also indicates that the measured-to-predicted  $V_{Top Flg}$  contributions are 4.5% and 4.5%, respectively, for a measured-to-predicted ratio of 1.00. Finally, it indicates that the measured and predicted  $V_{Bot. Flg}$  shear contributions are 4.6% and 4.1%, respectively, for a measured-to-predicted ratio of 1.12.

#### 4.9.1 Web and Flange Shear Contributions

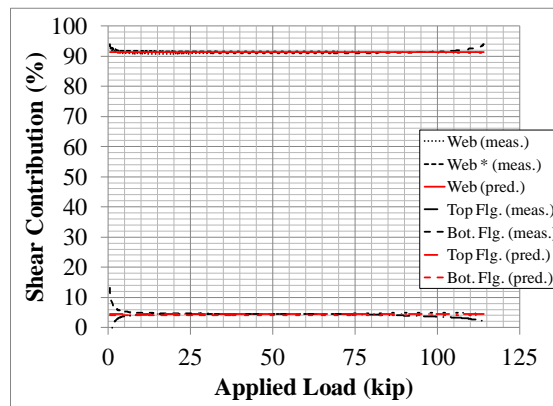


Figure 4-33 “Tapered 5”  $V_{meas.} / V_{pred.}$  (%)

In Figure 4-34,  $V_{meas.} / V_{pred.}$  for each component contributing to the resistance of the applied shear force at Station 1 and Station 2 was computed. At Station 1, the ratios were:  $V_{Web} = 1.00$ ,  $V_{Web^*} = 0.921$ ,  $V_{Top Flg} = 0.922$ , and  $V_{Bot. Flg} = 1.03$ .

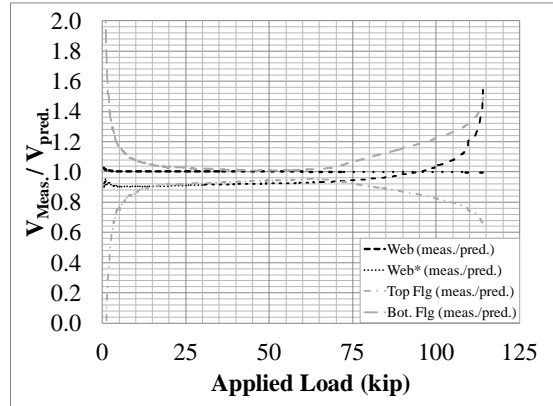


Figure 4-34 “Tapered 5”  $V_{meas.} / V_{pred.}$

#### 4.9.2 Failure Load

Figure 4-35 shows the measured load-displacement curve (shear buckling failure; ultimate load = 114 kip) and predicted failure loads using the AISC *Specification* (2010) Section G2. The lines labeled “AISC,” “AISC + Williams and Harris,” and “AISC + Blodgett” are the predicted failure loads without using modified shear, using the Williams and Harris (1957) modified shear, and using the Blodgett (1966) modified shear method, respectively. If a modified shear method is not used, the predicted failure load is 47.5 kip for a measured-to-predicted ratio of 2.40, indicating that this method is very conservative. Using the William and Harris modified shear, the predicted failure load is 60.2 kip for a measured-to-predicted ratio of 1.90, indicating that the method is very conservative. Similarly, using the Blodgett modified shear method, the predicted failure load is 61.8 for a measured-to-predicted ratio of 1.85, indicating that the method is very conservative.

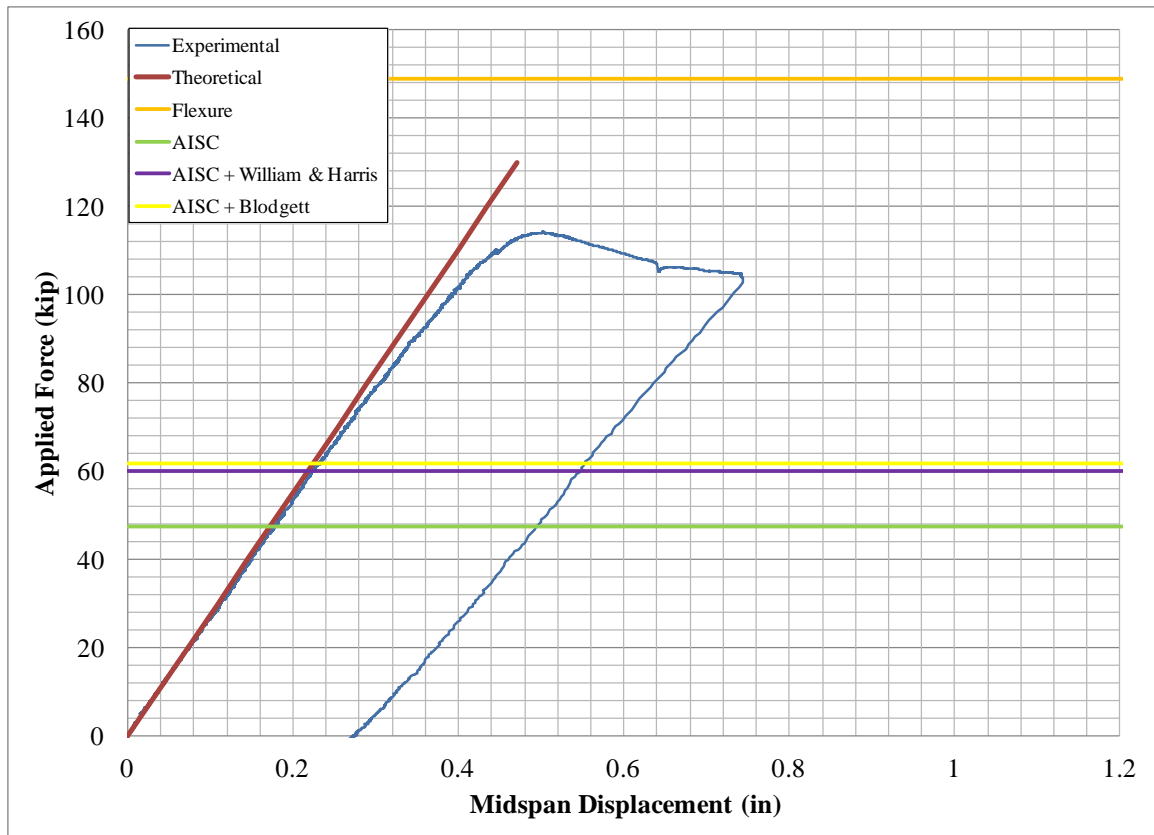


Figure 4-35 “Tapered 5” AISC Predicted Failure Loads

Figure 4-36 shows the measured load-displacement curve (shear buckling failure ½ ft near the support; ultimate load = 114 kip) and predicted failure loads using the method proposed by Lee et al. (2008). The lines labeled “Lee et al. (2008),” “Lee et al. (2008) + William and Harris,” and “Lee et al. (2008) + Blodgett” are at the predicted failure loads without using modified shear, using the William and Harris (1957) modified shear, and using the Blodgett (1966) modified shear method, respectively. If a modified shear method is not used, the predicted failure load is 97.0 kip for a measured-to-predicted ratio of 1.18, indicating that this method is slightly conservative. Using the William and Harris modified shear method, the predicted failure load is 105 kip for a measured-to-predicted ratio of 1.09, indicating that the method is slightly conservative.

Similarly, using the Blodgett modified shear method, the predicted failure load is 106 kip for a measured-to-predicted ratio of 1.08, indicating that the method is conservative.

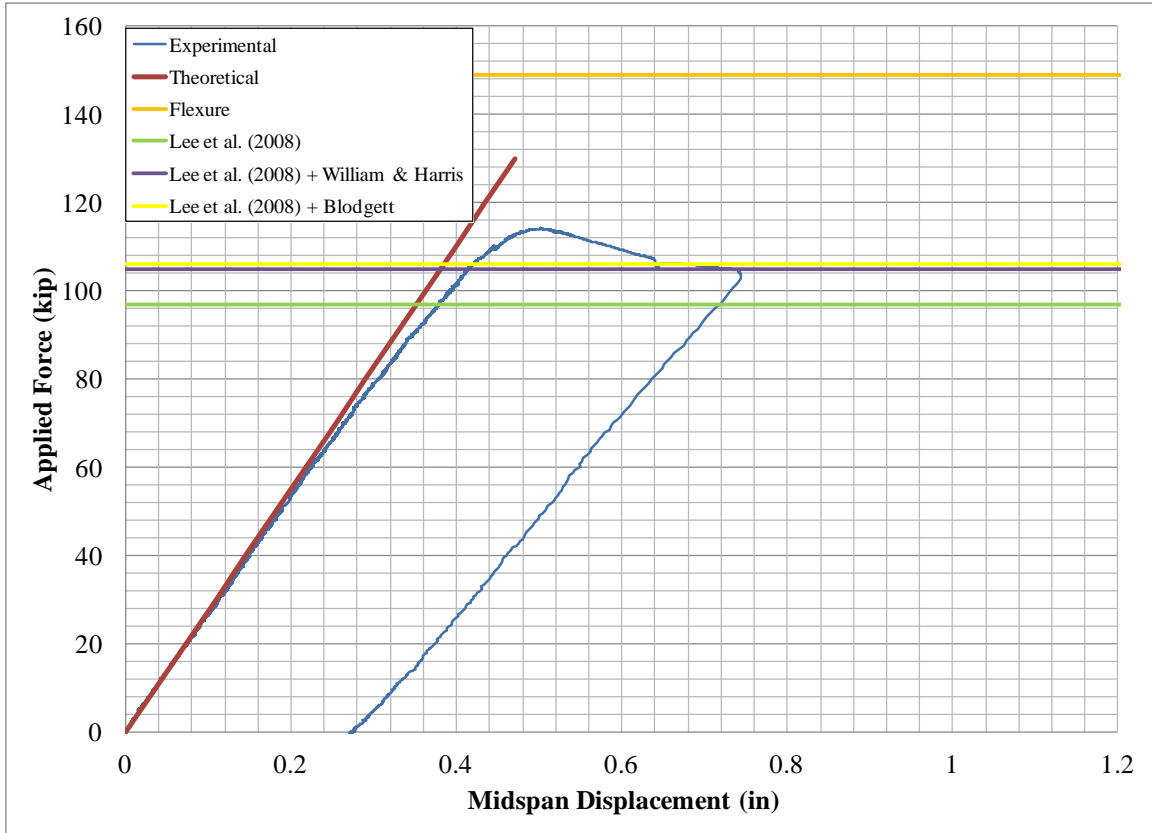


Figure 4-36 “Tapered 5” Lee et al. (2008) Predicted Failure Loads

#### 4.10 Tapered 6

A complete list of graphs for test “Tapered 6” can be found in Appendix J.

**Station 1.** Figure 4-37 indicates that the measured and predicted web shear contributions are 83.5% and 82.6% respectively, for a measured-to-predicted ratio of 1.01 for  $V_{Web}$ . For  $V_{Web^*}$  the measured and predicted web shear contributions are 84.0% and 82.6% respectively, for a measured-to-predicted ratio of 1.02 for  $V_{Web^*}$ . Figure 4-37 also indicates that the measured-to-predicted  $V_{Top Flg}$  contributions are 7.6% and 8.4%, respectively, for a measured-to-predicted ratio of 0.903. Finally, it indicates that the

measured and predicted  $V_{Bot. Flg}$  shear contributions are 8.4% and 9.0%, respectively, for a measured-to-predicted ratio of 0.939.

**Station 2.** Figure 4-37 indicates that the measured and predicted web shear contributions are 79.3% and 78.8% respectively, for a measured-to-predicted ratio of 1.01 for  $V_{Web}$ . For  $V_{Web^*}$  the measured and predicted web shear contributions are 80.1% and 78.8% respectively, for a measured-to-predicted ratio of 1.02 for  $V_{Web^*}$ . Figure 4-37 also indicates that the measured-to-predicted  $V_{Top Flg}$  contributions are 9.8% and 10.3%, respectively, for a measured-to-predicted ratio of 0.957. Finally, it indicates that the measured and predicted  $V_{Bot. Flg}$  shear contributions are 10.1% and 10.9%, respectively, for a measured-to-predicted ratio of 0.923.

#### 4.10.1 Web and Flange Shear Contributions

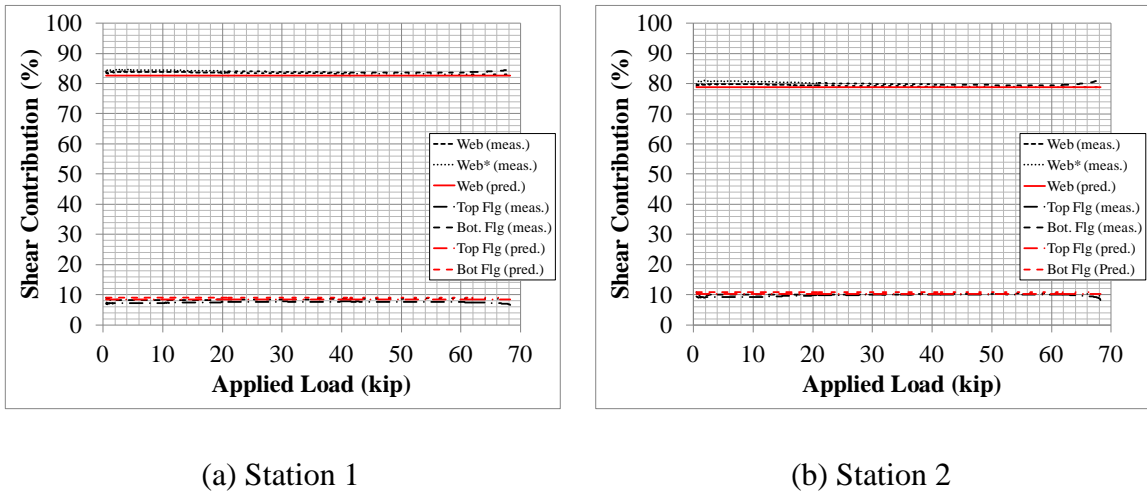


Figure 4-37 “Tapered 6”  $V_{meas.} / V_{pred.}$  (%)

In Figure 4-38,  $V_{meas.} / V_{pred.}$  for each component contributing to the resistance of the applied shear force at Station 1 and Station 2 was computed. At Station 1 the ratios

were:  $V_{Web} = 0.984$ ,  $V_{Web^*} = 1.02$ ,  $V_{Top Flg} = 0.905$ , and  $V_{Bot. Flg} = 0.942$ . At Station 2, the ratios were:  $V_{Web} = 0.989$ ,  $V_{Web^*} = 1.04$ ,  $V_{Top Flg} = 0.976$ , and  $V_{Bot. Flg} = 0.941$ .

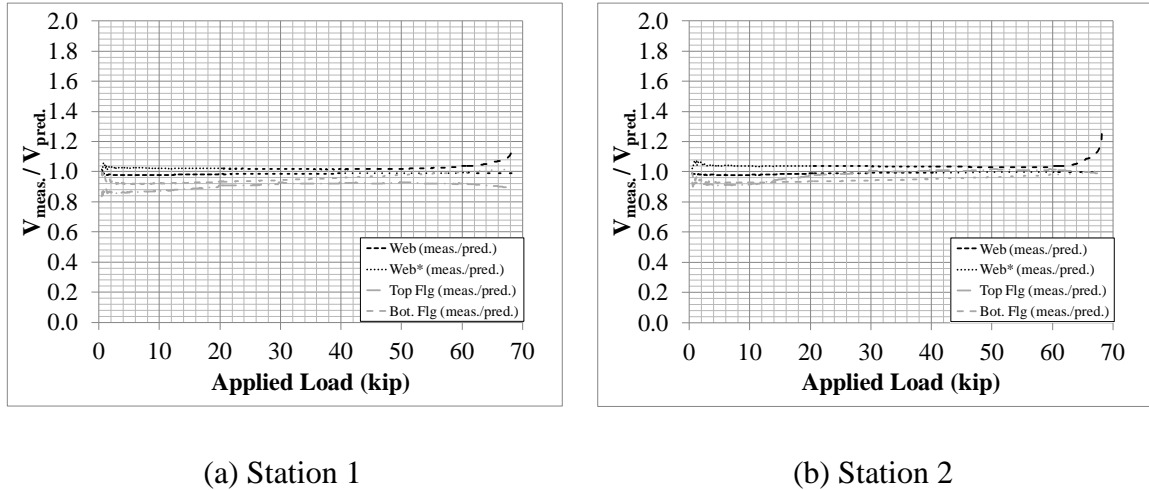


Figure 4-38 “Tapered 6”  $V_{meas.} / V_{pred.}$

#### 4.10.2 Failure Load

Figure 4-39 shows the measured load-displacement curve (shear buckling failure; ultimate load = 68.2 kip) and predicted failure loads using the AISC *Specification* (2010) Section G2. The lines labeled “AISC,” “AISC + Williams and Harris,” and “AISC + Blodgett” are the predicted failure loads without using modified shear, using the Williams and Harris (1957) modified shear, and using the Blodgett (1966) modified shear method, respectively. If a modified shear method is not used, the predicted failure load is 35.1 kip for a measured-to-predicted ratio of 1.94, indicating that this method is very conservative. Using the William and Harris modified shear, the predicted failure load is 31.6 kip for a measured-to-predicted ratio of 2.16, indicating that the method is very conservative. Similarly, using the Blodgett modified shear method, the predicted failure load is 31.3 for a measured-to-predicted ratio of 2.18, indicating that the method is very conservative.



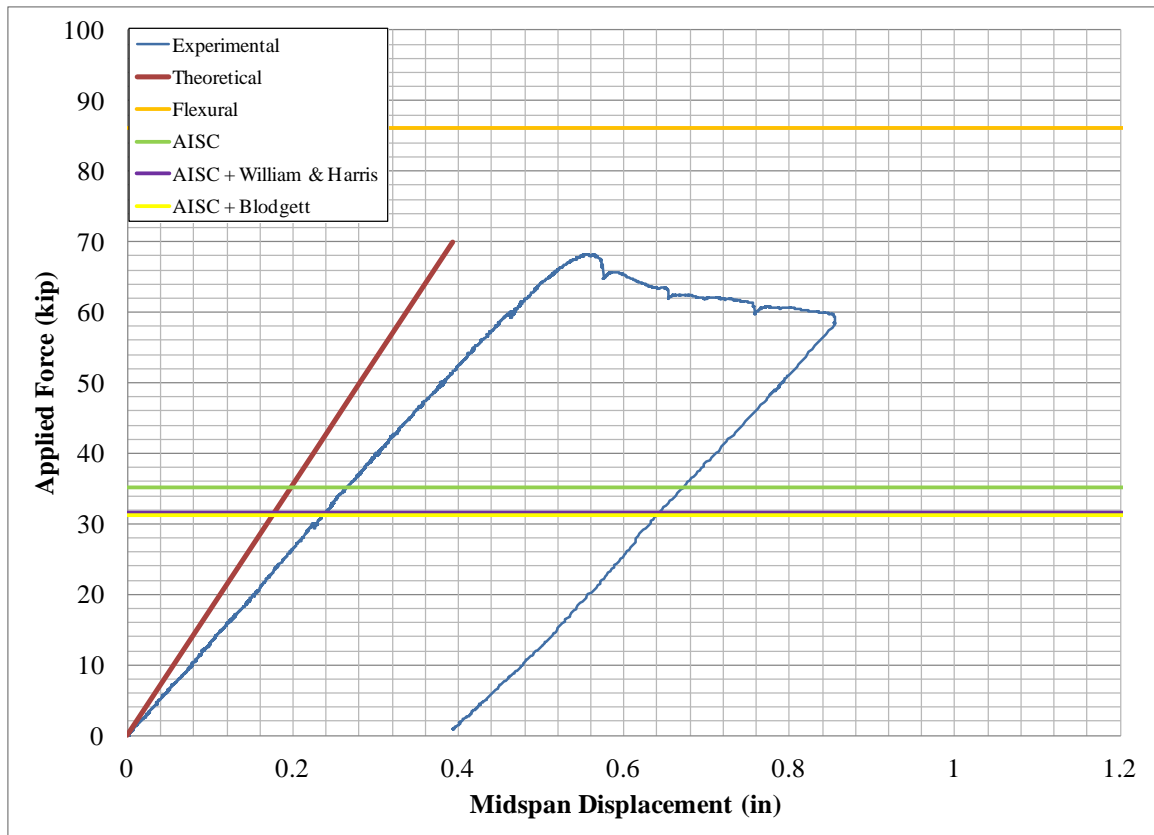


Figure 4-39 “Tapered 6” AISC Predicted Failure Loads

Figure 4-40 shows the measured load-displacement curve (shear buckling failure  $\frac{1}{2}$  ft near the support; ultimate load = 68.2 kip) and predicted failure loads using the method proposed by Lee et al. (2008). The lines labeled “Lee et al. (2008),” “Lee et al. (2008) + William and Harris,” and “Lee et al. (2008) + Blodgett” are at the predicted failure loads without using modified shear, using the William and Harris (1957) modified shear, and using the Blodgett (1966) modified shear method, respectively. If a modified shear method is not used, the predicted failure load is 82.0 kip for a measured-to-predicted ratio of 0.832, indicating that this method is unconservative. Using the William and Harris modified shear method, the predicted failure load is 63.8 kip for a measured-to-predicted ratio of 1.07, indicating that the method is slightly conservative. Similarly,

using the Blodgett modified shear method, the predicted failure load is 62.3 kip for a measured-to-predicted ratio of 1.10, indicating that the method is slightly conservative.

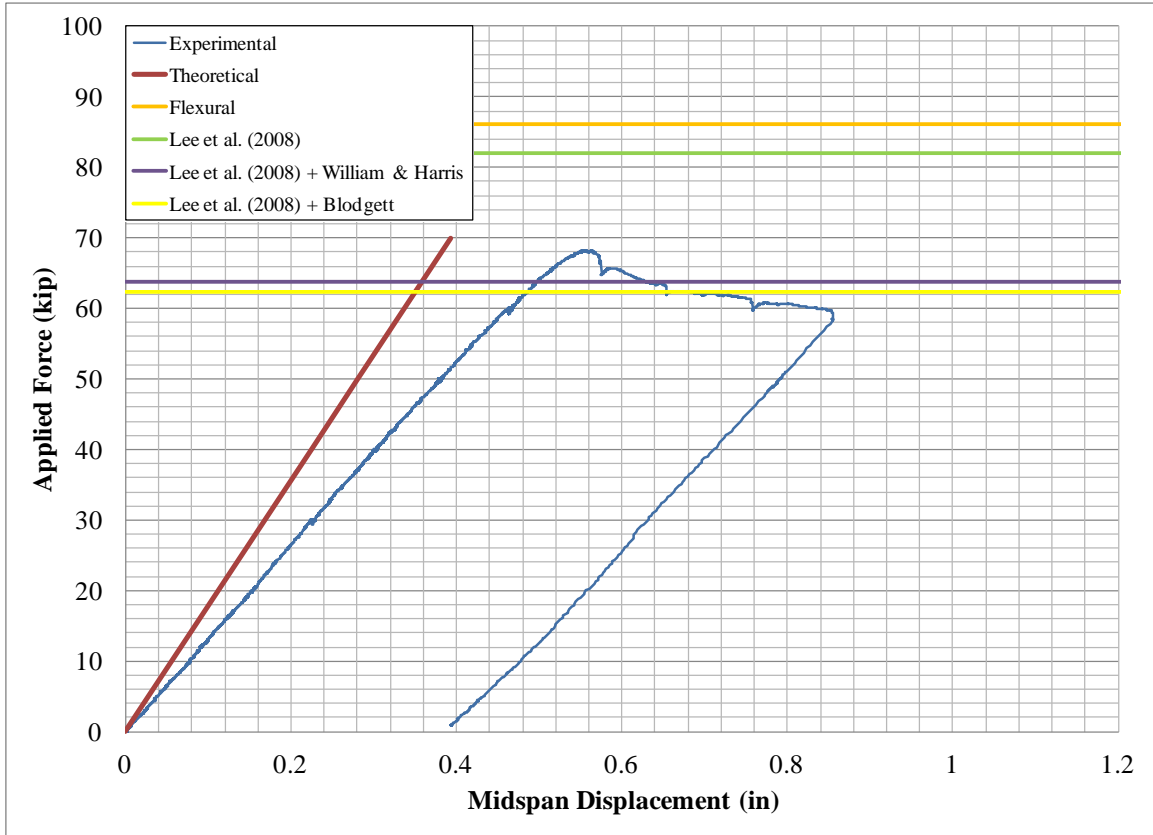


Figure 4-40 “Tapered 6” Lee et al. (2008) Predicted Failure Loads

#### 4.11 Prismatic 1

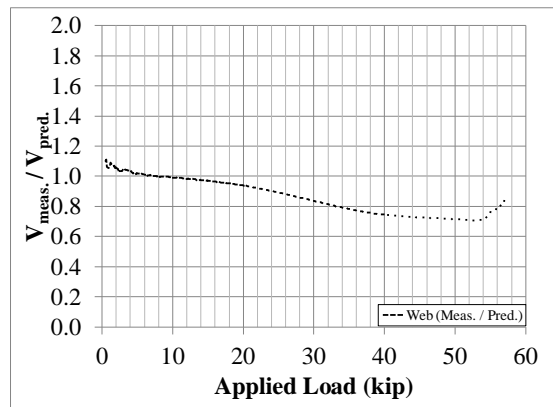


Figure 4-41 “Prismatic 1”  $V_{meas.} / V_{pred.}$

In Figure 4-38,  $V_{meas.} / V_{pred.}$  for each component contributing to the resistance of the applied shear force at Station 1 and Station 2 was computed. At Station 1 the ratio was:  $V_{Web*} = 0.908$ .

#### 4.11.1 Failure Load

Figure 4-42 shows the measured load-displacement curve (flexural flange local buckling failure near midspan; ultimate load = 57.2) and predicted failure loads using the AISC *Specification* (2010) Section G2 and Lee et al. (2008). Since the member is prismatic, a modified shear force is not applicable. The AISC *Specification* (2010) predicted failure load is 27.3 kip for a measured-to-predicted ratio of 2.09, indicating that this method is very conservative. Because the specimen failed in flexure at a load below the predicted shear failure loads, it is not possible to compare the measured and predicted failure loads. It can only be stated that the Lee et al. (2008) method did not produce an unconservative predicted failure load for this test.

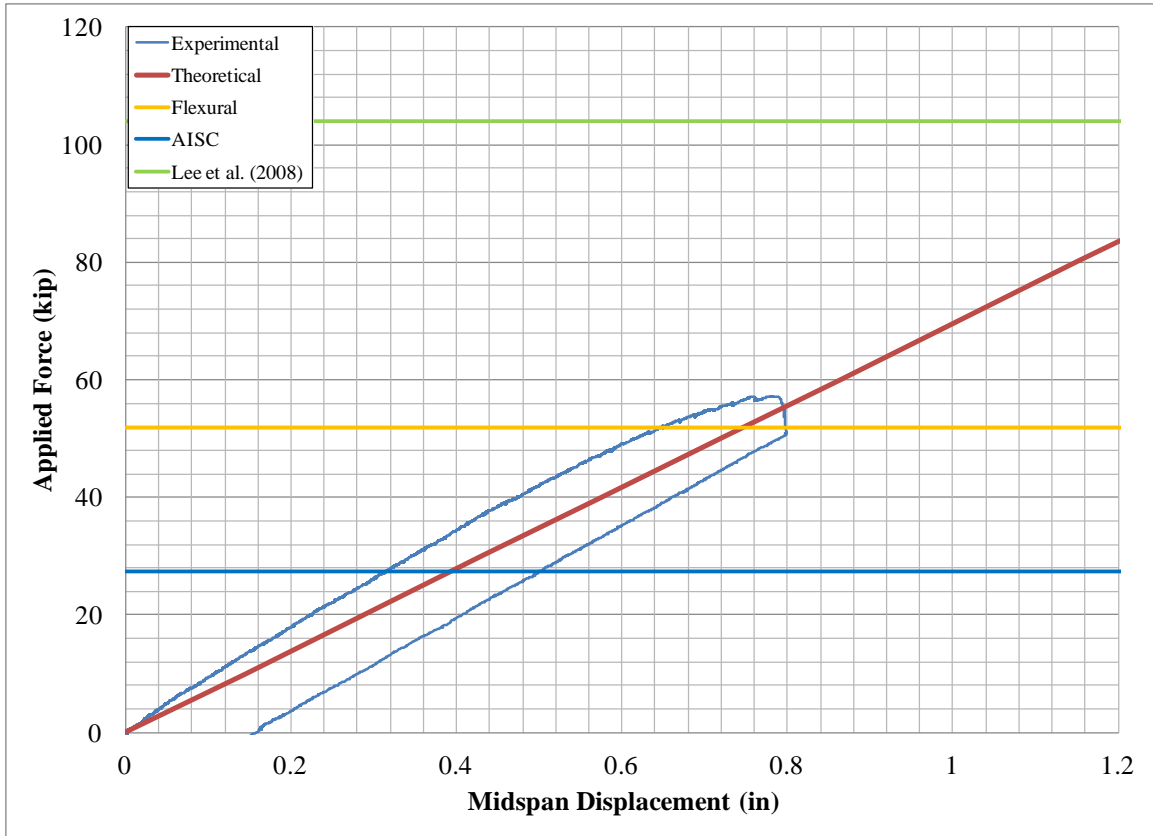
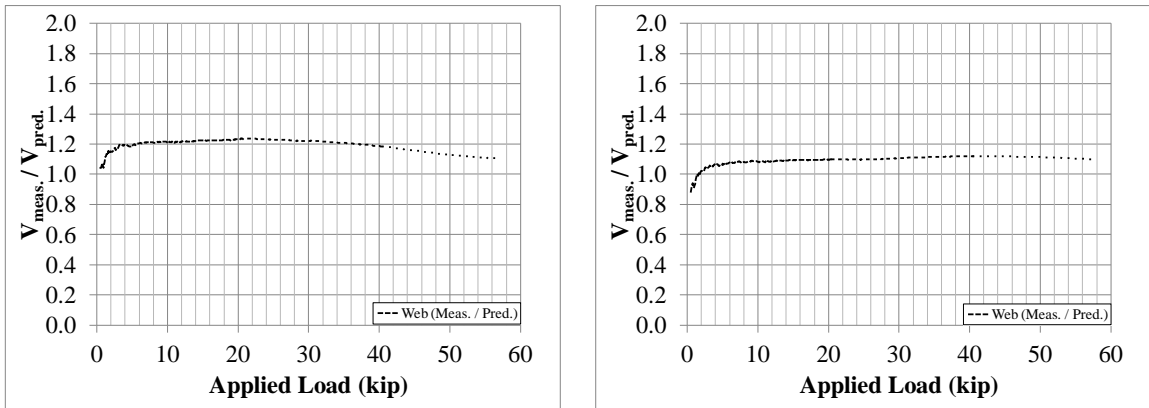


Figure 4-42 “Prismatic 1” Predicted Failure Loads

#### 4.12 Prismatic 2



(a) Station 1

(b) Station 2

Figure 4-43 “Prismatic 2”  $V_{meas.} / V_{pred.}$

In Figure 4-38,  $V_{meas.} / V_{pred.}$  for each component contributing to the resistance of the applied shear force at Station 1 and Station 2 was computed. At Station 1 the ratios were:  $V_{Web*} = 1.22$ . At Station 2, the ratios were  $V_{Web*} = 1.10$ .

#### 4.12.1 Failure Load

Figure 4-42 shows the measured load-displacement curve (flexural flange local buckling failure near midspan; ultimate load = 66.7) and predicted failure loads using the AISC *Specification* (2010) Section G2 and Lee et al. (2008). Since the member is prismatic, a modified shear force is not applicable. The AISC *Specification* (2010) predicted failure load is 29.2 kip for a measured-to-predicted ratio of 2.28, indicating that this method is very conservative. The Lee et al. (2008) predicted failure load is 99.8 kip for a measured-to-predicted ratio of 0.668, indicating that this method is unconservative.

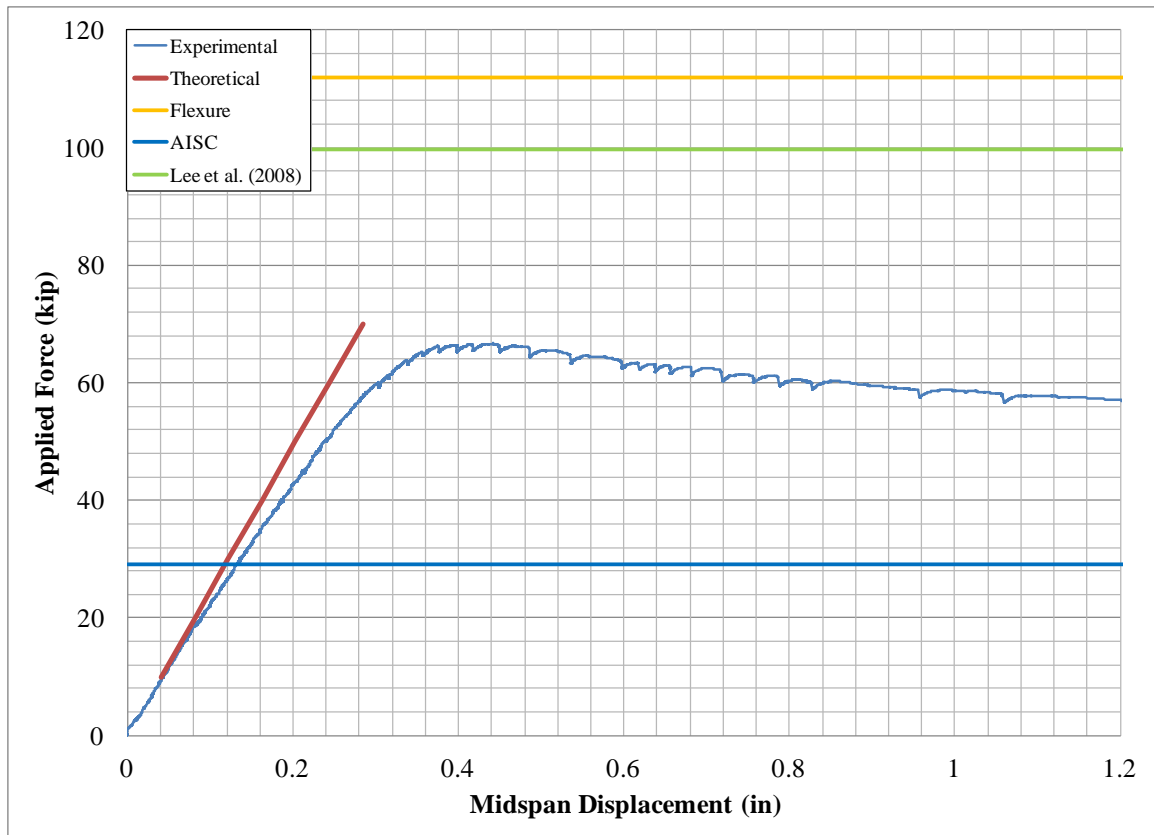


Figure 4-44 “Prismatic 2” Predicted Failure Loads

#### 4.13 Summary of Comparisons

Table 4-1 shows the measured-to-predicted shear force contribution for the web, top flange, and bottom flange at each strain gage station for each tapered specimen. Note that the primary method for computing the web contribution is  $V_{web}$ , while  $V_{web^*}$  is shown as an additional verification. Average measured-to-predicted ratios are shown for the specimens with normal taper angles (with transverse components decreasing the web shear as shown in Figures 1-1 and 1-2) and for all specimens.

The average measured  $V_{web}$  to predicted web shear for the normal taper specimens was 1.01, indicating that the prediction method described in Section 3.1 was very accurate. The COV was only 1.57%, and the worst predictions were within 5%,

indicating that the prediction method was consistent and precise also. The reverse taper specimen (flange transverse components increasing the web shear as shown in Figure 1-3), Taper 6, web shear force contribution predictions were similarly accurate.

For all specimens, the average measured-to-predicted shear contribution was 1.00 (COV=7.75%) and 1.00 (COV=11.6%) for the top and bottom flange, respectively, indicating that the predictions were very accurate on the average and fairly precise.

Table 4-1 Tapered Specimens Shear Force Contribution

Specimen	Strain Gage Station	$V_{Web}$	$V_{Web^*}$	$V_{Top\ Flg}$	$V_{Bot. Flg}$
		Meas. / Pred.	Meas. / Pred.	Meas. / Pred.	Meas. / Pred.
Tapered 1a	1	1.01	1.02	0.874	0.978
	2	1.01	1.00	1.01	1.00
Tapered 1b	1	1.01	1.01	0.979	0.969
	2	1.02	0.999	1.00	1.01
Tapered 1c	1	1.00	1.05	0.895	0.890
Tapered 2a	1	1.03	1.04	1.10	0.819
Tapered 2b	1	1.00	1.00	1.00	0.993
	2	1.01	1.01	0.987	0.954
Tapered 2c	1	1.00	1.00	1.00	1.01
	2	1.00	0.978	1.13	1.06
	3	1.05	1.11	1.04	0.743
Tapered 3	1	1.00	0.994	0.924	1.17
	2	0.998	0.970	1.16	1.11
Tapered 4	1	0.984	0.994	0.963	1.21
	2	0.991	0.994	1.04	1.02
Tapered 5	1	1.00	0.995	1.00	1.12
Tapered 6	1	1.01	1.02	0.903	0.939
	2	1.01	1.02	0.957	0.923
Specimens 1a-5 (Normal Tapers)	Average	1.01	1.01	1.01	1.00
	COV (%)	1.57	3.30	7.69	12.0
Specimens 1a-6	Average	1.01	1.01	1.00	1.00
	COV (%)	1.48	3.11	7.75	11.6

The predicted failure loads are divided into three different tables: AISC 2010 *Specifications* for tapered specimens, Table 4-2; Lee et al. (2008) for tapered specimens,

Table 4-3; and both design procedures evaluated together for the prismatic specimens, Table 4-4.

Table 4-2 indicates that the average ratio of measured ultimate strength to that predicted by the AISC *Specification* without use of a modified shear method was 2.36 with a 14.3% COV, indicating the method to be extremely conservative. When the AISC *Specification* web shear strength is used with the Williams and Harris (1957) and Blodgett (1966) modified shear methods, the average measured-to-predicted ratio was 1.55 (18.5% COV) and 1.44 (22.1% COV), respectively, indicating that both of those methods are very conservative also. The COVs listed in this paragraph indicate that the three methods are only moderately precise.

Table 4-2 Tapered Specimens AISC Measured / Predicted Failure Loads

Specimen	Measured Ultimate Strength (kip)	AISC		AISC + William & Harris		AISC + Blodgett	
		Pred. Strength (kip)	Meas. / Pred.	Pred. Strength (kip)	Meas. / Pred.	Pred. Strength (kip)	Meas. / Pred.
Tapered 1a	57.6	30.3	1.90	42.7	1.35	46.3	1.25
Tapered 1b	60.5	30.3	1.99	42.7	1.42	46.3	1.31
Tapered 1c	58.6	30.3	1.93	42.7	1.37	46.3	1.27
Tapered 2a	138	53.4	2.59	101	1.37	113	1.22
Tapered 2b	135	53.4	2.53	101	1.34	113	1.19
Tapered 2c	130	53.4	2.43	101	1.29	113	1.15
Tapered 3	84.6	32.5	2.61	43.5	1.95	44.8	1.89
Tapered 4	85.1	29.9	2.84	44.1	1.93	46.2	1.84
Tapered 5	114	47.5	2.40	60.2	1.90	61.8	1.85
Tapered 6	68.2	35.1	1.94	31.6	2.16	31.3	2.18
Specimen 1a-5 (Normal Tapers)		Average	2.36	Average	1.55	Average	1.44
		COV (%)	14.3	COV (%)	18.5	COV (%)	22.1
Specimen 1a-6		Average	2.32	Average	1.61	Average	1.51
		COV (%)	14.9	COV (%)	20.7	COV (%)	25.1



Table 4-3 indicates that the average ratio of measured ultimate strength to that predicted by Lee et al. (2008) without use of a modified shear method was 1.32 with a 9.57% COV, indicating the method to be conservative. When the Lee et al. (2008) web shear strength is used with the Williams and Harris (1957) and Blodgett (1966) modified shear methods, the average measured-to-predicted ratio was 1.16 (6.77% COV) and 1.15 (6.59% COV), indicating that both of those methods are quite accurate and slightly conservative. The COVs listed in this paragraph indicate that the three methods are precise. For Lee et al. (2008) with the Williams and Harris modified shear, the measured-to-predicted strength ratios ranged from 1.07 to 1.27, so the method was not unconservative for any specimen. The range was similar for Lee et al. with the Blodgett modified shear.

Table 4-3 Tapered Specimens Lee et al. (2008) Measured / Predicted Failure Loads

Specimen	Measured Ultimate Strength (kip)	Lee et al. (2008)		Lee et al. (2008) + William & Harris		Lee et al. (2008) + Blodgett	
		Pred. Strength (kip)	Meas. / Pred.	Pred. Strength (kip)	Meas. / Pred.	Pred. Strength (kip)	Meas. / Pred.
Tapered 2a	138	93.4	1.48	109	1.27	110	1.26
Tapered 2b	135	95.1	1.42	111	1.22	112	1.21
Tapered 2c	130	97.3	1.33	114	1.14	115	1.13
Tapered 3	84.6	72.3	1.17	79.5	1.06	80.0	1.06
Tapered 4	85.1	64.6	1.32	73.6	1.16	74.2	1.15
Tapered 5	114	97.0	1.18	105	1.09	106	1.08
Tapered 6	68.2	82.0	0.832	63.8	1.07	62.3	1.10
Specimen 1a-5 (Normal Tapers)		Average	1.32	Average	1.16	Average	1.15
		COV (%)	9.57	COV (%)	6.77	COV (%)	6.59
Specimen 1a-6		Average	1.25	Average	1.14	Average	1.14
		COV (%)	17.3	COV (%)	6.86	COV (%)	6.28

Table 4-4 shows the measured and predicted results for the two prismatic specimens. Prismatic 1 failed by flange local buckling, so it is not possible to directly compare the measured and predicted shear failure strengths for either the AISC

*Specification* (2010) or Lee et al. (2008) method. However, the measured failure load exceeded the AISC predicted failure load by a factor of 2.09, indicating that the prediction method is very conservative. As for the Lee et al. (2008) method, it can only be said to have *not* unconservatively predicted the Prismatic 1 failure load. Prismatic 2 failed in shear. The AISC method underpredicted the failure load by a factor of 2.28, indicating that the prediction method was extremely conservative. The method by Lee et al. (2008) over predicted the failure load (0.668 measured-to-predicted ratio), so was unconservative for that specimen.

Table 4-4 Prismatic Specimens Measured / Predicted Failure Loads

Specimen	Measured Ultimate Strength (kip)	AISC		Lee et al. (2008)	
		Pred. Strength (kip)	Meas. / Pred.	Pred. Strength (kip)	Meas. / Pred.
Prismatic 1	57.2	27.3	NA	104	NA
Prismatic 2	66.7	29.2	2.28	99.8	0.668

## Chapter 5 Conclusions

### 5.1 Web and Flange Shear Contributions

The first primary objective of this research is to investigate the internal force distribution in tapered members to determine if the web resists the portion of the shear predicted using a modified shear approach such as those proposed by Williams and Harris (1957) or Blodgett (1966). Because the method by Williams and Harris is more consistent with basic mechanics of materials and because it provided more accurate predictions of the web shear, its predictions are shown in this section. Table 5-1 shows that the average ratio of measured-to-predicted web shear for every measurement station in this study was 1.01 with a COV of 1.48%. It is concluded that the Williams and Harris (1957) method very accurately predicted the web shear, with very small scatter in the data, so it is recommended for design use.

Table 5-1 Summary of Web Shear Prediction Accuracy

Specimen	Station	$V_{Web}$ Measured / Predicted
Tapered 1a	1	1.01
	2	1.01
Tapered 1b	1	1.01
	2	1.02
Tapered 1c	1	1.00
Tapered 2a	1	1.03
Tapered 2b	1	1.00
	2	1.01
Tapered 2c	1	1.00
	2	1.00
	3	1.05
Tapered 3	1	1.00
	2	0.998
Tapered 4	1	0.984
	2	0.991
Tapered 5	1	1.00
Tapered 6	1	1.01
	2	1.01
Average		1.01
COV (%)		1.48

## 5.2 Ultimate Shear Strength of Tapered Members

The second primary objective of this research is to determine an accurate method for checking tapered member shear strength. Table 5-2 provides a summary of the measured and predicted failure loads for the tapered specimens that failed by shear buckling. Each predicted strength is the midspan point load which results in  $V_{WebApplied} = V_n$ , computed using the references indicated in Table 5-3.

Predictions generated using the AISC *Specification* Section G2 without a modified shear approach were very conservative, with an average measured-to-predicted ratio of 2.32. If the AISC *Specification* Section G2 is used with a modified shear approach, the predictions are still quite conservative, with an average measured-to-

predicted ratio of 1.61. Predictions generated using the equations proposed by Lee et al. (2008) combined with Williams and Harris (1957) were accurate and slightly conservative, with an average measured-to-predicted ratio of 1.14 (COV=6.86%). Because this method is slightly conservative and the most accurate of the methods studied it is recommended for design use. (Lee et al. (2008) combined with Blodgett (1966) is approximately as accurate, but the method by Blodgett (1966) is less consistent with fundamental mechanics.)

Table 5-2 Summary of Shear Strength Measurements and Predictions

Specimen	Measured Ultimate Strength (kip)	AISC		AISC + William & Harris		Lee et al. (2008) + William & Harris	
		Predicted Strength (kip)	Meas. / Pred.	Predicted Strength (kip)	Meas. / Pred.	Predicted Strength (kip)	Meas. / Pred.
Tapered 2a	138	53.4	2.59	101	1.37	109	1.27
Tapered 2b	135	53.4	2.53	101	1.34	11	1.22
Tapered 2c	130	53.4	2.43	101	1.29	114	1.14
Tapered 3	84.6	32.5	2.61	43.5	1.95	79.5	1.06
Tapered 4	85.1	29.9	2.84	44.1	1.93	73.6	1.16
Tapered 5	114	47.5	2.40	60.2	1.90	105	1.09
Tapered 6	68.2	35.1	1.94	31.6	2.16	63.8	1.07
		Average:	2.32	Average:	1.61	Average:	1.14
		COV (%):	14.9	COV (%):	20.7	COV (%):	6.86

Table 5-3 Shear Strength Prediction Methods

Method	$V_{WebApplied}$	$V_n$
AISC	Entire Shear	AISC <i>Specification</i> (2010) Section G2
AISC + William & Harris	Modified shear per Williams and Harris (1957)	AISC <i>Specification</i> (2010) Section G2
Lee et al. (2008) + William & Harris	Modified shear per Williams and Harris (1957)	Lee et al. (2008)

### **5.3 Ultimate Shear Strength of Prismatic Members**

Only one prismatic specimen in this study failed by shear (Prismatic 2) and its failure load was 66.7 kip. The AISC *Specification* (2010) Section G2 predicted failure load was 29.2 kip for a measured-to-predicted ratio of 2.28. It is not surprising that the AISC *Specification* Section G2 method is conservative because it uses the shear buckling load as the nominal strength even though significant postbuckling strength of long panels has been reported by Lee et al. (2008). The method by Lee et al. (2008) predicted a 101 kip failure load, which was on the unconservative side—measured-to-predicted ratio = 0.663. However, Lee et al. (2008) reported that their method very accurately predicted the measured failure load for a test specimen. It also very accurately matched the failure loads computed using sophisticated geometric and material nonlinear finite element analysis for a large database of hypothetical plate girders. As of the completion of the current study, there is inadequate evidence to allow a conclusion to be made except to say that the AISC *Specification* Section G2 method appears to be very conservative and that significant postbuckling strength appears to exist even for unstiffened panels such as the ones tested in this study.

### **5.4 Flexural Strength**

Investigation of the flexural strength of tapered members is not within the scope of the project, but a MBMA 2011 Researchers Symposium attendee asked whether or not the use of a modified shear approach affects the flexural design. The question was (paraphrase): “The flanges are already resisting the moment, so how can they also be used to help resist the shear?”

The modified shear procedure is a refinement and recognition of the flange stresses, not a method that seeks to make the flanges perform an additional duty, as explained in the following paragraphs.

Consider the flange stresses computed when checking shear and flexure using the current method (entire shear resisted by the web) and a modified shear method. For the sake of discussion, the member is slender for flexure so the AISC *Specification* (2010) Section F5 applies. The  $R_{pg}$  and  $\Omega$  factors are left out because they are not relevant.

Current Method: when comparing the required and available flexural strengths, one is comparing the applied stress  $M / S_x$  (parallel to the longitudinal axis) to the buckling or yield stress. This is not technically correct for a tapered member because the flange principal stress,  $M / (S_x \cos(\theta_{Taper} / 2))$  parallel to the flange, should actually be compared to the buckling or yield stress. However, the error is insignificant because  $M / S_x$  is practically identical to the principal stress for taper angles used by MBMA companies. The quantity  $1 / \cos(\theta_{Taper} / 2)$  is almost unity—ranging from 1.001 to 1.009.

Modified Shear Method: Using the modified shear approach, the engineer recognizes that the flange principal stress is  $M / (S_x \cos(\theta_{Taper} / 2))$ , parallel to the flange. The vertical component of the flange stress resultant works with the web to resist the shear. The longitudinal component of the flange stress is practically equal to the principal stress, so the flexural unity check is unaffected by the choice between them. Interestingly, basic trigonometry results for the maximum taper angle can help to understand why the transverse component is able to offer a significant offset of the shear

while the longitudinal component is practically identical to the resultant:  
 $\sin(7.5^\circ) = 0.131$  and  $\cos(7.5^\circ) = 0.991$ .

The three identical “Tapered 1” specimens each failed by compression flange local buckling (FLB), so they provide experimental evidence. The measured failure loads for those specimens were 57.6 kip, 60.5 kip, and 58.6 kip and the predicted flexural failure load (AISC *Specification* (2010) Section F5) was 56.6 kip. The average measured-to-predicted flexural failure ratio is 1.04 with a 2.5% COV, indicating that the flexural strength was very accurately predicted using the AISC *Specification* Section F5 FLB equations without considering whether or not part of the flange stress also served to resist some of the shear force. Each of the three identical “Tapered 2” specimens, none of which failed by flexure, had a measured failure load within 10% of the flexural failure load predicted using Section F5. None of the other specimens provide useful data toward answering this question.

Therefore, the investigators see no reason to modify the flexural strength calculations and recommend continuing using the AISC *Specification* and AISC *Design Guide 25* flexural calculation methods unless other research indicates otherwise.



## Chapter 6 Recommendations for Future Research

Future research needs to be taken to verify the accuracy of the Lee et al. (2008) method for prismatic built-up plate girders with long shear panels by experimental laboratory work. A larger data base might verify that Lee et al. (2008) will perform satisfactory in all design cases unlike the “Prismatic 2” specimen in the current study. The experimental test specimens would be supported by finite element analysis in the hopes of either supporting or refuting the design procedures proposed by Lee et al. (2008). Note that the MBMA initial out-of-flat tolerance ( $h/72$ ) is larger than that used by Lee et al. ( $h/12$ ) to develop their initial imperfection adjustment factor,  $R$ , discussed in Section 1.2.2. It might be necessary to use a smaller  $R$  factor for MBMA members.

The recommended study mentioned above should further investigate the post-buckling effect of long web panels and the mechanics behind it. A dense distribution of rosette strain gages could be installed to check the theory proposed by Lee et al. (1999) that re-distribution of stresses does occur after initial buckling and principal compressive stresses do increase near support conditions.

## Appendices

## Appendix A Tapered 1a Results

PROJECT: Metal Building Manufacturers Association  
TEST NAME: Tapered 1a  
TEST DATE: December 3, 2010

### MOMENT END PLATE CONNECTION DESCRIPTION:

Nominal Yield Stress	55 ksi
Gage	3.5 in.
Width	8 in.
Thickness	1 in.
Bolt Hole Locations	2.00 in., 13.88 in., 17.88 in., and 21.88 in.
Bolt Hole Size	1.1875 in.
Bolt Type	1.125" x 3.75" A325 Bolts
Bolt Pretension	Snug Tightened
Nuts	1.125" -7 Heavy Hex Nuts (A563 Grade C, C3, D or DH)

### TEST SPECIMEN GEOMETRY:

Total Taper Angle	5.09°
Total Length	15ft
Test Length	7.5 ft
$d_{End}$	12 in.
$d_{Midspan}$	20 in.
$t_w$	0.125 in.
$t_{f,bottom}$	0.3125 in.
$b_{f,bottom}$	6 in.
$t_{f,top}$	0.3125 in.
$b_{f,top}$	6 in.
$t_{stiffener}$	0.5 in.
$a/h_{ave.}$	5.53

Notes: Test length measured from centerline of stiffener to midspan. Total length measured from centerline of stiffener to centerline of stiffener

### LVDT AND STRAIN GAGE LOCATIONS:

LVDT Station 1	22.5 in.
LVDT Station 2	45 in.
LVDT Station 3	67.5 in.
Strain Gage Station 1	36 in.
Strain Gage Station 2	72 in.

Notes: Distances measured from outside face of stiffener. LVDT stations placed on near side of specimen

### EXPERIMENTAL:

Maximum Load	57.6 kips
Failure Mode	Flange local buckling

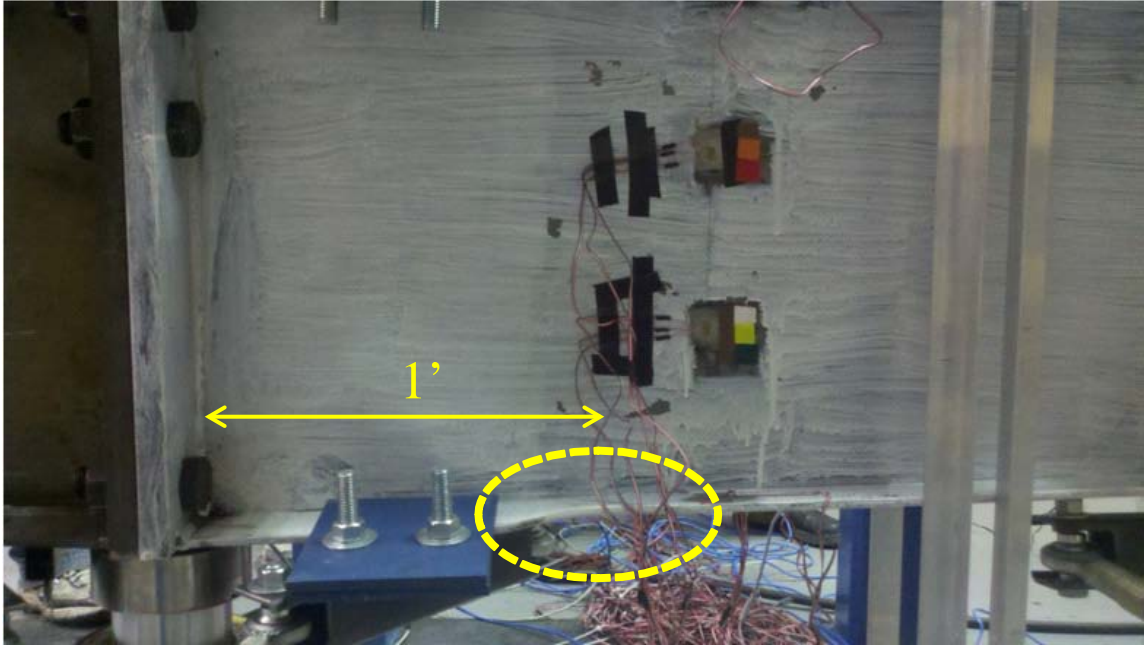


Figure A-1 Flange Local Buckling

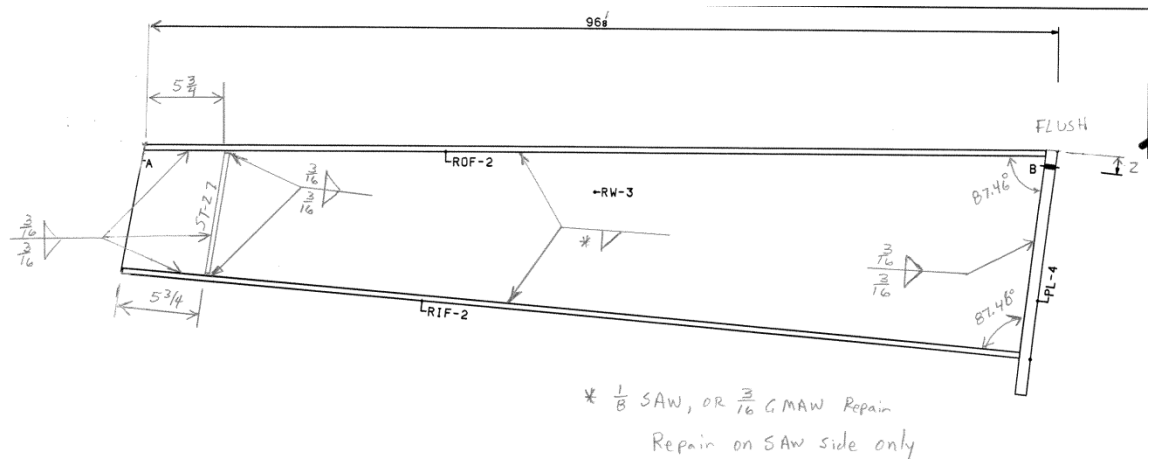


Figure A-2 Dimensions

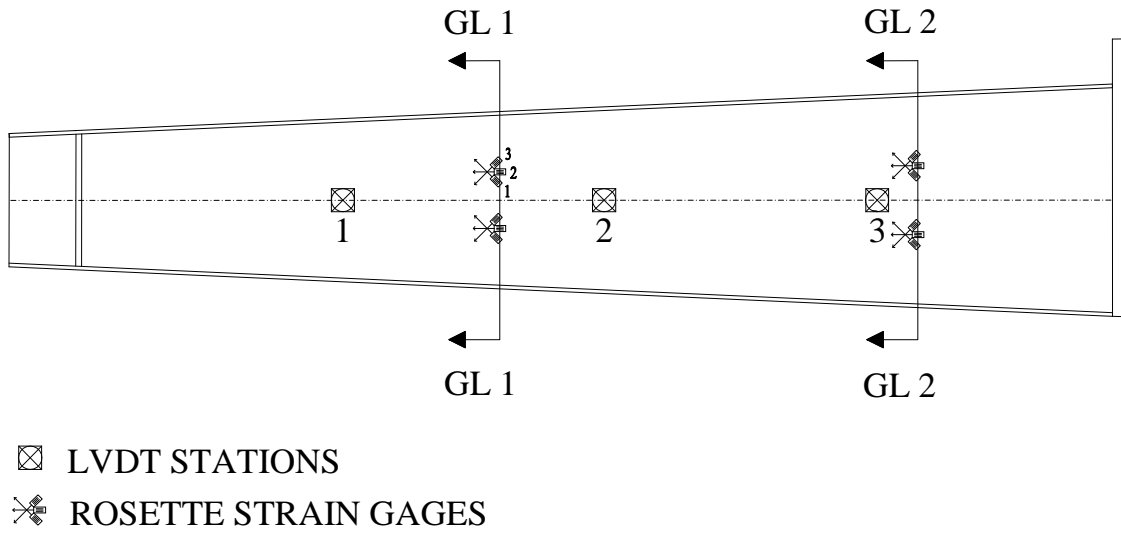


Figure A-3 Near Side Elevation

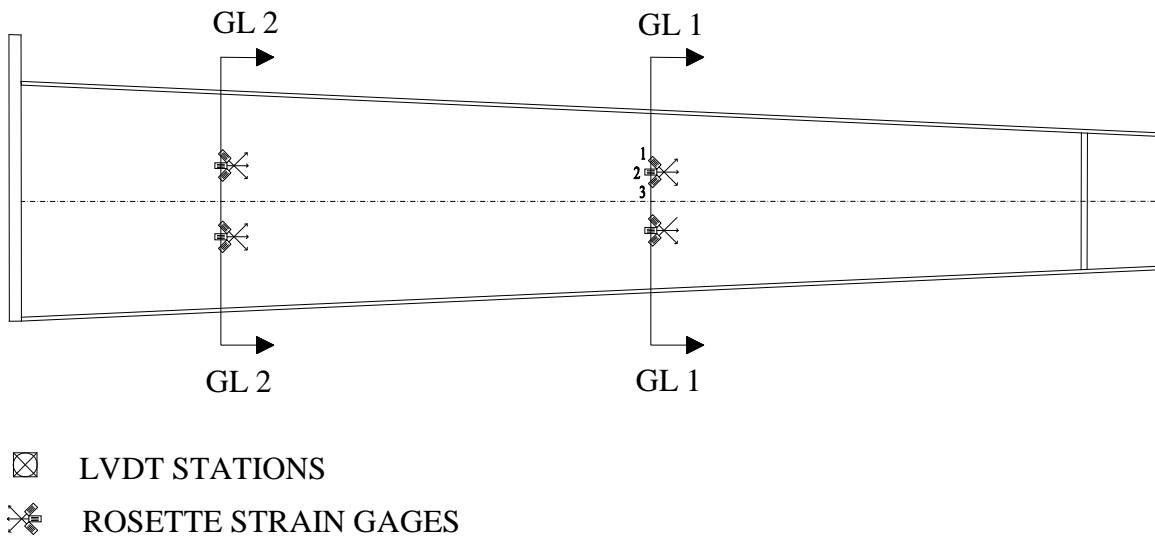


Figure A-4 Far Side Elevation

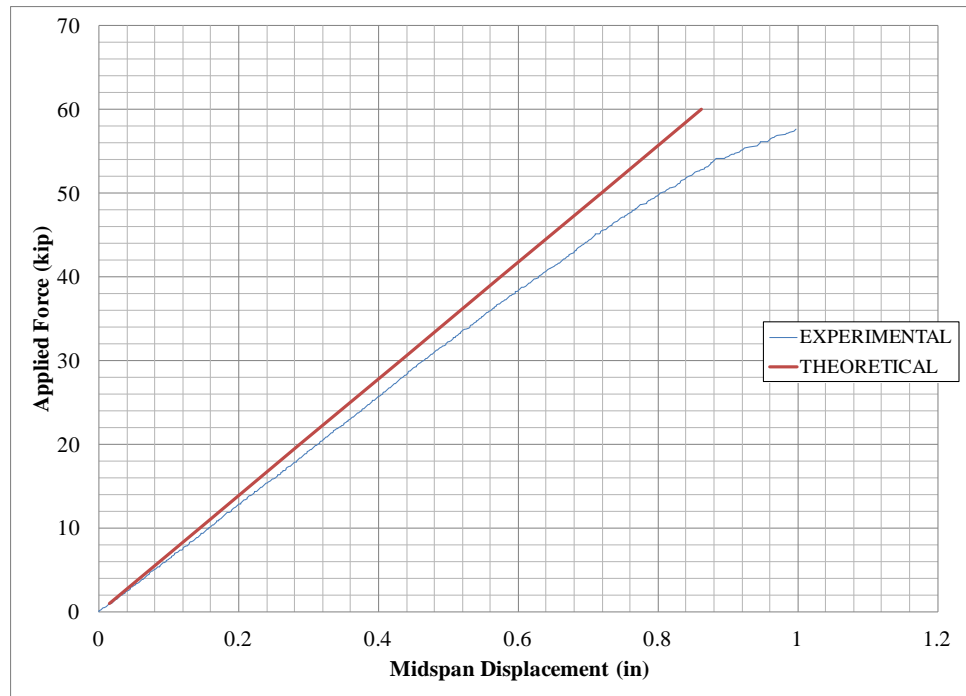


Figure A-5 Applied Force vs. Midspan Displacement

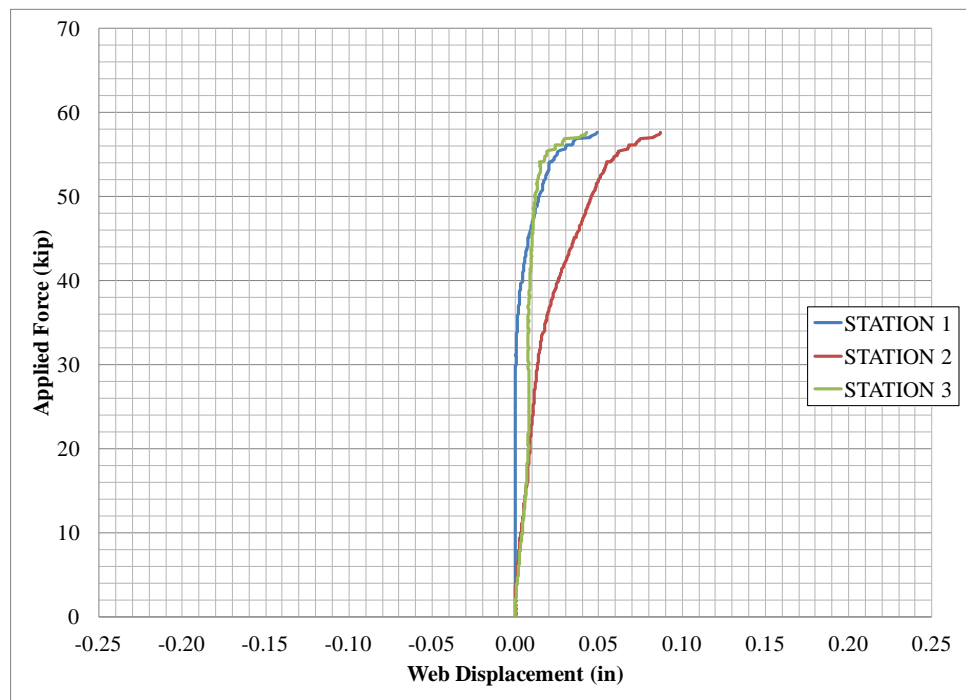
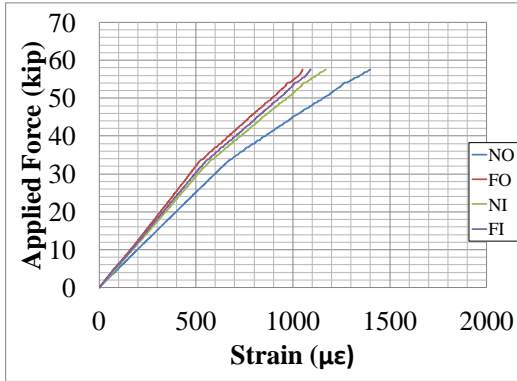
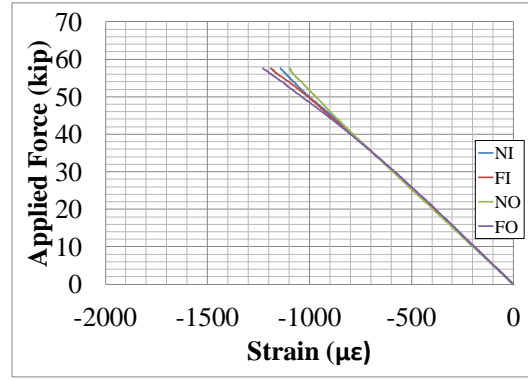


Figure A-6 Applied Force vs. Web Displacement

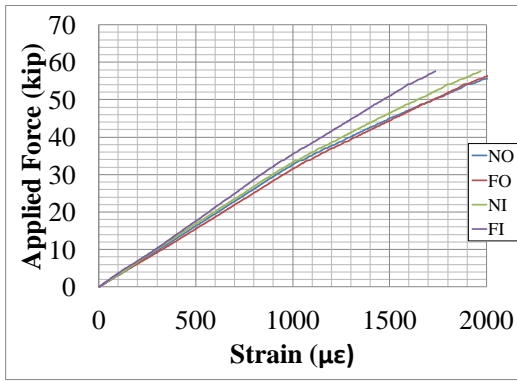


(a) Top Flange

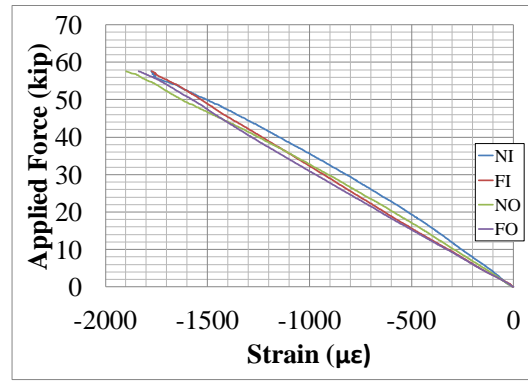


(b) Bottom Flange

Figure A-7 Applied Force vs. Uniaxial Strains at Strain Gage Station 1

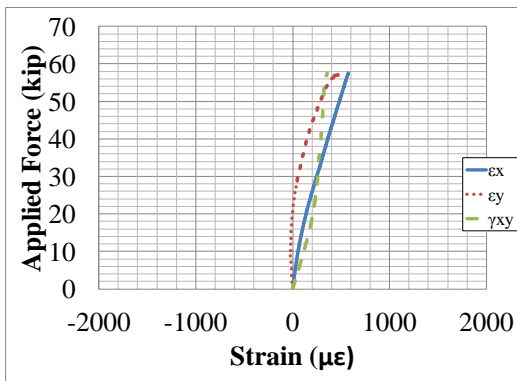


(a) Top Flange

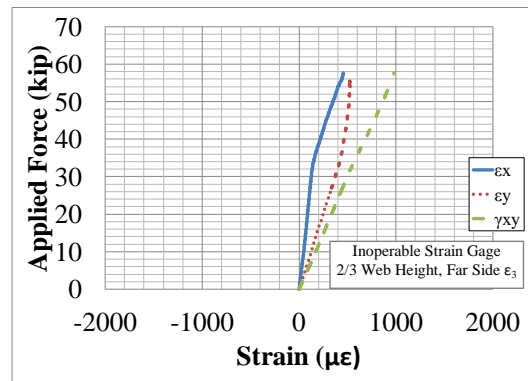


(b) Bottom Flange

Figure A-8 Applied Force vs. Uniaxial Strains at Strain Gage Station 2

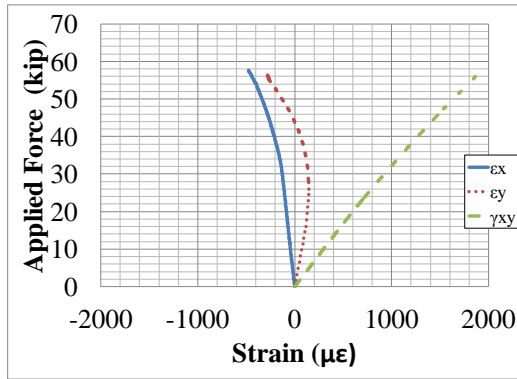


(a) Near Side

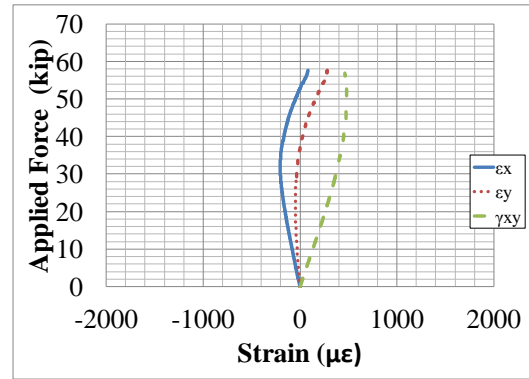


(b) Far Side

Figure A-9 Applied Force vs. 2/3 Web Height Rosette Strains at Strain Gage Station 1

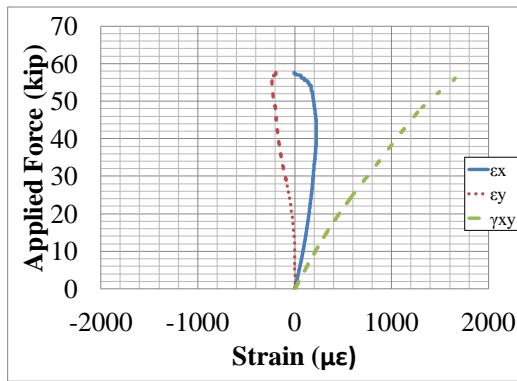


(a) Near Side

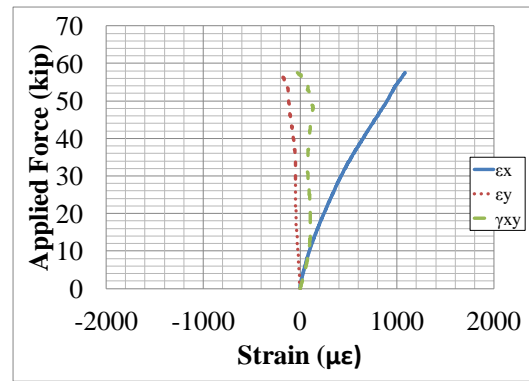


(b) Far Side

Figure A-10 Applied Force vs. 1/3 Web Height Rosette Strains at Strain Gage Station 1

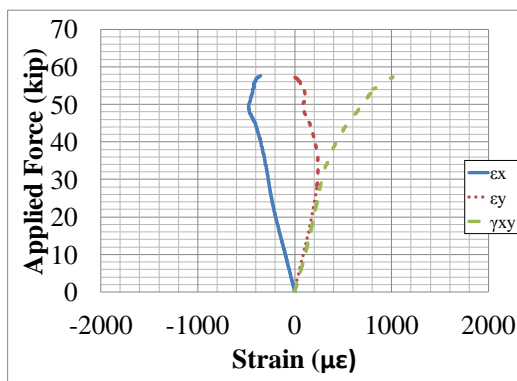


(a) Near Side

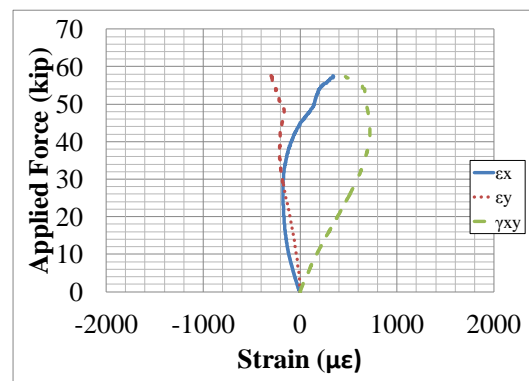


(b) Far Side

Figure A-11 Applied Force vs. 2/3 Web Height Rosette Strains at Strain Gage Station 2



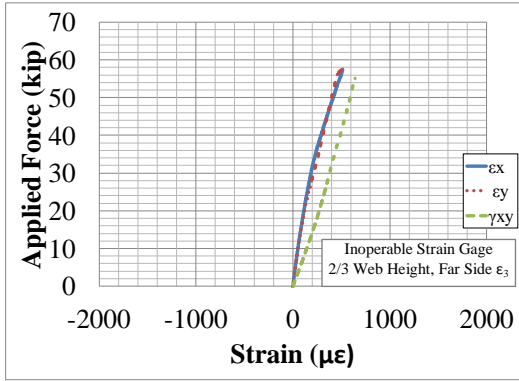
(a) Near Side



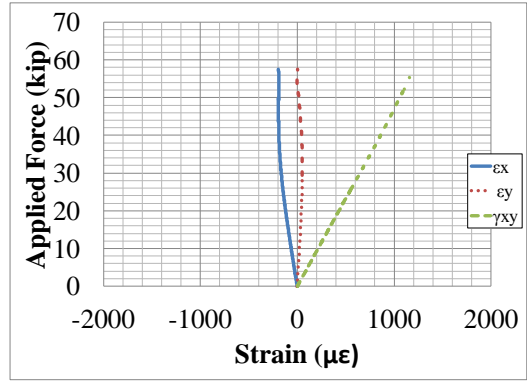
(b) Far Side

Figure A-12 Applied Force vs. 1/3 Web Height Rosette Strains at Strain Gage Station 2



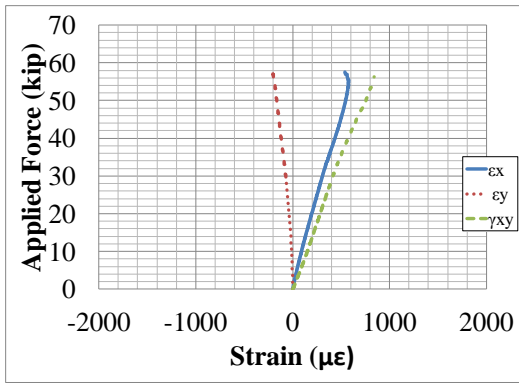


(a) 2/3 Web Height

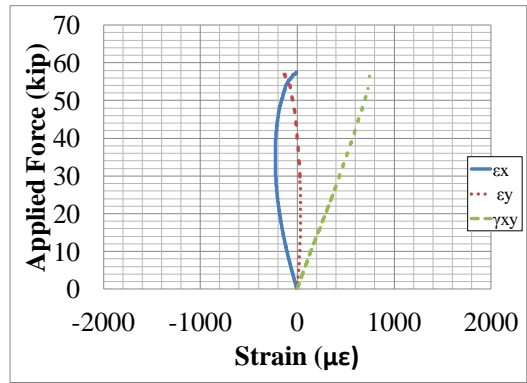


(b) 1/3 Web Height

Figure A-13 Applied Force vs. In Plane Rosette Strains at Strain Gage Station 1



(a) 2/3 Web Height



(b). 1/3 Web Height

Figure A-14 Applied Force vs. In Plane Rosette Strains at Strain Gage Station 2

## Appendix B Tapered 1b Results

PROJECT: Metal Building Manufacturers Association  
TEST NAME: Tapered 1b  
TEST DATE: February 22, 2011

### MOMENT END PLATE CONNECTION DESCRIPTION:

Nominal Yield Stress	55 ksi
Gage	3.5 in.
Width	8 in.
Thickness	1 in.
Bolt Hole Locations	2.00 in., 13.88 in., 17.88 in., and 21.88 in.
Bolt Hole Size	1.1875 in.
Bolt Type	1.125" x 3.75" A325 Bolts
Bolt Pretension	Snug tightened
Nuts	1.125" -7 Heavy Hex Nuts (A563 Grade C, C3, D or DH)

### TEST SPECIMEN GEOMETRY:

Total Taper Angle	5.09°
Total Length	15ft
Test Length	7.5 ft
$d_{End}$	12 in.
$d_{Midspan}$	20 in.
$t_w$	0.125 in.
$t_{f,bottom}$	0.3125 in.
$b_{f,bottom}$	6 in.
$t_{f,top}$	0.3125 in.
$b_{f,top}$	6 in.
$t_{stiffener}$	0.5 in.
$a/h_{ave.}$	5.53

Notes: Test length measured from centerline of stiffener to midspan. Total length measured from centerline of stiffener to centerline of stiffener

### LVDT AND STRAIN GAGE LOCATIONS:

LVDT Station 1	65 in.
LVDT Station 2	71 in.
LVDT Station 3	77 in.
Strain Gage Station 1	35 in.
Strain Gage Station 2	71 in.

Notes: Distances measured from outside face of stiffener. LVDT stations placed on near side of specimen

### EXPERIMENTAL:

Maximum Load	60.5 kip
Failure Mode	Flange local buckling

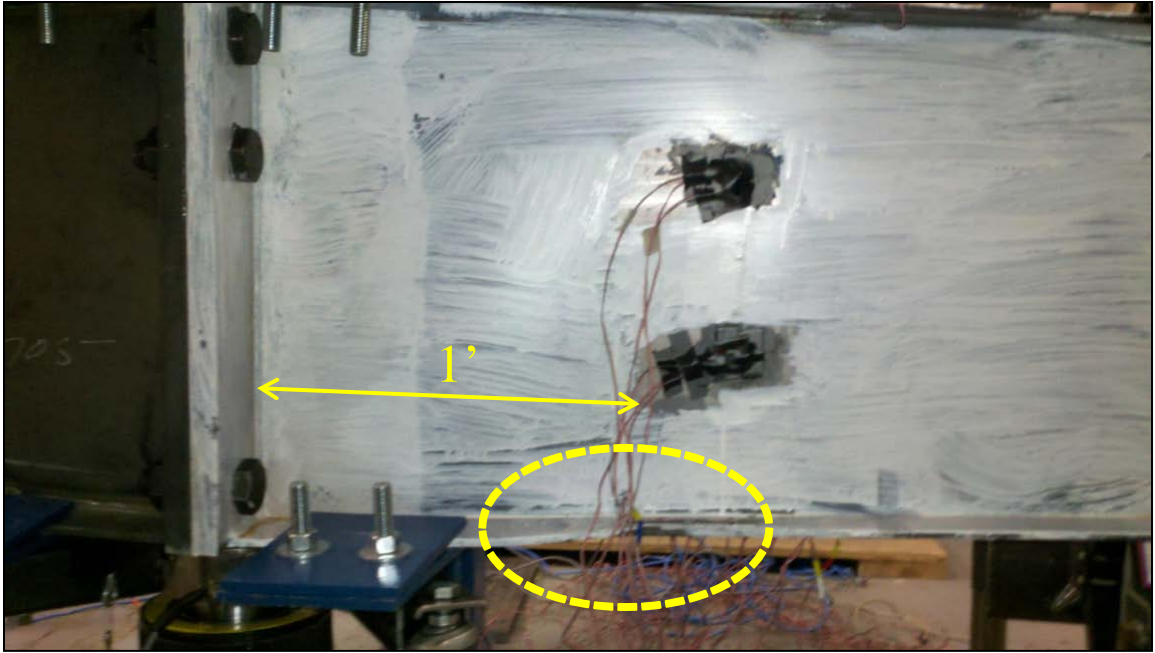


Figure B-1 Flange Local Buckling

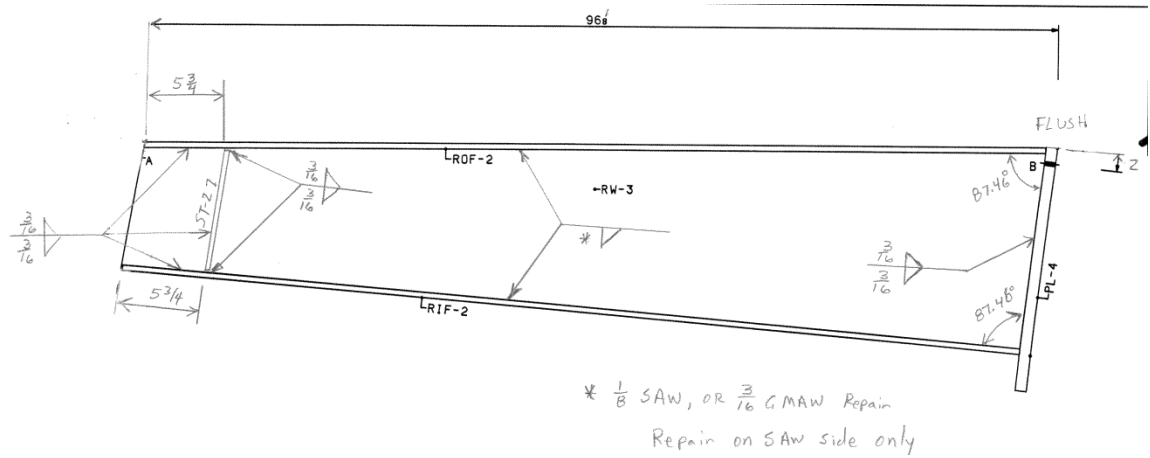


Figure B-2 Dimensions

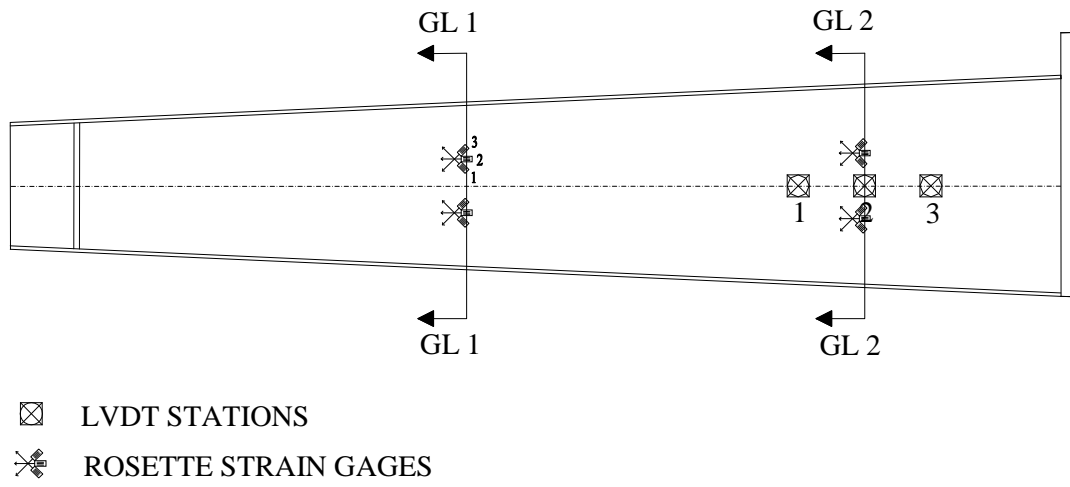
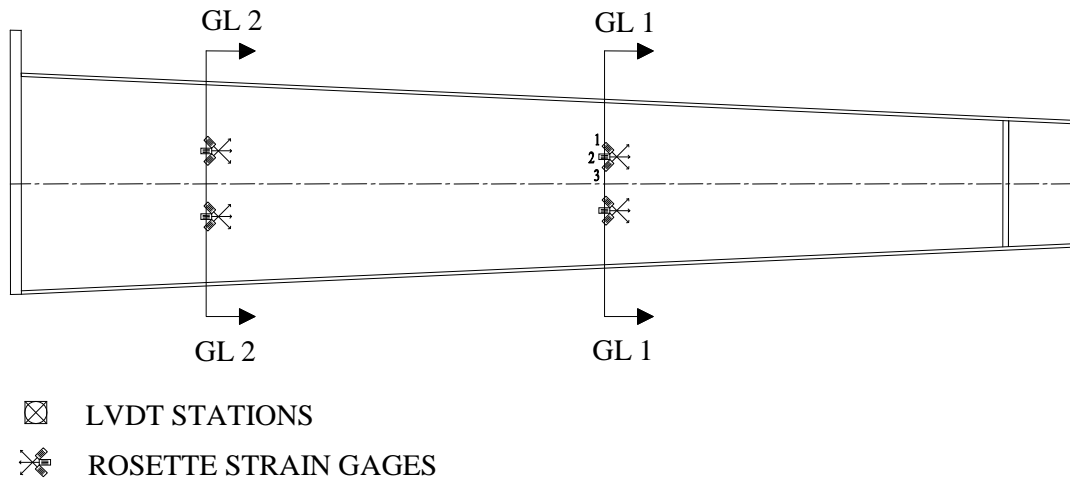


Figure B-3 Near Side Elevation



(d) Figure B-4 Far Side Elevation

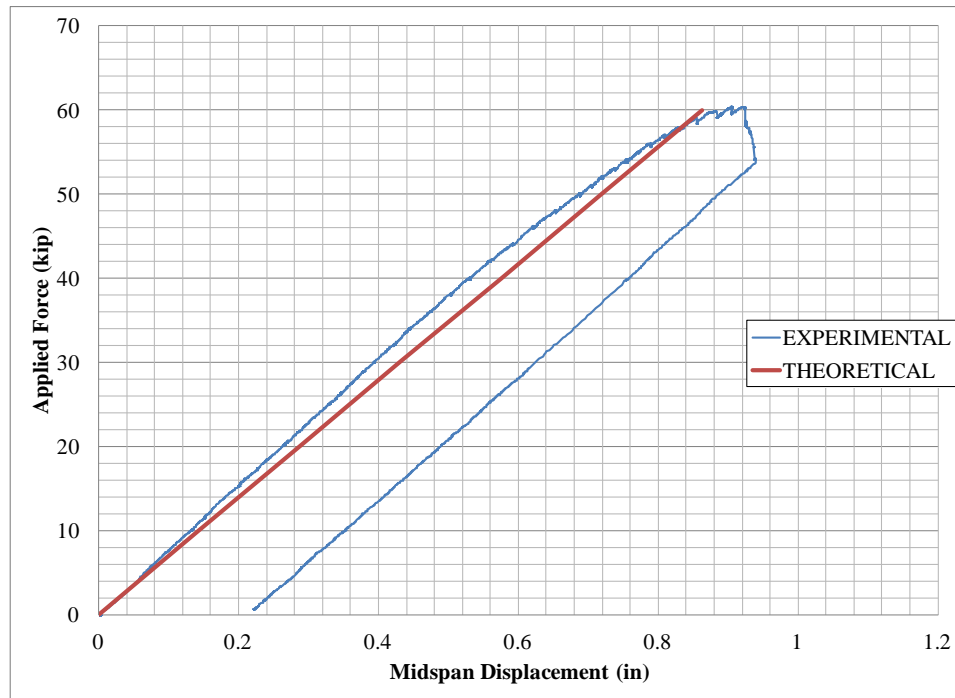


Figure B-5 Applied Force vs. Midspan Displacement

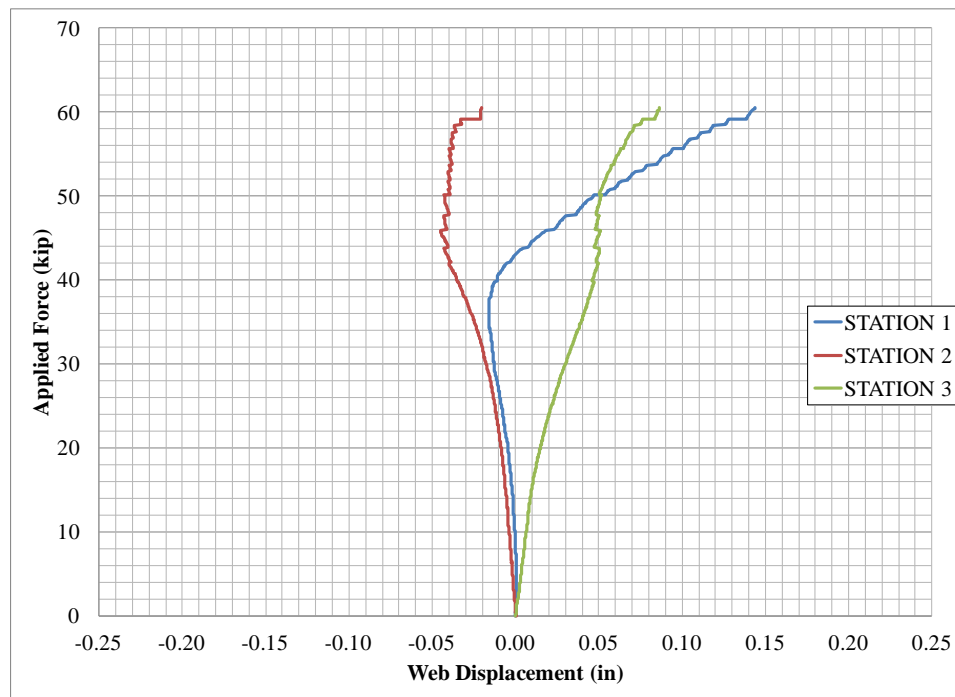
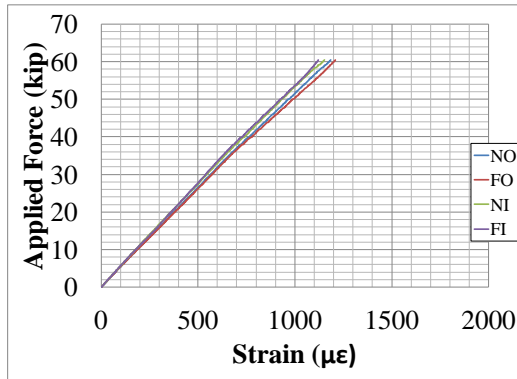
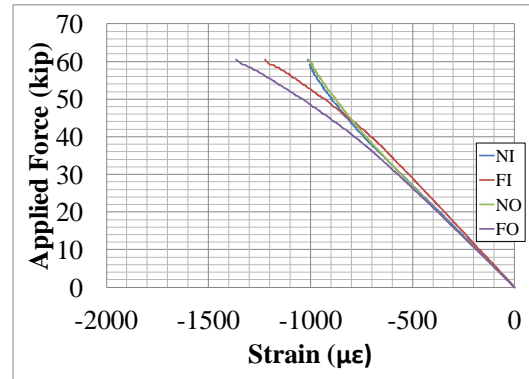


Figure B-6 Applied Force vs. Web Displacement

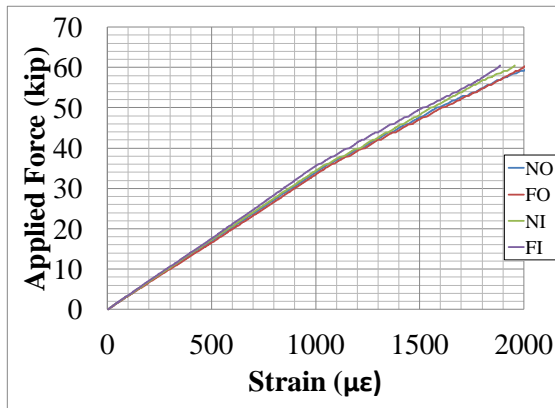


(a) Top Flange

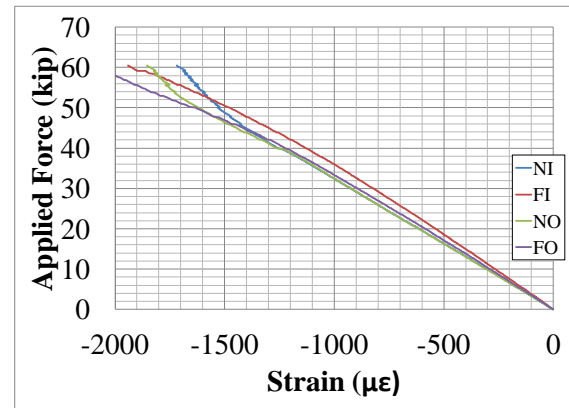


(b) Bottom Flange

Figure B-7 Applied Force vs. Uniaxial Strains at Strain Gage Station 1

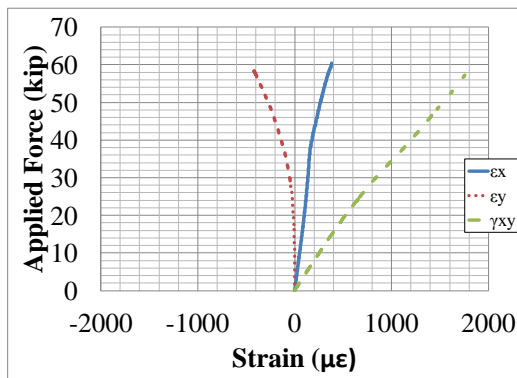


(a) Top Flange

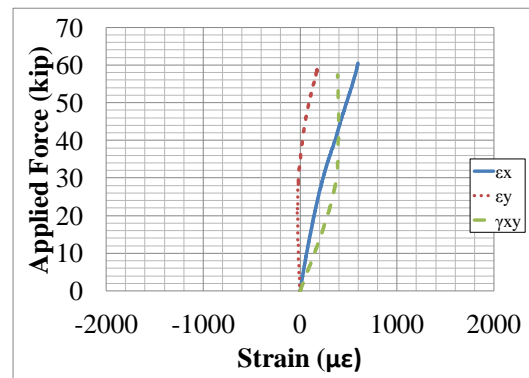


(b) Bottom Flange

Figure B-8 Applied Force vs. Uniaxial Strains at Strain Gage Station 2

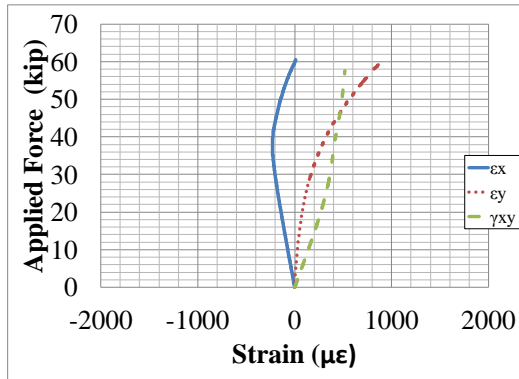


(a) Near Side

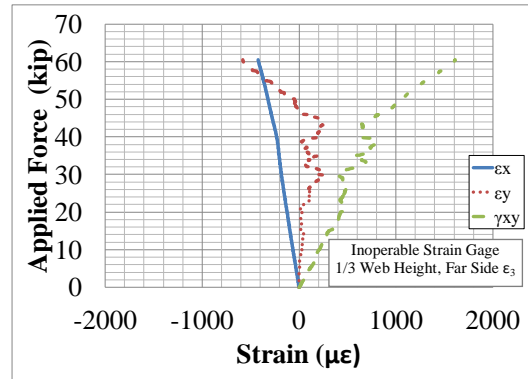


(b) Far Side

Figure B-9 Applied Force vs. 2/3 Web Height Rosette Strains at Strain Gage Station 1

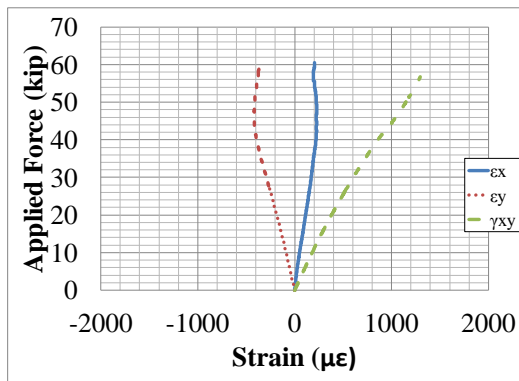


(a) Near Side

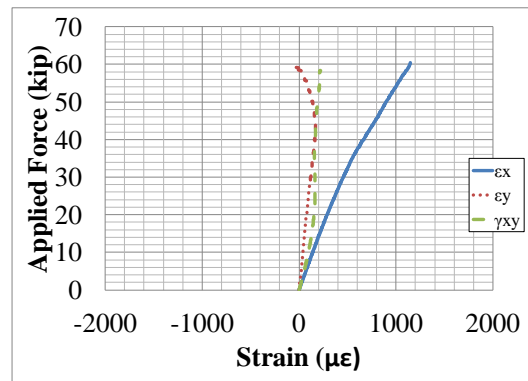


(b) Far Side

Figure B-10 Applied Force vs. 1/3 Web Height Rosette Strains at Strain Gage Station 1

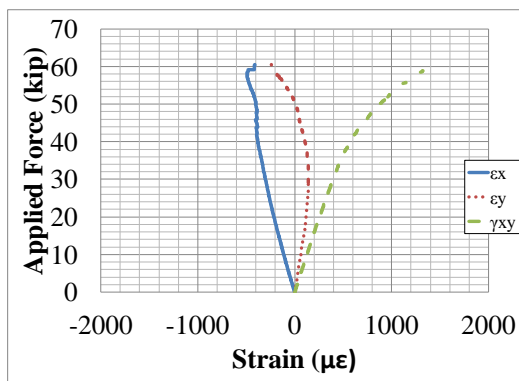


(a) Near Side

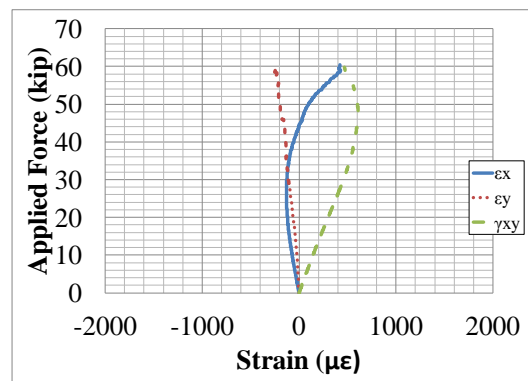


(b) Far Side

Figure B-11 Applied Force vs. 2/3 Web Height Rosette Strains at Strain Gage Station 2

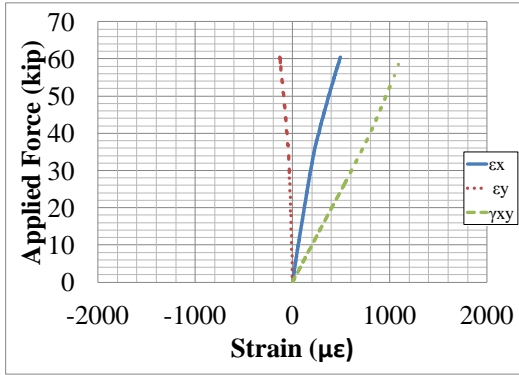


(a) Near Side

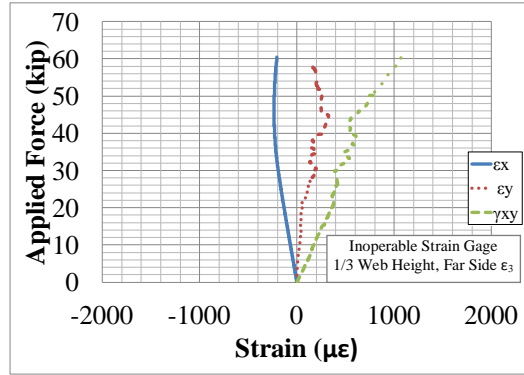


(b) Far Side

Figure B-12 Applied Force vs. 1/3 Web Height Rosette Strains at Strain Gage Station 2

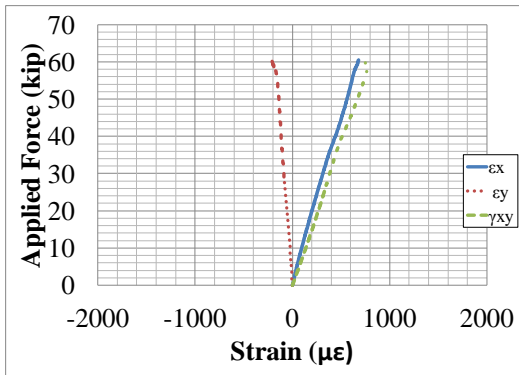


(a) 2/3 Web Height

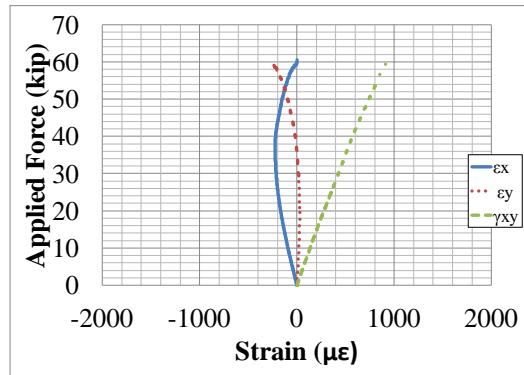


(b) 1/3 Web Height

Figure B-13 Applied Force vs. In Plane Rosette Strains at Strain Gage Station 1



(a) 2/3 Web Height



(b) 1/3 Web Height

Figure B-14 Applied Force vs. In Plane Rosette Strains at Strain Gage Station 2



## Appendix C Tapered 1c Results

PROJECT: Metal Building Manufacturers Association  
TEST NAME: Tapered 1c  
TEST DATE: March 4, 2011

### MOMENT END PLATE CONNECTION DESCRIPTION:

Nominal Yield Stress	55 ksi
Gage	3.5 in.
Width	8 in.
Thickness	1 in.
Bolt Hole Locations	2.00 in., 13.88 in., 17.88 in., and 21.88 in.
Bolt Hole Size	1.1875 in.
Bolt Type	1.125" x 3.75" A325 Bolts
Bolt Pretension	Snug tightened
Nuts	1.125" -7 Heavy Hex Nuts (A563 Grade C, C3, D or DH)

### TEST SPECIMEN GEOMETRY:

Total Taper Angle	5.09°
Total Length	15ft
Test Length	7.5 ft
$d_{End}$	12 in.
$d_{Midspan}$	20 in.
$t_w$	0.125 in.
$t_{f,bottom}$	0.3125 in.
$b_{f,bottom}$	6 in.
$t_{f,top}$	0.3125 in.
$b_{f,top}$	6 in.
$t_{stiffener}$	0.5 in.
$a/h_{ave.}$	5.53

Notes: Test length measured from centerline of stiffener to midspan. Total length measured from centerline of stiffener to centerline of stiffener

### LVDT AND STRAIN GAGE LOCATIONS:

LVDT Station 1	73 in.
LVDT Station 2	78.125 in.
LVDT Station 3	84.125 in.
Strain Gage Station 1	71 in.
Strain Gage Station 2 (Rosette Gages Only)	77.125 in.
Strain Gage Station 3 (Rosette Gages Only)	83.125 in.

Notes: Distances measured from outside face of stiffener. LVDT stations placed on far side of specimen

### EXPERIMENTAL:

Maximum Load	58.6 kip
Failure Mode	Flange local buckling



Figure C-1 LVDTs Near Failure Location

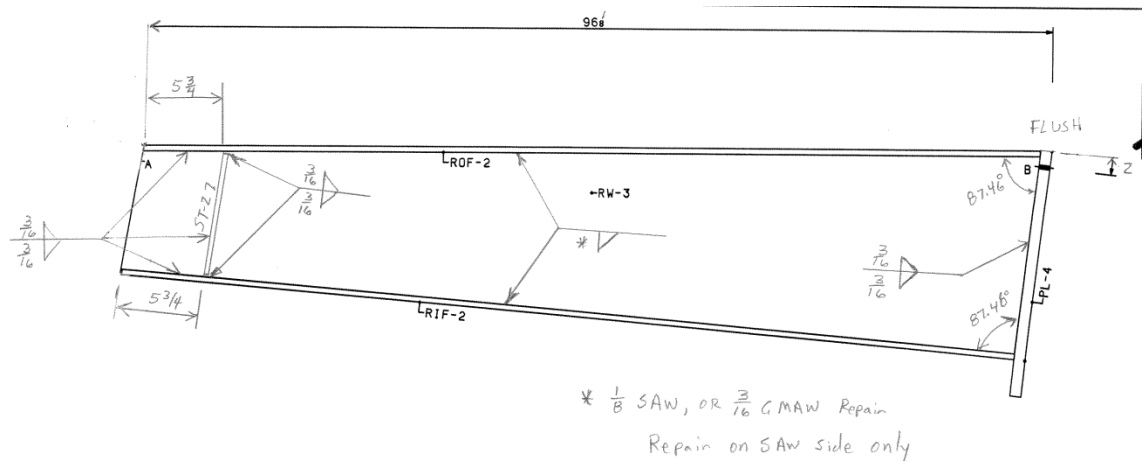


Figure C-2 Dimensions

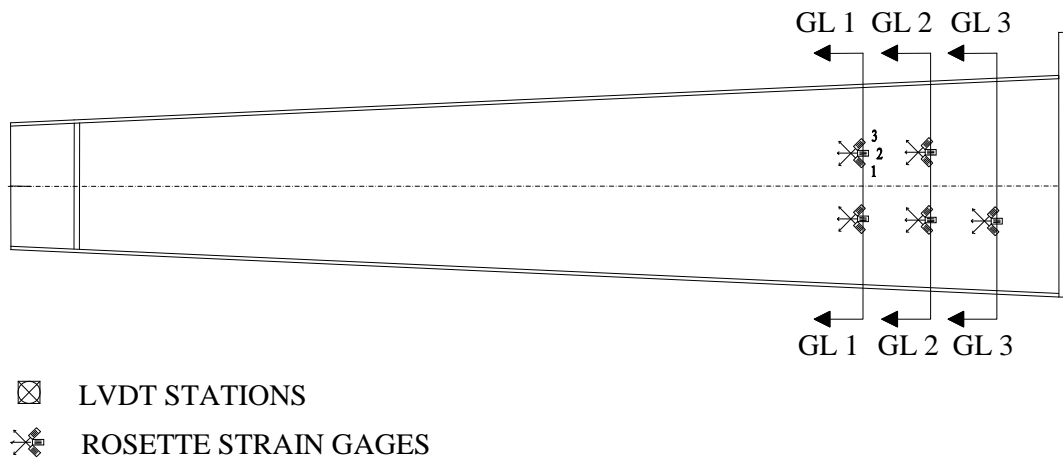


Figure C-3 Near Side Elevation



Figure C-4 Far Side Elevation

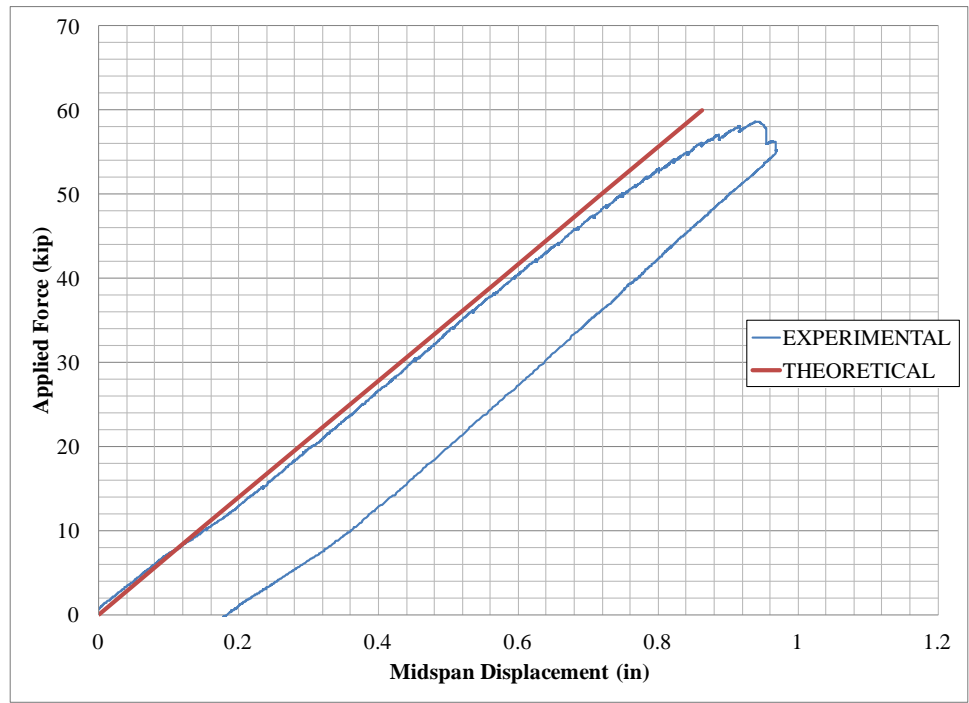


Figure C-5 Applied Force vs. Midspan Displacement

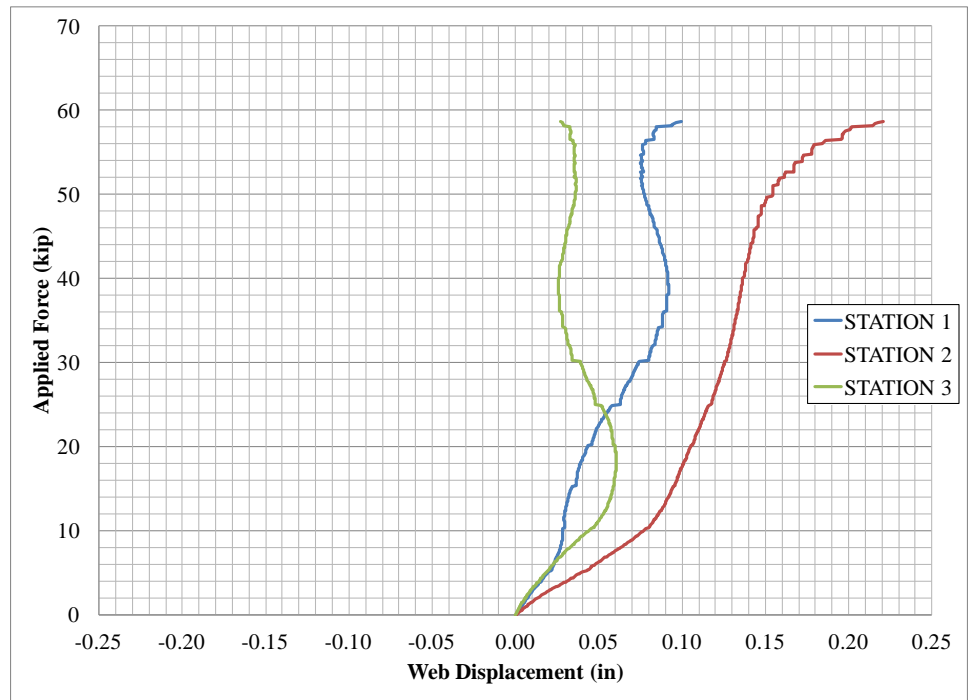
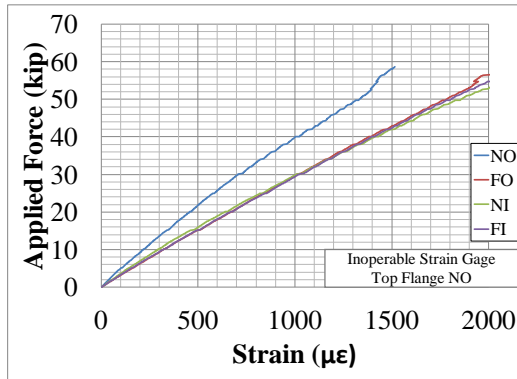
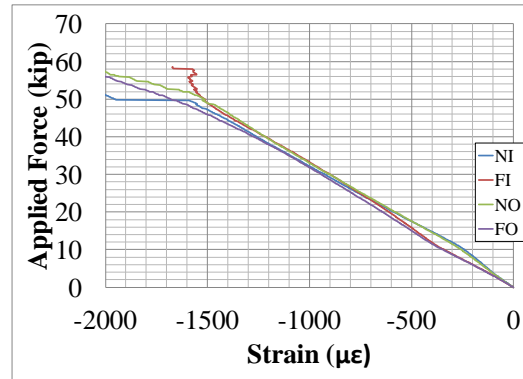


Figure C-6 Applied Force vs. Web Displacement

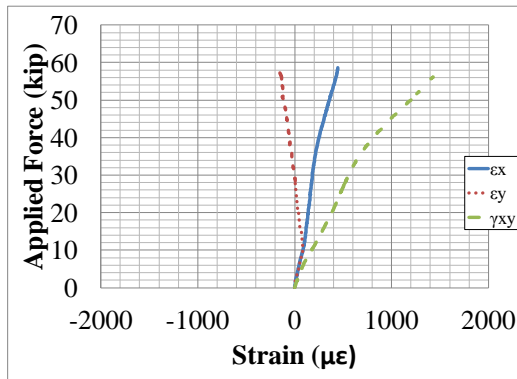


(a) Top Flange

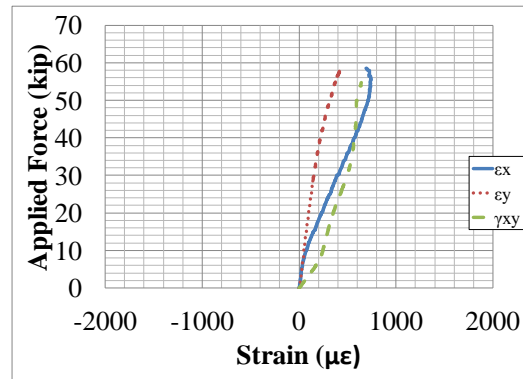


(b) Bottom Flange

Figure C-7 Applied Force vs. Uniaxial Strains at Strain Gage Station 1

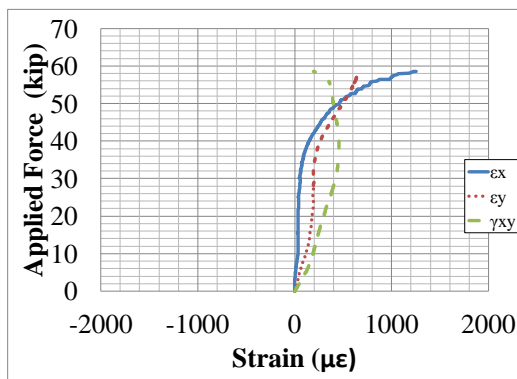


(a) Near Side

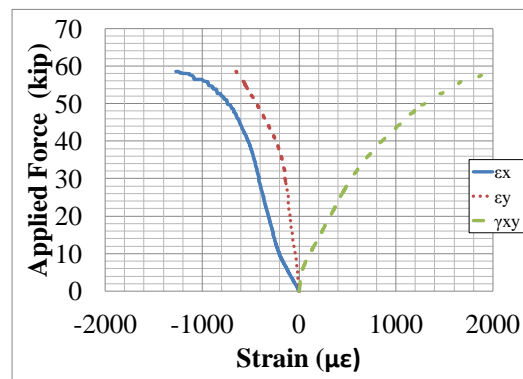


(b) Far Side

Figure C-8 Applied Force vs. 2/3 Web Height Rosette Strains at Strain Gage Station 1

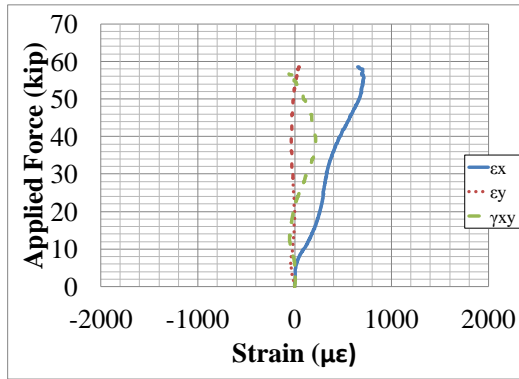


(a) Near Side

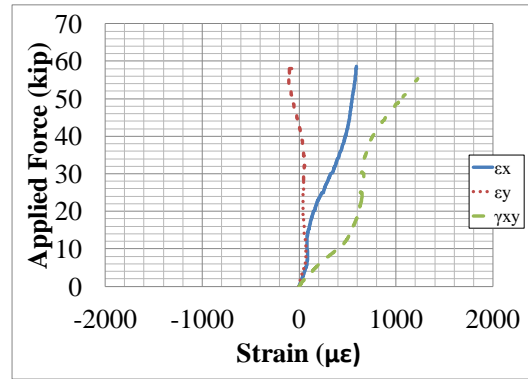


(b) Far Side

Figure C-9 Applied Force vs. 1/3 Web Height Rosette Strains at Strain Gage Station 1

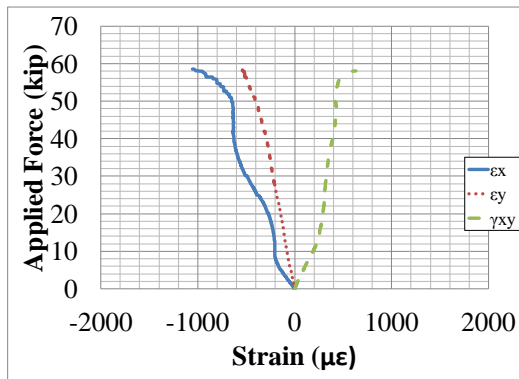


(a) Near Side

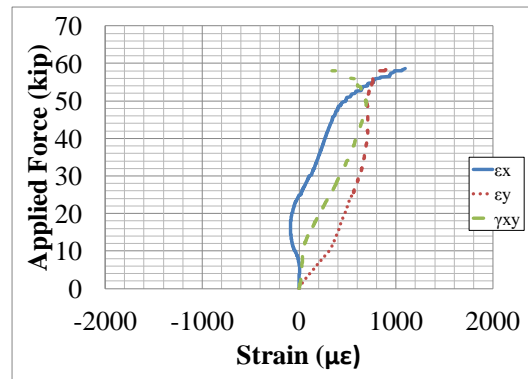


(b) Far Side

Figure C-10 Applied Force vs. 2/3 Web Height Rosette Strains at Strain Gage Station 2

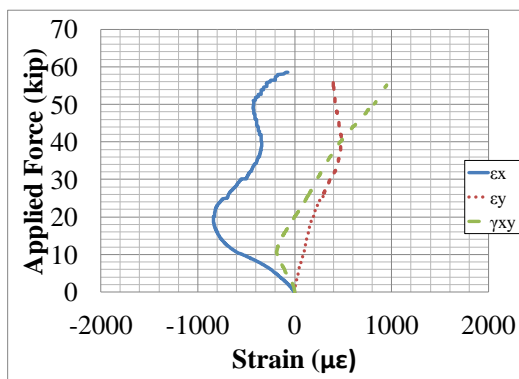


(a) Near Side

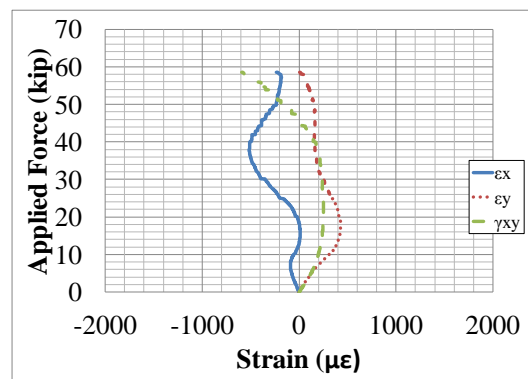


(b) Far Side

Figure C-11 Applied Force vs. 1/3 Web Height Rosette Strains at Strain Gage Station 2

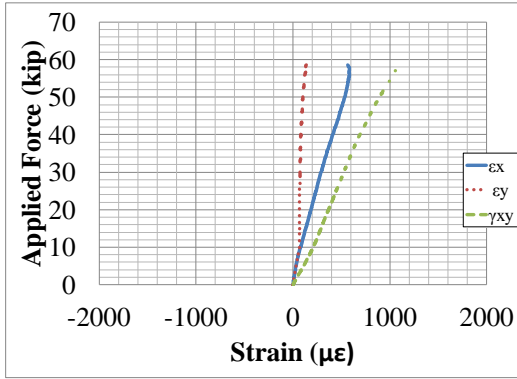


(a) Near Side

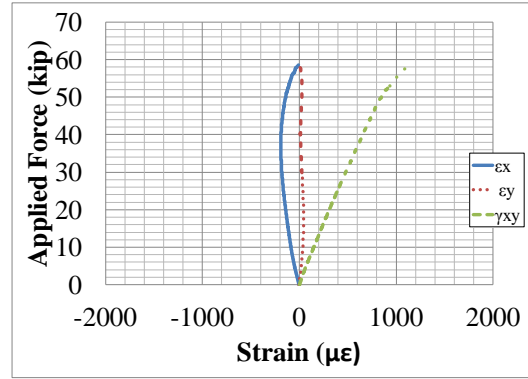


(b) Far Side

Figure C-12 Applied Force vs. 1/3 Web Height Rosette Strains at Strain Gage Station 3

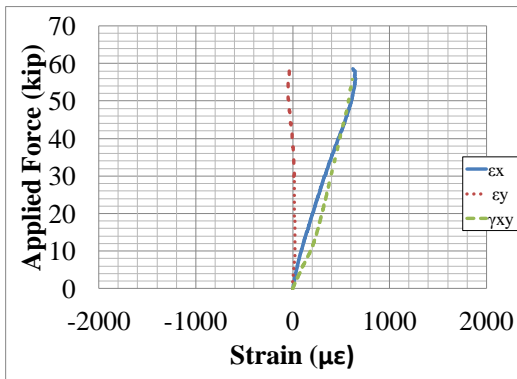


(a) 2/3 Web Height

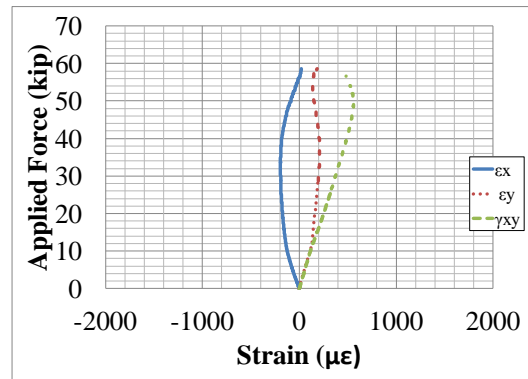


(b) 1/3 Web Height

Figure C-13 Applied Force vs. In Plane Rosette Strains at Strain Gage Station 1



(a) 2/3 Web Height



(b) 1/3 Web Height

Figure C-14 Applied Force vs. In Plane Rosette Strains at Strain Gage Station 2

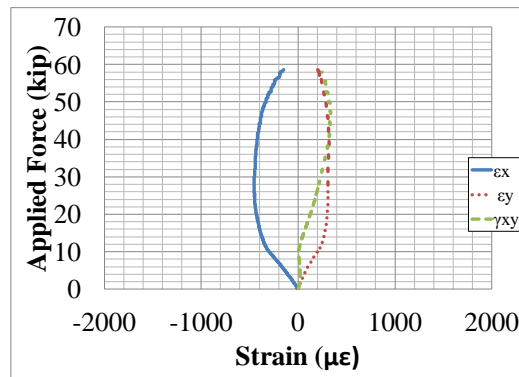


Figure C-15 Applied Force vs. 1/3 Web Height In Plane Rosette Strains at Strain Gage Station 3

## Appendix D Tapered 2a Results

PROJECT: Metal Building Manufacturers Association

TEST NAME: Tapered 2a

TEST DATE: April 14, 2011

### MOMENT END PLATE CONNECTION DESCRIPTION:

Nominal Yield Stress	55 ksi
Gage	5.5 in.
Width	10 in.
Thickness	1.25 in.
Bolt Hole Locations	3.06, 16.62, 22.12, 27.62 in.
Bolt Hole Size	1.8125 in.
Bolt Type	1.75" x 4.5" A354 Bolts Grade BC
Bolt Pretension	Snug tightened
Nuts	1.75" -8 Heavy Hex Nuts (A194 Grade 2H) to match A354 bolts

### TEST SPECIMEN GEOMETRY:

Total Taper Angle	9.53°
Total Length	15 ft
Test Length	7.5 ft
$d_{End}$	10 in.
$d_{Midspan}$	25 in.
$t_w$	0.156 in.
$t_{f,bottom}$	0.5 in.
$b_{f,bottom}$	8 in.
$t_{f,top}$	5 in.
$b_{f,top}$	8 in.
$t_{stiffener}$	0.5 in.
$a/h_{ave.}$	5.06

Notes: Test length measured from centerline of stiffener to midspan. Total length measured from centerline of stiffener to centerline of stiffener

### LVDT AND STRAIN GAGE LOCATIONS:

LVDT Station 1	60 in.
LVDT Station 2	66 in.
LVDT Station 3	72 in.
Strain Gage Station 1	77.25 in.

Notes: Distances measured from outside face of stiffener. LVDT stations placed on far side of specimen

### EXPERIMENTAL:

Maximum Load	138 kip
Failure Mode	Web Shear Buckling



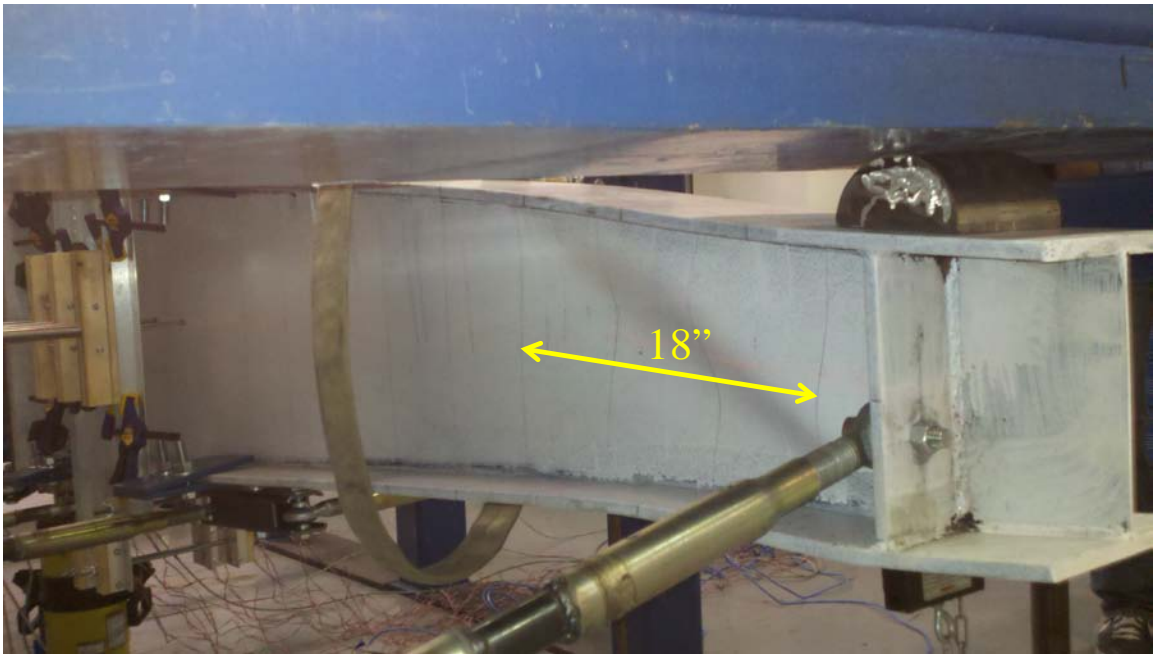


Figure D-1 Web Shear Buckling

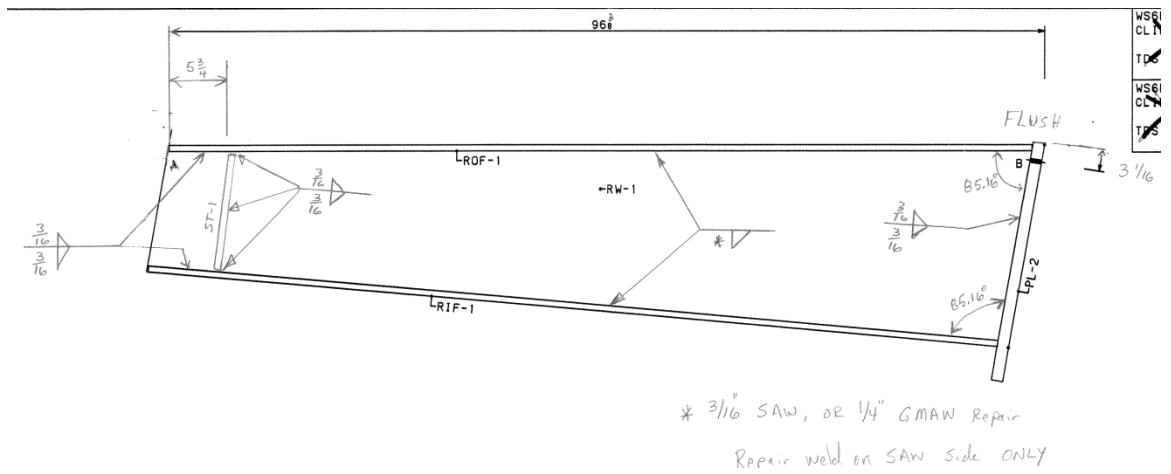


Figure D-2 Dimensions

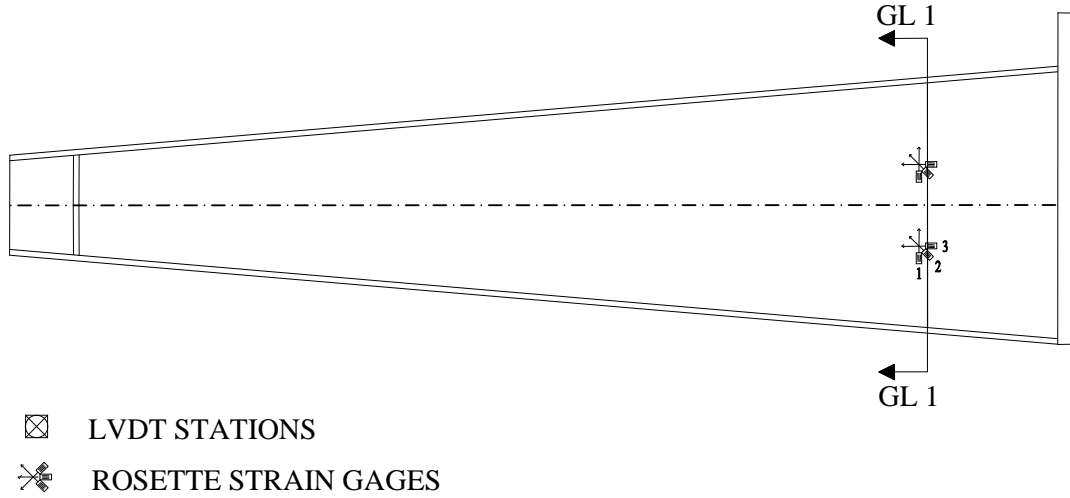


Figure D-3 Near Side Elevation

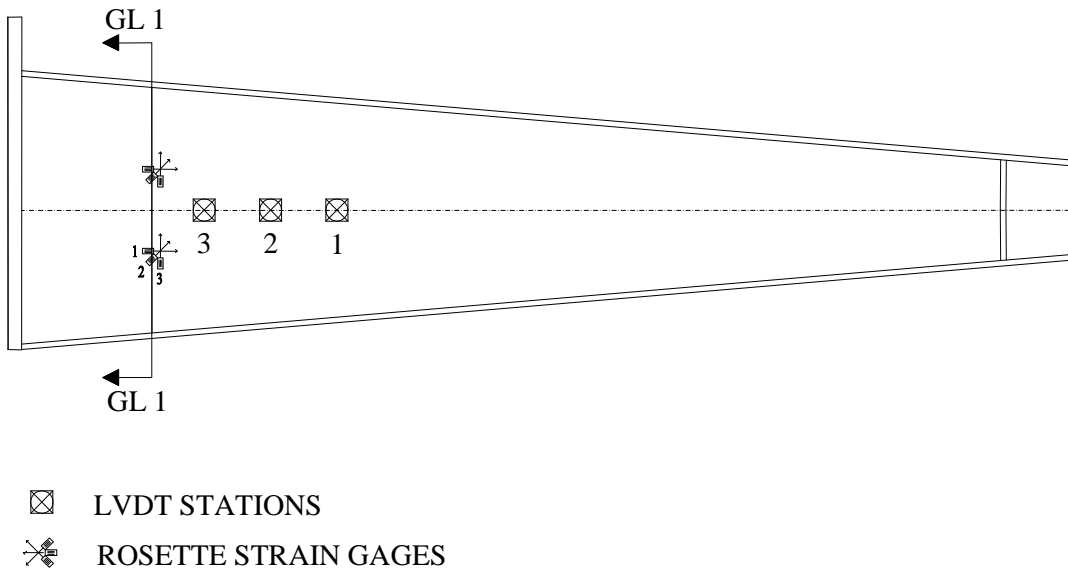


Figure D-4 Far Side Elevation

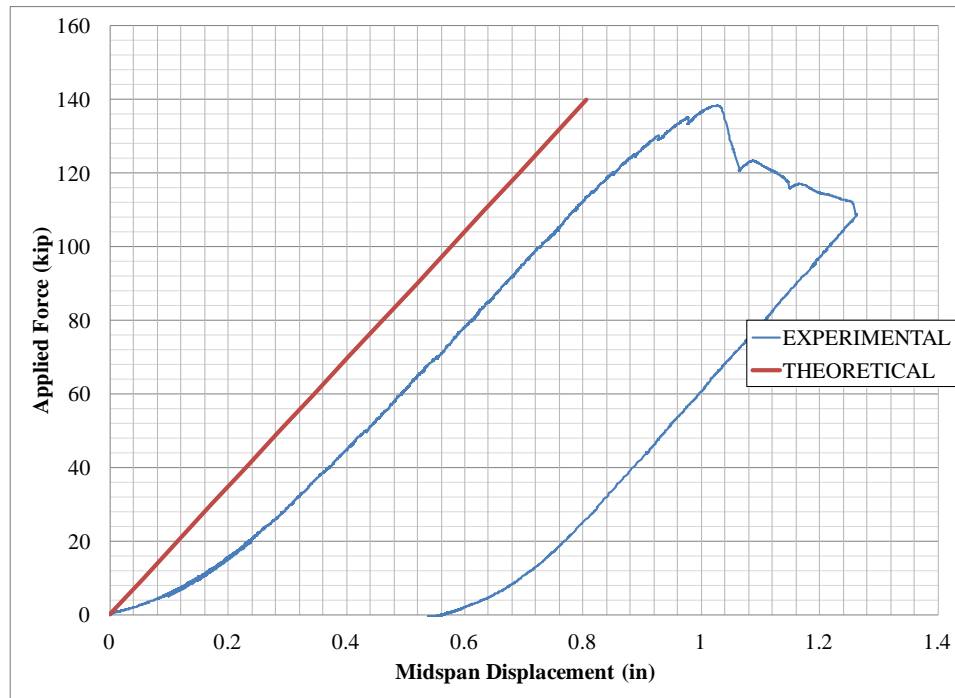


Figure D-5 Applied Force vs. Midspan Displacement

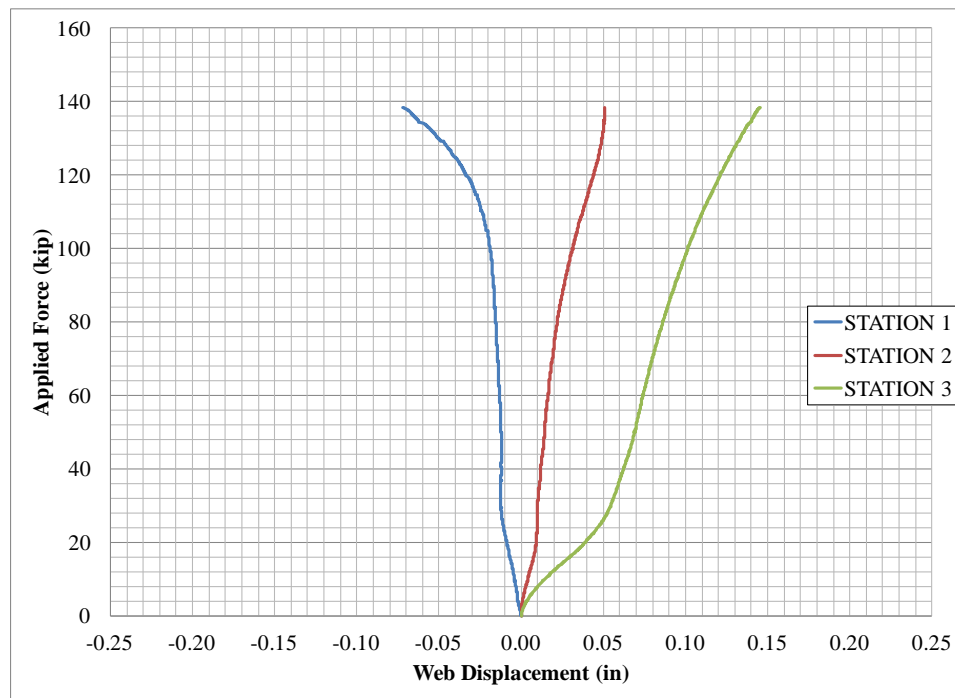
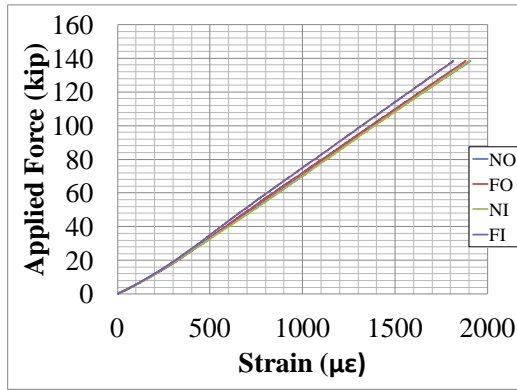
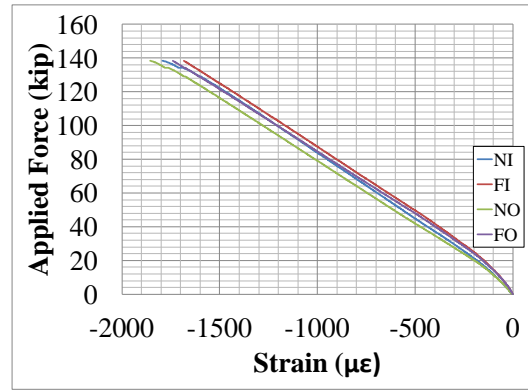


Figure D-6 Applied Force vs. Web Displacement

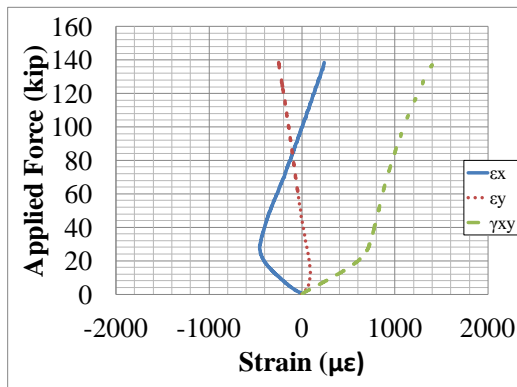


(a) Top Flange

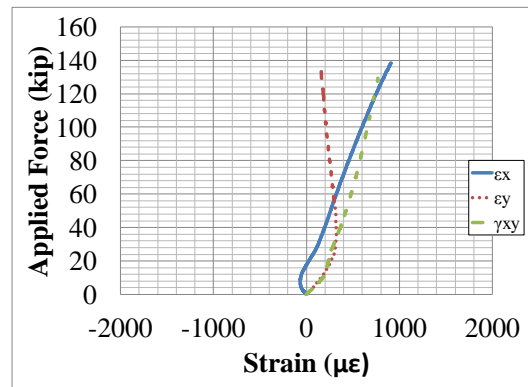


(b) Bottom Flange

Figure D-7 Applied Force vs. Uniaxial Strains at Strain Gage Station 1

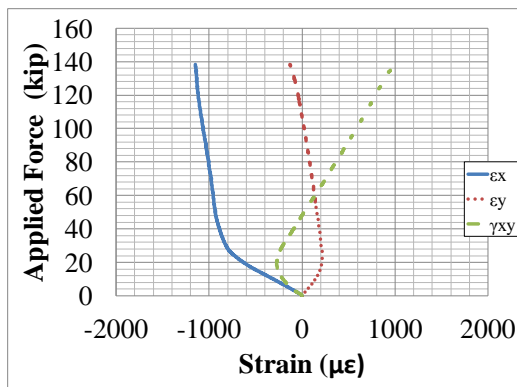


(a) Near Side

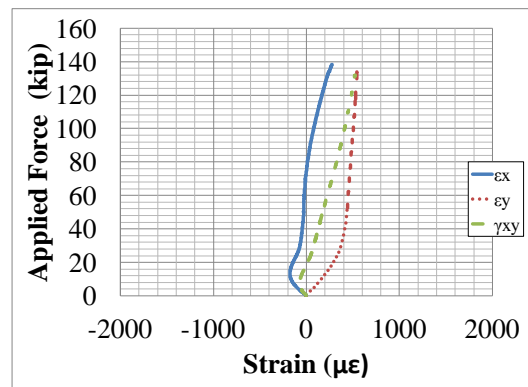


(b) Far Side

Figure D-8 Applied Force vs. 2/3 Web Height Rosette Strains at Strain Gage Station 1

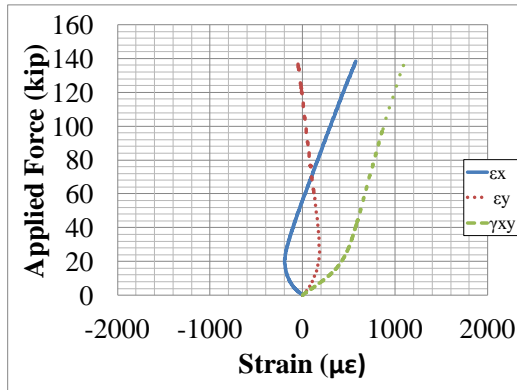


(a) Near Side

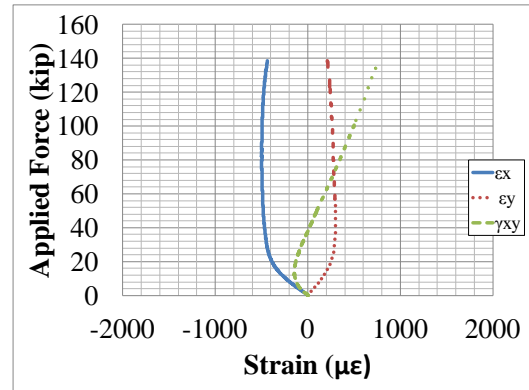


(b) Far Side

Figure D-9 Applied Force vs. 1/3 Web Height Rosette Strains at Strain Gage Station 1



(a) 2/3 Web Height



(b) 1/3 Web Height

Figure D-10 Applied Force vs. In Plane Rosette Strains at Strain Gage Station 1

## Appendix E Tapered 2b Results

PROJECT: Metal Building Manufacturers Association  
TEST NAME: Tapered 2b  
TEST DATE: May 4, 2011

### MOMENT END PLATE CONNECTION DESCRIPTION:

Nominal Yield Stress	55 ksi
Gage	5.5 in.
Width	10 in.
Thickness	1.25 in.
Bolt Hole Locations	3.06, 16.62, 22.12, 27.62 in.
Bolt Hole Size	1.8125 in.
Bolt Type	1.75" x 4.5" A354 Bolts Grade BC
Bolt Pretension	Snug tightened
Nuts	1.75" -8 Heavy Hex Nuts (A194 Grade 2H) to match A354 bolts

### TEST SPECIMEN GEOMETRY:

Total Taper Angle	9.53°
Total Length	15 ft
Test Length	7.5 ft
$d_{End}$	10 in.
$d_{Midspan}$	25 in.
$t_w$	0.156 in.
$t_{f,bottom}$	0.5 in.
$b_{f,bottom}$	8 in.
$t_{f,top}$	5 in.
$b_{f,top}$	8 in.
$t_{stiffener}$	0.5 in.
$a/h_{ave.}$	5.06

Notes: Test length measured from centerline of stiffener to midspan. Total length measured from centerline of stiffener to centerline of stiffener

### LVDT AND STRAIN GAGE LOCATIONS:

LVDT Station 1	8 in.
LVDT Station 2	14 in.
LVDT Station 3	20 in.
Strain Gage Station 1	7.75 in.
Strain Gage Station 2	11.625 in.

Notes: Distances measured from outside face of stiffener. LVDT stations placed on far side of specimen

### EXPERIMENTAL:

Maximum Load	135 kips
Failure Mode	Web Shear Buckling

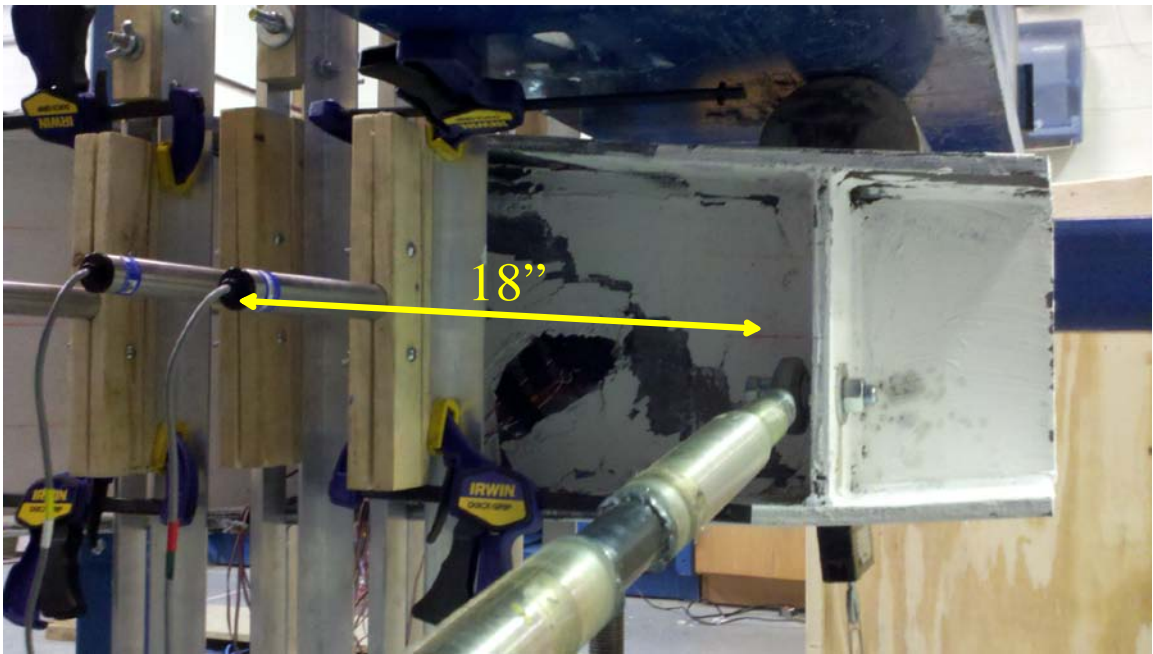


Figure E-1 Web Shear Buckling

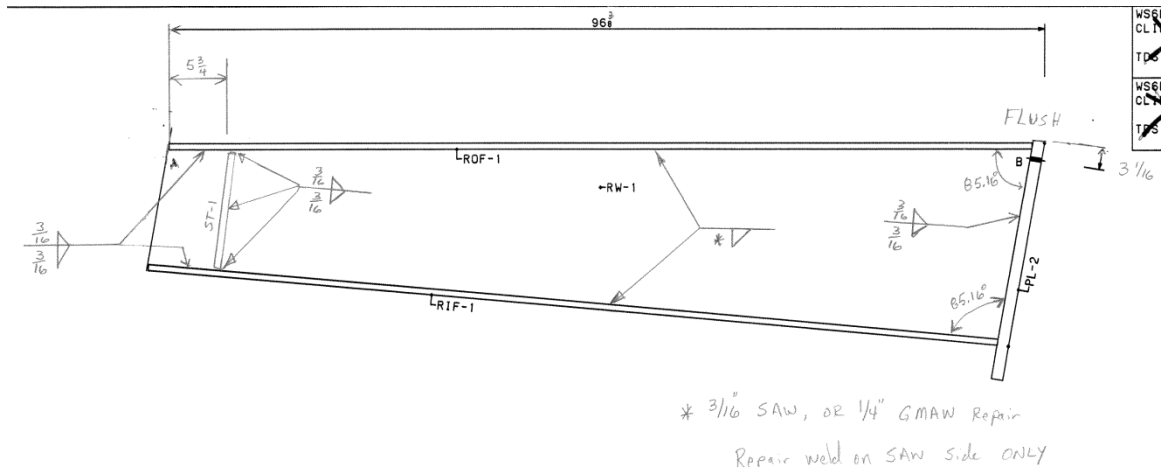


Figure E-2 Dimensions

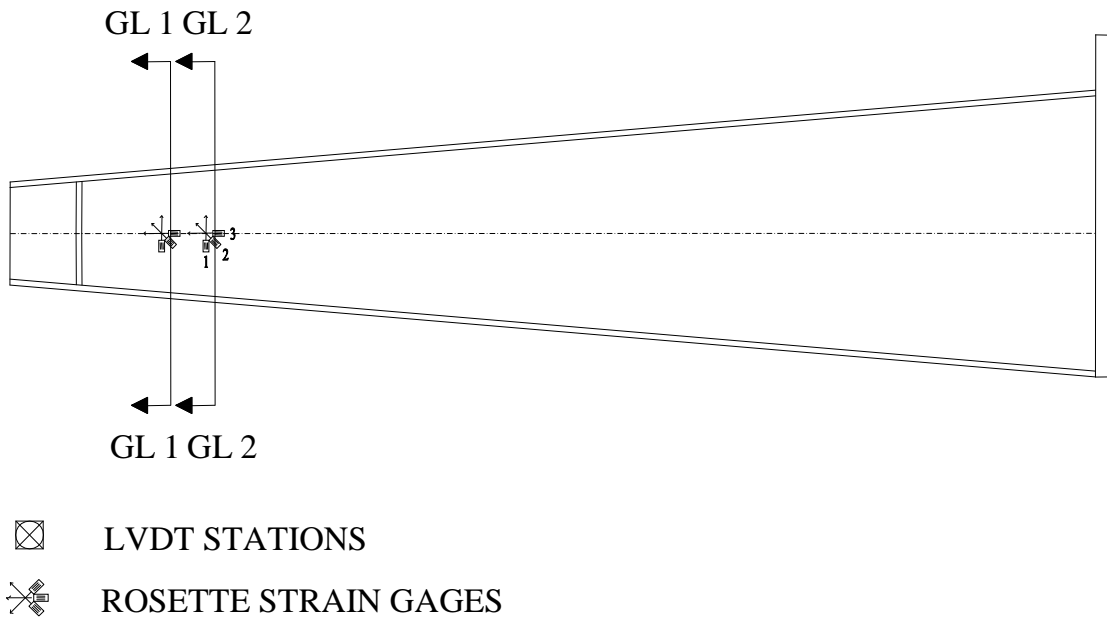


Figure E-3 Near Side Elevation

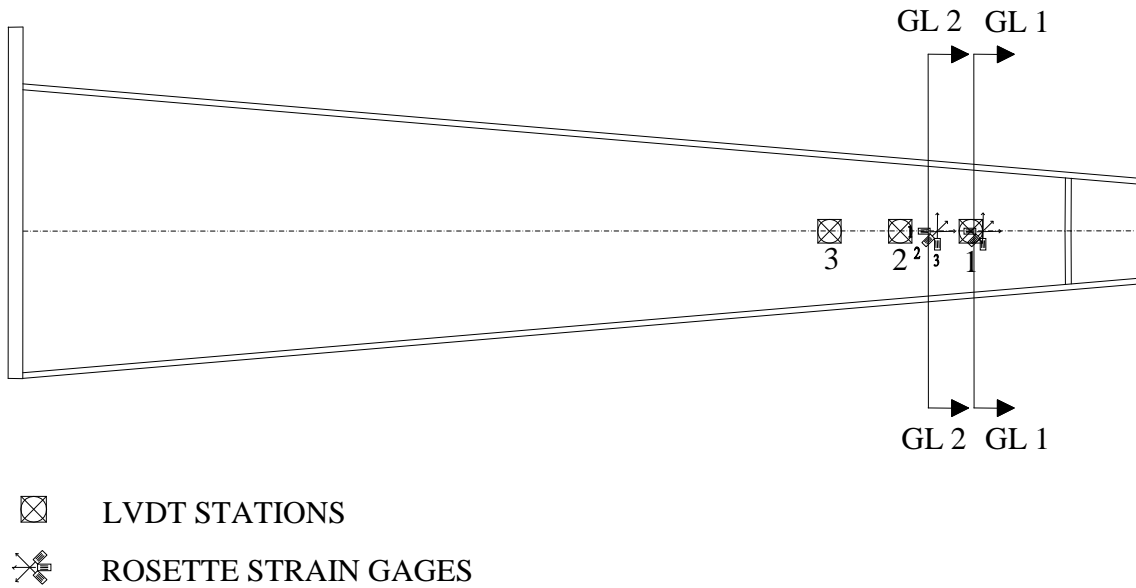


Figure E-4 Far Side Elevation



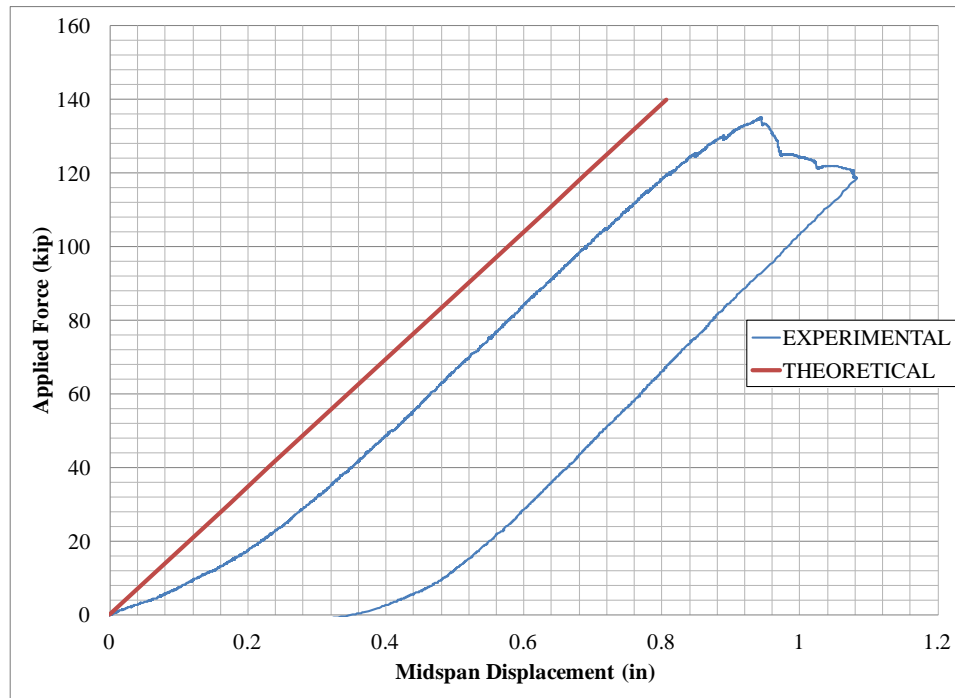


Figure E-5 Applied Force vs. Midspan Displacement

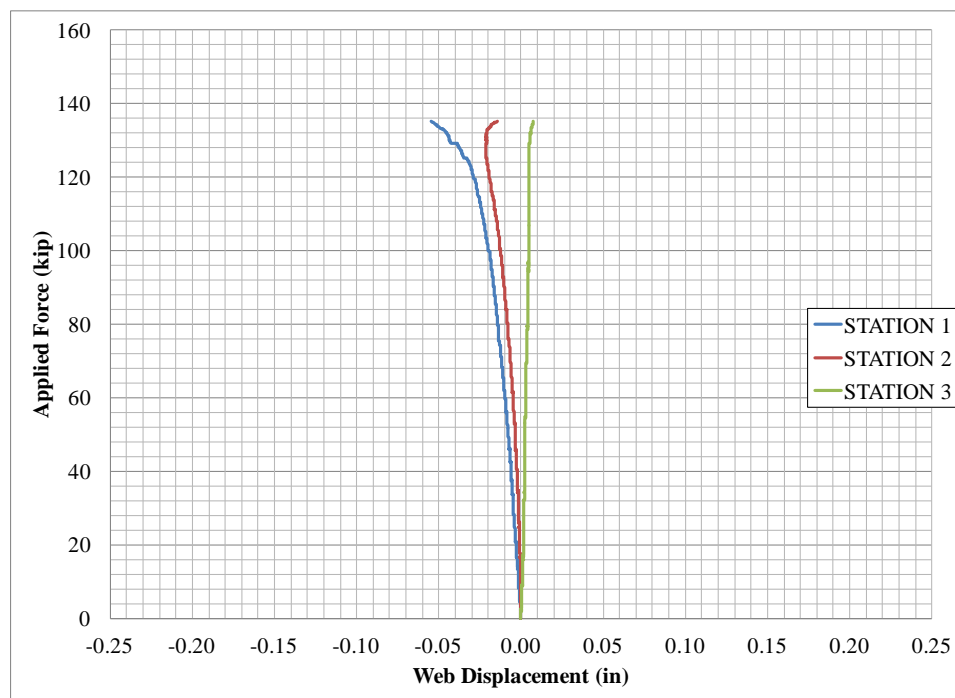
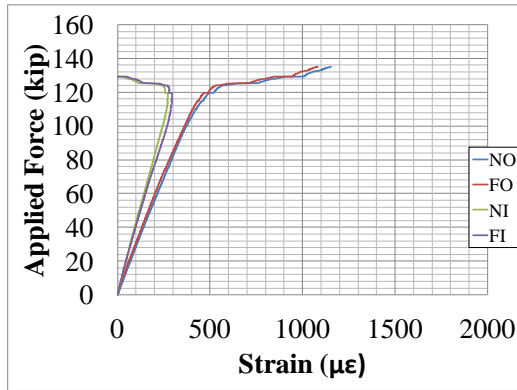
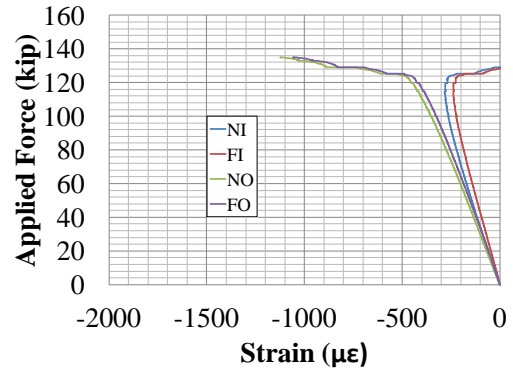


Figure E-6 Applied Force vs. Web Displacement

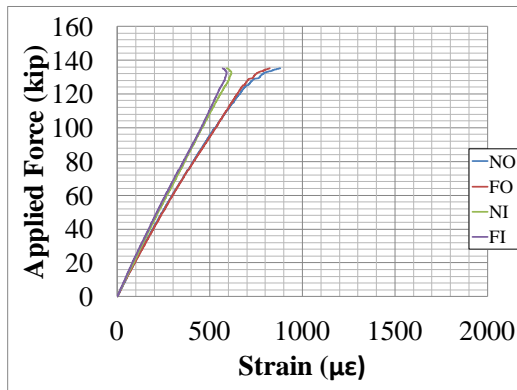


(a) Top Flange

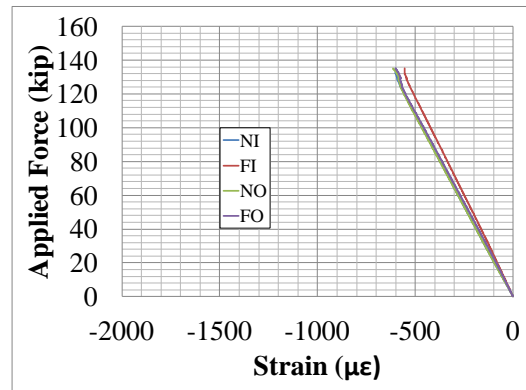


(b) Bottom Flange

Figure E-7 Applied Force vs. Uniaxial Strains at Strain Gage Station 1

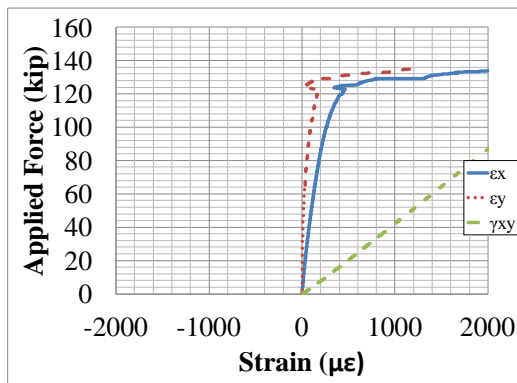


(a) Top Flange

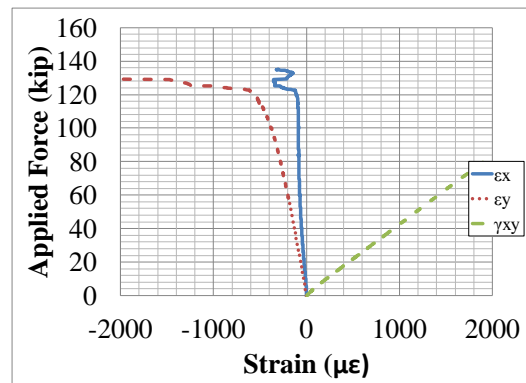


(b) Bottom Flange

Figure E-8 Applied Force vs. Uniaxial Strains at Strain Gage Station 2

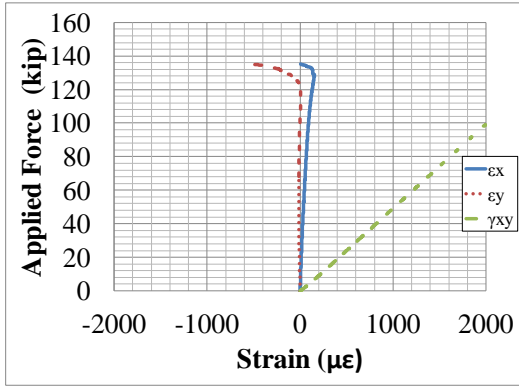


(a) Near Side

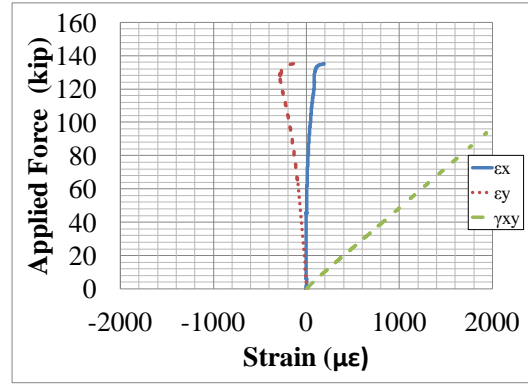


(b) Far Side

Figure E-9 Applied Force vs. 1/2 Web Height Rosette Strains at Strain Gage Station 1



(a) Near Side



(b) Far Side

Figure E-10 Applied Force vs. 1/2 Web Height Rosette Strains at Strain Gage Station 2

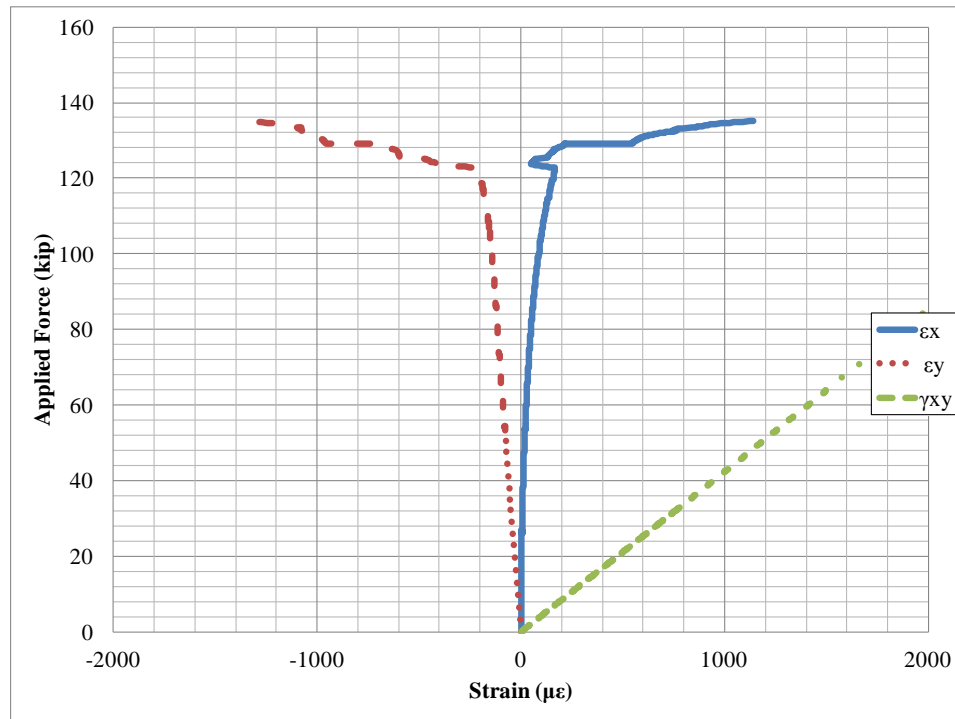


Figure E-11 Applied Force vs. 1/2 Web Height In Plane Rosette Strains at Strain Gage Station 1

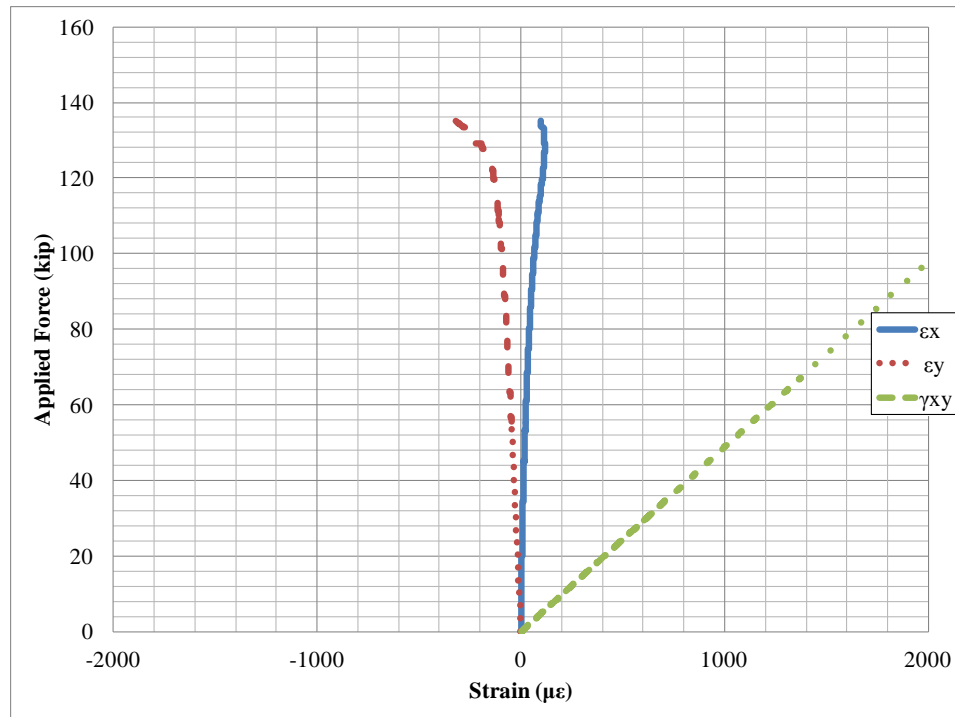


Figure E-12 Applied Force vs. 1/2 Web Height In Plane Rosette Strains at Strain Gage Station 2

## Appendix F Tapered 2c Results

PROJECT: Metal Building Manufacturers Association

TEST NAME: Tapered 2c

TEST DATE: May 25, 2011

### MOMENT END PLATE CONNECTION DESCRIPTION:

Nominal Yield Stress	55 ksi
Gage	5.5 in.
Width	10 in.
Thickness	1.25 in.
Bolt Hole Locations	3.06, 16.62, 22.12, 27.62 in.
Bolt Hole Size	1.8125 in.
Bolt Type	1.75" x 4.5" A354 Bolts Grade BC
Bolt Pretension	Snug tightened
Nuts	1.75" -8 Heavy Hex Nuts (A194 Grade 2H) to match A354 bolts

### TEST SPECIMEN GEOMETRY:

Total Taper Angle	9.53°
Total Length	15 ft
Test Length	7.5 ft
$d_{End}$	10 in.
$d_{Midspan}$	25 in.
$t_w$	0.156 in.
$t_{f,bottom}$	0.5 in.
$b_{f,bottom}$	8 in.
$t_{f,top}$	5 in.
$b_{f,top}$	8 in.
$t_{stiffener}$	0.5 in.
$a/h_{ave.}$	5.06

Notes: Test length measured from centerline of stiffener to midspan. Total length measured from centerline of stiffener to centerline of stiffener

### LVDT AND STRAIN GAGE LOCATIONS:

LVDT Station 1	7.75 in.
LVDT Station 2	11.625 in.
Strain Gage Station 1	7.75 in.
Strain Gage Station 2	11.625 in.
Strain Gage Station 3	78 in.

Notes: Distances measured from outside face of stiffener. LVDT stations placed on far side of specimen

### EXPERIMENTAL:

Maximum Load	129 kips
Failure Mode	Web Shear Buckling

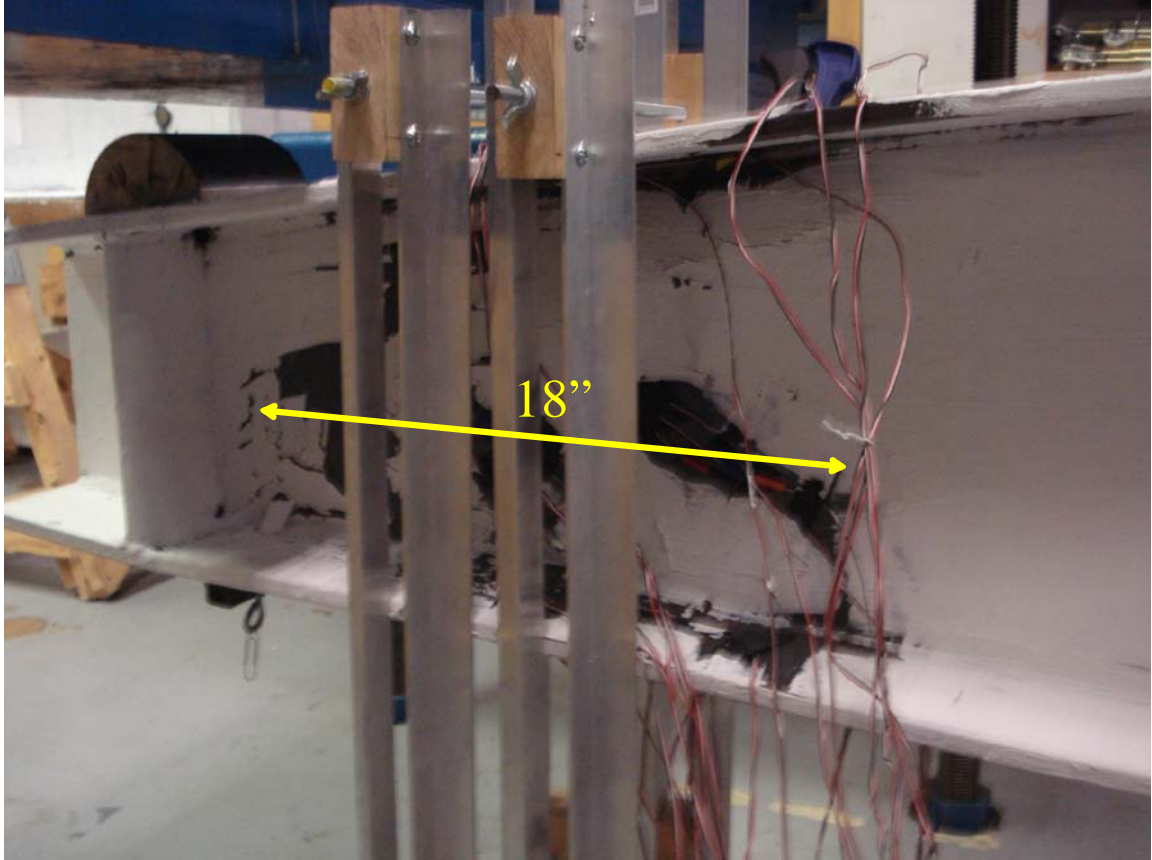


Figure F-1 Web Shear Buckling

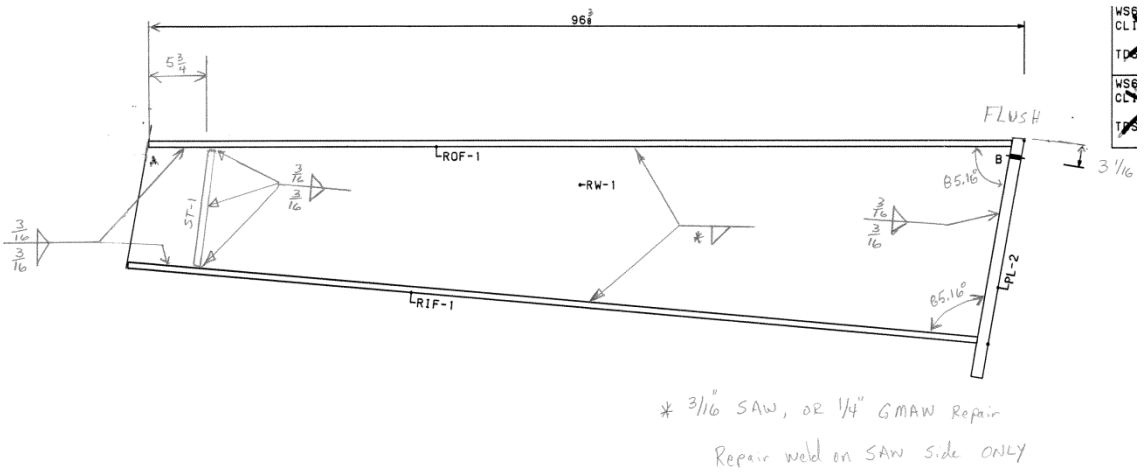


Figure F-2 Dimensions

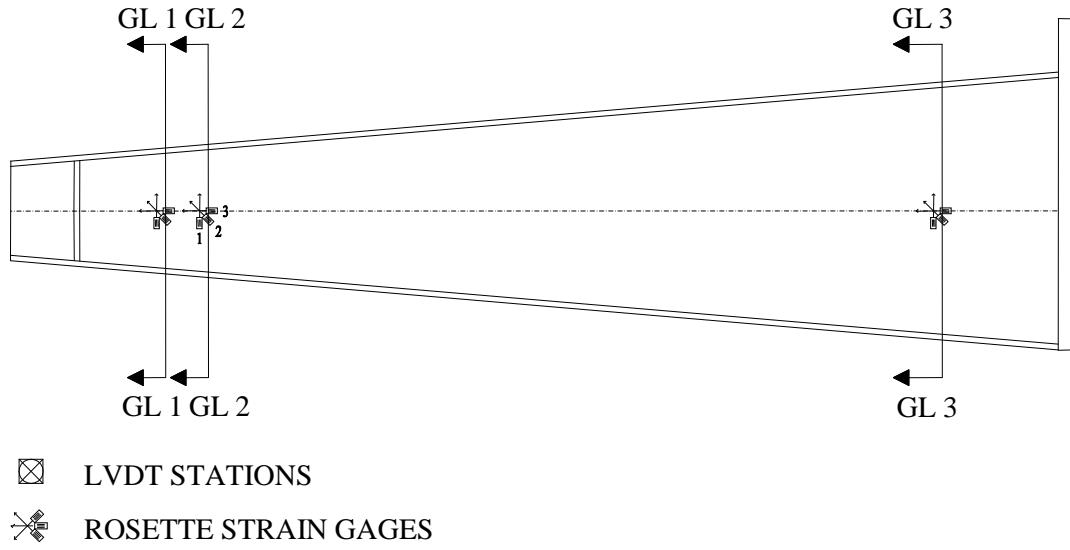


Figure F-3 Near Side Elevation

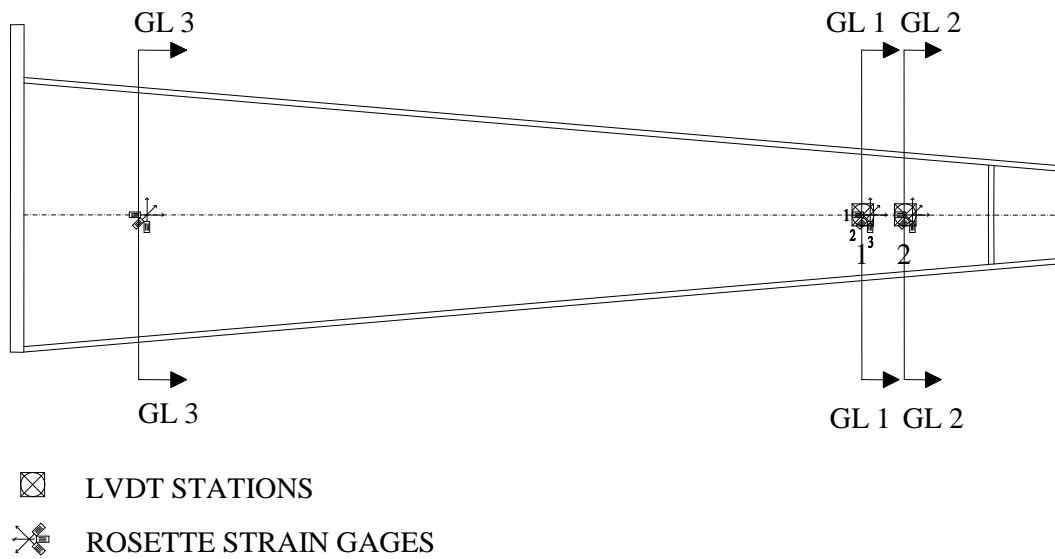


Figure F-4 Far Side Elevation

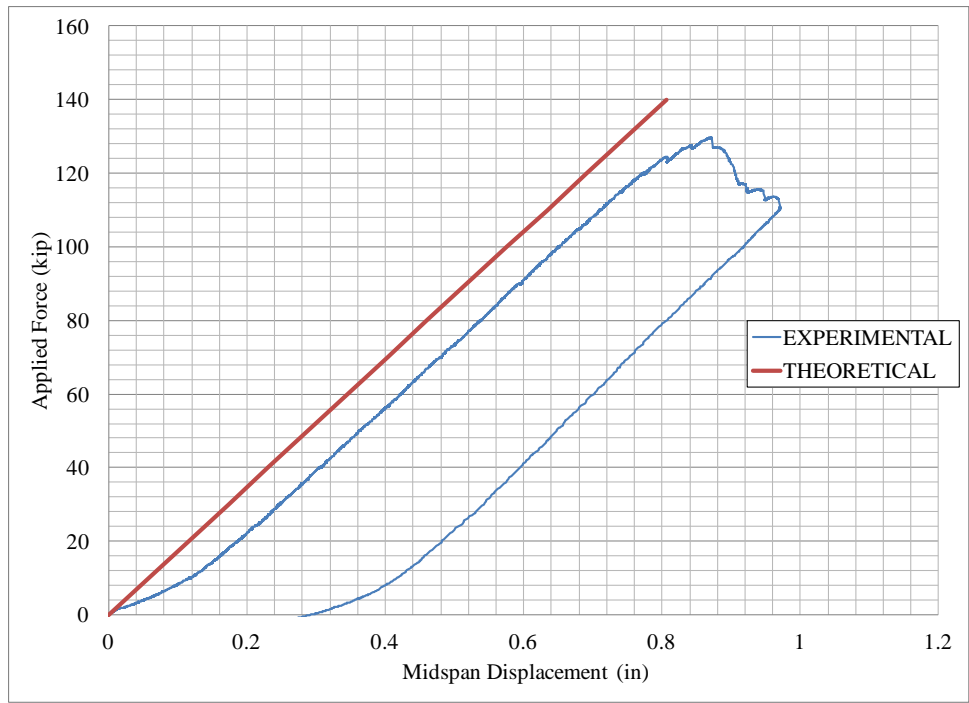


Figure F-5 Applied Force vs. Midspan Displacement

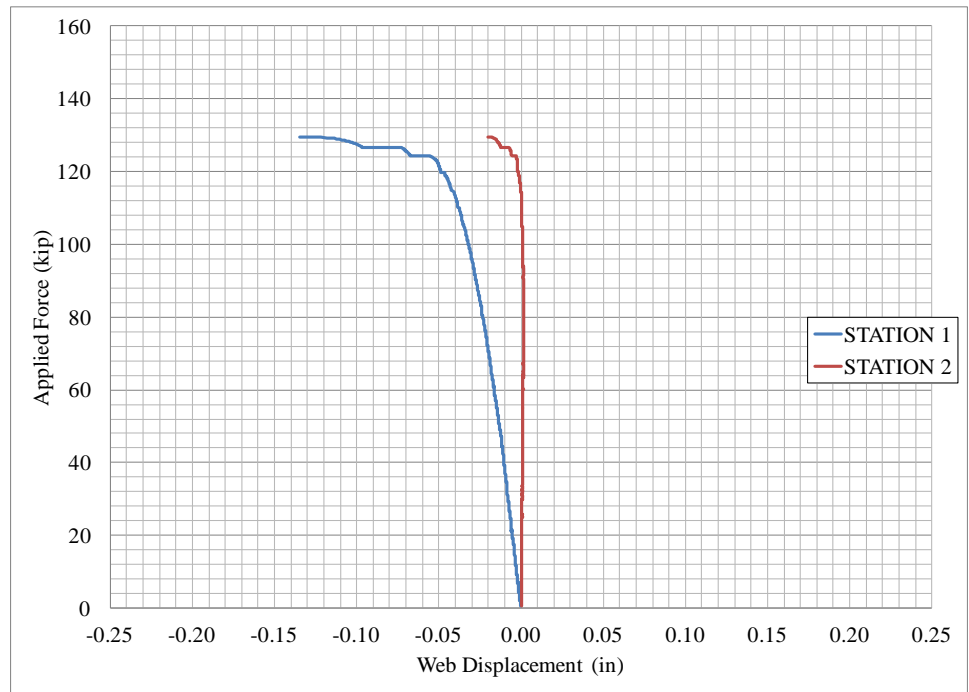
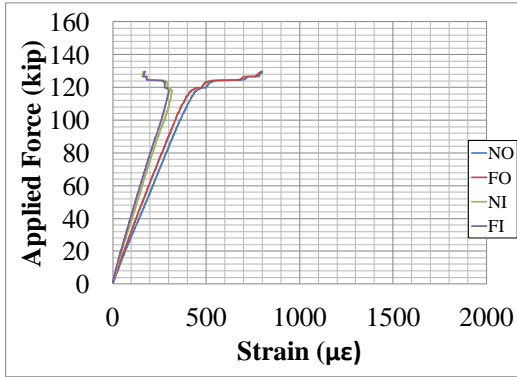
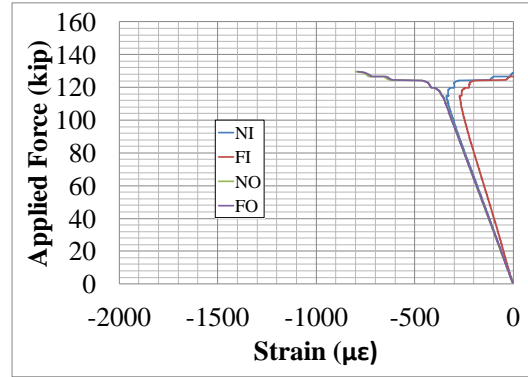


Figure F-6 Applied Force vs. Web Displacement



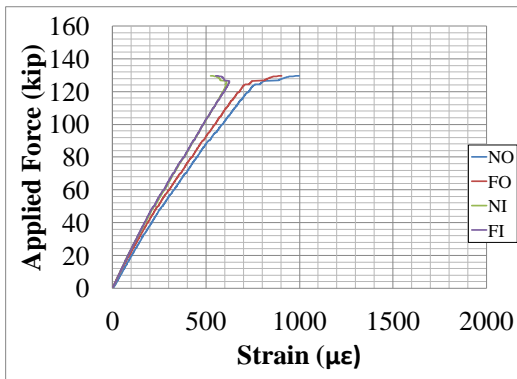


(a) Top Flange

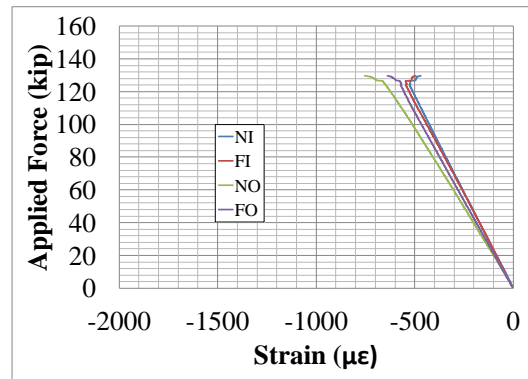


(b) Bottom Flange

Figure F-7 Applied Force vs. Uniaxial Strains at Strain Gage Station 1

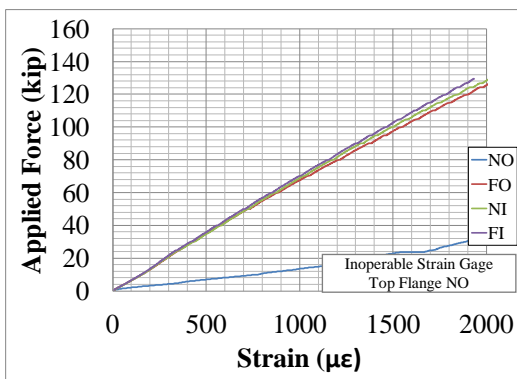


(a) Top Flange

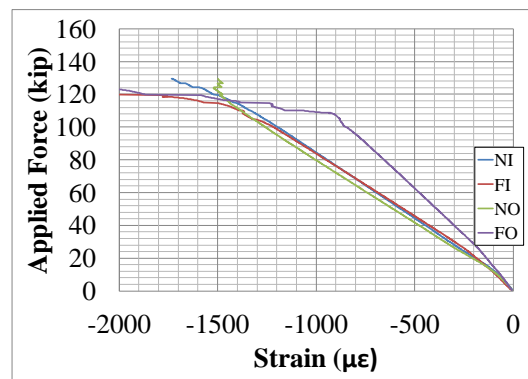


(b) Bottom Flange

Figure F-8 Applied Force vs. Uniaxial Strains at Strain Gage Station 2

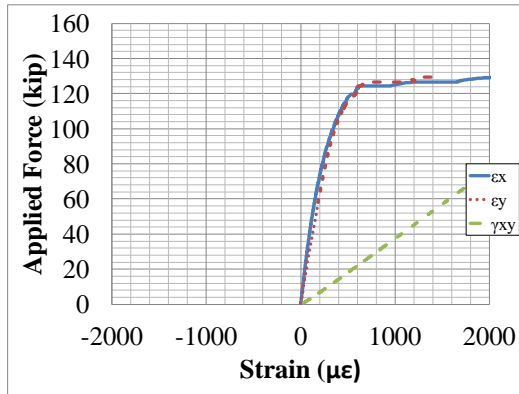


(a) Top Flange

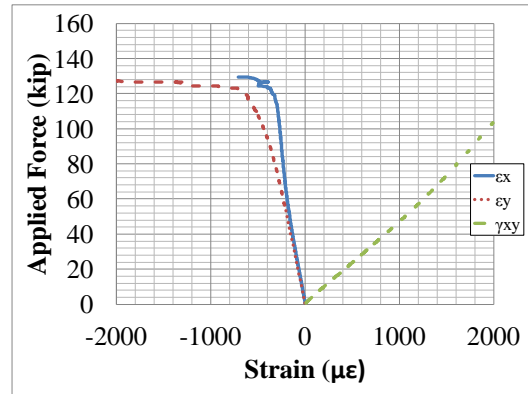


(b) Bottom Flange

Figure F-9 Applied Force vs. Uniaxial Strains at Strain Gage Station 3

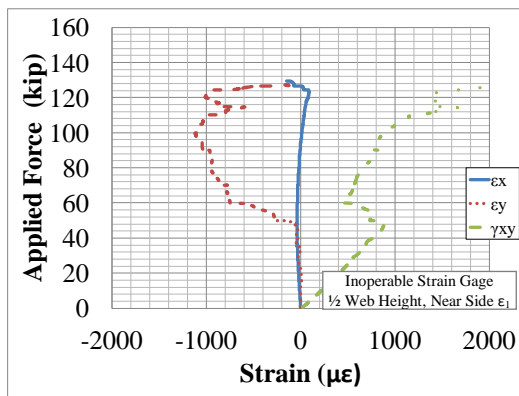


(a) Near Side

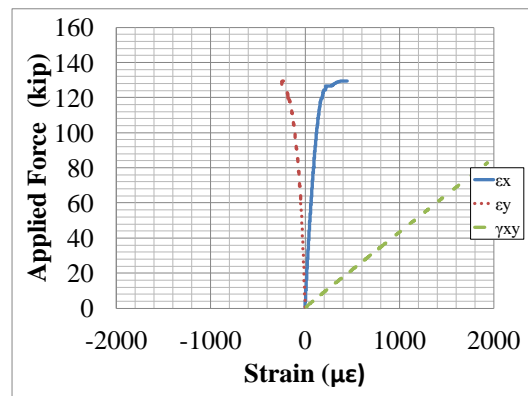


(b) Far Side

Figure F-10 Applied Force vs. 1/2 Web Height Rosette Strains at Strain Gage Station 1

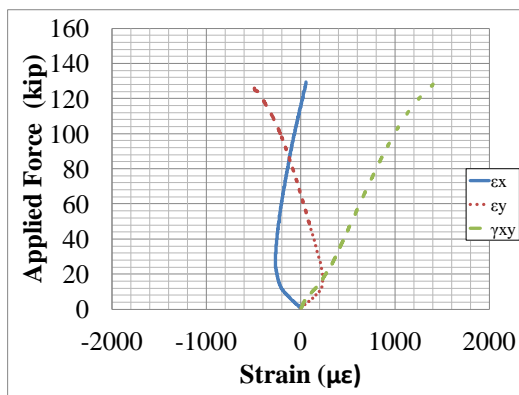


(a) Near Side

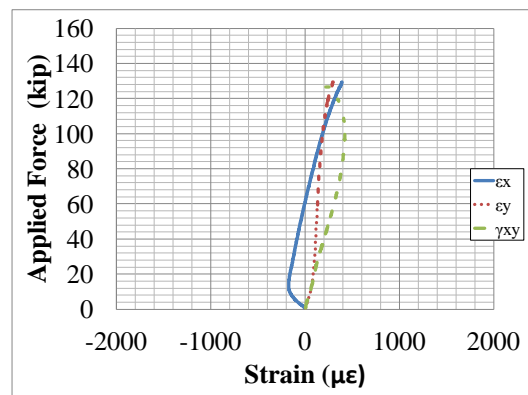


(b) Far Side

Figure F-11 Applied Force vs. 1/2 Web Height Rosette Strains at Strain Gage Station 2



(a) Near Side



(b) Far Side

Figure F-12 Applied Force vs. 1/2 Web Height Rosette Strains at Strain Gage Station 3

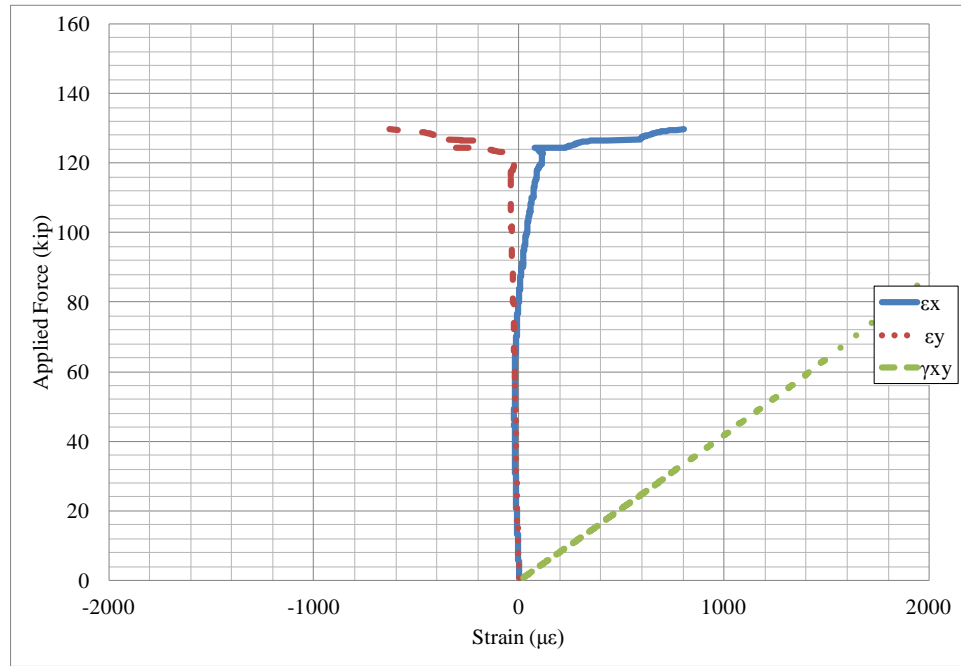


Figure F-13 Applied Force vs. 1/2 Web Height In Plane Rosette Strains at Strain Gage Station 1

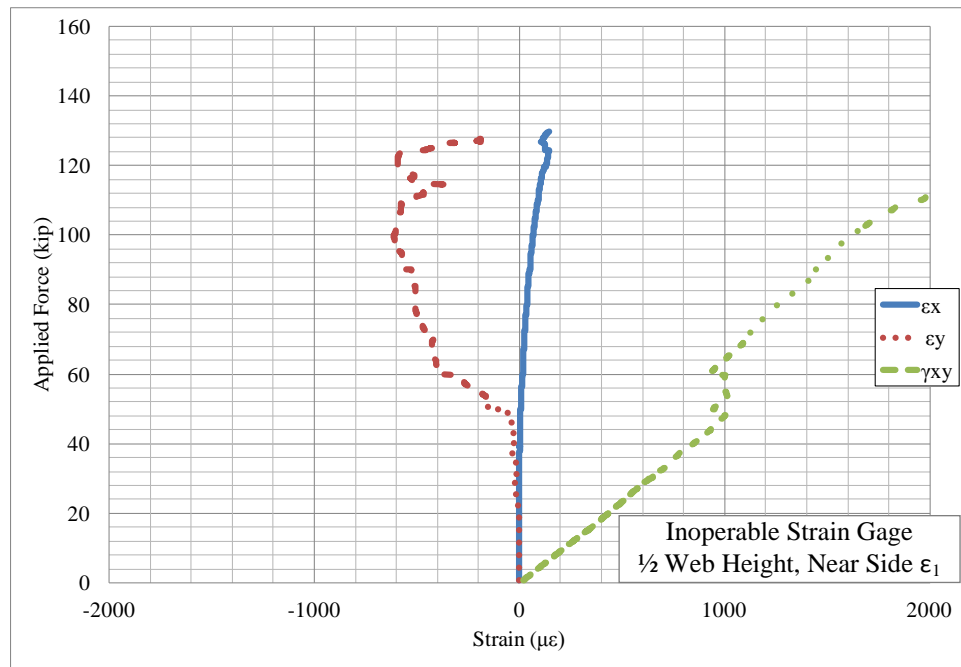


Figure F-14 Applied Force vs. 1/2 Web Height In Plane Rosette Strains at Strain Gage Station 2

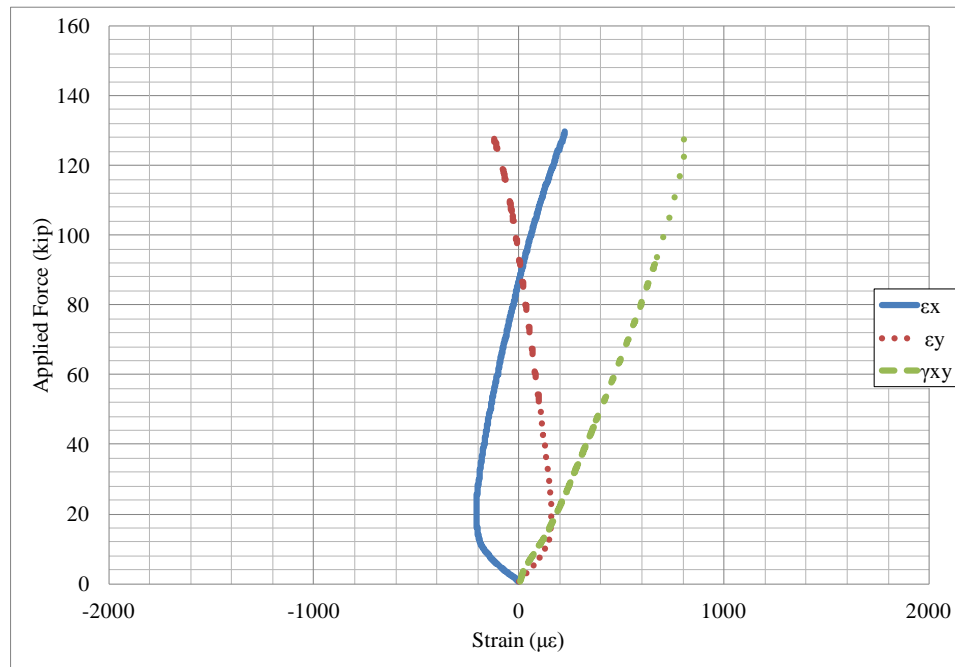


Figure F-15 Applied Force vs. 1/2 Web Height In Plane Rosette Strains at Strain Gage Station 3

## Appendix G Tapered 3 Results

PROJECT: Metal Building Manufacturers Association  
TEST NAME: Tapered 3  
TEST DATE: October 15, 2011

### MOMENT END PLATE CONNECTION DESCRIPTION:

Nominal Yield Stress	55 ksi
Gage	4 in.
Width	12 in.
Thickness	1 in.
Bolt Hole Locations	2.25 in., 6.5 in., 10 in., and 21.125 in.
Bolt Hole Size	1.3125 in.
Bolt Type	1.25" - 7 x 4.25" A490 Hex Bolt
Bolt Pretension	Snug tightened
Nuts	1.25" - 7 A563 GR DH Heavy Hex Nut

### TEST SPECIMEN GEOMETRY:

Total Taper Angle	5.75°
Total Length	11.44 ft
Test Length	5.71 in.
$d_{End}$	13.125 in.
$d_{Midspan}$	20 in.
$t_w$	0.156 in.
$t_{f,bottom}$	0.625 in.
$b_{f,bottom}$	6 in.
$t_{f,top}$	0.625 in.
$b_{f,top}$	6 in.
$t_{stiffener}$	0.5 in.
$a/h_{ave.}$	4.05

Notes: Test length measured from centerline of stiffener to midspan. Total length measured from centerline of stiffener to centerline of stiffener

### LVDT AND STRAIN GAGE LOCATIONS:

LVDT Station 1	9 in.
LVDT Station 2	18 in.
Strain Gage Station 1	18.125 in.
Strain Gage Station 2	30.125 in.

Notes: Distances measured from outside face of stiffener. LVDT stations placed on near side of specimen

### EXPERIMENTAL:

Maximum Load	84.6 kip
Failure Mode	Web Shear Buckling



Figure G-1 Web Shear Buckling

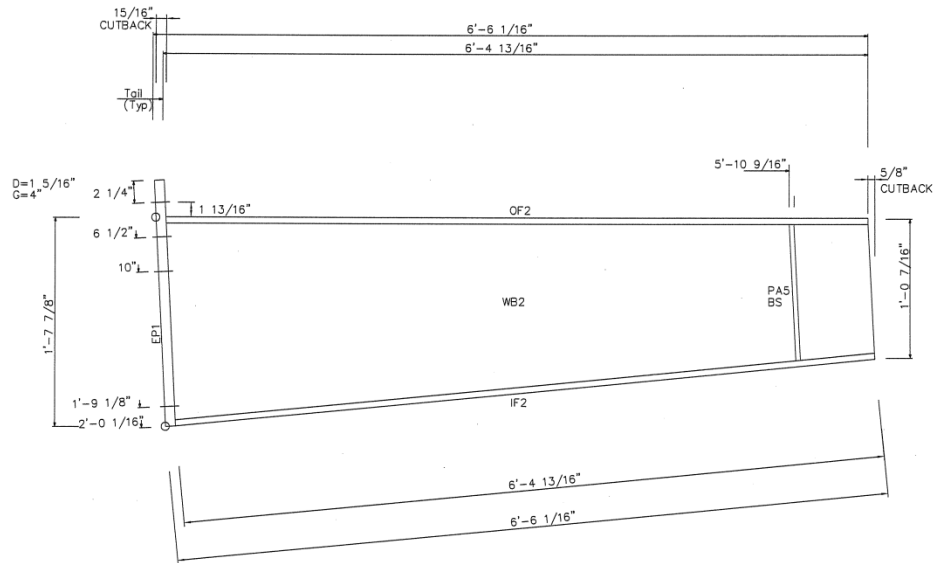


Figure G-2 Dimensions

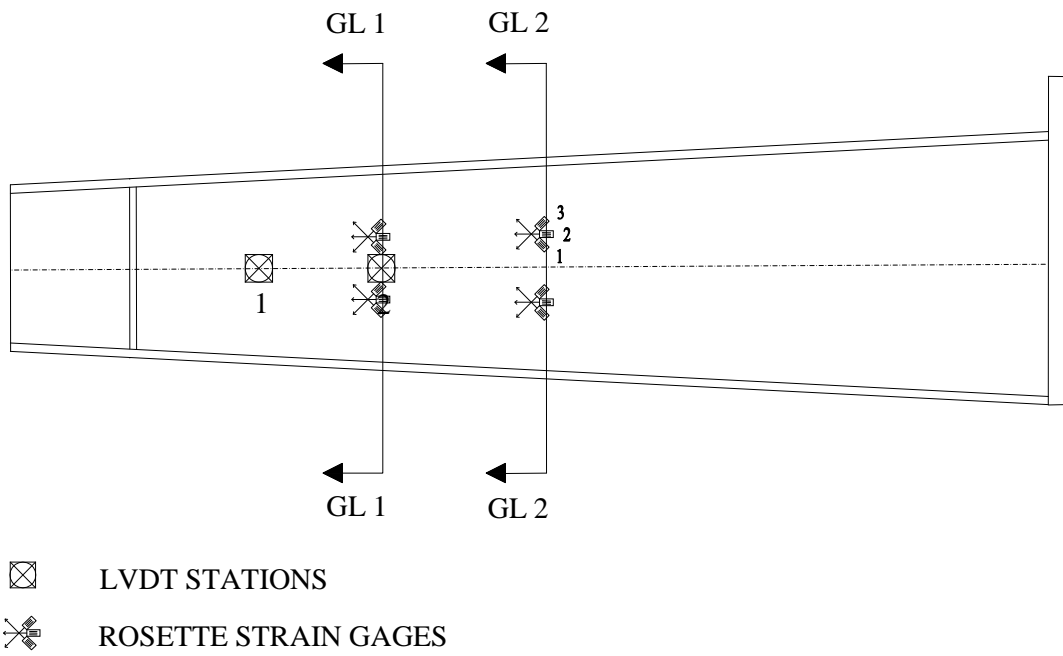


Figure G-3 Near Side Elevation

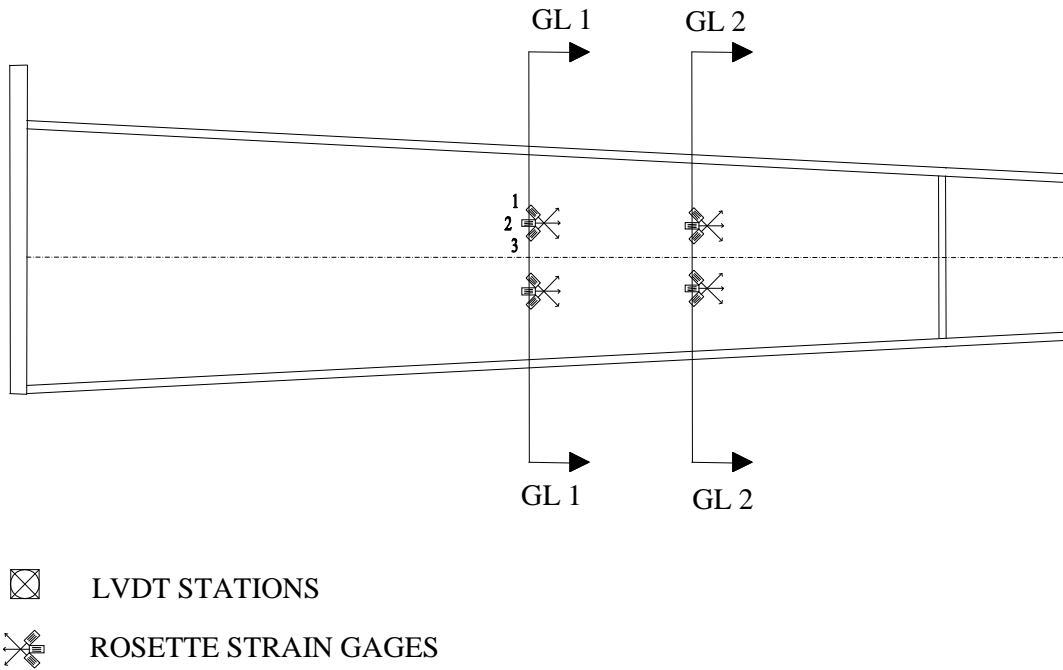


Figure G-4 Far Side Elevation

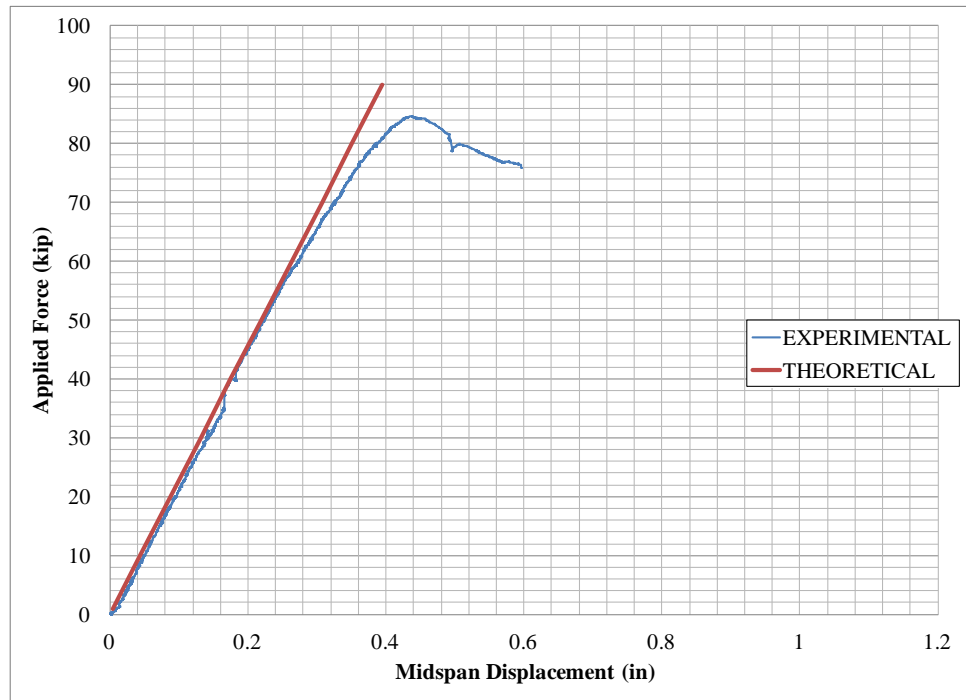


Figure G-5 Applied Force vs. Midspan Displacement

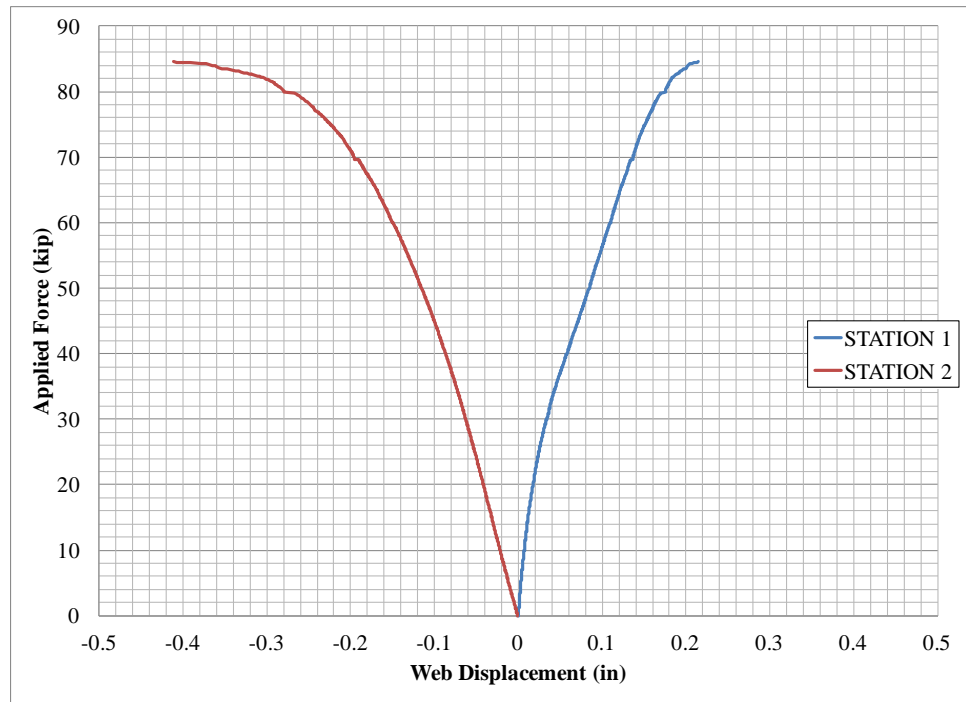
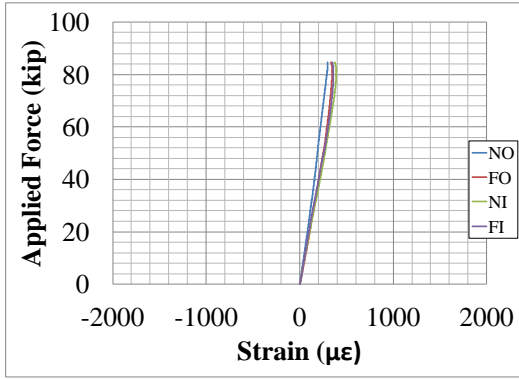
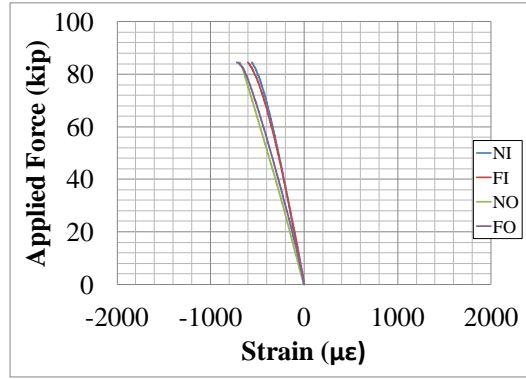


Figure G-6 Applied Force vs. Web Displacement



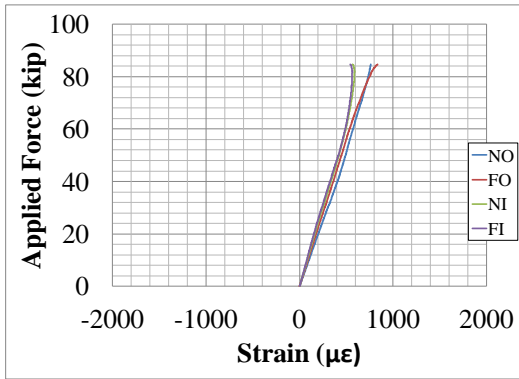


(a) Top Flange

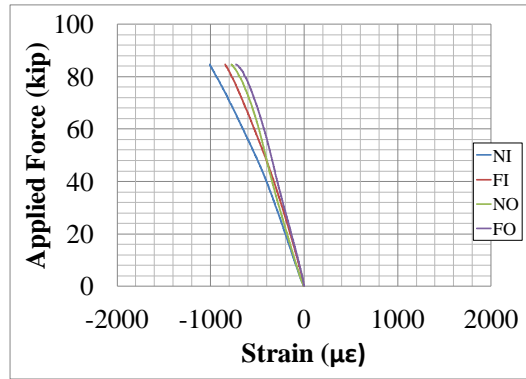


(b) Bottom Flange

Figure G-7 Applied Force vs. Uniaxial Strains at Strain Gage Station 1

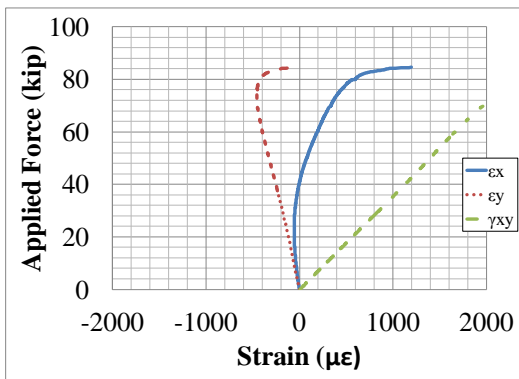


(a) Top Flange

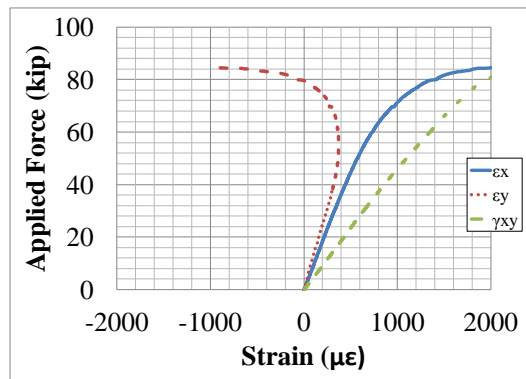


(b) Bottom Flange

Figure G-8 Applied Force vs. Uniaxial Strains at Strain Gage Station 2

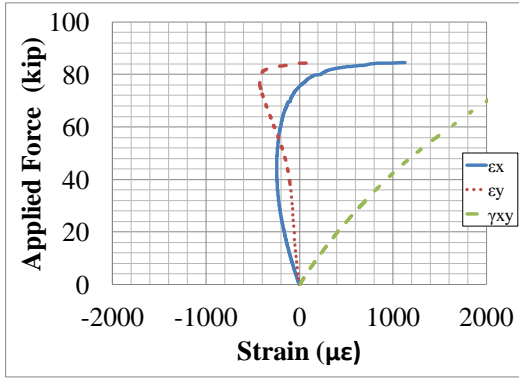


(a) Near Side

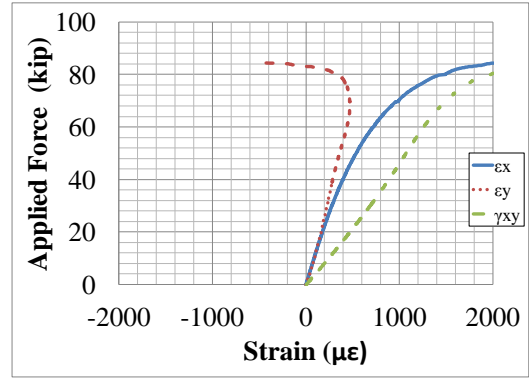


(b) Far Side

Figure G-9 Applied Force vs. 2/3 Web Height Rosette Strains at Strain Gage Station 1

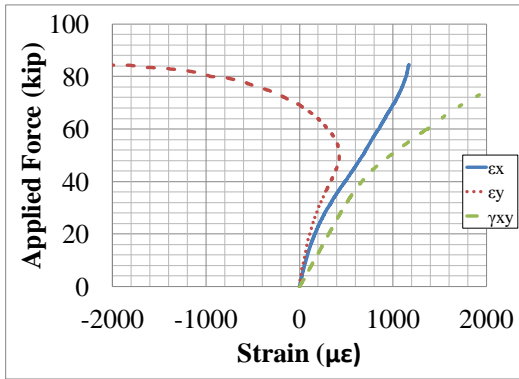


(a) Near Side

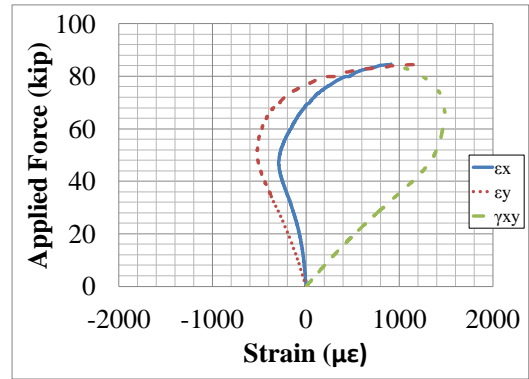


(b) Far Side

Figure G-10 Applied Force vs. 1/3 Web Height Rosette Strains at Strain Gage Station 1

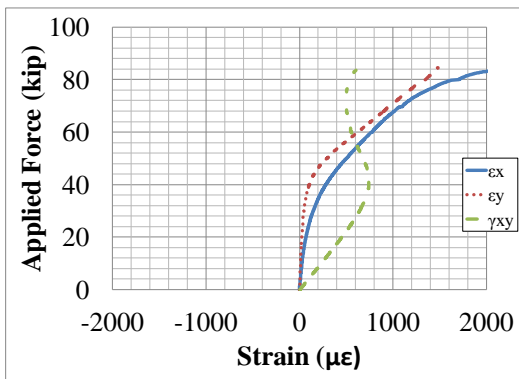


(a) Near Side

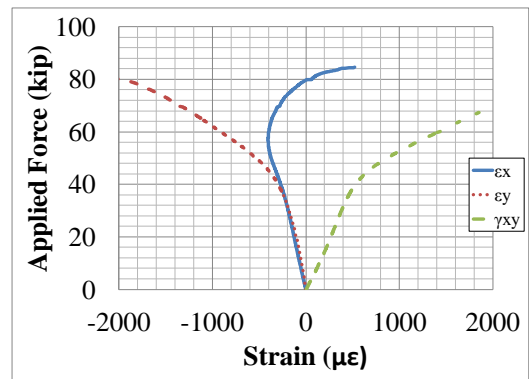


(b) Far Side

Figure G-11 Applied Force vs. 2/3 Web Height Rosette Strains at Strain Gage Station 2

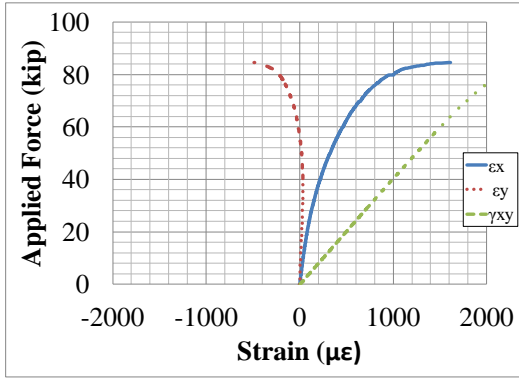


(a) Near Side

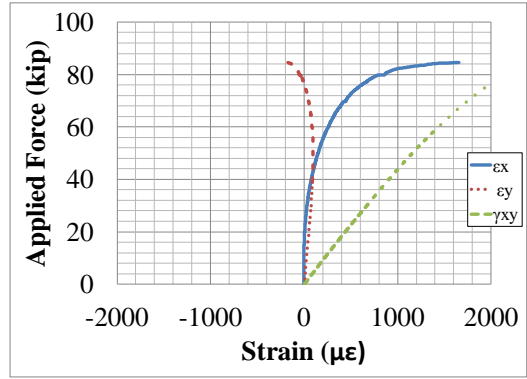


(b) Far Side

Figure G-12 Applied Force vs. 1/3 Web Height Rosette Strains at Strain Gage Station 2

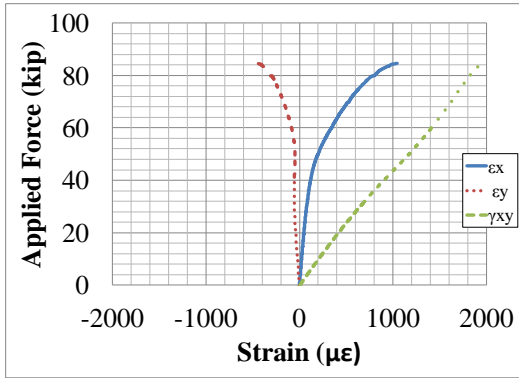


(a) 2/3 Web Height

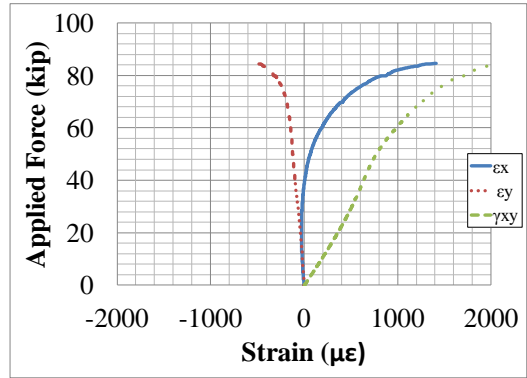


(b) 1/3 Web Height

Figure G-13 Applied Force vs. In Plane Rosette Strains at Strain Gage Station 1



(a) 2/3 Web Height



(b). 1/3 Web Height

Figure G-14 Applied Force vs. In Plane Rosette Strains at Strain Gage Station 2

## Appendix H Tapered 4 Results

PROJECT: Metal Building Manufacturers Association  
TEST NAME: Tapered 4  
TEST DATE: October 3, 2011

### MOMENT END PLATE CONNECTION DESCRIPTION:

Nominal Yield Stress	55 ksi
Gage	4 in.
Width	12 in.
Thickness	1.25 in.
Bolt Hole Locations	2.25 in., 6.5 in., 10in., 21.125in.
Bolt Hole Size	1.3125 in.
Bolt Type	1.25" -7 x 4.25" A490 Hex Bolt
Bolt Pretension	Snug tightened
Nuts	1.25" - 7 A563 GR DH Heavy Hex Nut

### TEST SPECIMEN GEOMETRY:

Total Taper Angle	8.09°
Total Length	11.74 ft
Test Length	5.71 ft
$d_{End}$	12.3125 in.
$d_{Midspan}$	22 in.
$t_w$	0.125 in.
$t_{f,bottom}$	0.625 in.
$b_{f,bottom}$	8 in.
$t_{f,top}$	0.625 in.
$b_{f,top}$	8 in.
$t_{stiffener}$	0.5 in.
$a/h_{ave.}$	3.91

Notes: Test length measured from centerline of stiffener to midspan. Total length measured from centerline of stiffener to centerline of stiffener

### LVDT AND STRAIN GAGE LOCATIONS:

LVDT Station 1	6 in.
LVDT Station 2	18 in.
LVDT Station 3	30 in.
Strain Gage Station 1	6 in.
Strain Gage Station 2	18 in.

Notes: Distances measured from outside face of stiffener. LVDT stations placed on near side of specimen

### EXPERIMENTAL:

Maximum Load	85.1 kip
Failure Mode	Web Shear Buckling



Figure H-1 Web Shear Buckling

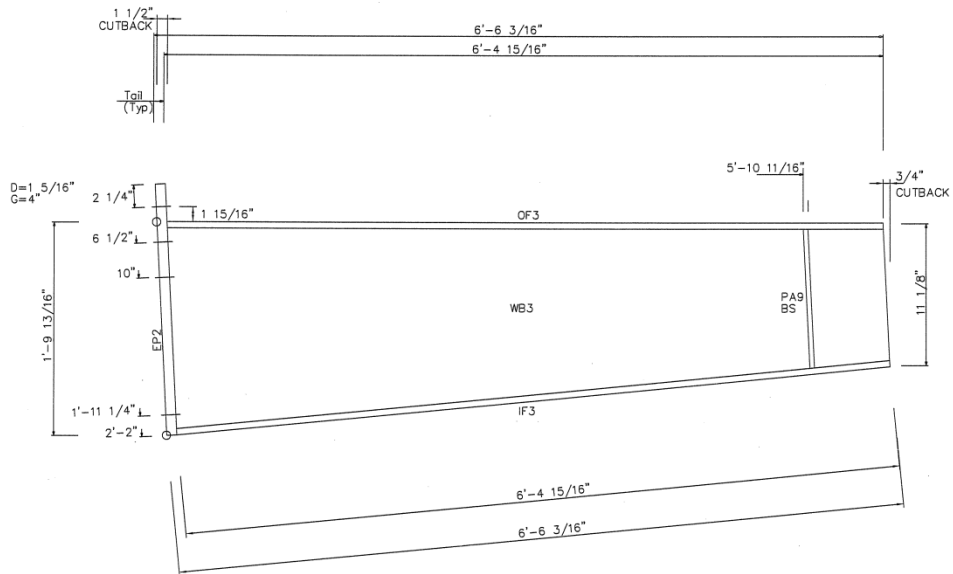


Figure H-2 Dimensions

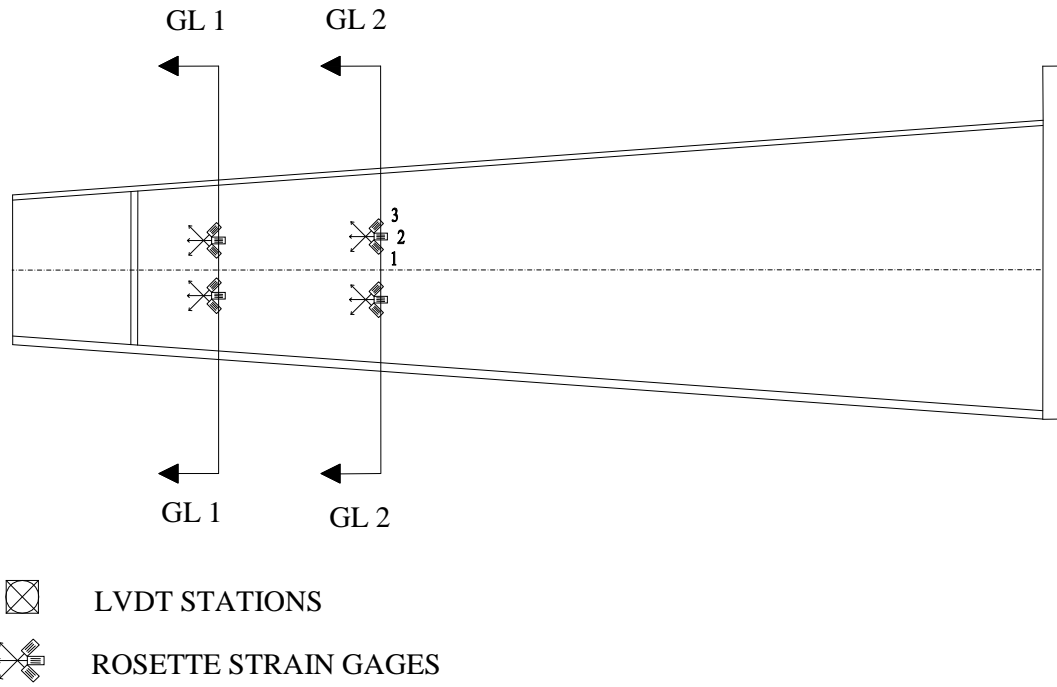


Figure H-3 Near Side Elevation

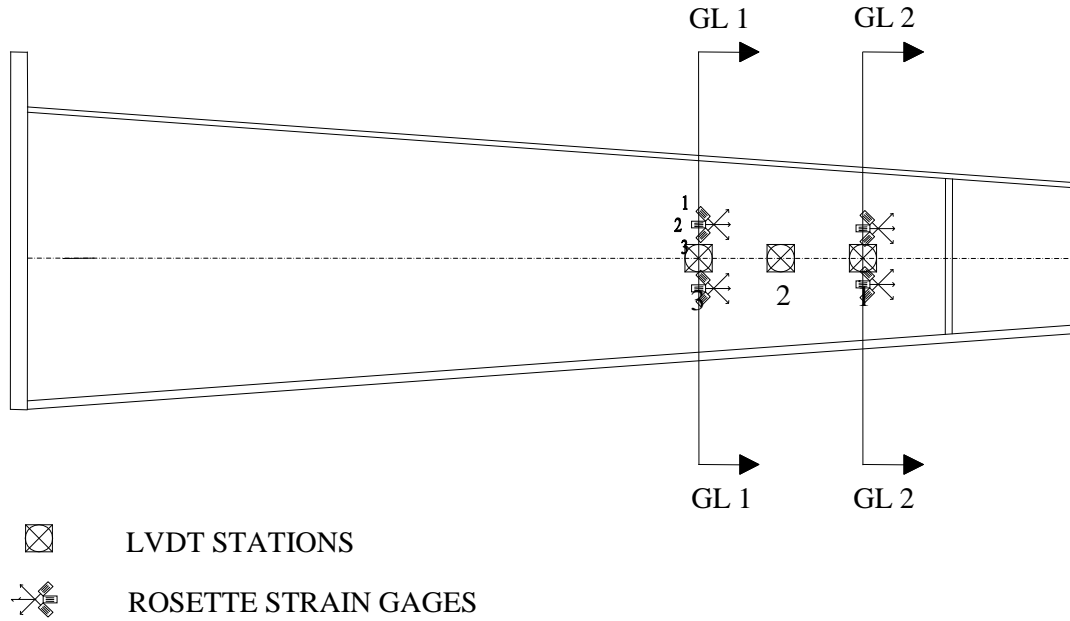


Figure H-4 Far Side Elevation

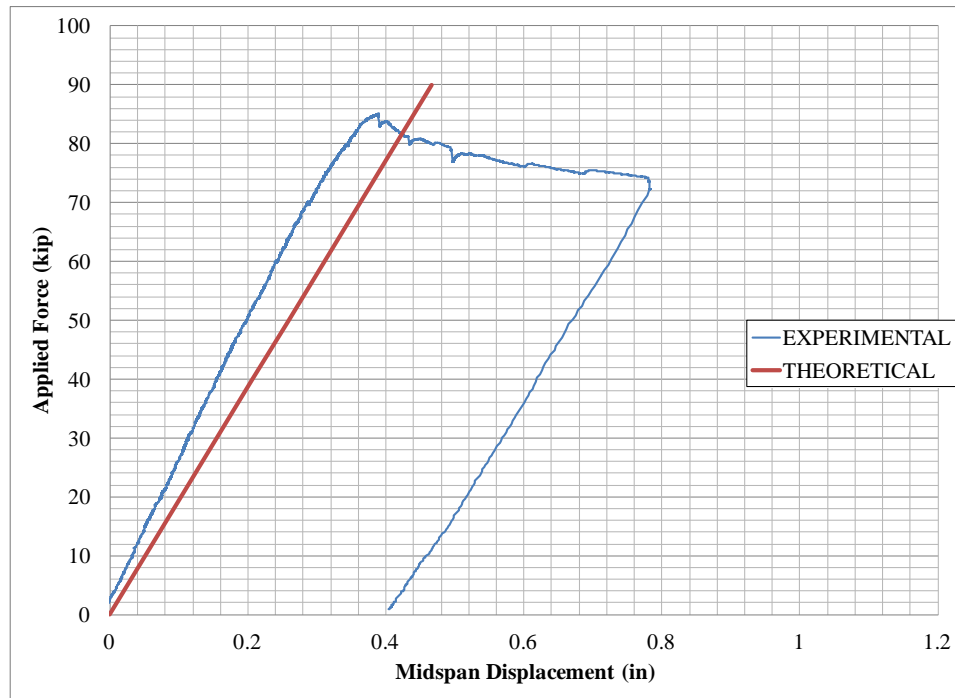


Figure H-5 Applied Force vs. Midspan Displacement

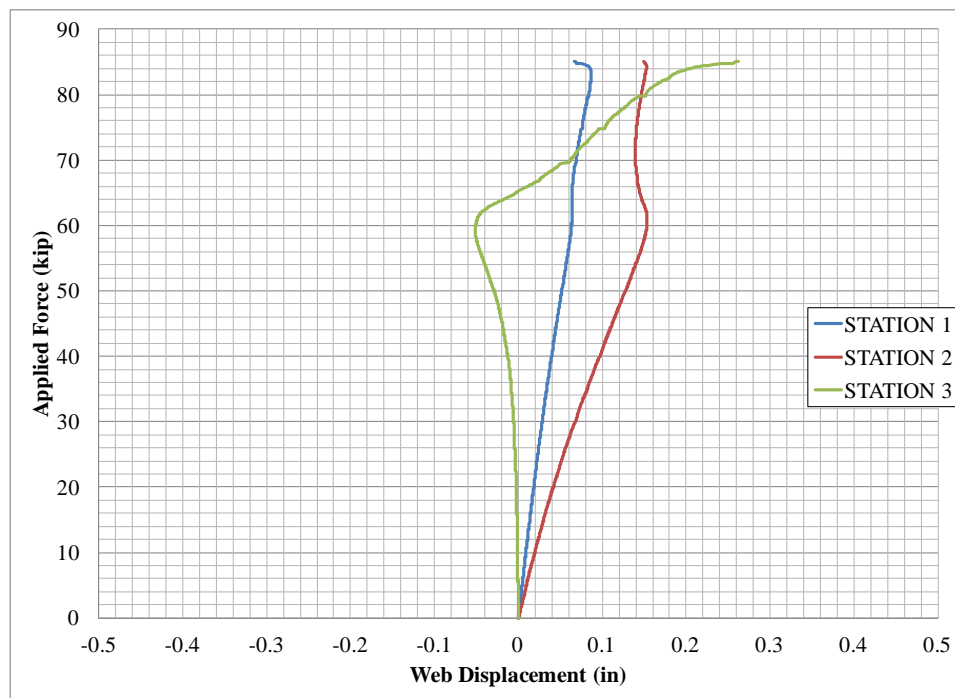
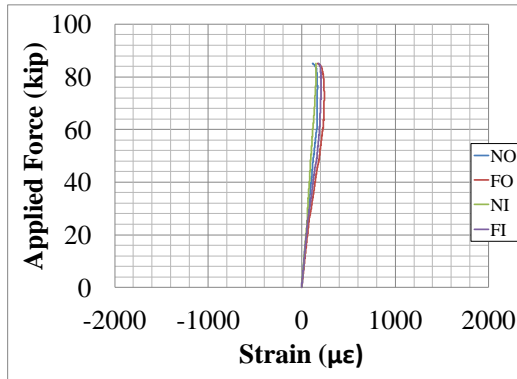
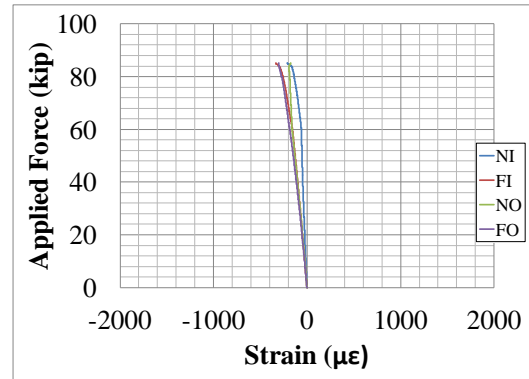


Figure H-6 Applied Force vs. Web Displacement

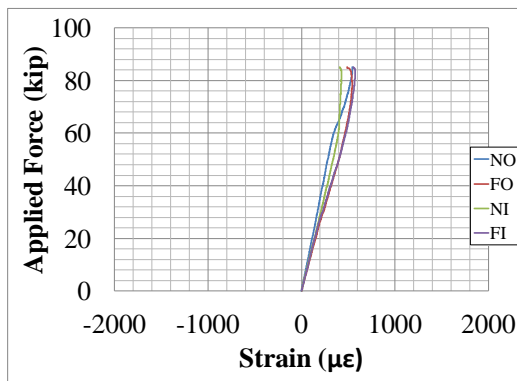


(a) Top Flange

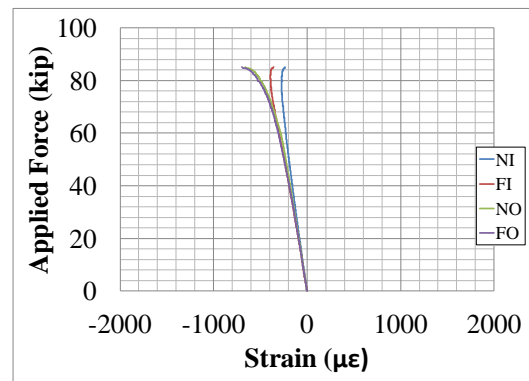


(b) Bottom Flange

Figure H-7 Applied Force vs. Uniaxial Strains at Strain Gage Station 1

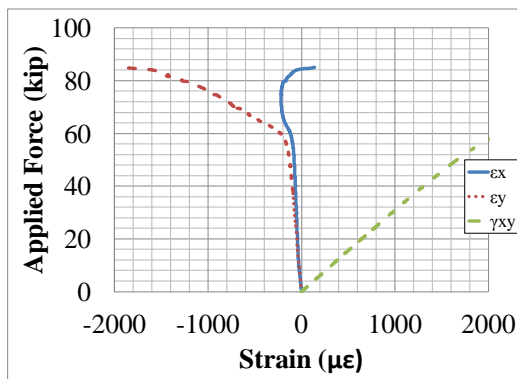


(a) Top Flange

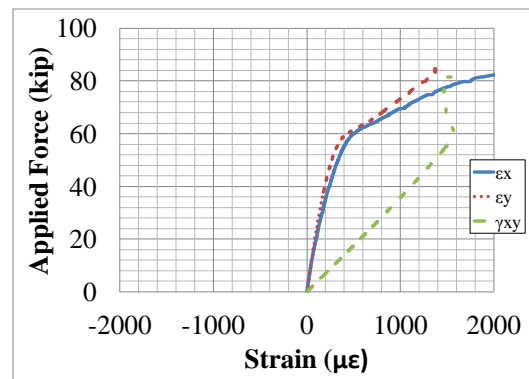


(b) Bottom Flange

Figure H-8 Applied Force vs. Uniaxial Strains at Strain Gage Station 2



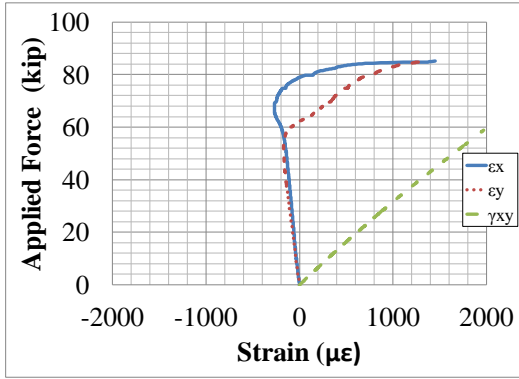
(a) Near Side



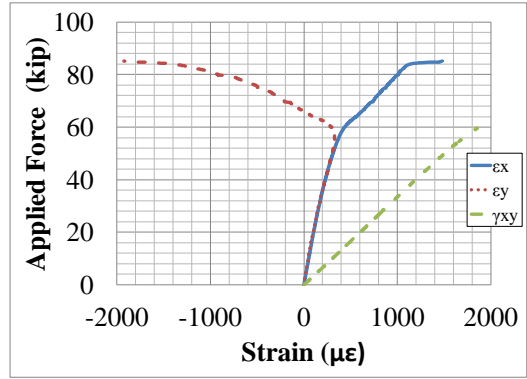
(b) Far Side

Figure H-9 Applied Force vs. 2/3 Web Height Rosette Strains at Strain Gage Station 1



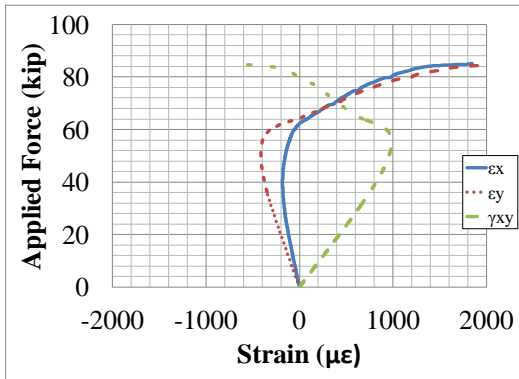


(a) Near Side

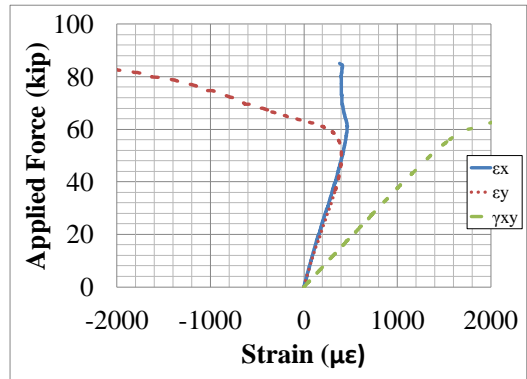


(b) Far Side

Figure H-10 Applied Force vs. 1/3 Web Height Rosette Strains at Strain Gage Station 1

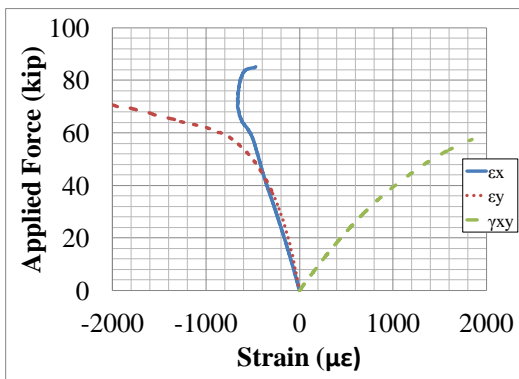


(a) Near Side

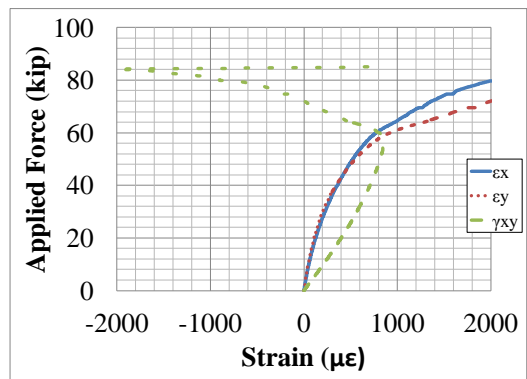


(b) Far Side

Figure H-11 Applied Force vs. 2/3 Web Height Rosette Strains at Strain Gage Station 2

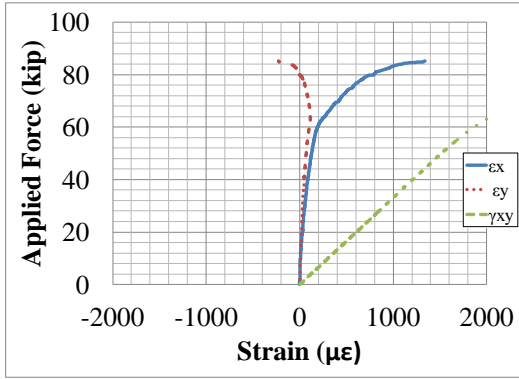


(a) Near Side

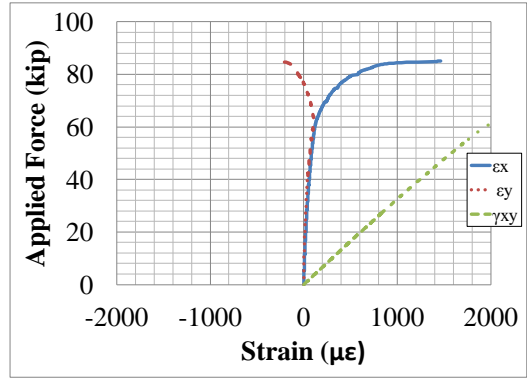


(b) Far Side

Figure H-12 Applied Force vs. 1/3 Web Height Rosette Strains at Strain Gage Station 2

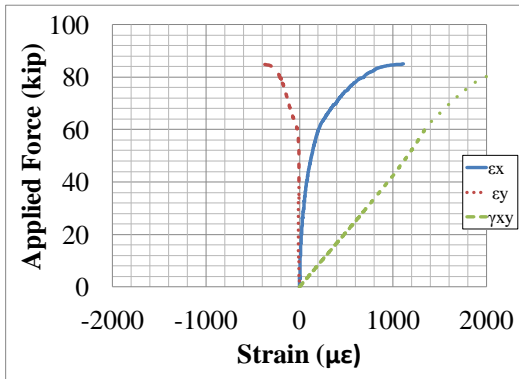


(a) 2/3 Web Height

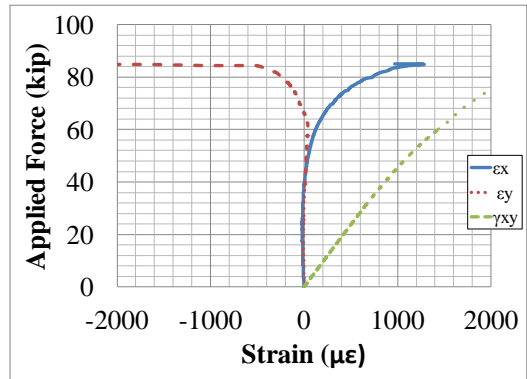


(b) 1/3 Web Height

Figure H-13 Applied Force vs. In Plane Rosette Strains at Strain Gage Station 1



(a) 2/3 Web Height



(b) 1/3 Web Height

Figure H-14 Applied Force vs. In Plane Rosette Strains at Strain Gage Station 2

## Appendix I Tapered 5 Results

PROJECT: Metal Building Manufacturers Association  
TEST NAME: Tapered 5  
TEST DATE: November 4, 2011

### MOMENT END PLATE CONNECTION DESCRIPTION:

Nominal Yield Stress	55 ksi
Gage	4 in.
Width	12 in.
Thickness	1.25 in.
Bolt Hole Locations	2.25 in., 6.5in., 10in., 24.0625 in.
Bolt Hole Size	1.3125 in.
Bolt Type	1.25" - 7 x 4.25" A490 Hex Bolt
Bolt Pretension	Snug tightened
Nuts	1.25" - 7 A563 GR DH Heavy Hex Nut

### TEST SPECIMEN GEOMETRY:

Total Taper Angle	4.97°
Total Length	13.1875 ft
Test Length	6.48 ft
$d_{End}$	16.125 in.
$d_{Midspan}$	22.875 in.
$t_w$	0.150 in.
$t_{f,bottom}$	0.5 in.
$b_{f,bottom}$	8 in.
$t_{f,top}$	0.75 in.
$b_{f,top}$	8 in.
$t_{stiffener}$	0.5 in.
$a/h_{ave.}$	3.91

Notes: Test length measured from centerline of stiffener to midspan. Total length measured from centerline of stiffener to centerline of stiffener

### LVDT AND STRAIN GAGE LOCATIONS:

LVDT Station 1	12.0625 in.
LVDT Station 2	18.0625 in.
Strain Gage Station 1	18.0625 in.

Notes: Distances measured from outside face of stiffener. LVDT stations placed on near side of specimen

### EXPERIMENTAL:

Maximum Load	114 kip
Failure Mode	Web Shear Buckling

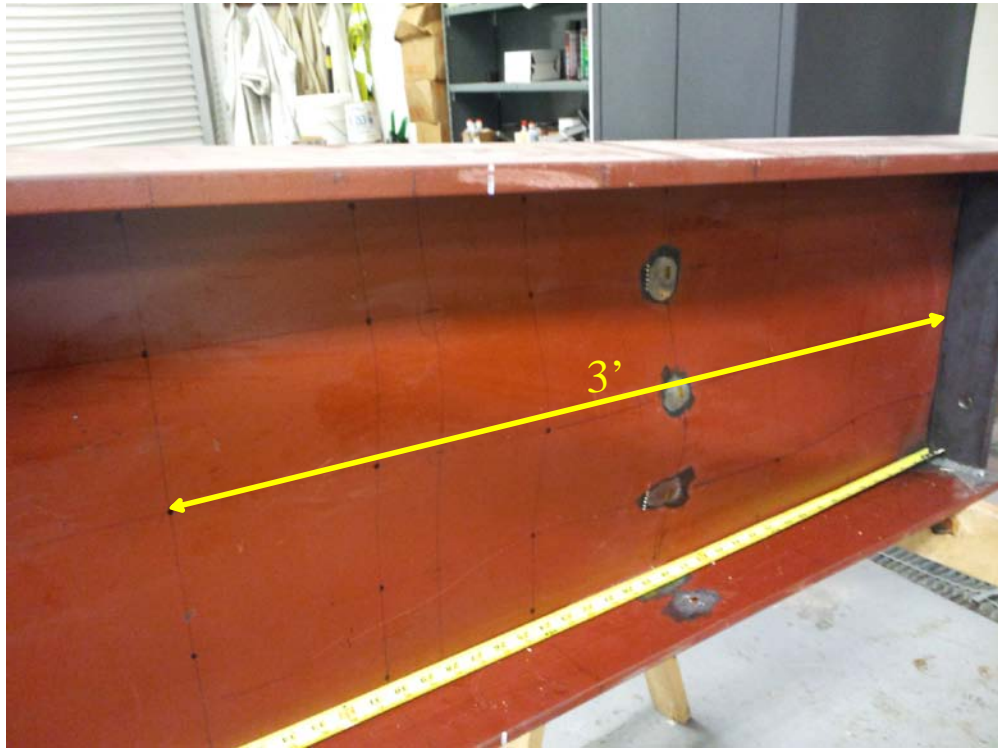


Figure I-1 Web Shear Buckling

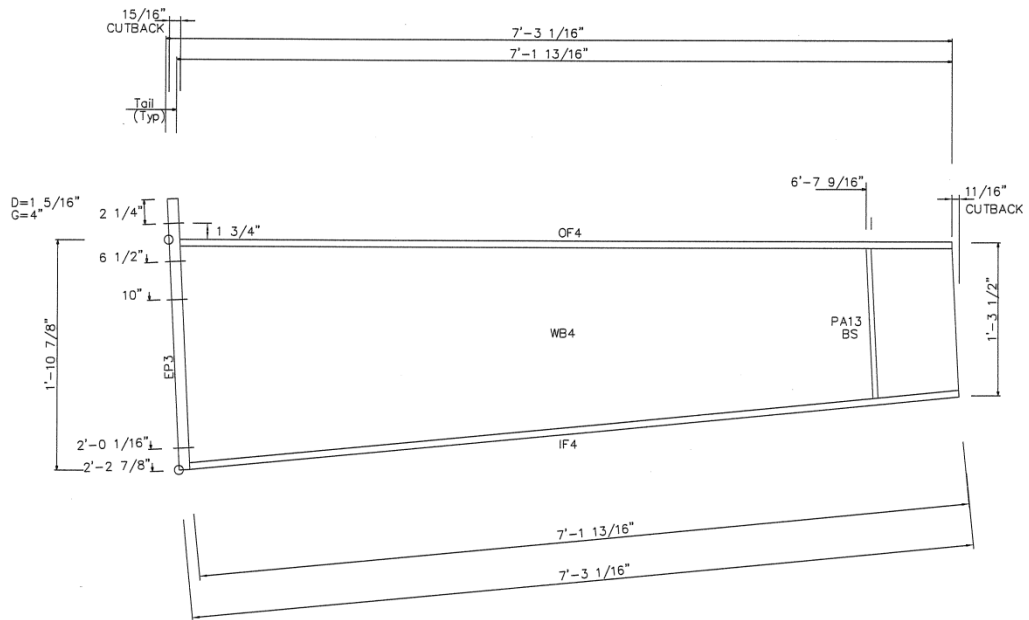


Figure I-2 Dimensions

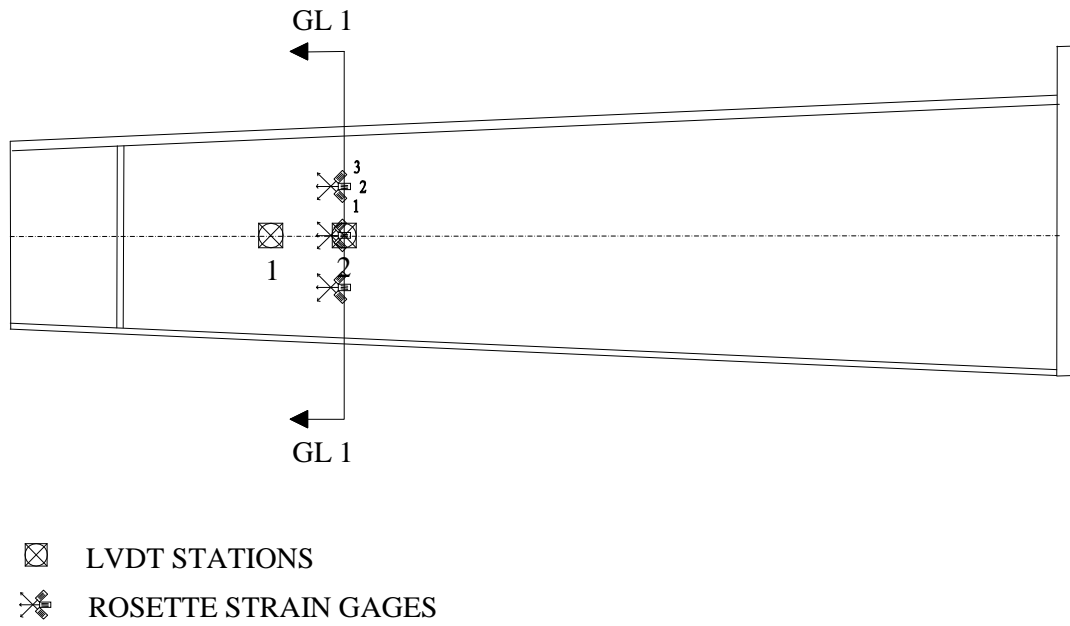


Figure I-3 Near Side Elevation

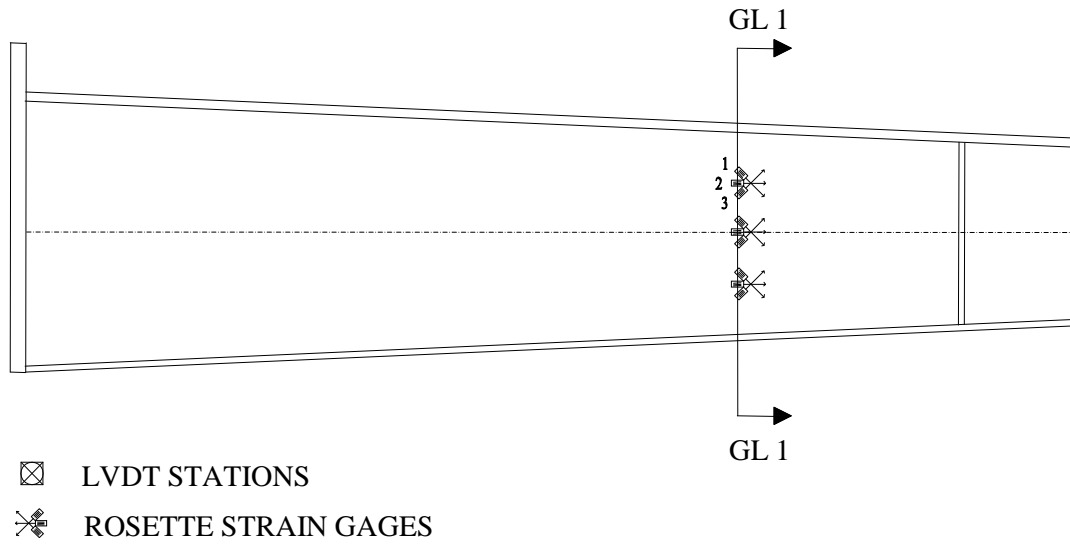


Figure I-4 Far Side Elevation

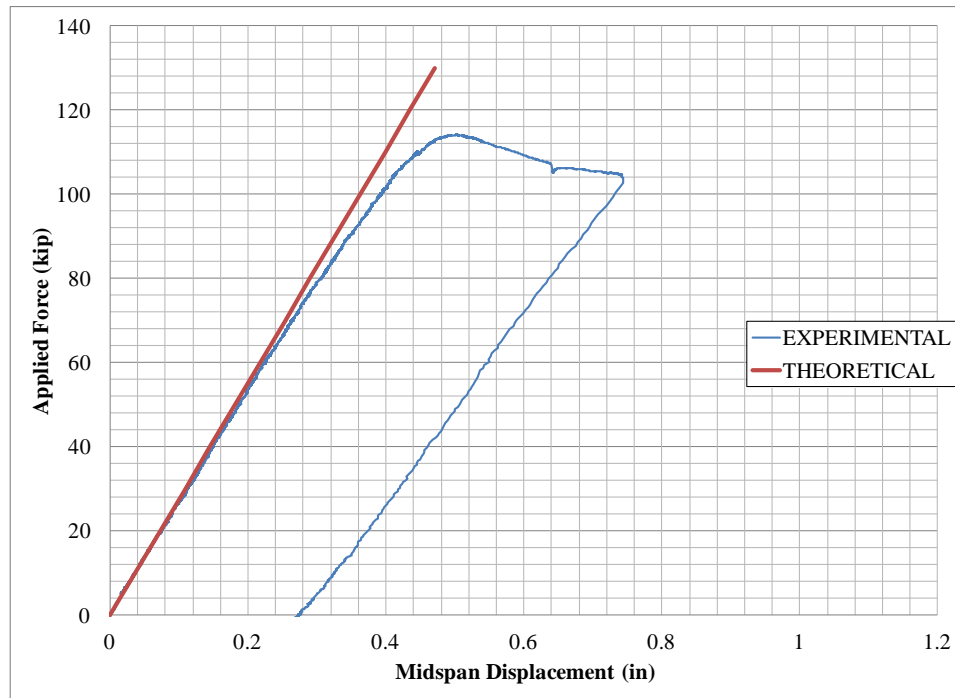


Figure I-5 Applied Force vs. Midspan Displacement

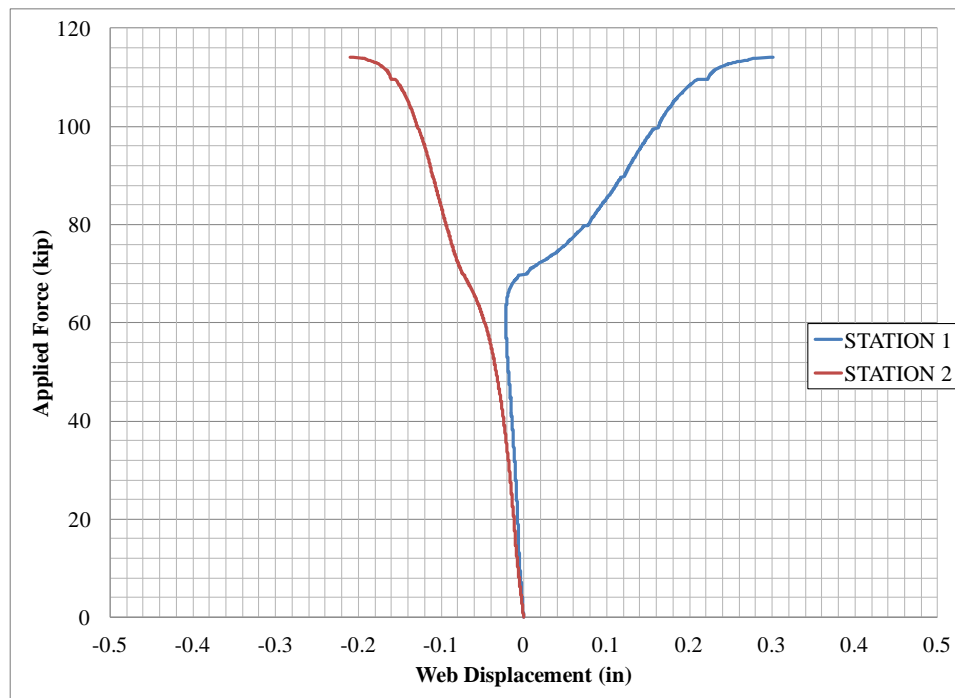
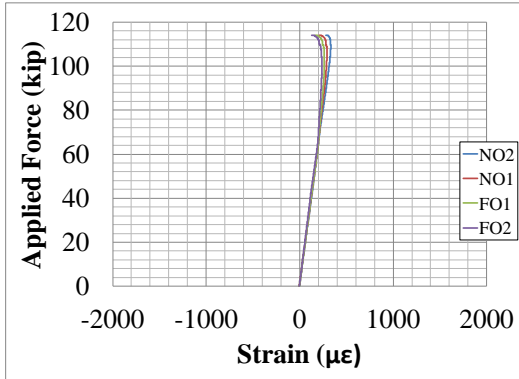
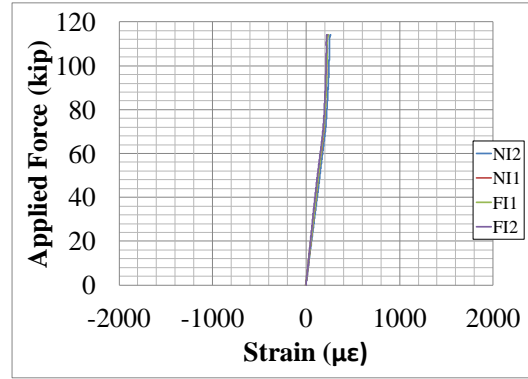


Figure I-6 Applied Force vs. Web Displacement



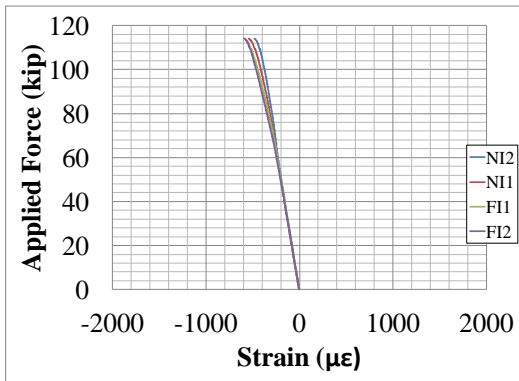
(a) Outside Flange



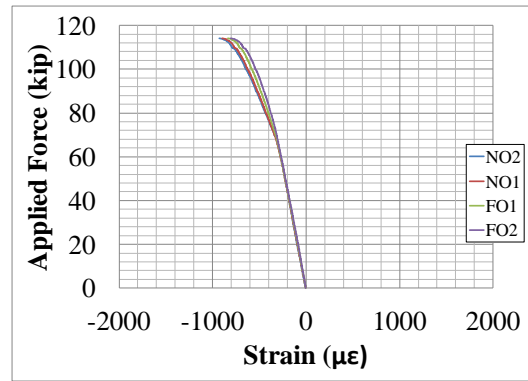
(b) Inside Flange

2 = Outer Strain Gages      1 = Inner Strain Gages      2 = Outer Strain Gages      1 = Inner Strain Gages

Figure I-7 Applied Force vs. Top Flange Uniaxial Strains at Strain Gage Station 1



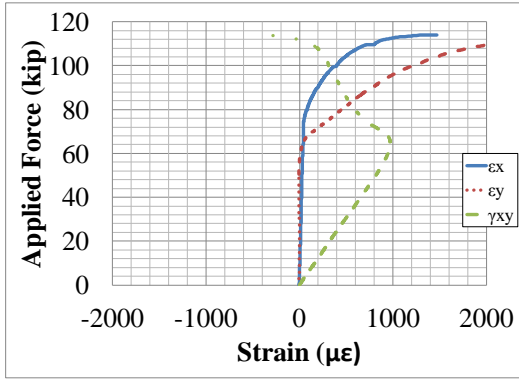
(a) Inside Flange



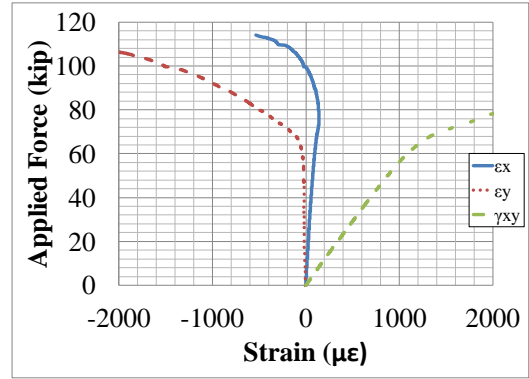
(b) Outside Flange

2 = Outer Strain Gages      1 = Inner Strain Gages      2 = Outer Strain Gages      1 = Inner Strain Gages

Figure I-8 Applied Force vs. Bottom Flange Uniaxial Strains at Strain Gage Station 1

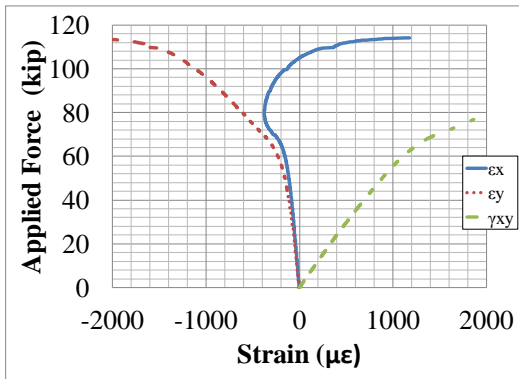


(a) Near Side

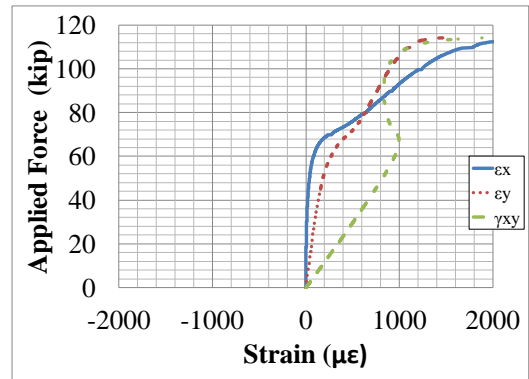


(b) Far Side

Figure I-9 Applied Force vs. 3/4 Web Height Rosette Strains at Strain Gage Station 1

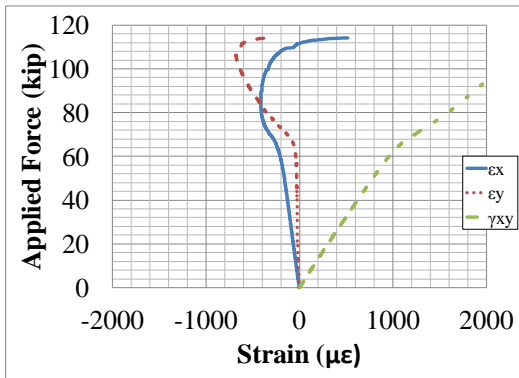


(a) Near Side

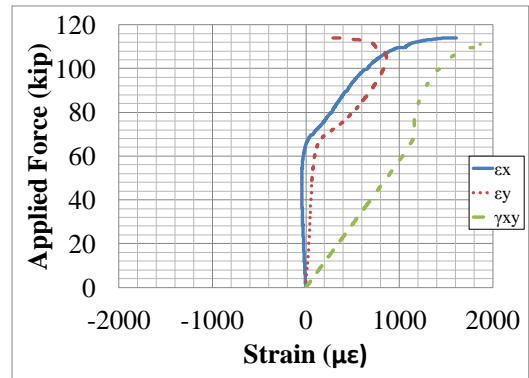


(b) Far Side

Figure I-10 Applied Force vs. 1/2 Web Height Rosette Strains at Strain Gage Station 1



(a) Near Side



(b) Far Side

Figure I-11 Applied Force vs. 1/4 Web Height Rosette Strains at Strain Gage Station 1



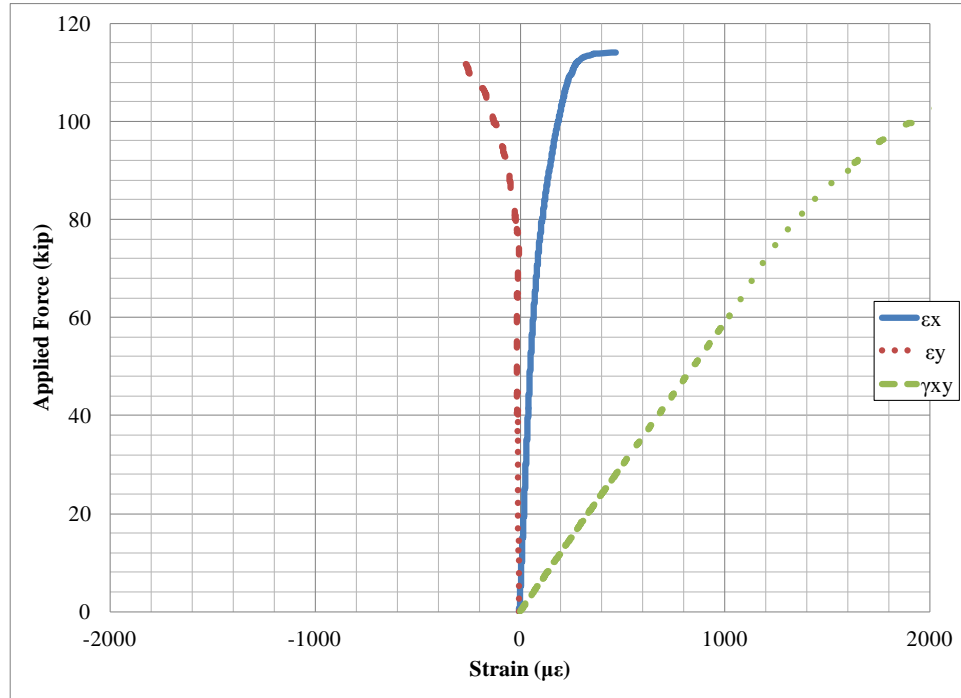


Figure I-12 Applied Force vs. 3/4 Web Height In Plane Rosette Strains at Strain Gage Station 1

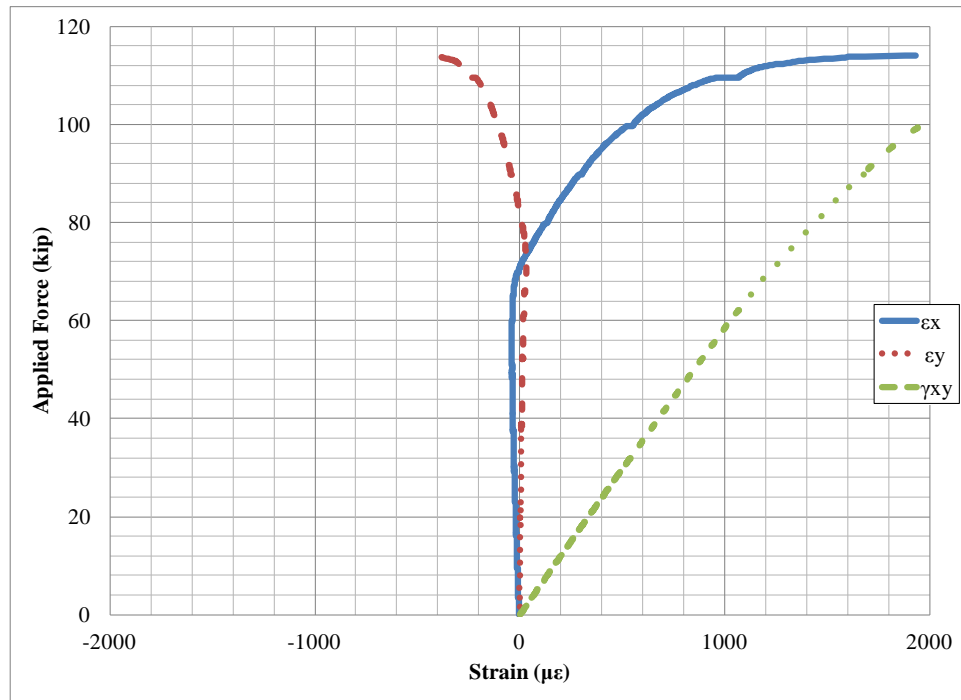


Figure I-13 Applied Force vs. 1/2 Web Height In Plane Rosette Strains at Strain Gage Station 1

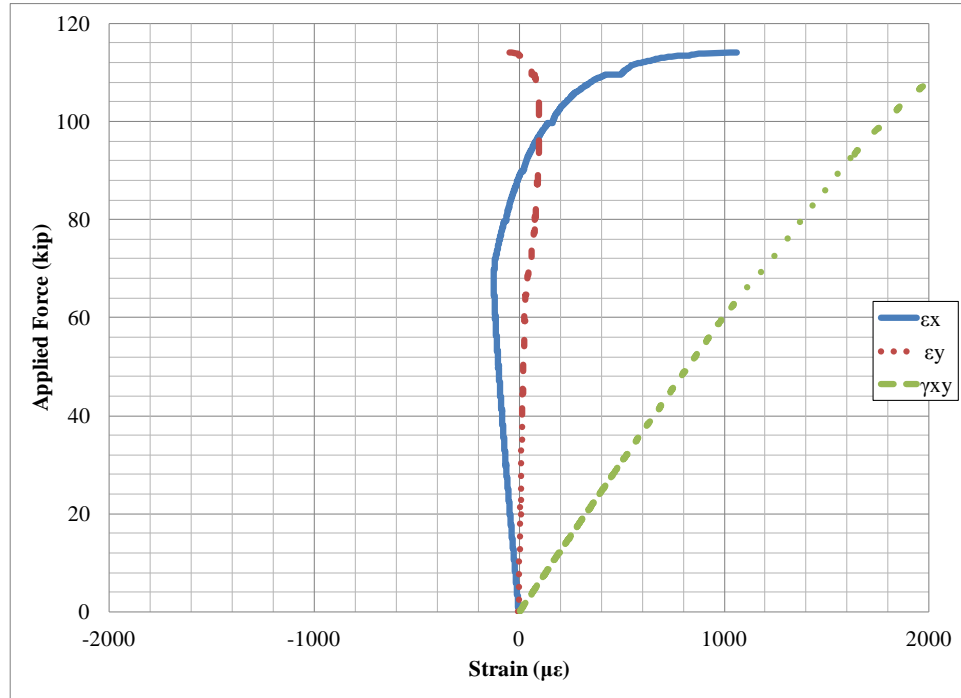


Figure I-14 Applied Force vs. 1/4 Web Height In Plane Rosette Strains at Strain Gage Station 1

## Appendix J Tapered 6 Results

PROJECT: Metal Building Manufacturers Association  
TEST NAME: Tapered 6  
TEST DATE: October 21, 2011

### MOMENT END PLATE CONNECTION DESCRIPTION:

Nominal Yield Stress	55 ksi
Gage	4 in.
Width	12 in.
Thickness	1.25 in.
Bolt Hole Locations	2.25 in., 6.5 in., 15.375 in.
Bolt Hole Size	1.3125 in.
Bolt Type	1.25" - 7 x 4.25" A490 Hex Bolt
Bolt Pretension	Snug
Nuts	1.25" - 7 A563 GR DH Heavy Hex Nut

### TEST SPECIMEN GEOMETRY:

Total Taper Angle	6.05°
Total Length	11.77 ft
Test Length	5.71 ft
$d_{End}$	14.125 in.
$d_{Midspan}$	21.5 in.
$t_w$	0.134 in.
$t_{f,bottom}$	0.5 in.
$b_{f,bottom}$	8 in.
$t_{f,top}$	0.375 in.
$b_{f,top}$	8 in.
$t_{stiffener}$	0.5 in.
$a/h_{ave.}$	3.75

Notes: Test length measured from centerline of stiffener to midspan. Total length measured from centerline of stiffener to centerline of stiffener

### LVDT AND STRAIN GAGE LOCATIONS:

LVDT Station 1	40.5 in.
LVDT Station 2	28 in.
LVDT Station 3	9 in.
Strain Gage Station 1	24 in.
Strain Gage Station 2	12 in.

Notes: Distances measured from outside face of moment plate. LVDT stations placed on near side of specimen

### EXPERIMENTAL:

Maximum Load	68.2 kips
Failure Mode	Web Shear Buckling



Figure J-1 Web Shear Buckling

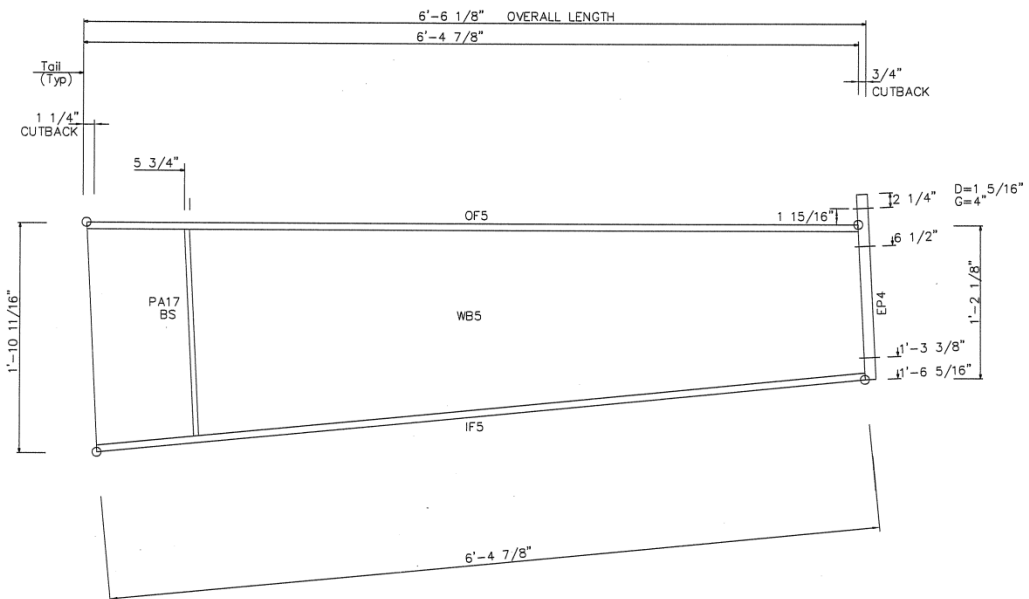


Figure J-2 Dimensions

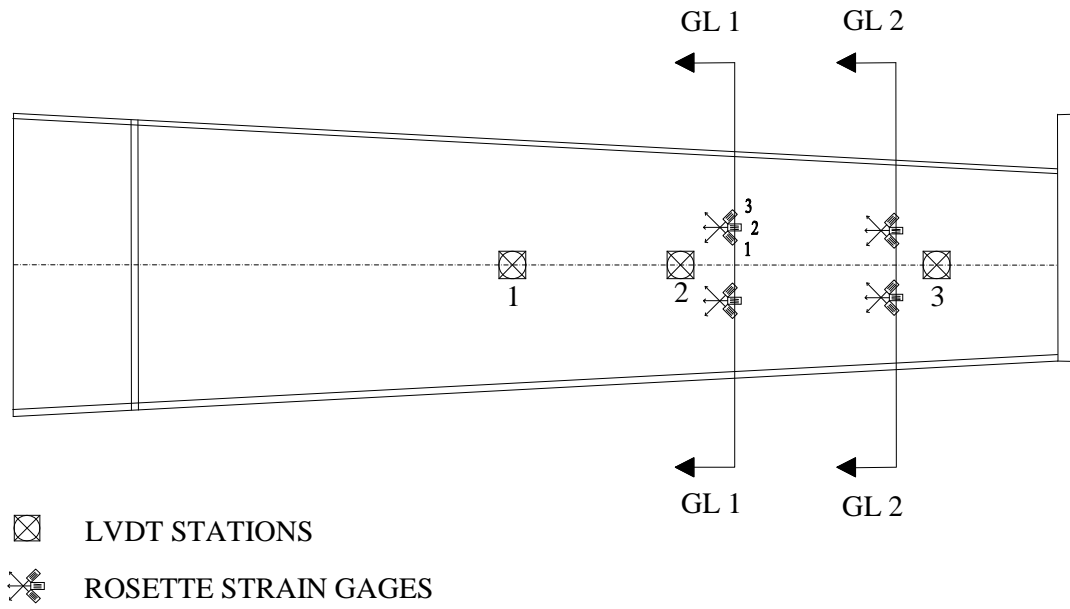


Figure J-3 Near Side Elevation

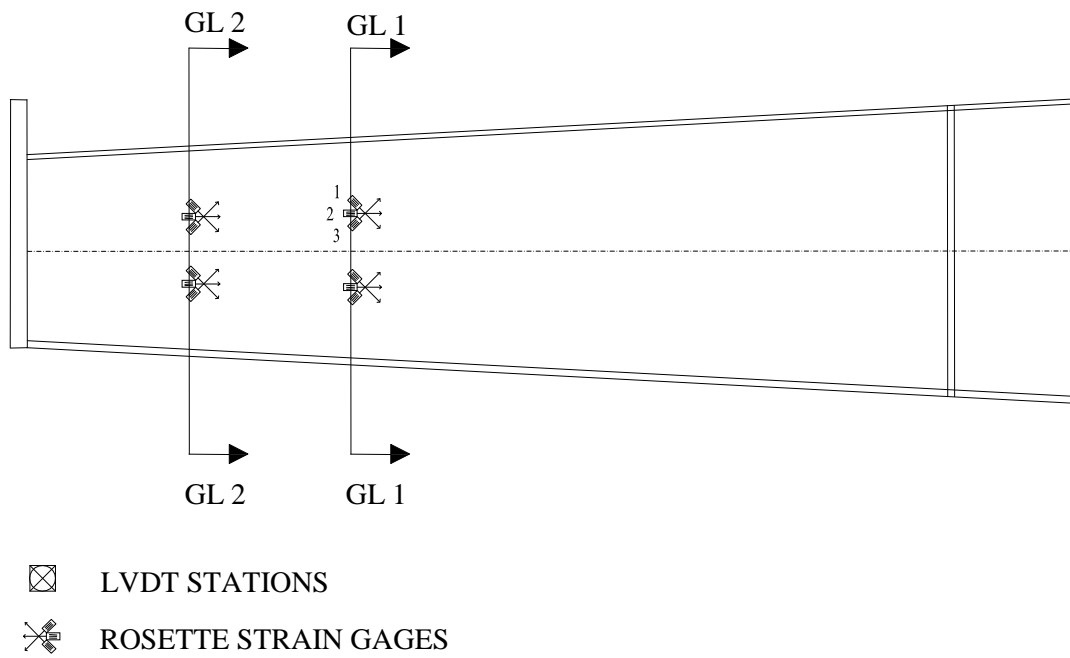


Figure J-4 Far Side Elevation

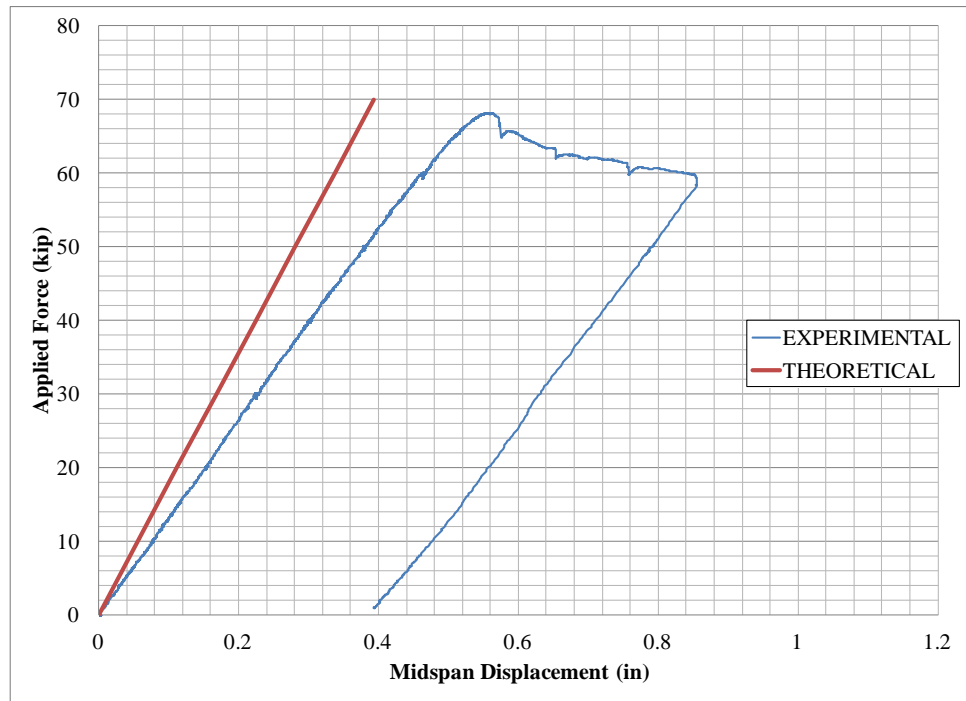


Figure J-5 Applied Force vs. Midspan Displacement

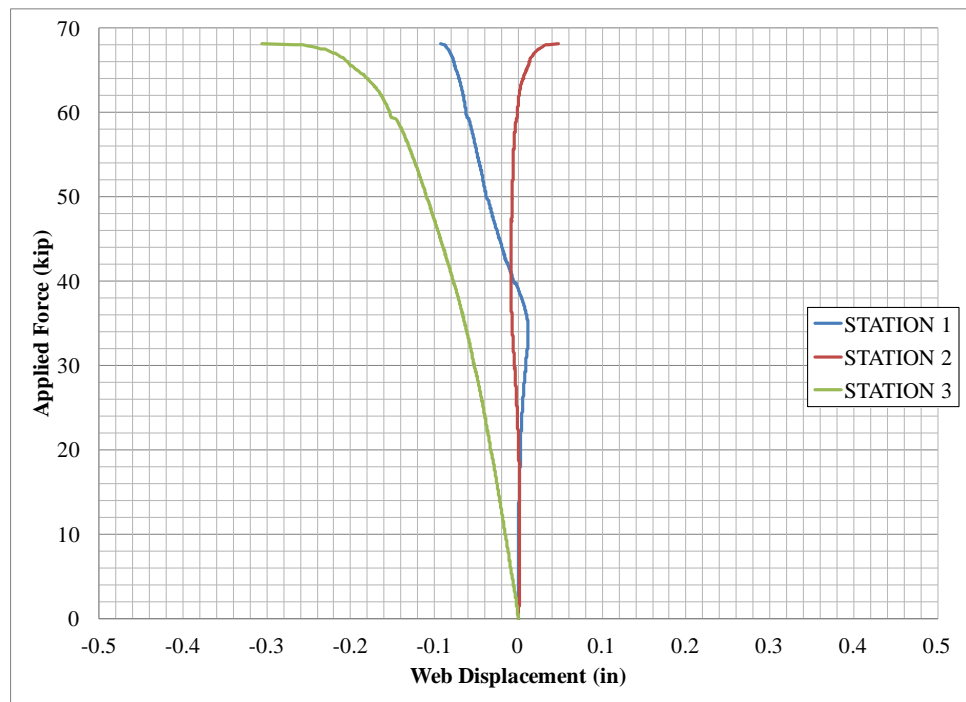
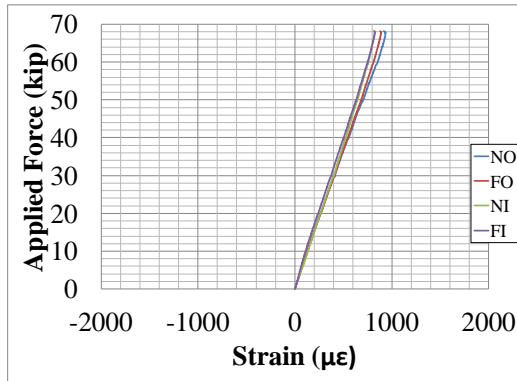
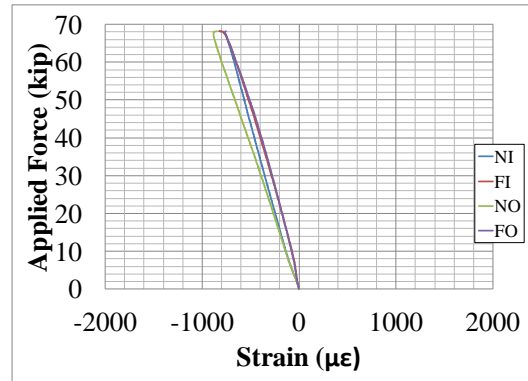


Figure J-6 Applied Force vs. Web Displacement

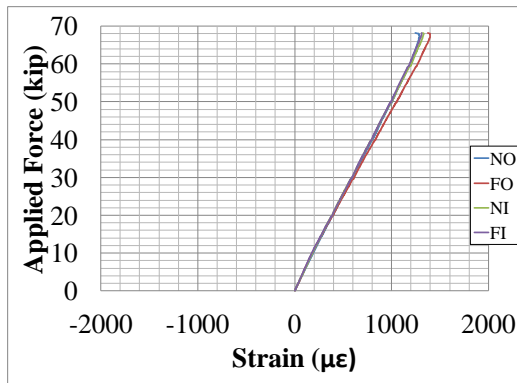


(a) Top Flange

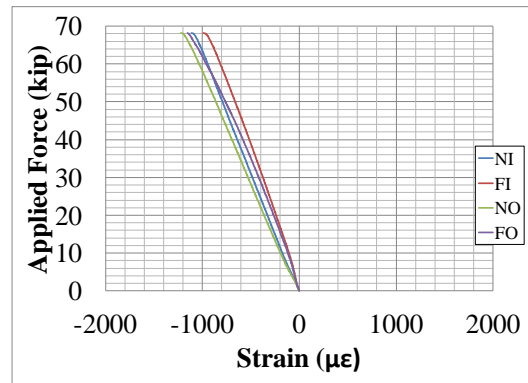


(b) Bottom Flange

Figure J-7 Applied Force vs. Uniaxial Strains at Strain Gage Station 1

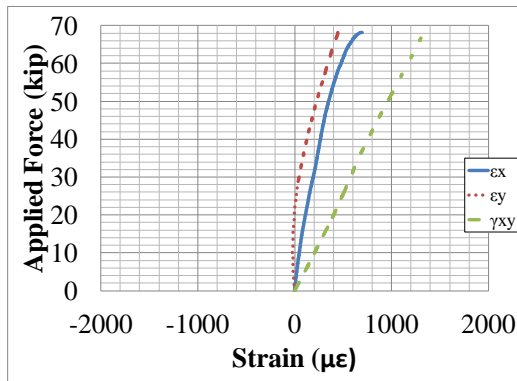


(a) Top Flange

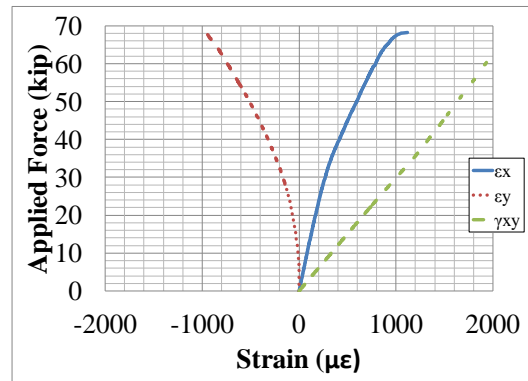


(b) Bottom Flange

Figure J-8 Applied Force vs. Uniaxial Strains at Strain Gage Station 2

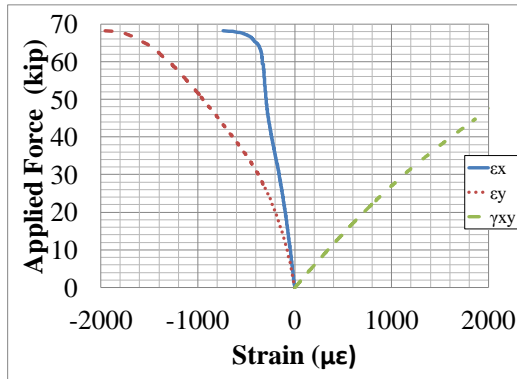


(a) Near Side

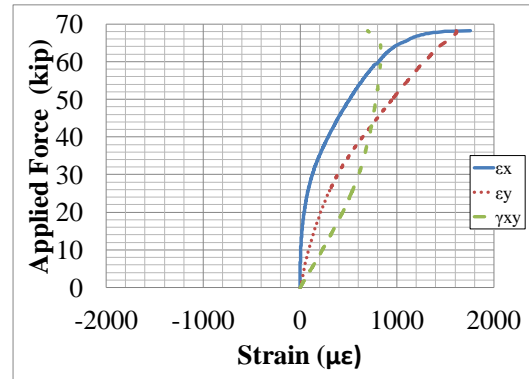


(b) Far Side

Figure J-9 Applied Force vs. 2/3 Web Height Rosette Strains at Strain Gage Station 1

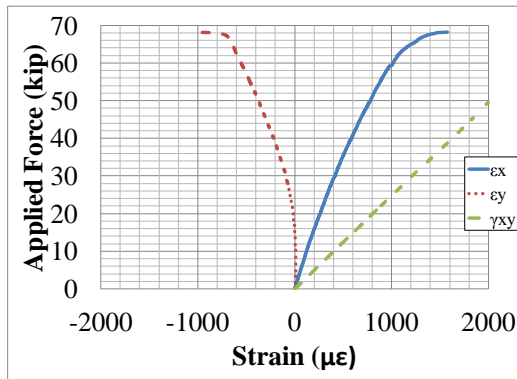


(a) Near Side

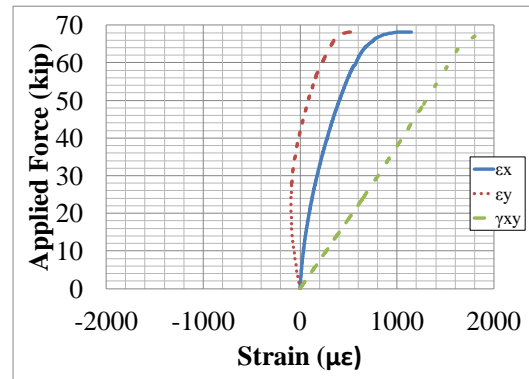


(b) Far Side

Figure J-10 Applied Force vs. 1/3 Web Height Rosette Strains at Strain Gage Station 1

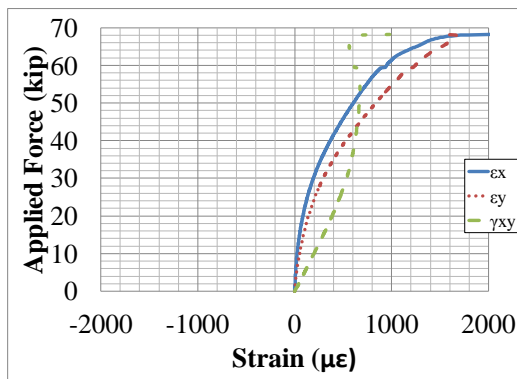


(a) Near Side

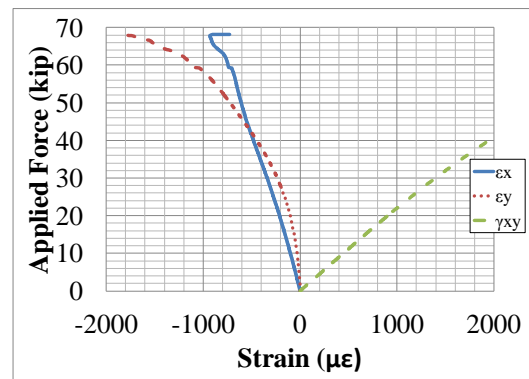


(b) Far Side

Figure J-11 Applied Force vs. 2/3 Web Height Rosette Strains at Strain Gage Station 2



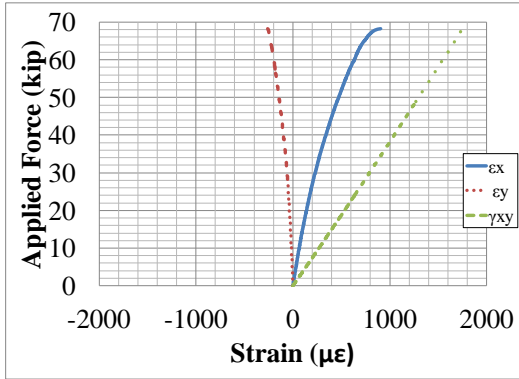
(a) Near Side



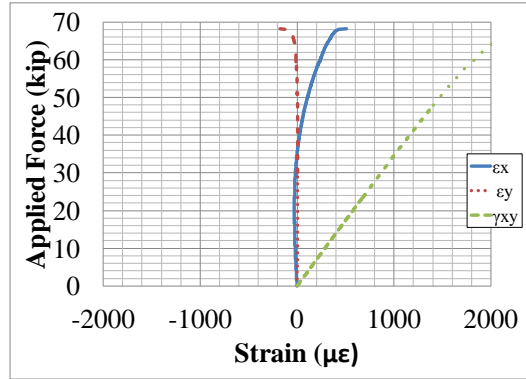
(b) Far Side

Figure J-12 Applied Force vs. 1/3 Web Height Rosette Strains at Strain Gage Station 2



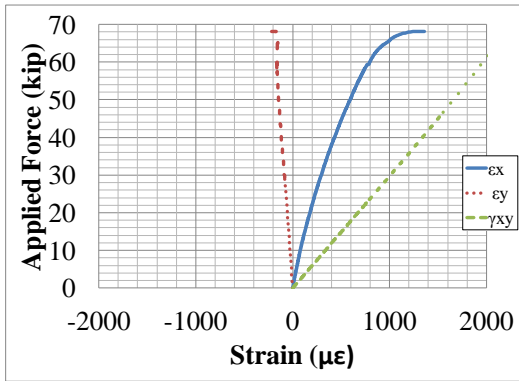


(a) 2/3 Web Height

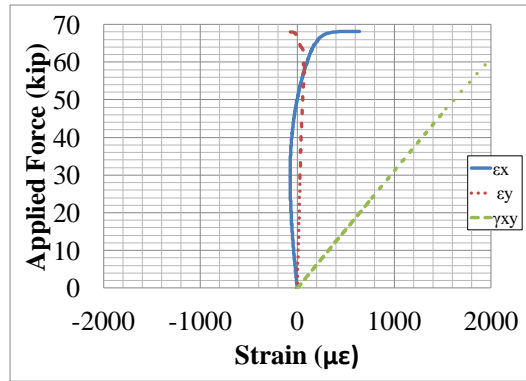


(b) 1/3 Web Height

Figure J-13 Applied Force vs. In Plane Rosette Strains at Strain Gage Station 1



(a) 2/3 Web Height



(b) 1/3 Web Height

Figure J-14 Applied Force vs. In Plane Rosette Strains at Strain Gage Station 2

## Appendix K Prismatic 1 Results

PROJECT: Metal Building Manufacturers Association  
TEST NAME: Prismatic 1  
TEST DATE: April 1, 2011

### MOMENT END PLATE CONNECTION DESCRIPTION:

Nominal Yield Stress	55 ksi
Gage	3.50 in.
Width	8 in.
Thickness	1 in.
Bolt Hole Locations	2 in., 13.88 in., 17.88 in., and 21.88 in.
Bolt Hole Size	1.1875 in.
Bolt Type	1.125" x 3.75" A325 Bolts
Bolt Pretension	Snug tightened
Nuts	1.125" -7 Heavy Hex Nuts (A563 Grade C, C3, D or DH)

### TEST SPECIMEN GEOMETRY:

Total Taper Angle	0°
Total Length	15 ft
Test Length	7.5 ft
$d_{End}$	20 in.
$d_{Midspan}$	20 in.
$t_w$	0.125 in.
$t_{f,bottom}$	0.3125 in.
$b_{f,bottom}$	6 in.
$t_{f,top}$	0.3125 in.
$b_{f,top}$	6 in.
$t_{stiffener}$	0.5 in.
$a/h_{ave.}$	4.43

Notes: Test length measured from centerline of stiffener to midspan. Total length measured from centerline of stiffener to centerline of stiffener

### LVDT AND STRAIN GAGE LOCATIONS:

LVDT Station 1	66 in.
LVDT Station 2	72 in.
LVDT Station 3	78 in.
Strain Gage Station 1	72 in.

Notes: Distances measured from outside face of stiffener. LVDT stations placed on near side of specimen

### EXPERIMENTAL:

Maximum Load	57.2 kip
Failure Mode	Web Shear Buckling

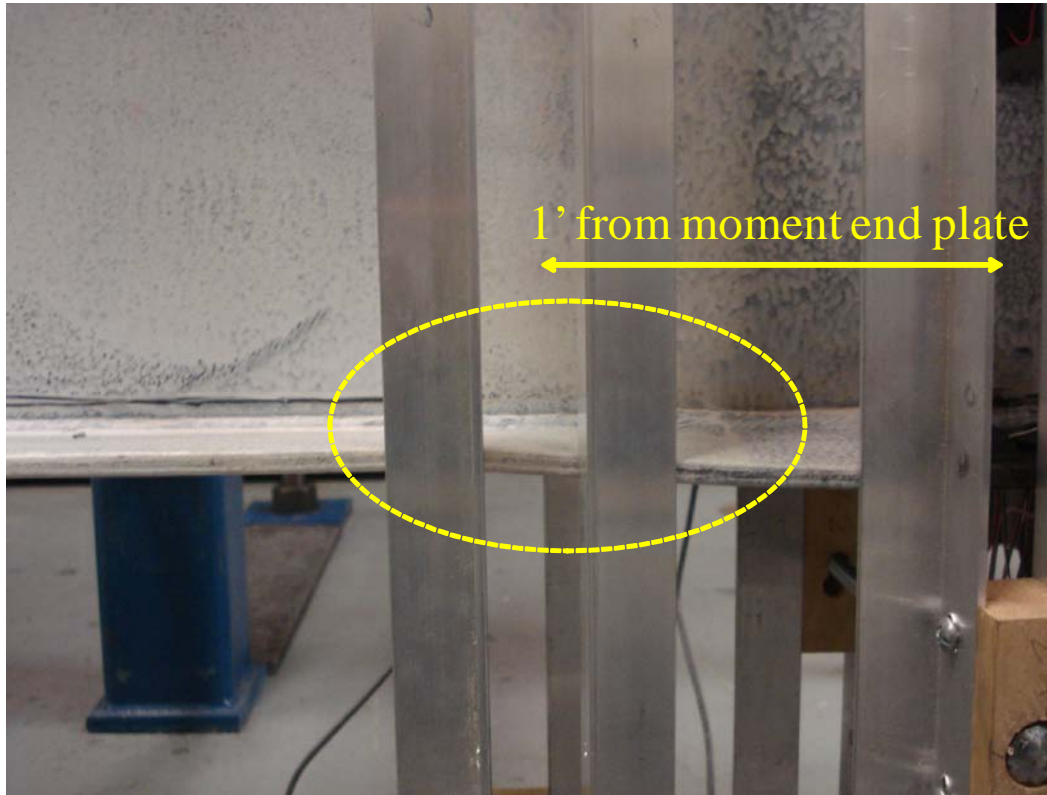


Figure K-1 Flange Local Buckling

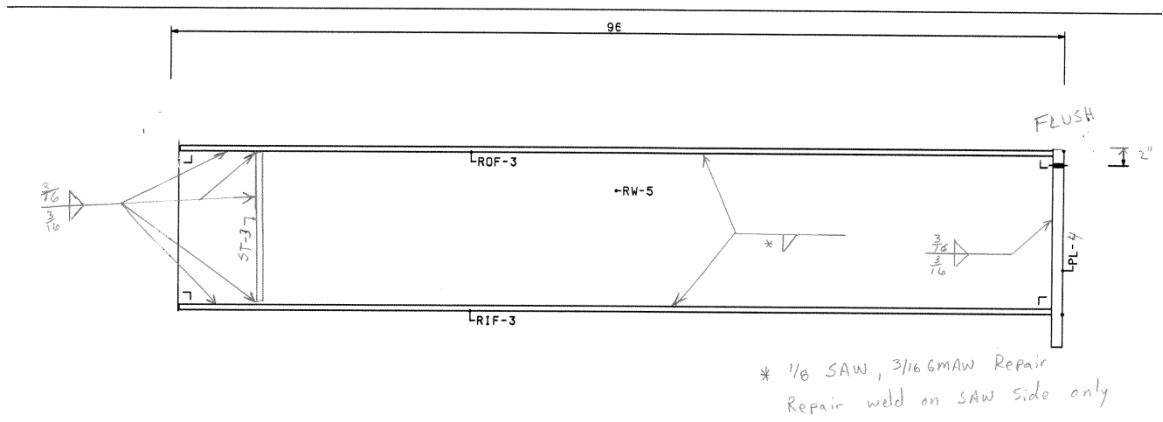


Figure K-2 Dimensions

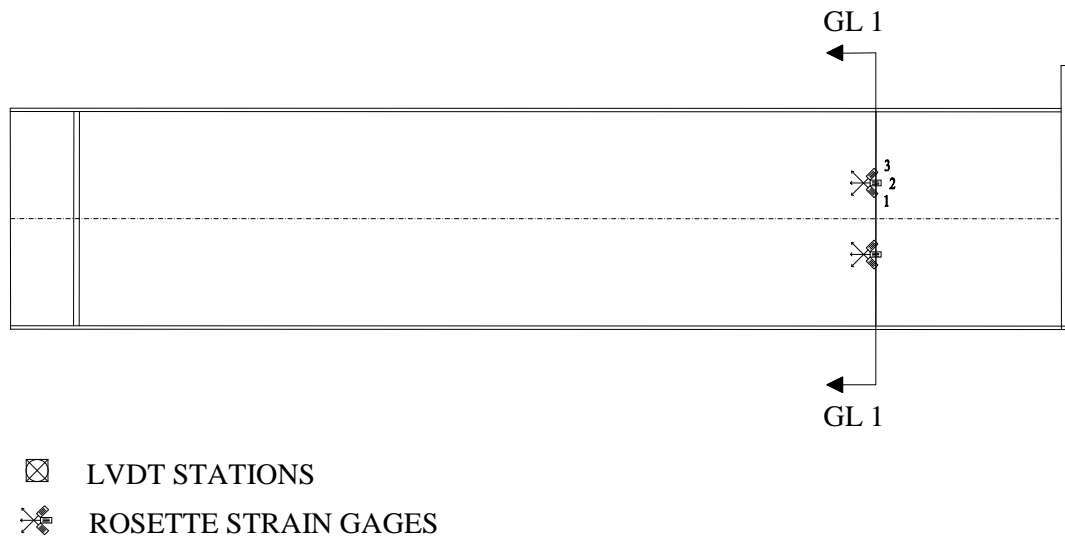


Figure K-3 Near Side Elevation

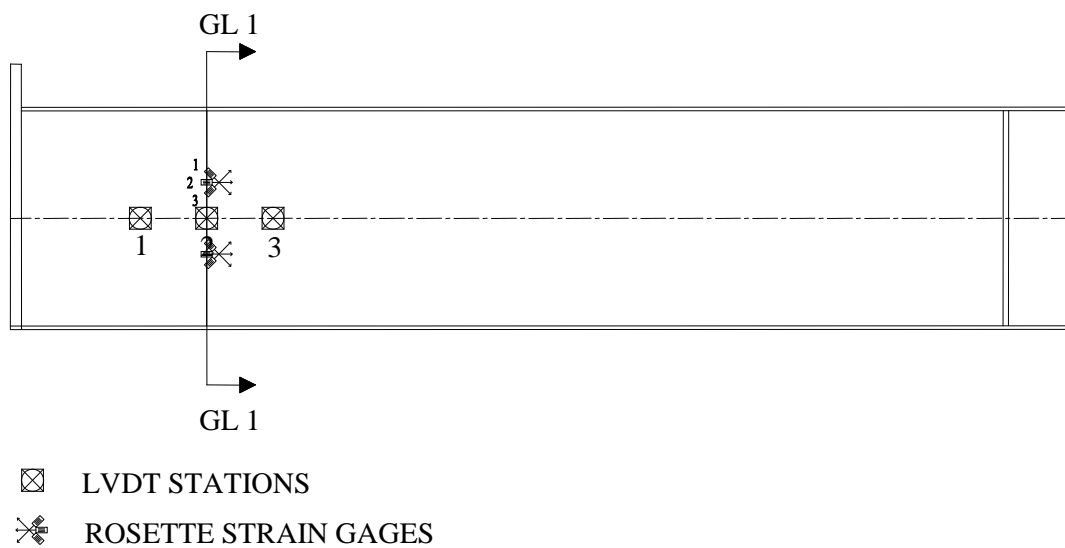


Figure K-4 Far Side Elevation

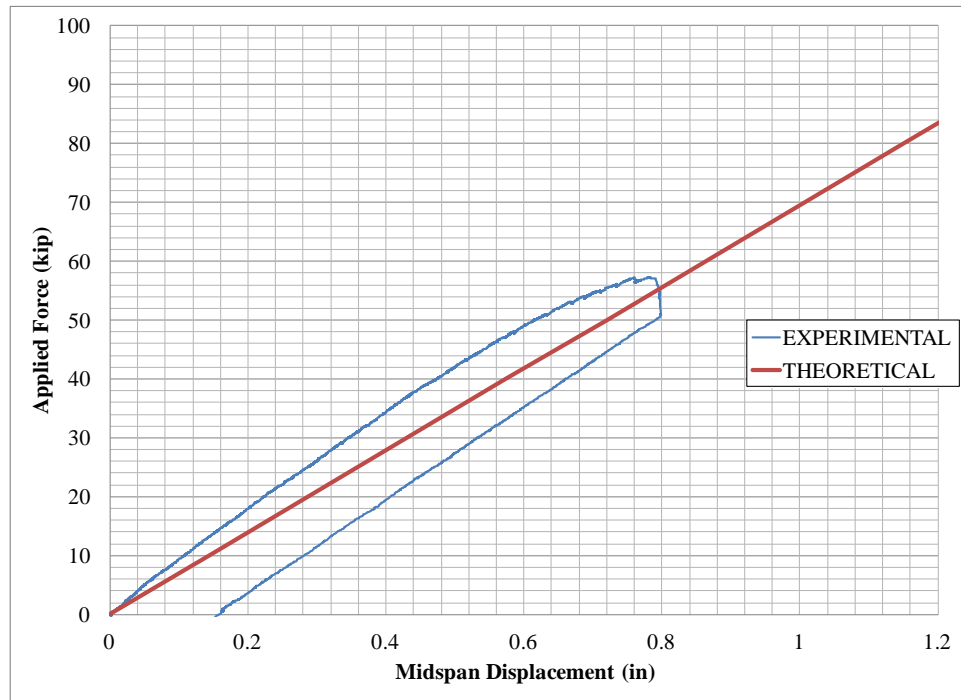


Figure K-5 Applied Force vs. Midspan Displacement

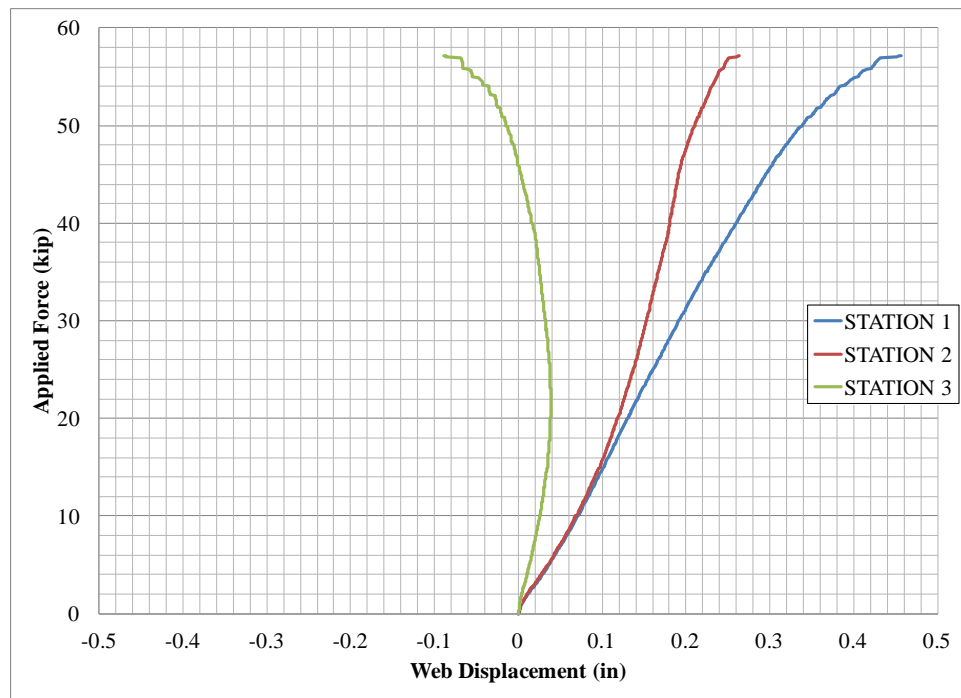
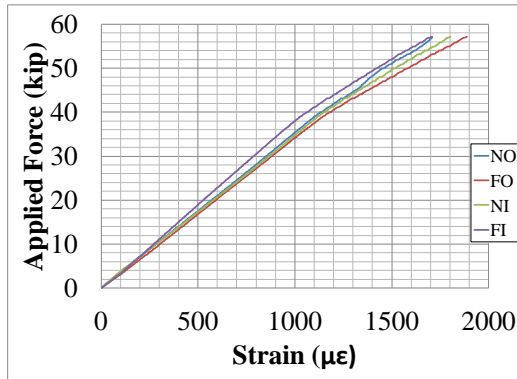
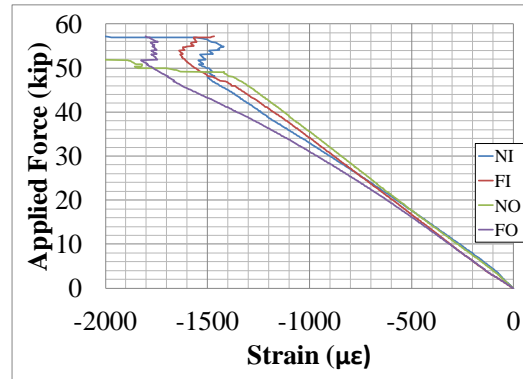


Figure K-6 Applied Force vs. Web Displacement

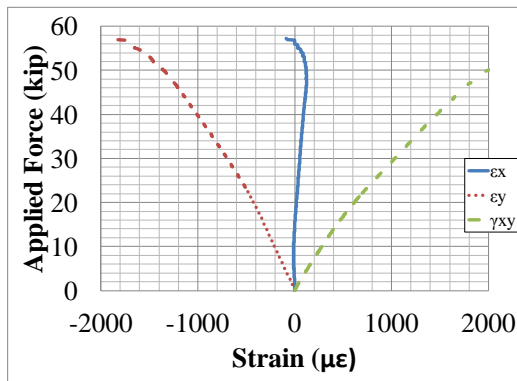


(a) Top Flange

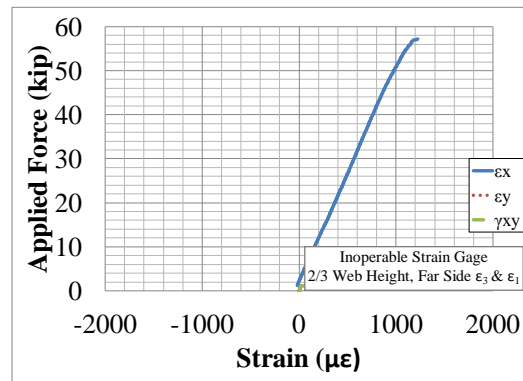


(b) Bottom Flange

Figure K-7 Applied Force vs. Uniaxial Strains at Strain Gage Station 1

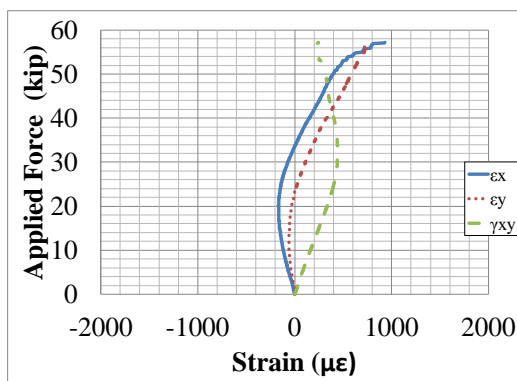


(a) Near Side

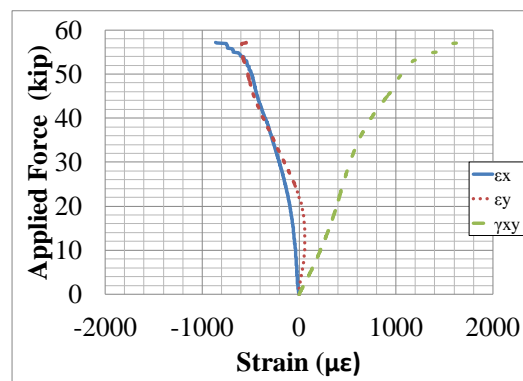


(b) Far Side

Figure K-8 Applied Force vs. 2/3 Web Height Rosette Strains at Strain Gage Station 1

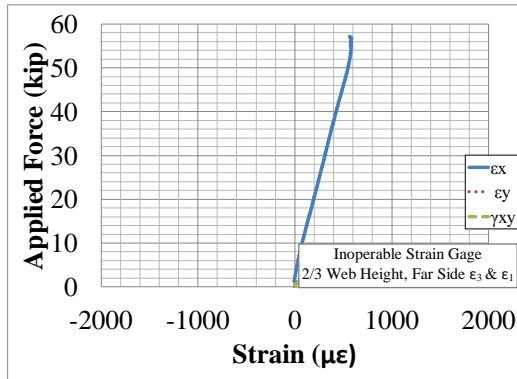


(a) Near Side

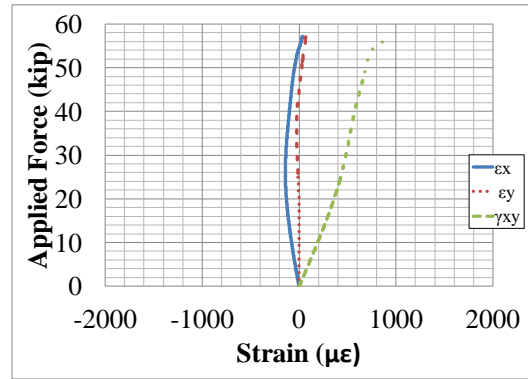


(b) Far Side

Figure K-9 Applied Force vs. 1/3 Web Height Rosette Strains at Strain Gage Station 1



(a) 2/3 Web Height



(b) 1/3 Web Height

Figure K-10 Applied Force vs. In Plane Rosette Strains at Strain Gage Station 1

## Appendix L Prismatic 2 Results

PROJECT: Metal Building Manufacturers Association  
TEST NAME: Prismatic 2  
TEST DATE: September 28, 2011

### MOMENT END PLATE CONNECTION DESCRIPTION:

Nominal Yield Stress	55 ksi
Gage	4 in.
Width	12 in.
Thickness	1.25 in.
Bolt Hole Locations	2.25 in., 6.5 in., 10in., 21.125 in.
Bolt Hole Size	1.3125 in.
Bolt Type	1.25" -7 x 4.25" A490 Hex Bolt
Bolt Pretension	Snug tightened
Nuts	1.25" - 7 A563 GR DH Heavy Hex Nut

### TEST SPECIMEN GEOMETRY:

Total Taper Angle	0°
Total Length	12 ft
Test Length	6 ft
$d_{End}$	20 in.
$d_{Midspan}$	20 in.
$t_w$	0.125 in.
$t_{f,bottom}$	0.625 in.
$b_{f,bottom}$	6 in.
$t_{f,top}$	0.625 in.
$b_{f,top}$	6 in.
$t_{stiffener}$	0.5 in.
$a/h_{ave.}$	3.53

Notes: Test length measured from centerline of stiffener to midspan. Total length measured from centerline of stiffener to centerline of stiffener

### LVDT AND STRAIN GAGE LOCATIONS:

LVDT Station 1	54 in.
LVDT Station 2	36 in.
LVDT Station 3	18 in.
Strain Gage Station 1	46 in.
Strain Gage Station 2	23 in.

Notes: Distances measured from outside face of moment plate. LVDT stations placed on near side of specimen

### EXPERIMENTAL:

Maximum Load	66.7 kip
Failure Mode	Web Shear Buckling





Figure L-1 Web Shear Buckling

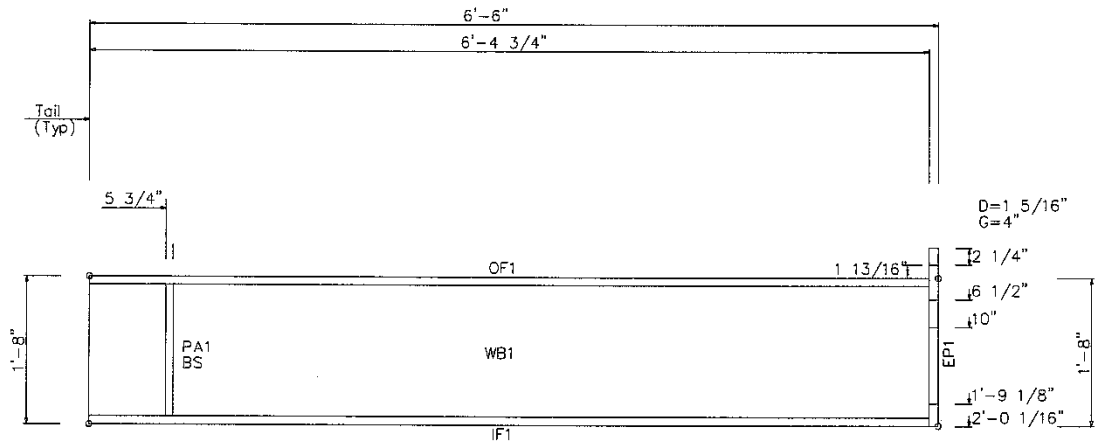


Figure L-2 Dimensions

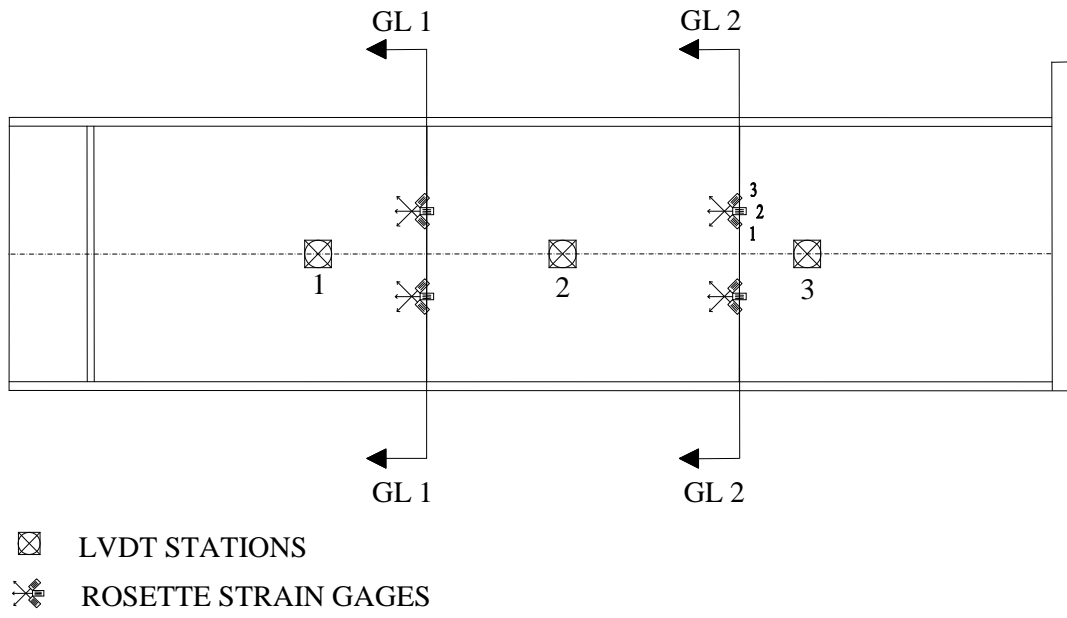


Figure L-3 Near Side Elevation

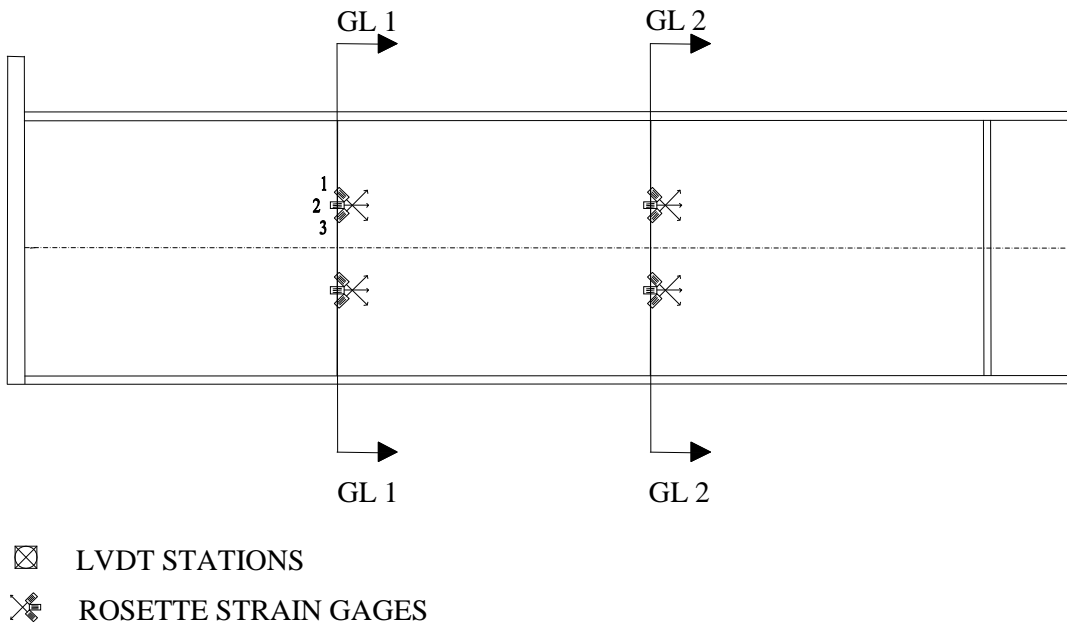


Figure L-4 Far Side Elevation

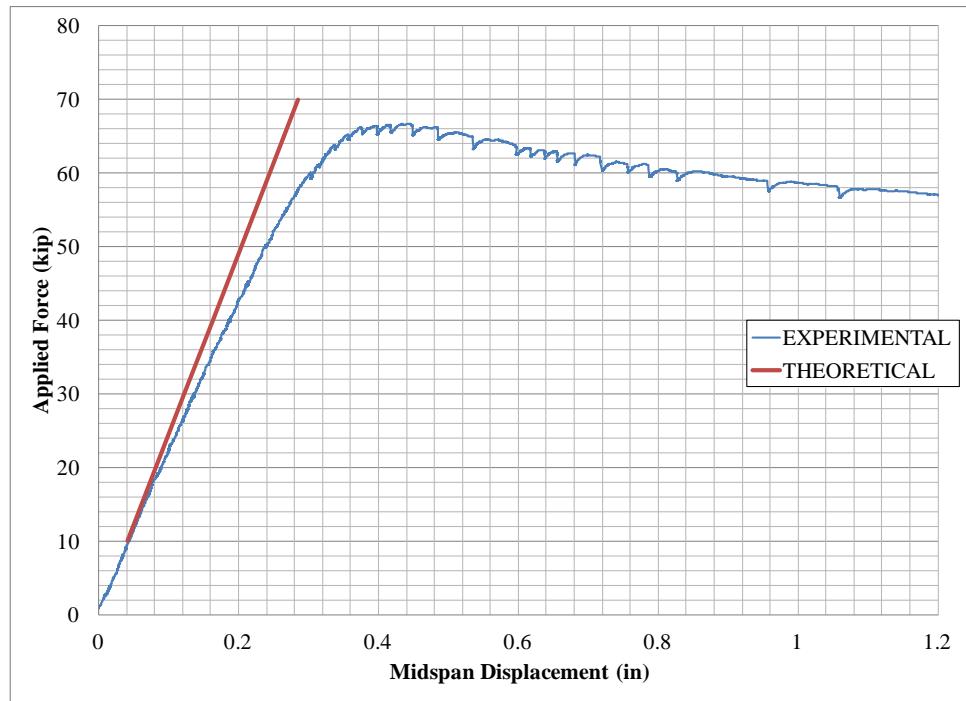


Figure L-5 Applied Force vs. Midspan Displacement

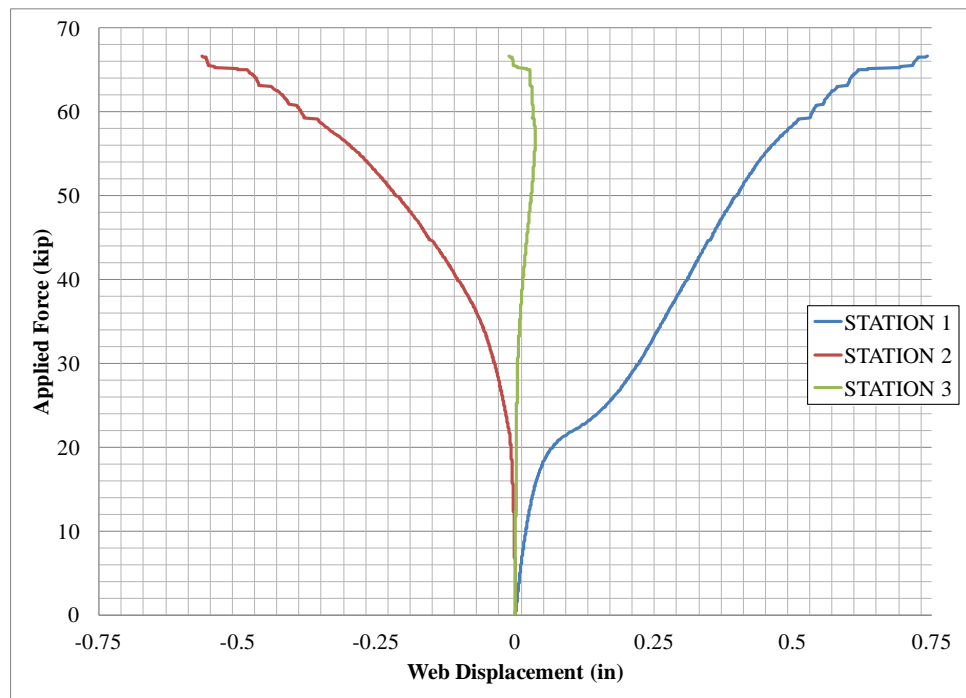
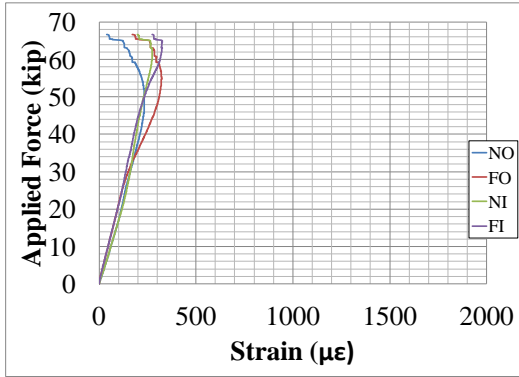
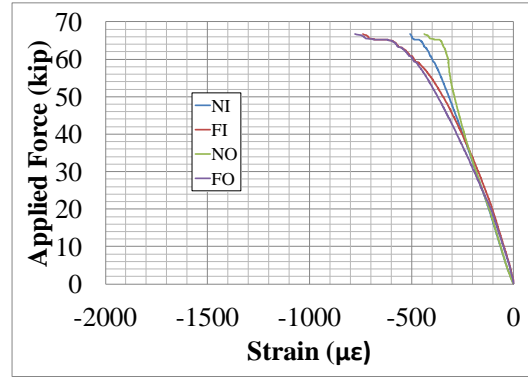


Figure L-6 Applied Force vs. Web Displacement

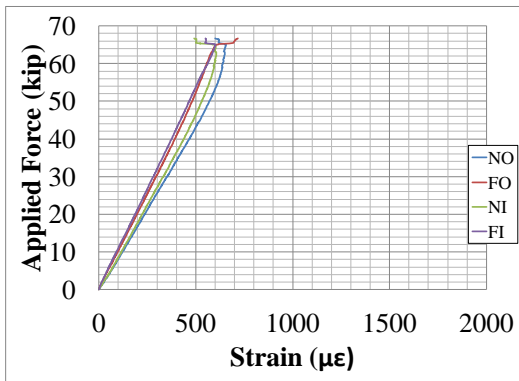


(a) Top Flange

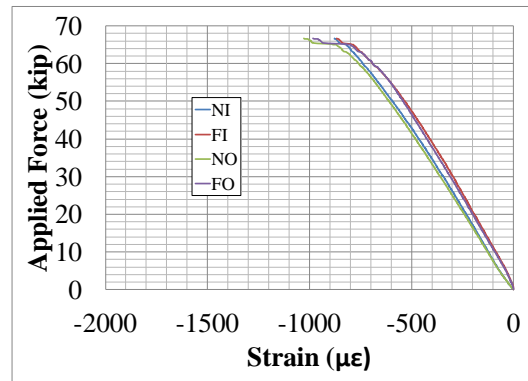


(b) Bottom Flange

Figure L-7 Applied Force vs. Uniaxial Strains at Strain Gage Station 1

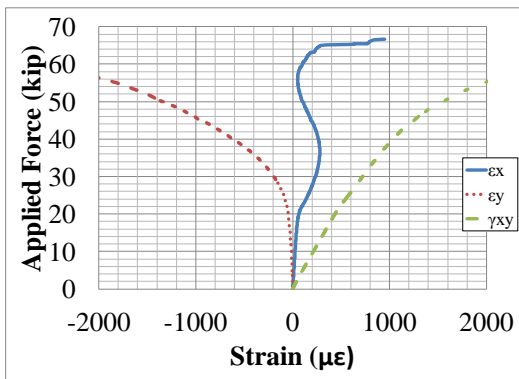


(a) Top Flange

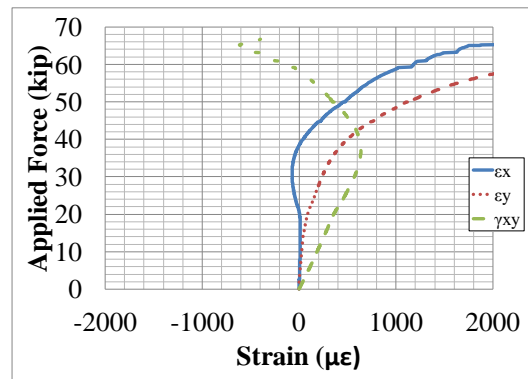


(b) Bottom Flange

Figure L-8 Applied Force vs. Uniaxial Strains at Strain Gage Station 2

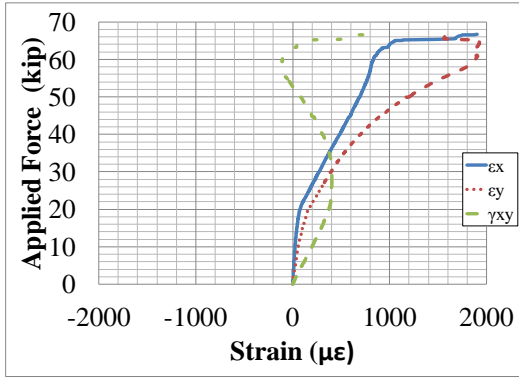


(a) Near Side

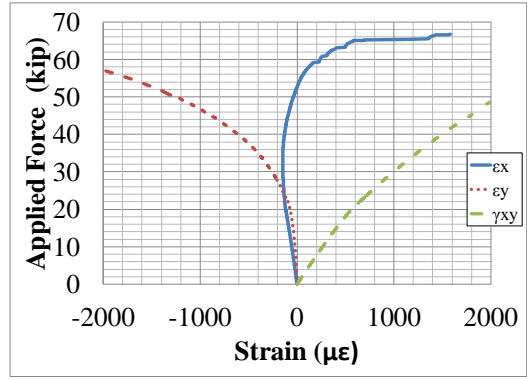


(b) Far Side

Figure L-9 Applied Force vs. 2/3 Web Height Rosette Strains at Strain Gage Station 1

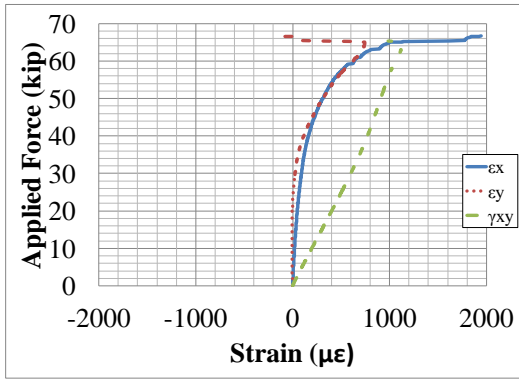


(a) Near Side

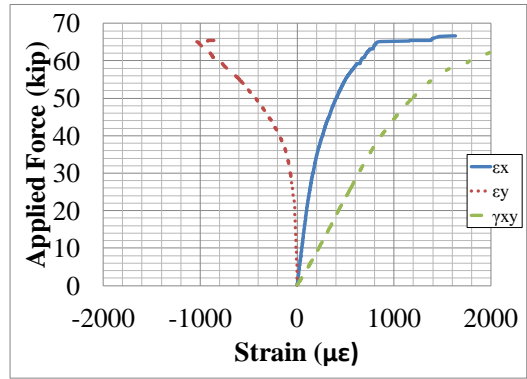


(b) Far Side

Figure L-10 Applied Force vs. 1/3 Web Height Rosette Strains at Strain Gage Station 1

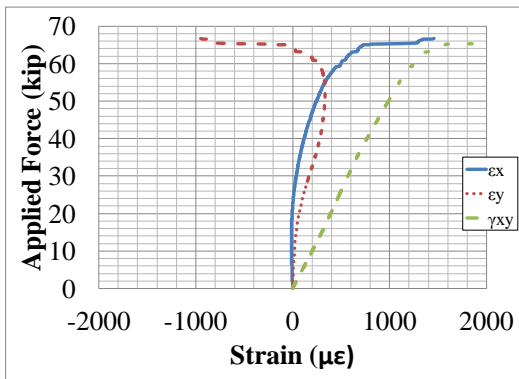


(a) Near Side

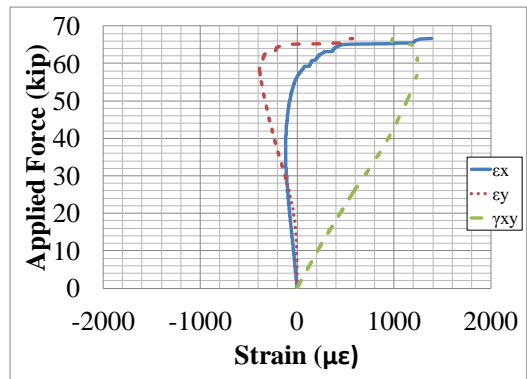


(b) Far Side

Figure L-11 Applied Force vs. 2/3 Web Height Rosette Strains at Strain Gage Station 2

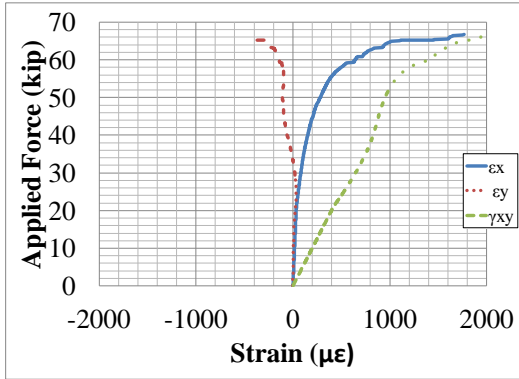


(a) Near Side

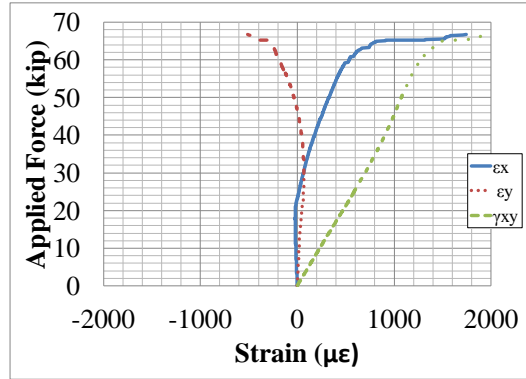


(b) Far Side

Figure L-12 Applied Force vs. 1/3 Web Height Rosette Strains at Strain Gage Station 2

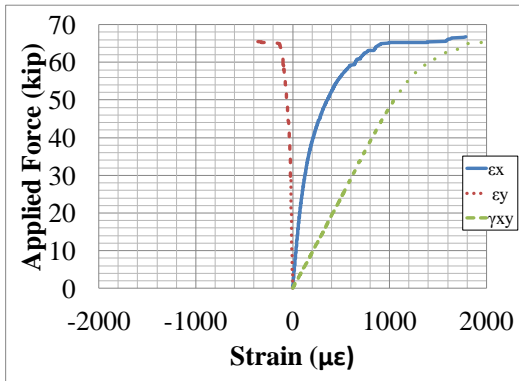


(a) 2/3 Web Height

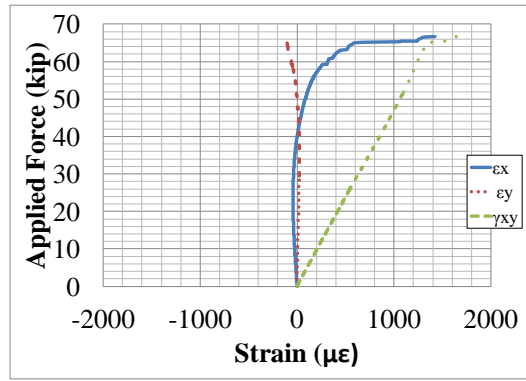


(b) 1/3 Web Height

Figure L-13 Applied Force vs. In Plane Rosette Strains at Strain Gage Station 1



(a) 2/3 Web Height



(b) 1/3 Web Height

Figure L-14 Applied Force vs. In Plane Rosette Strains at Strain Gage Station 2

## References

- AISC (2010). *Specification for Structural Steel Buildings*, American Institute of Steel Construction, Inc., Chicago, IL.
- Basler, K. (1960a). *Strength of plate girders in shear*. [Bethlehem, Pa.]: Lehigh University Institute of Research.
- Basler, K. (1960b). Web buckling tests on welded plate girders. Bethlehem, Pa.: Fritz Engineering Laboratory, Lehigh University.
- Basler, K. (1961). Strength of plate girders in shear. *Structural Division*, 87.
- Beer, F. P., Johnston, E. R., & DeWolf, J. T. (2006). *Mechanics of materials* (4th ed.). Boston: McGraw-Hill Higher Education.
- Bleich, F. (1952). *Buckling strength of metal structures*. New York: McGraw-Hill.
- Blodgett, O. W., & James, F. L. A. W. F. (1966). *Design of welded structures*. Cleveland: James F. Lincoln Arc Welding Foundation.
- Bresler, B., Lin, T. Y., & Scalzi, J. B. (1968). *Design of steel structures* (2d ed.). New York,: Wiley.
- Lee, S. C., Davidson, J. S., & Yoo, C. H. (1996). Shear buckling coefficients of plate girder web panels. *COMPUTERS AND STRUCTURES*, 59(5), 789-795.
- Lee, S. C., Lee, D. S., Park, C. S., & Yoo, C. H. (2009). Further Insights into Postbuckling of Web Panels. II: Experiments and Verification of New Theory. *Journal of Structural Engineering*, 135(1), 11-18.
- Lee, S. C., Lee, D. S., & Yoo, C. H. (2008). Ultimate shear strength of long web panels. *Journal of Constructional Steel Research*, 64(12), 1357-1365.
- Lee, S. C., & Yoo, C. H. (1998). Strength of Plate Girder Web Panels under Pure Shear. *JOURNAL OF STRUCTURAL ENGINEERING -NEW YORK-*, 124(2), 184-194.
- Lee, S. C., & Yoo, C. H. (1999). TECHNICAL PAPERS - Experimental Study on Ultimate Shear Strength of Web Panels. *Journal of structural engineering.*, 125(8), 838.
- Redmond, N. A. (2007). *Experimental and analytical investigation of the shear strength of unstiffened tapered steel members*. University Libraries, Virginia Polytechnic Institute and State University, Blacksburg, Va.

- Salmon, C. G., Johnson, J. E., & Malhas, F. A. (2009). *Steel structures : design and behavior : emphasizing load and resistance factor design*. Upper Saddle River, NJ: Pearson/Prentice Hall.
- Sumner, E. A. (1995). *Experimental and analytical investigation of the LRFD strength of tapered members*. University Libraries, Virginia Polytechnic Institute and State University, Blacksburg, Va.
- Timoshenko, S., & Gere, J. M. (1961). *Theory of elastic stability*. New York: McGraw-Hill.
- Williams, C. D., & Harris, E. C. (1949). *Structural Design In Metals*. New York: The Ronald Press Company.
- Yoo, C. H., & Lee, S. C. (2006). Mechanics of Web Panel Postbuckling Behavior in Shear. *Journal of structural engineering.*, 132(10), 1580.
- Ziemian, R. D. (2010). *Guide to stability design criteria for metal structures* (6th ed.). Hoboken, N.J.: John Wiley & Sons.



## Vita

Name: Ryan Paul Studer  
Date of Birth: October 7, 1985  
Place of birth: Cincinnati, OH

Education: Bachelor of Science in Civil Engineering  
University of Kentucky  
(August 2004 – May 2009)

Scholarships: Downey Academic Scholarship  
Paul A. Faulkner Scholarship

Ryan Paul Studer  
April 30, 2012